

https://dspace.org/

Design and development of thin polymeric membranes for modulated release of chemotherapeutic agents

Sibeko, Bongani

2014-02-13
http://hdl.handle.net10539/13756

Downloaded from a DSpace repository. https://dspace.org/

DESIGN AND DEVELOPMENT OF THIN POLYMERIC MEMBRANES FOR MODULATED RELEASE OF CHEMOTHERAPEUTIC AGENTS

BONGANI SIBEKO

A Dissertation Submitted to the Faculty of Health Sciences, University of the Witwatersrand, in Fulfilment of the Requirements for the Degree for the Master of Pharmacy

Supervisor:

Professor Viness Pillay

Department of Pharmacy and Pharmacology, University of the Witwatersrand, South Africa

Co-Supervisors:

Professor Michael P. Danckwerts

Department of Pharmacy and Pharmacology, University of the Witwatersrand

Parktown, Johannesburg, 2011

Professor Girish Modi

Department of Neurosurgery, Division of Neurosciences

Professor Sunny E. Iyuke

School of Chemical and Metallurgical Engineering, University of the Witwatersrand

DECLARATION

I, Bongani Sibeko declare this dissertation as my own work. It is being submitted for the degree of Master of Pharmacy in the Faculty of Health Sciences in the University of the Witwatersrand, Johannesburg. It has not been submitted before for any degree or examination at this or any other University.

.....

This 22nd day of February 2012

ACKNOWLEDGEMENTS

- I thank God, the Father to the Lord Jesus Christ for being my source of strength throughout this research project, everything has been possible through Him.
- A special thanks to my pastor, pastor Ladi A.Lloyd-Kuyinu and his wife pastor Pamela Lloyd-Kuyinu for the words of faith that renewed my strength and made this journey an enjoyable learning experience.
- I would like to thank my family and friends for the support and the encouragement when things seemed to be impossible.
- I would like to extend my gratitude and many thanks to my supervisor Professor Viness Pillay for granting me the opportunity to undertake this research project under his supervision. It was a life time privilege to have been nutured by a first class researcher with a broad scientific knowledge and expertise.
- To Dr Yahya E. Choonara, thank you for your advice, sharing of valuable information and willingness to help at all times.
- This research was made possible by the National Research Foundation (NRF), Department of Labour (DoL) and Adcock Ingram Limited.

SUMMARY

Primary Central Nervous System Lymphoma (PCNSL) is an aggressive form of non-Hodgkin's lymphoma (NHL) with a lymphocytic origin that arises within the brain parenchyma, leptomeninges, spinal cord and rarely the eye. This neuropathological condition is characterized by few lesions (1-3), large lesions (2-4cm) confined to the central nervous system. PCNSL is often associated with poor prognosis and may affect all age groups with peak incidence in the fifth to seventh decade in immunocompetent patients. Recently, there has been an increased incidence rate of this condition and it is thought to be attributable to increasing incidence of AIDS and hence PCNSL is gradually becoming the most common tumor in AIDS patients. The most common presenting signs and symptoms in both immunocompromised and non-immunocompromised patients are neurological deficits, mental status changes, seizures and evidence of increased intracranial pressure.

Radiation therapy has generally been the mainstay of treatment for PCNSL, whether associated or not with HIV infection. Whole brain radiation therapy results in high response rates but rapid relapse and delayed neurotoxicity. Methotraxate (MXT) based chemotherapy has improved survival for patient population with PCNSL and further studies have been conducted to evaluate the benefits of combined irradiation chemotherapy with MTX being the main cytostatic agent. MXT is administered in high-doses in order to facilitate penetration into the central nervous system. First generation chemotherapeutic regimens used successfully in systemic Non-Hodgkin's lymphoma are ineffective in PCNSL in part because the drugs do not penetrate the intact BBB. Compared to other chemotherapeutic agents, MTX has an added advantage in that it can penetrate the BBB at high doses making it the most effective cytostatic agent for the treatment of PCNSL. However, the high MTX dose results in severe systemic side effects and a poor risk to benefit profile.
In this regard, this study was aimed at developing an implantable polymer-based drug delivery system for local delivery of MTX in the brain parenchyma. This drug delivery strategy has been shown to improve drug efficacy and therapeutic responses in the management of localized tumors. A biocompatible and biodegradable device consisting of poly(lactic acid)/methacrylic acid copolymer (PLA/MAA) nanosystems embedded within a poly(lactic acid)/poly(vinyl alcohol) (PLA/PVA) biopolymeric membrane was developed and assessed for its suitability for the intended application. In addition to extensive *in vitro* studies, *in vivo* animal studies were conducted in the Sprague Dawley rat model in order to elucidate information on MTX biodistribution and toxicity profile after device implantation.

The (NSBBM) Nanosystems Based Biopolymeric Membrane device was capable of releasing MTX for over an extend period of more than 30 days. The device degraded by surface erosion and textural profiling demonstrated that the device was tough and elastic. The device showed a morphing mechanical behaviour. It was hard and tough during storage and handling and became soft and elastic upon hydration with deionised water. These mechanical properties would allow easy handling during surgical procedure and smooth integration into the viscoelastic neural tissue environment. Histological findings revealed that the NBBM device was biocompatible with the brain tissue.

PUBLICATIONS, PRESENTATIONS AND PATENTS

PUBLICATIONS:

I. Computational and Molecular Modeling and Structural Rationalization for the Design of a Drug-loaded PLLA/PVA Biopolymeric Membrane. Bongani Sibeko, Viness Pillay, Yahya E. Choonara, Riaz A. Khan, GirishModi, Sunny E. Iyuke, Dinesh Naidoo and Michael P. Danckwerts, Journal of Biomedical Materials, 2009, (4) 1:15014.

PRESENTATIONS:

I. A podium presentation entitled "Fabrication of Synthetic Biopolymeric Membranes for Various Biomedical Applications". Bongani Sibeko, Viness Pillay, Yahya E. Choonara, GirishModi, Sunny E. Iyuke and Michael P. Danckwerts.Research day and postgrad expo, University of the Witwatersrand, Faculty of Health Sciences, 2007.

II. A poster entitled"Synthetic Approaches for Fabricating Biopolymeric Membranes for Rate-modulated Drug Delivery". Bongani Sibeko, Viness Pillay, Yahya E. Choonara, GirishModi, Sunny E. Iyuke and Michael P. Danckwerts.Workshop on Structure and properties of Nanomaterials, University of Zululand, 2007.

III. A poster entitled"Influence of complex oxidizing agents on the physicochemical and physicomechanical properties of crosslinked co-blended polymeric membranes." Bongani Sibeko, Viness Pillay, Yahya E. Choonara, GirishModi, Sunny E. Iyuke and Michael P. Danckwerts.28th Annual Conference of the Academy of the Pharmaceutical Sciences, Athene Conference Centre, Club Mykonos, and Langerbaan, Cape Town, 2007.

IV. A podium presentation entitled "An implantable hydrogel drug delivery system for chemotherapeutic applications". Bongani Sibeko, Viness Pillay, Yahya E. Choonara, Girish Modi, Sunny E. Iyuke and Michael P. Danckwerts. Research day and postgrad expo, University of the Witwatersrand, Faculty of Health Sciences, 2008.

V. A podium presentation entitled "Fabrication and Characterization of MTX-loaded PLA/PVA biopolymeric membranous drug delivery device". Bongani Sibeko, Viness

Pillay, Yahya E. Choonara, GirishModi, Sunny E. Iyuke and Michael P. Danckwerts.29th Annual Conference of the Academy of the Pharmaceutical Sciences, Hunters Rest, Rustenburg on the, 2008.

PATENTS:

I. Title: Polymeric Pharmaceutical Dosage Form in Sustained Released

International Application No.: PCT/IB2009/007598

Applicants: **University of the Witwatersrand, Johannesburg**, 1 Smuts Avenue 2050 Johannesburg, Pillay Viness; Choonara, Yahya Essop; Sibeko, Bongani; Harilall, Sheri-Lee; Pillay, Samantha; Modi, Girish; Iyuke, Sunny Esayegbemu; Naidoo, Dinesh.

TABLE OF CONTENTS

Declaration	ii
Acknowledgements	iii
Summary	iv
Publications, Presentations and Patents	v-vi
Table of Contents	viii-xvi
List of Tables	Xvii
List of Figures	xviii-xxii

CHAPTER ONE

INTRODUCTION AND MOTIVATION FOR THE STUDY

1.1	**Background**	1
1.2	**Primary Central Nervous System Lymphoma**	2
1.3	**The Blood Brain Barrier: Physiology, Anatomy and Transport of Therapeutic Molecules**	5
1.4	**Strategies for Enhancing the Delivery of Therapeutic Active Compounds into the Brain Parenchyma**	9
1.5	**Physiological Response Following Implantation of a Biomaterial into the Brain Parenchyma**	12
1.6	**Rationale and Motivation for the Study**	14
1.7	**Aims and Objectives of this Study**	15
1.8	**Overview of the Dissertation**	17

CHAPTER TWO

DESIGN AND DEVELOPMENT OF POLYMERIC MEMBRANES AND SCAFFOLDS FOR CONTROLLED DELIVERY OF BIOACTIVE MOLECULES AND DRUG COMPOUNDS

2.1	**Introduction**	20
2.2	**Design and Preparation of Polymeric Scaffolds**	23
2.2.1	Solid Phase Separation	23
2.2.2	Electrospinning Technology	24
2.2.3	Foaming Using Supercritical Carbondioxide (CO_2)/Supercritical Fluid Technology	26
2.2.4	Melt Molding Particulate Leaching Technology/Injection Molding/Micromolding	28
2.2.5	Selective Laser Sintering (SLS)	29
2.2.6	Solid Free Form Fabrication (SFF)	30
2.2.7	Computer Aided Design (CAD) and Computer-Aided Manufacturing (CAM) of Polymer Scaffolds	32
2.3	**Processing Techniques for Control and Optimization of Pore Size, Mechanical Properties and Morphology**	32
2.3.1	Particulate Seeding	33
2.3.2	Thermal Treatments	33
2.3.2	Coating of Polymer Scaffolds	33
2.3.4	Topological Optimization	34
2.3.5	Crosslinking of Polymer Scaffolds (Photocrosslinking and Chemical Crosslinking)	34

2.4 **Drug Delivery (Protein, DNA and Drug Compounds) from Polymer Scaffolds** 35

2.4.1 Matrix-Mediated Drug Delivery 35

2.4.2 Microsphere-Mediated Drug Delivery 37

2.5 **Concluding Remarks** 38

CHAPTER THREE

COMPUTATIONAL AND MOLECULAR MODELING AND STRUCTURAL RATIONALIZATION FOR THE DESIGN OF A DRUG-LOADED PLLA/PVA BIOPOLYMERIC MEMBRANE

3.1 **Introduction** 40

3.2 **Materials and Methods** 43

3.2.1 Preparation of the Biopolymeric Membrane 43

3.2.2 Computational and Molecular Structural Modeling of the Biopolymeric Membrane Formation 44

3.2.3 Analysis of the Biopolymeric Membrane Swelling Potential 44

3.2.4 Assessment of Biopolymeric Membrane Morphology 45

3.2.5 Determination of Membrane Toughness and Bi-Axial Extensibility 45

3.2.6 Determination of the Drug Entrapment Efficiency within the Biopolymeric Membrane 48

3.2.7 *In vitro* Release of MTX from the Biopolymeric Membranes 48

3.3 **Results and Discussions** 49

3.3.1 Formulation of the MTX-PLLA-TEA-PVA Biopolymeric Membrane 49

3.3.2 The Effect of the Addition of AmphiphilicTriethanolamine (TEA) 51

3.3.3 Computational Molecular Structural Modeling of the Proposed Mechanism of Biopolymeric Membrane Layering 53
3.3.4 Assessment of the Surface Morphology of the Biopolymeric Membranes 56
3.3.5 Membrane Toughness and Bi-axial Extensibility 58
3.3.6 Drug Entrapment Efficiency and Swelling Studies 60
3.3.7 *In vitro* MTX Release Studies 61
3.3.8 Hypothetical Drug Release Mechanism 62
3.4 **Concluding Remarks** 62

CHAPTER FOUR

PREPARATION, CHARACTERIZATION AND OPTIMISATION OF POLY(VINYL ALCOHOL)/POLY (LACTIC ACID) BIOPOLYMERIC MEMBRANES FOR DRUG DELIVERY APPLICATIONS

4.1 **Introduction** 64
4.2 **Materials and Methods** 66
4.2.1 Materials 66
4.2.2 Preliminary Studies 66
4.2.3 Preparation of the PLA/PVA Drug-Loaded Biopolymeric Membrane 67
4.2.4 Construction of a Randomized Box-Bhenken Experimental Design for Biopolymeric Membrane Preparation and Optimisation 68
4.2.5 Assessment of the *In vitro* Degradation of PLA/PVA Biopolymeric Membranes 69
4.2.6 Analysis of Membrane Swellability 69
4.2.7 Analysis of Drug Entrapment Efficiency 70

4.2.8 *In vitro* Drug Release Studies 70

4.2.9 Tensile Mechanical Testing 71

4.2.10 Analysis of the Membrane Surface Morphology 72

4.2.11 Surface Plots and Constrained Optimisation 72

4.3 **Results and Discussions** 73

4.3.1 Mechanical Properties of the Membranes 73

4.3.2 Swelling Behaviour of the Biopolymeric Membranes 77

4.3.3 Drug Entrapment Efficiency(DEE) Studies 78

4.3.4 Degradation Behaviour of the PLA/PVA Biopolymeric Membranes 80

4.3.5 *In vitro* Drug Release Studies 82

4.3.6 Analysis of Membrane Surface Morphology 84

4.3.7 Surface Plots for Drug Entrapment Efficiency (DEE) 85

4.3.8 Surface Plots for Matrix Erosion 87

4.3.9 Surface Plots for Swellability of the Biopolymeric Membranes 89

4.3.10 Constrained Optimisation 90

4.4 **Concluding Remarks** 92

CHAPTER FIVE

A COMPOSITE METHOTREXATE-LOADED NANOCARRIER FOR THE LOCALISED TREATMENT OF PRIMARY CENTRAL NEVOUS SYSTEM LYMPHOMA

5.1 **Introduction** 93

5.2 **Materials and Methods** 95

5.2.1 Materials 95

5.2.2 Preparation of the MTX-PLA/MAA-Loaded Nanoparticles 96
5.2.3 Determination of Size Distribution, Zeta Potential and Polydispersity Index of all Formulations 97
5.2.4 Enhancement of Drug-Loading Capacity of the Optimised Nanoparticle Formulation 97
5.2.5 Determination of Drug Entrapment Efficiency of all Formulations 98
5.2.6 *In vitro* Drug Release Studies 98
5.2.7 Fourier-Transform Infrared Spectroscopic Investigations 98
5.2.8 Assessment of the Size and Shape of the Nanoparticles 99
5.2.9 Temperature Modulated Differential Scanning Calorimetry on Poly(lactic acid)/Methacrylic Acid Copolymer Nanoparticles 99
5.2.10 Molecular Simulation of the Potential Mechanisms of Polymeric Nanoparticle Formation 100
5.3 **Results and Discussions** 101
5.3.1 Preparation and Constrained Optimisation of the Nanoparticles 101
5.3.2 Effects of Formulation Variables on the Size of the Nanoparticles 103
5.3.3 Effects of Formulation Variables on the Zeta Potential of the Nanoparticles 107
5.3.4 Effect of Formulation Variables on the Drug Entrapment Efficiency of the Nanoparticles 107
5.3.5 Effect of Formulation Variables on the Yield of the Nanoparticles 109
5.3.6 Fourier-Transform Infrared Spectroscopic Investigations 112
5.3.7 *In vitro* Drug Release Studies 113
5.3.8 Morphological Characterization of the Nanoparticles 114
5.3.9 Temperature Modulated Differential Scanning Calorimetry on Poly(lactic acid)/ Methacrylic Acid Copolymer Nanoparticles and Characterization Thereof 115

5.3.10 Molecular Simulation of the Potential Mechanisms of Polymeric Nanoparticle Formation and Characterization thereof 117

5.4 **Concluding Remarks** 122

CHAPTER SIX

***IN VITRO* AND *IN VIVO* EVALUATION OF THE PLA/MAA MTX-LOADED NANOPARTICLE BASED PLA/PVA BIOPOLYMERIC MEMBRANE**

6.1 **Introduction** 124

6.2 **Materials and Methods** 126

6.2.1 Materials 126

6.2.2 Preparation of the PLA/PVA Composite Polymer 126

6.2.3 Preparation of MTX-Loaded PLA/MAA Nanoparticles 126

6.2.4 Preparation of the MTX-Loaded PLA/MAA Nanoparticle Based PLA/PVA Biopolymeric Membrane (NBBM) 127

6.2.5 Analysis of Swellability 127

6.2.6 Tensile Mechanical Testing 127

6.2.7 Assessment of the Degradation Behaviour 128

6.2.8 *In vivo* Drug Release Studies 128

6.2.9 Animal Preparation 128

6.2.10 Intravenous Bolus Administration of MTX 129

6.2.11 Surgical Implantation of the NBBM into the Brain Parenchyma 129

6.2.12 Plasma and CSF Sampling 129

6.2.13 Brain Tissue Harvesting 130

6.2.14 Histological Evaluation 131

6.2.15 Ultra Performance Liquid Chromatographic (UPLC) Separations 132

6.2.16 Preparation of aCSF, Standard Solutions and Calibration Curve 132
6.2.17 Preparation of Plasma Stock Solutions and Calibration Curve 133
6.2.18 Determining Optimal Conditions for Solid Phase Extraction (SPE) 133
6.2.19 Analysis of MTX Levels in Plasma and CSF Samples 134
6.2.20 Assay of MTX in Rat Brain Regions 134
6.3 **Results and Discussion** 134
6.3.1 Description and Dimensions of the NBBM 134
6.3.2 Surgical Procedure and Wellbeing of the Animals 134
6.3.3 Swellability and Tensile Mechanical Testing 135
6.3.4 Evaluation of the Degradation Behaviour 136
6.3.5 *In vitro* Drug Release 137
6.3.6 Histological Findings 138
6.3.6.1 Drug-Loaded Implant 138
6.3.6.2 Placebo Implant 141
6.3.7 MTX and AZT Chromatographic Separations and Calibration in aCSF and Plasma 143
6.3.8 CSF, Plasma, and Brain Tissue Concentration Profiles Following Intravenous Administration of MTX and Surgical Implantation of MTX-Loaded NBBM 145
6.3.9 **Concluding Remarks** 147

CHAPTER SEVEN

CONCLUSIONS AND RECOMMENDATIONS

7.1	**Conclusions**	148
7.2	**Recommendations**	150
8	**REFERENCES**	151
9	**APPENDICES**	176

LIST OF TABLES

Table 1.1	Considerations for drug transport into the brain	9
Table 2.1	Biopolymers used for preparing scaffolds	22
Table 3.1	Test parameter settings employed for bi-axial extensibility testing of biopolymeric membranes	46
Table 3.2	Hyperchem® V 7.5 (Hypercube Inc., Gainesville, FL, USA) computational molecular attributes at *ab initio* and Density Functional Theory (DFT) (6-31G)	56
Table 4.1	Independent formulation factors selected for biopolymeric membrane preparation and optimization	67
Table 4.2	Formulation of PLA/PVA biopolymeric membranes using a 3-Factor Box-Bhenken design with values of variables	69
Table 4.3	Test parameter settings employed for textural profiling	72
Table 4.4	Elastic modulus and factor change in modulus for various PLA/PVA biopolymeric membranes	74
Table 5.1	Arrangement of the 3-Factor Box-Bhenken Design for PLA/MAA nanoparticle formulations	96
Table 5.2	Temperature modulated differential scanning calometry settings employed for thermal analysis	100
Table 5.3	Response obtained for studied formulation variables from the 3-Factor Box-Bhenken design	102
Table 5.4	Formulation constrains obtained for response optimization	103
Table 5.5	Calculated energy parameters (kcal/mol) and molecular attributes of the complexes involving PLA, MAA and MTX	120
Table 5.6	Calculated molecular attributes of the complexes involving PLA,MAA and MTX	120
Table 6.1	Test parameters employed for bi-axial extensibility testing of the NBBM device	128

LIST OF FIGURES

Figure 1.1	Transportation mechanisms at the blood brain-barrier	8
Figure 2.1	A schematic of binary phase diagram of a polymer solution showing liquid-liquid demixing gap and possible structure formation in different part of liquid-liquid demixing gap: nucleation and growth of polymer rich phase (left picture),bicontinous morphology due to spinodal decomposition (middle picture), nucleation and growth of polymer poor phase (right picture)	24
Figure 2.2	A schematic diagram showing a micromolding technique	28
Figure 2.3	A schematic diagram of PCL FDM extrusion and deposition process	31
Figure 3.1	A schematic depicting the experimental configuration for assessing the toughness and bi-axial extensibility of biopolymeric membrane employing textural profile analysis. Step I, involves securing of the samples; Step II, securing the sample platform to textural stage and Step III, lowering the textural probe during test mode for biopolymeric membrane	47
Figure 3.2	Digital images of (a) MTX-PLLA-PVA, (b) PLLA-PVA, (c) MTX-TEA-PLLA-PVA and (d) TEA-PLLA-PVA biopolymeric membranes, where MTX=methotrexate, TEA=triethanolamine, PLLA= poly(L-lactic acid) and PVA= poly(vinyl alcohol)	50
Figure 3.3	Schematic of (a) A 1D representation of MTX-loaded biopolymeric membrane entity conjugation MTX-PLLA-PVA, (b) initial induction of structure layering and (c) A 3D representation of the conformationally evolved biopolymeric membrane showing inter-layering of PLLA and MTX conjugated to the PVA backbone	50
Figure 3.4	Schematic of (a) MTX molecules bound to a PLLA-TEA-PVA backbone of the biopolymeric membrane where R=PVA polymeric chain, R1=PLLA-TEA-MTX linkage and R2=a MTX molecule and (b) A 3D structural model of the biopolymeric membrane depicting the multilayers representing PLLA, TEA and MTX conjugated onto the PVA backbone	52
Figure 3.5	Schematic depicting (a) a cube representing the diverse model contours of the conjugated MTX-TEA-PLLA-PVA-PLLA-PVA-TEA-MTX entity due to matrix stereo-electronic factors, (b) formation of self-assembled mono-layered isomers, (c) end chain activation of fusion based on chirality of mono-layered and (d) isomeric conjugation into an ordered multi-layered biopolymeric membrane	54

Figure 3.6	SEM photomicrographs of the biopolymeric membrane depicting (a) and (b) layered architecture and crystalline structure, (c) the aerial surface and (d) bottom surface morphology of the membrane	57
Figure 3.7	Typical bi-axial extensibility profiles generated for (a) a MTX-PLLA-PVA membrane and (b) a MTX-TEA-PLLA-PVA membrane system. I= phase of linear extensibility, II= maximum extensibility, III= membrane fracture, *P* = region of extended membrane plasticity due to addition of TEA	59
Figure 3.8	Histograms comparing (a) the drug entrapment efficiency and (b) the dynamic swelling potential of MTX-PLLA-PVA and MTX-TEA-PLLA-PVA biopolymeric membrane	60
Figure 3.9	MTX release profiles from (a) the MTX-PLLA-PVA and MTX-TEA-PLLA-PVA biopolymeric membrane formulation showing triphasic release kinetics with I-initial burst effect, II-diffusional phase of MTX release, and III- a final controlled MTX release phase	61
Figure 4.1	Bar graph depicting the elastic modulus for various biopolymeric membrane formulations at different physicochemical states (a) drug-loaded, (b) hydrated and (c) plain	75
Figure 4.2	Bar graph depicting a factor change in modulus for various biopolymeric membranes (d) upon hydration and (e) drug-loading	76
Figure 4.3	Bar graph depicting swelling potential (Sw) of various biopolymeric membrane formulations obtained from the experimental design	78
Figure 4.4	Bar graph depicting drug entrapment efficiency (DEE) of various biopolymeric membrane formulations obtained from the experimental design	79
Figure 4.5	Degradation profiles for various biopolymeric membrane formulations in PBS (pH 7.4; 37°C) (a) Formulation 3-6, Formulation 7-10 and (c) Formulation 12, 14 and 16.	81
Figure4.6	Drug release profiles for various biopolymeric membrane formulations in PBS (pH 7.4, 37°C) (a) Formulation 2-5, Formulation 6-9 and (c) Formulation 15 and 16.	83
Figure 4.7	Scanning electron micrographs depicting (a) the surface of the biopolymeric membrane that was directly in contact with the non-solvent and (b) the surface of the membrane that was in contact with the support	84
Figure 4.8	Response surface plots depicting the effect of (a) PVA concentration and PVA volume ratio, (b) the effect of PVA concentration and quantity of TEC and (c) the effect of PVA volume ratio and quantity of TEC on DEE.	86

Figure 4.9	Response surface plots depicting the effect of (a) PVA concentration and quantity of TEC, (b) PVA volume ratio and quantity of TEC and (c) PVA concentration and PVA volume ratio on biopolymeric membrane erosion	88
Figure 4.10	Response surface plots depicting the effect of (a) PVA concentration and PVA volume ratio, PVA concentration and quantity of TEC and (c) PVA volume ratio and quantity of TEC on the swellebility of the biopolymeric membranes	90
Figure 4.11	Desirability plot depicting the requisite variables for producing PVA/PLA biopolymeric membrane with the desired targeted responses.	91
Figure 5.1	Desirability plots depicting the requisite variables for producing PLA/MAA nanoparticles with the desired targeted responses	103
Figure 5.2	(a) Size-plot depicting the sizes of different PLA/MAA nanoparticle formulations, (b) monomodal size distribution for the optimized PLA/MAA nanoparticle formulation (n=3, SD≤1.53) and (c) monomodal size distribution for the final PLA/MAA formulation (n=3, SD≤1.0).	105
Figure 5.3	Response surface plots depicting the effect of (a) quantity of PLA and quantity of ES (MAA), (b) quantity of PLA and phase volume ratio and (c) quantity of ES (MAA) and phase volume ratio on the size of the nanoparticles	106
Figure 5.4	Bar-plots depicting differences in DEE within various PLA/MAA nanoparticle formulations	108
Figure 5.5	Response surface plots depicting the effect of (a) quantity of PLA and quantity of ES (MAA), (b) quantity of PLA and phase volume ratio and (c) quantity of ES (MAA) and phase volume ratio on theDEE of the nanoparticles	109
Figure 5.6	Bar chart plots depicting differences in the yield within various PLA/MAA nanoparticle formulations.	110
Figure 5.7	Response surface plots depicting the effect of (a) amount of PLA and amount of ES (MAA), (b) amount of PLA and phase volume ratio and (c)amount of ES (MAA) and phase volume ratio on the yield of nanoparticles	111
Figure 5.8	FT-IR spectra of (a) methotrexate (MTX), poly(DL-lactic acid) (PLA) and methacrylic acid copolymer (1:2) (MAA)	112
Figure 5.9	FT-IR spectra of (a) drug-free PLA/MAA NP's, (b) MTX-loaded PLA/MAA nanoparticles and (c) the difference in spectra.	113
Figure 5.10	Release profile of MTX from an optimized PLA/MAA nanoparticle with highest drug incorporation efficiency (n=3, SD≤0,34).	114

Figure 5.11	Transmission electron micrograph (TEM) of the PLA/MAA nanoparticles.	115
Figure 5.12	Temperature modulated DSC thermograms of PLA/MAA nanoparticles showing the endothermic and exothermic peaks generated from the reversible, non-reversible, total heat flow curves and *Cp*-complex, outphase and inphase profiles that generated the reversible curves	117
Figure 5.13	Energy minimised geometrical preferences of the drug-polymer complexes derived from molecular mechanics calculations (a) MAA-MTX, (b) PLA-MTX, (c) depiction of adsorption of MTX on MAA nanoparticle (shown coloured-tube rendered). MTX is rendered in spheres and polymer are ball/cylinder rendering. Colour codes for elements are Carbon: cyan, Nitrogen: blue, Oxygen: red and Hydrogen: white	119
Figure 5.14	(a) Polymer-drug composite showing the interspersed load and polymer outer wall, (b) MTX-PLA/MAA linkage depicted in a stereo-orientation pattern, (c) the 3D sketch depicting the polymer surface embedded the MTX-PLA/MAA and (d) surrounding medium in an un-hydrated condition	121
Figure 5.15	A computographics representation depicting (a) formation of uniform nanoparticle molecules, (b) cluster of grouping of molecules, (c) nanoparticles, (d) ion fill with synthetic PLA/MAA coating, (e) MTX-PLA/MAA fill with MTX coating or wrapping, (f) heterogenous fill depicting the adsorption of MTX onto the PLA/MAA composite	122
Figure 6.1	Flow diagram showing the layout of the *in vivo* studies	131
Figure 6.2	Textural profile for the (a) unhydrated NBBM and (b) hydrated NBBM	135
Figure 6.3	Degradation profile of the NBBM device in PBS (pH 7.4; 37°C), (n=3, SD≤0.36).	137
Figure 6.4	4 MTX release profile from the NBBM device in PBS (pH 7.4; 37°C), (n=3, SD≤0,74)	138

Figure 6.5 (a) the homogenous implant is present in the one part of the section, while the inflammatory process could be demonstrated in the neurocortex of the cerebrum, (b)mild inflammation observed in the neurocortex associated with the drug-loaded polymeric implant,(c) edge of the implant and neuroparenchyma with microglia as well as gitter cells visible (d), bright eisinophilic material at the edge of the surface with mild granulomatous inflammation in the neuroparenchyma, (e) gitter cells and microglia in the inflammatory region adjacent to the drug-loaded polymeric implant and (f) mild inflammatory process in the leptomeninges and neuroparenchyma with microglia visible 140

Figure 6.6 (a) the edge between the polymeric placebo implant and the brain tissue showing minimal inflammation,(b) at higher magnification, (c) minimal inflammation in the neuroparenchyma, (d) inflammatory area with few glitter cells in the neuroparenchyma and (e) minimal inflammation in cortical neuroparenchyma 142

Figure 6.7 Chromatogram showing separation and retention times of (a) MTX and (b) AZT in aCSF (n=3, SD≤0.62) 143

Figure 6.8 Chromatogram showing separation and retention times of (a) MTX and (b) AZT in plasma (n=3, SD≤0.73) 144

Figure 6.9 MTX calibration curve in aCSF 144

Figure 6.10 MTX calibration curve in plasma 145

Figure 6.11 (a) Plasma concentration-time profile following bolus intravenous administration of MTX (n=3, SD≤0.53), CSF concentration-time profile following bolus intravenous administration of MTX (n=3, SD≤0,62) and (c) Brain tissue concentration-time profile following implantation with MTX-loaded NBBM device(n=3, SD≤0.67). 146

CHAPTER ONE

INTRODUCTION AND MOTIVATION FOR THIS STUDY

1.1 Background

Trees bear perfect resemblance of the evolution of drug delivery systems. Starting from the deep roots of ancient medicine which gave rise to altitude climbing stems representing various branches of drug delivery technologies such as tablets, hard and soft capsules, controlled and modulated release systems, stimuli sensitive drug delivery systems, sophisticated programmable systems, microparticles and nanosystems. These novel drug delivery formulations eventually blossom into innovative commercial products possessing superior therapeutic properties. Drug delivery research is devoted to maximising therapeutic efficacy, minimising dose frequency and reducing side effects and reducing toxicities. It is committed to developing suitable vehiculant systems for existing and newly discovered drug entities. Over the years, the amalgamation of polymer science and pharmaceutical science has gradually led to the establishment polymer fabrication technologies which gave birth to many innovative polymer-based drug delivery systems for treating various disease conditions.

Polymers have been studied and employed extensively in the field of drug delivery design. They are versatile materials with inherent diversity of chemical structures which can be modified through different polymer processing technologies to obtain desired physical and chemical properties. Polymers are available as natural, synthetic or semi-synthetic materials. They can be classified as biodegradable or non-biodegradable. Natural polymers include chitosan, gelatin, agarose and hyaluronic acid. Biodegradable synthetic polymers include polyesters, polyanhydrides and polyamides and non-biodegradable polymers include cellulose derivatives, silicones and acrylic polymers. Some polymers such as PLGA, PVA, PCL, and PLGA have

been found to be biocompatible with physiological tissues and have been employed extensively to in the field of drug delivery implantable biomaterials.

Biocompatibility is an important property of polymers used for drug delivery applications. According to the Williams Dictionary of Biomaterials, biocompatibility does not only consist in not having harmful effects nor, in observing a tissue response comparable to test materials. The definition proposed by Williams in 1987 refers to "the ability of a material to perform with an appropriate host response in a specific application". The biocompatibility of a biomaterial relies on various parameters depending on the host and the material itself. The site of implantation is one of the principal host factors while factors depending on the material are shape, size, surface chemistry and roughness, design, morphology and porosity, composition, sterility issues, contact duration and degradation behaviour.

To date, the fabrication of many novel drug delivery technologies is still based on polymer materials. These systems have proved to be potent novel therapeutics for new diseases and diseases which lack efficient treatment with conventional dosage forms. Therefore this study was focused on using polymers and polymer processing technologies for developing an implantable drug delivery device for modulated release of chemotherapeutic agents such as methotrexate in the treatment of primary brain tumors.

1.2 Primary Central Nervous System Lymphoma (PCNSL)

Primary central nervous system lymphomas (PCNSL) once called microgliomas reticular cell sarcomas or perivuscular sarcomas are malignant non-Hodgkin's (NHL's) B-cell lymphomas confined to the CNS (Henry et al.,1974; Lai et al., 2002). Most PCNSL are predominantly histologically high grade B phenotype and more than 90% fall within groups G (diffuse with large

cells) and H (immunoblastic) and 5% are group J (Burkitt). PCNSL tend to localise in deep regions of the brain (cerebral, cerebellar and brain stem parenchyma) and can present as single or multiple lesions. The histological margins are cloudy (because of infiltrative growth and vasogenic oedema) and sometimes the neoplasm symmetrically infiltrates the both cerebral hemispheres giving origin to the radiographic "butterfly" image (Ferreri et al., 1995; Basso and Brandes, 2002; Andres and Michele, 2007). PCNS lymphoma affects all age groups with a peak incidence in the 5th to 7th decade in non-acquired immunodeficiency syndrome patients (Deangelis, 1994; Ferreri et al., 1995; Yamanaka et al., 2005). Within the last two to three decades there has been a significant increase in the incidence of PCNSL in immunocompromised as well as immunocompetent individuals.

Some authors have reported that its increase in incidence exceeds that of gliomas, and the entire group of non-Hodgkin's lymphomas (NHLs) (Lutz and Coleman, 1994; Werner et al., 1995). The dramatic increase in incidence that is independent of age and gender could not solely be attributed to the changes in medical practise such as improved diagnostic techniques, the use of magnetic resonance imaging (MRI) or stereotactic surgery. Indirect evidence implicates the acquired immune deficiency syndrome (AIDS) epidemic as a contributor to this trend (Beral et al., 1991; Cote et al., 1996; Lantos et al., 1997; Eby et al., 1998). PCNSL arising in HIV patients is different to those affecting immunocompetent patients. The two forms display different pathogenic and clinical aspects and require different therapeutic approaches (Basso and Brandes, 2002). In HIV patients, Epstein-Bar virus (EBV) and c-myc proto-oncogene translocation induce proliferation of PCNL by a known mechanism while it arises by an unknown mechanism in immunocompetent patients (Andres and Michele, 2007).

While the quest for finding a cure for HIV/AIDS continues and the number of people being infected increasing daily, PCNSL is gradually progressing to being the most common brain

tumor in AIDS patients with 2-6% of patients showing clinical symptoms during the course of the disease (Rosenblum et al., 1988; Cammilleri-Broet et al., 1997; Chamberlain et al., 1999; Schabeth, 1999). Most of the patients diagnosed with PCNSL die within a year or two if appropriate treatment is not initiated. PCNSL is a highly aggressive malignant brain tumor characterised by rapid growth that is equally paralled by rapid clinical evolution. The disease is extremely fatal if correct treatment is not initiated immediately. The prognosis for patients with PCNSL is very poor with the median survival rate of only 3-5 months if untreated (Pollack et al., 1989; Andres and Michele, 2007). The prognosis in immunocompromised patients is even lower, with the median survival of 1 month for untreated patients.

Radiotherapy (RT) has been the mainstay therapy for years achieving complete response in most patients receiving 40-50 Gy (Schlegel et al., 2000). However, the improvement in median survival has been singularly poor with a median survival time of 12 – 42 months and a 5 year survival rate of less than 10% (Hochberg and Miller, 1988; Nelson et al., 1992; DeAngelis et al., 1995; Shibamoto et al., 1999; Schlegel et al., 2000). Surgical resection of the tumor is contraindicated because of the diffusely infiltrative nature of PCNSL. In addition, surgery may result in neurological deficit and it is therefore restricted to diagnostic biopsy (Fine and Mayer, 1993; Bataille et al., 2000). In an attempt to improve the dismal prognosis and improve the patient's survival, researchers have investigated several different therapeutic strategies involving combination of chemotherapy with radiotherapy, chemotherapy alone using a single chemotherapeutic agent or treatment protocols consisting of a combination of chemotherapeutic compounds. A number of studies have shown that addition of high-dose methotrexate (MTX) - based chemotherapy to RT substantially improves survival (median survival: 2 to 4 years) compared with RT alone (median survival: 1 year) (Nelson et al., 1992; Abrey et al., 1998; Glass et al., 1994; Neuwelt et al., 1998). Unfortunately this combined treatment has been shown to expose the surviving patients especially the elderly to severe delayed neurotoxicity (Hoang-

Xuan et al., 2004). Unlike malignant gliomas, appropriate treatment of PCNSL can result in prolonged survival and even cure when chemotherapy is incorporated into treatment (DeAngelis, 2003).

Treatment of PCNSL with MTX has proved to be beneficial and this drug has since been regarded as the most efficient cytostatic drug in PCNSL. Thus, MTX-based chemotherapy has gained wider acceptance as initial therapy for PCNSL (Reni et al., 1997;Conroy et al., 1998; Blay et al., 2000). Several trials of high-dose systemic MTX (HD-MTX) alone have been conducted and these suggest comparable survival with less long-term neurotoxicity compared with combination chemotherapy plus whole brain radiation therapy (WBRT) (Cher et al., 1996; Guha-Thakurta et al., 1999; Batchelor et al., 2003). In patients treated only with MTX-based chemotherapy, no gross cognitive decline was observed as a long term treatment effect (Fliesbach et al., 2005). HD-MTX alone produced a 52-100% response rate and a 2-year survival of 61-63% (Cher et al., 1996; Batchelor et al., 2003).

1.3. The Blood-Brain Barrier: Physiology, Anatomy and Transport of Therapeutic Molecules

The blood-brain barrier (BBB) is critically important when it comes to the effective management of PCNSL since this tumor resides behind the intact BBB which limits the accessibility of antineoplastic drugs to the lymphomatous cells (Hoang-Xuan et al., 2004). It has been observed that standard chemotherapy regimens useful for comparable systemic lymphoma are ineffective against PCNSL in part because the drugs do not penetrate the intact blood-brain barrier (BBB) (Brada et al., 1990; O' Neill et al., 1995). The BBB restricts entry of applicable compounds depending on their size and permeability. The barrier is selective in the passage of desired molecules into the brain parenchyma. Therefore MTX has to be administered intravenously at

very high doses in order to reach effective therapeutic concentrations at the tumor site. It has been shown that the response to chemotherapy also depends on the integrity of the BBB (Andres and Michele, 2007).

The primary function of the BBB is of a protective nature, with various cells regulating the entry of compounds in and out of the brain tissue. However it is this primary function that ultimately frustrates therapeutic interventions directed at treating brain tumors or any other CNS disease for that matter. A basic understanding of the physiology and the anatomy of the BBB and transport mechanisms across the BBB is crucial when designing and synthesizing new chemical entities or developing drug delivery devices for therapeutic advancement of brain diseases. Cerebral capillaries are created by the process of angiogenesis, which is the development of blood vessels from those existing in previously formed complexes. In the early stages of development, the endothelial cells transverse the extracellular matrix and degrade the basement membrane to create a microvuscular network (Reese and Karnovsky et al., 1967; Nag, 2003). Neural determinants confer characteristic physiological properties of the BBB and consequently cerebral endothelial cells (EC) are distinguished from the EC of the periphery. The brain EC have fewer endocytotic vessels than peripheral EC, which limits the transcellular flux at the BBB. The endothelial cells are joined by occluded tight junctions which imposes barriers to paracellular flux. The cerebral EC have more mitochondria than the peripheral EC, which drives the increased metabolic workload necessary to maintain ionic gradients across the BBB (Nag, 2003). These unique structural properties of the cerebral EC define the selectiveness of the BBB.

The EC and the astrocytes are fused by an electron dense basement membrane which also divides the EC and the pericytes from the surrounding extracellular space. Pericytes are thought to indirectly regulate EC activity and BBB transport. In addition, pericytes could also manage

endothelial growth and development by inhibiting cell proliferation and contribute to angiogenesis (Hirshi and D'Armore, 2007). More than 99% of the basal capillary membrane is enveloped by the astrocytes which also play a role in the BBB induction of high paracellular resistance (Johanson, 1980). There is a significant interplay between the EC, astrocytes and the pericytes which govern solute transportation.

Transporters, receptors and enzymes located on the plasma membranes of the astrocytes and pericytes dictate the fates of solutes before they reach the EC (Johanson, 1980; Pardridge, 2003). The increased electrical resistance between the EC at the tight junctions restricts solute entry into the brain by the transcellular route (Crone and Olesen, 1982).The tight junction (TJ) is composed of proteins, claudin 1-, 3-, and 5-, occludin and the junctional adhesion molecule (JAM) (Martin-Padura et al., 1998; Furuse et al., 2003; Wolburg and Lippoldt, 2000; Wolburg et al., 2003,). The claudins form the seal of the tight junction by binding to each other on adjacent EC (Mitie et al., 1998). The occluding protein is also responsible for directing the paracellular permeability. These proteins localize into intramembrane strands of the TJ and direct the BBB to decrease paracellular permeability. The extent of solute impedance is directly proportional to the number of localized proteins (Mitte et al., 2000; Furuse et al., 2003). Leukocyte transmigration at the BBB is regulated by JAM (Martin-Padura et al., 1998). Thus, the three integral proteins as well as transmembrane proteins are responsible for controlling the passage of molecules into the CNS.

Drug compounds can be afforded entry into the CNS via various transport mechanisms at the BBB depending on their physical and chemical properties (Figure 1.1). The BBB is also equipped with efflux protein which expels drugs with poor affinity for these proteins. Therefore,

several considerations need to be made when designing drug delivery systems intended for the treatment of brain tumors (Table 1.1).

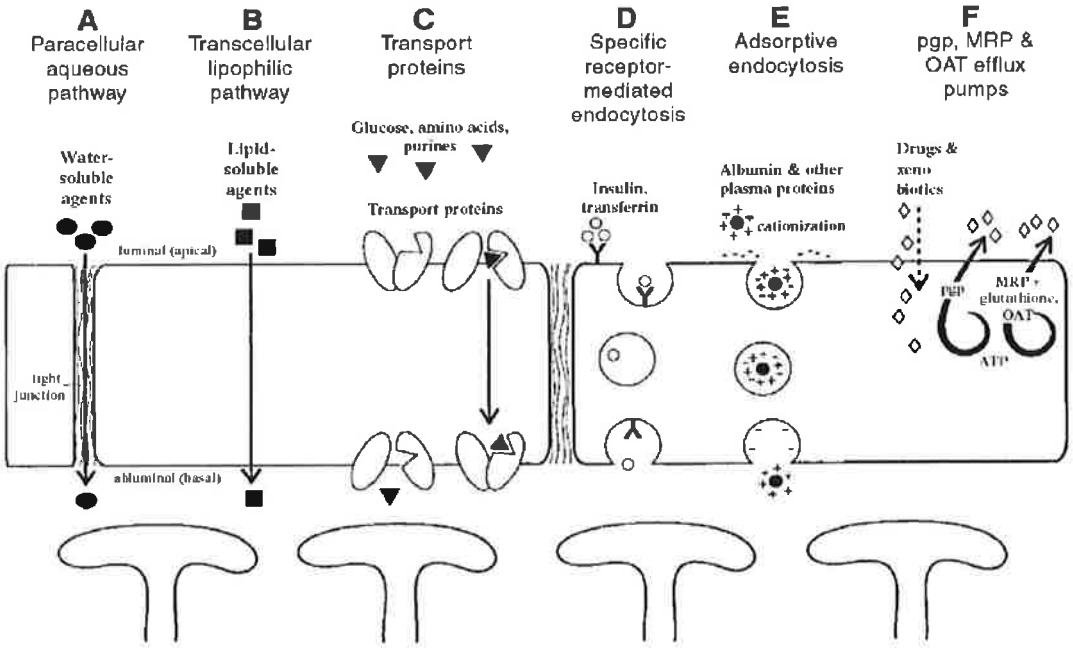

Figure 1.1. Transportation mechanisms at the blood brain-barier (Source: Neuwelt et al., 2004)

Table 1.1. Considerations for drug transport into the brain

Factors at the BBB	Peripheral factors
Concentration gradients of drug/ polymer	Systemic enzymatic stability
Molecular weight (of drug)	Affinity for plasma proteins
Flexibility, conformation of drug/polymer	Cerebral blood flow
Molecular charge (of drug/polymer)	Clearance rate of drug polymer
Affinity for receptors or carriers	Effects of existing pathological conditions
Affinity for efflux proteins	
Existing pathological conditions	

1.4 Strategies for Enhancing the Delivery of Therapeutically Active Compounds into the Brain Parenchyma

Several therapeutic approaches aimed at by-passing the BBB and subsequently improving drug concentrations in the tumor microenvironment have been investigated in the past. These include chemical modification of drugs, osmotic disruption of the BBB by intracarotid administration of vasoactive molecules such as bradykinin or hypotonic solutions of mannitol, convection enhanced drug delivery and interstitial administration of therapeutic agents by polymeric materials placed directly into the brain tissue. In chemical modification, drugs are complexed to agents that render drug molecules more lipophilic or by coupling drugs to molecules that have a specific transport mechanism (Bodor and Simpkins, 1983). Chemical modification processes alters the chemical properties and enables drugs to cross the BBB. Poor therapeutic outcome and treatment failure have been strongly linked to disease progression at the primary site of the tumor (Pollack and Keating, 2005). Interstitial chemotherapy and convection-enhanced drug delivery have been considered the most effective strategies for addressing this treatment shortfall. These treatment strategies have become the focus of research and are considered novel and feasible for enhancing local delivery of drugs to the CNS tumor microenvironment (Pollack and Keating, 2005). Delivery of chemotherapeutic drugs to the tumor site with polymeric carrier systems requires careful considerations concerning practical

problems related to the design of the drug delivery device that may be encountered. The design challenges fall within four different areas: (a) loading capacity, (b) controlled and sustained release of active agent, (c) drug instability and degradation and (d) drug penetrability and device biocompatibility (Popovic and Brundin, 2006).

Carmustine-impregnated polymeric drug delivery device has been the most widely applied in interstitial delivery for adult patients with brain tumors. Gliadel® is a wafer composed of a copolymer matrix with carmustine, which can be directly implanted into the tumor resection cavity at the time of surgery. The copolymer matrix contains bis (*p*-carboxyphenoxy) propane and sebacic acid in 20:80 molar ratios. Each 200mg wafer contains 7.7mg of carmustine. Effectiveness of Gliadel is based on the release of carmustine as the wafer matrix in hydrolyzed in the aqueous environment of the tumor resection cavity (Sipos et al., 1997; Wang et al., 1999). Studies in *in vitro* model systems have demonstrated that approximately 75% of the carmustine is released within 60 hours of wafer implantation and nearly 100% is released by 120 hours post-operatively (Dang et al., 1996). *In vivo* studies have shown clinically significant drug levels for several weeks up to 2 cm from the polymer matrix (Fung et al., 1996). Interstitial delivery of carmustine with polymer material resulted in sustained high local concentrations of the drug in and around the resection cavity. Thus, it was demonstrated that interstitial delivery has a great potential of achieving high intratumoral concentrations of the active agent without corresponding systemic toxicities. Clinical studies showed that adults who underwent surgery for recurrent malignant glioma had a longer median survival after treatment with Gliadel wafer 3.85%, compared with patient who received polymer wafers without carmustine (Brem et al., 1995; Valtonen et al., 1997). The US Food and Drug Administration (FDA) approved Gliadel® in 1996 (Guerin et al., 2004). In addition to Gliadel®, other controlled-release delivery strategies have been explored in preclinical models and/preliminary clinical trials. These include the delivery of other active chemotherapeutic compounds, such as taxol, using polymer-based delivery (Fung

et al., 1998). Poly (DL-lactide) microspheres have been employed to deliver 5-fluorouracil (5-FU) to tumor infiltrated brain around a resection cavity (Menei et al., 1996).

Interstitial delivery with polymer-based drug delivery systems exposes cancer cells to sufficiently high concentrations of drug for long enough duration. A major advantage of polymer-based systems is that, they ensure long-time exposure at modest concentrations and the drug concentration is optimised between its effectiveness and tolerability throughout the treatment period (Feng and Chien, 2003). In contrast, intravenous administration of high doses of cancer drugs lead to unavoidable fluctuations in blood concentrations. Convection-enhanced delivery involves administration of chemotherapeutic drugs directly into the brain tissue (intracranially) by using a motor driven syringe or some other suitable pumping mechanism to drive a flow of a suitable agent through a cannula or catheter, the tip of which is stereotactically guided to the target site within the brain. The development of self-regulated polymer based systems designed for localized, modulated and sustained delivery of chemotherapeutic compounds offers several advantages over other therapies. Polymeric materials can be processed into matrices that represent a diffusion-controlled system where control over drug release is accompanied by polymer degradation and drug release rate is proportional to polymer erosion rate. Local delivery of chemotherapeutic compounds with degradable polymers eliminates the possibility of accidental release, improves device safety and release rates can be modulated by changing the device parameters such as thickness, total drug content, copolymer ratio and type of polymers used (Duce et al., 2006).

1.5 Physiological Response Following Implantation of a Biomaterial into the Brain Parenchyma

Drug incorporation into an implantable polymeric carrier for controlled release was first inventedby Folkman and Long in 1964 who implanted digoxine-releasing silicone rubber devices into myocardium of dogs (Benoit et al., 2000). Since then, many polymeric materials have been implanted in different organs for various applications including drug delivery. Following implantation of a polymeric drug carrier in the brain tissue, a cascade of inflammatory response is initiated consisting of a complex series of reactions aimed at halting the ongoing tissue damage, isolate and destroy the foreign body material and activate the major processes. The foreign body reaction proceeds by two stages, the first stage is the acute phase response (APR) which is directed at destroying the implanted system or may proceed as chronic inflammation phase and/or granulation tissue development. The second stage is the chronic phase response (CPR) characterised by the proliferation of fibroblasts and macrophages.

A polymer-blood interface is inevitably created once the polymeric drug carrier system is successfully implanted at the target site resulting in non-specific spontaneous changes in serum levels of plasma proteins such as amyloid A, C-reactive protein and alpha-1-antitrypsin. A turbulent flow of increased blood supply by the dilated vessels directed at the injured tissue gradually comes to a halt when the blood starts to clot due to increased viscosity resulting from the loss of water to the surrounding tissue. Blood proteins and tissue fluid proteins (immunoglobulins, complement components, antithrombin III, transferrin, fibronectin, laminin, albumin, growth factors, and ect.) cover the drug carrier system strategically implanted at or in the proximity of the diseased site in the CNS in a matter of few hours. In parallel, leucocytes, monocytes, neutrophils and lymphocytes are recruited by the triggered cascade to perform their specific functions.

The initiation of the chronic phase response is characterised by the proliferation of macrophages and fibroblasts which direct their energy and expertise in engulfing the foreign material. A change in morphological structure of the macrophages is and indication that the effort is worthless and hence a more advanced strategy is require in order to successfully complete the assigned task. Macrophages fuse to form multinucleated foreign body giant cells (FBGC) which are supposed to be more efficient. FBGC accumulate, spread onto the implant and send out signals indicating a large foreign body to be walled off. The implant is ultimately encapsulated in a fibrous capsule composed of collagen and proteoglycans synthesized by the fibroblasts. The formation of a fibrous capsule around an implant is considered as a normal response and is not a confirmation of non-biocompatibility state. In fact, the brain tissue response is similar to nearly all the materials considered biocompatible in their application by walling them off in a fibrous capsule. Toxicity occurs when the macrophages fail to digest what they have engulfed, die and release enzymes in the surrounding tissue leading to tissue damage which is followed by cell death and ultimately lead to the formation of necrotic tissue.

The fibrous capsule forms an additional barrier for the encapsulated drug to diffuse in the surrounding tissue and may to some extent affect the pharmacokinetics of the drug-delivery system. The thickness of the fibrous capsule formed around the drug-delivery device is a major factor that determines drug release retardation. Other criteria required for a successful long-term implantation include the size and shape of the device which must be adapted to the anatomy of the implantation site.

1.6 Rationale and Motivation for the Study

It has been postulated that efficient treatment of PCNSL with MTX can result in complete tumor remission. However, the BBB restricts the adequate entry of intravenously administered MTX into the tumor microenvironment. As a result, high doses of MTX are required in order to reach effective therapeutic concentrations at the target site. High-dose intravenous schedules of MTX have been shown to be non-specific and require short dosing frequencies and this leads to severe side effect profile and poor treatment outcomes. Drug interactions in immunocompromised patients on antiretroviral treatment are prone to occur with high frequency and this often complicates treatment. In addition, poor treatment outcomes may be prompted by tumor recurrence at the initial site or distant site and drug resistance. Tumor recurrence has been associated with failure to achieve sufficient drug concentrations at sites furthest from the tumor due to rapidly declining drug concentrations. Thus, despite the good response of PCNSL to high-dose MTX treatment, patient survival period is still poor.

Local delivery of chemotherapeutic agents to the tumor site via drug- loaded polymer systems has been shown to possess major advantages over conventional routes of drug administration and other drug delivery strategies that have been developed to improve entry of drug compounds into the CNS. Interstitial delivery with polymer engineered drug delivery systems localizes therapy to the tumor site, provides a continuous sustained release of chemotherapeutic drugs and minimizes systemic exposure. Biodegradable polymers are used for such applications since they are able to degrade *in vivo*, therefore there is no need for a second surgery to remove the implanted device.

In this view, this study was aimed at designing and developing an implantable biodegradable and biocompatible drug delivery system comprising of a polymeric membrane embedded with

polymeric nanosystemsfor the management of PCNSL. The conceptualised model of the drug delivery system is one that is capable of attaining higher drug loading capacity and release the drug in a controlled and prolonged manner. This high MTX loading capacity would ensure maintenance of adequate drug concentrations at the tumor site and biodistribution to site furthest from the tumor. I addition, the treatment duration would be prolonged in order to eradicate tumor cells completely. Thus, the potential for tumor recurrence at the initial site and also at distant sites would be minimised if not completely addressed. Localized delivery of MTX promises greater specificity and favourable side effect profile due to minimal systemic exposure. A suitable device will improve patient compliance, reduce hospitalization time, reduce the cost of treatment and improve the patient quality of life.

1.7 Aims and Objectives of this Study

The aim of this study was to design, develop and characterize different types of drug-loaded polymeric based membranes for modulated and prolonged release of MTX.

In order to achieve this, the following objectives were outlined:

I. Preparation of drug-free and drug-loaded polymeric membranes.

Phase sparation process will be employed to prepare drug-free and drug-loaded membranes. The physicochemical properties of the drug-free and drug loaded polymer membranes will be studied in order elucidate information on influence of various formulation variables on the behavior of these systems. Furtheremore, the mechanism of drug association with the membrane will be studied.

II. Preparation of drug-loaded nanoparticles.

Polymer based nanocarriers will be prepared by double emulsion solvent evaporation technique. The nanocarriers will be analysed for size distribution, drug-loading capacity and yield. The shape of the nanocarriers will be evaluated by transmission electron microscopy.

III. Fixation of nanoparticles within the polymeric membranes.

The concept of combining the two systems (polymer membrans and the nanocarriers) will be explored. The nanocarriers will be prepared and incooporated into the polymer membranes. The postulated advantage of improved drug-loading will be discussed and the physicochemical properties of the system will be evaluated.

IV. Morphological observation of all membranes and nanoparticles formed.

Scanning electron microscopy will be used to analyse the surface of the polymer membranes. The shape of the nanocarriers will be analysed by transmission electron microsopy.

V. Characterization of the physicochemical and physicomechanical properties of membranes and of nanoparticles.

VI. Performance of matrix erosion and *in vitro* drug release studies.

The mechanism of degradation of the polymer membranes will be determined and the drug release mechanism will be studied.

VII. Performance of *in vivo* animal biodistribution studies.

The combined drug delivery system consisting of nanocarrires incooporated in a polymer membrane will be implanted in the brain parenchyma of male sprague rats. Histological evaluation will be performed on brain tissue samples harvested at a 7 day interval. In-vivo bioditribution of the drug released from the implanted device will be studied by high performance liquid chromatography.

1.8 Overview of the Dissertation

This dissertation consists of seven chapters, and each chapter can be regarded as a step towards the realization of an ultimate drug delivery system for the management of PCNSL.

Chapter One is an introductory chapter and focuses on the evolution of conventional therapeutic modalities to sophisticated drug delivery systems. It highlights the superior therapeutic advantages offered by polymer based drug delivery systems in addressing treatment challenges posed by disease conditions. Primary central nervous system lymphoma is presented as a model tumor (PCNSL) that lacks adequate therapeutic treatment with conventional (systemic) routes of drug administration. The Blood-Brain Barrier (BBB) restricts entry of drug molecules into the brain parenchyma and prevents optimal treatment. The physiology and molecular structure of the BBB is discussed in order to understand its underlying barrier and drug transport mechanisms. The inflammatory response of the brain tissue to implanted biomaterials is also discussed. A guideline pertaining to the factors that need to be considered with respect to interstitial delivery are highlighted. Various treatment modalities that have been used to improve entry of drug compounds into the brain are discussed. This chapter puts into perspective the pre-meditated purpose and rationale of this study and outlines the planned objectives towards the attainment of an optimal drug delivery system for the management of PCNSL.

Chapter Two is a review on the design and development of polymer based scaffolds and membranes for drug delivery applications. Various techniques for preparing polymer scaffolds and membranes such as phase separation, melt molding, electrospinning and supercritical fluid technology are discussed. The advantages and limitations of employing some of the techniques are highlighted. Scaffold modification strategies which have been explored by different researchers in the field in an attempt to improve the mechanical properties and performance are briefly discussed. This chapter also focuses on different polymer scaffolds formulations which have been successfully used for protein and drug delivery application.

Chapter Three describes the application of a computational simulation technique supported by experimental results in gaining a deeper insight into the molecular structure, physicomechanical and physicochemical properties of a composite poly (D, L-lactide) (PLA) and poly (vinyl alcohol) (PVA) methotrexate (MTX)-loaded biopolymeric membranes. Computational and structural molecular modeling was employed to rationalise the potential mechanisms of membrane formation and the release of MTX from the fabricated biopolymeric membranes. It was shown that this tool can be successfully employed in preliminary formulation studies for understanding the molecular basis of membranes formation and predict their performance. The computational modeling approach holds the economic benefits of reducing the time spent in the lab during the development of biomaterials for medical applications.

Chapter Four is based on the preparation, characterization and optimisation of MTX-loaded PLLA/PVA biopolymeric membranes. A Box-Behnken statistical experimental design was employed to generate a total of fifteen various formulations. These formulations were tested for swelling behaviour, degradation kinetics, mechanical properties and *in vitro* drug release behaviour. The influence of selected formulation variables on the response parameters were

studied in detail. Optimization technique was employed in order to obtain a biopolymeric membrane formulation with desired properties. In addition, the surface morphology of the membranes was studied by scanning electron microscopy.

Chapter Five elaborates on the fabrication, characterization and optimization of MTX-loaded PLA/MAA nanoparticles. Polymer-based nanoparticles have demonstrated their applicability as powerful drug delivery systems which possess great advantages such as the ability to penetrate cellular structures and increasing the half life of drug compounds. A Box-Behnken design was employed for generating various nanoparticle formulations. The influence of selected formulation variables on the response parameters was studied. The data obtained was used to prepare an optimized formulation with desired properties. The formulations were tested for size distribution, yield and drug entrapment efficiency. The surface morphology and the structure of the nanoparticles were studied by scanning electron microscopy and transmission electron microscopy. All the formulations demonstrated low drug entrapment efficiencies which prompted an investigation into a strategy that would overcome this formulation shortfall.

Chapter Six is on the development and characterization of a combined drug delivery devise based on PLA/PVA biopolymeric membrane embedded with PLA/MAA nanoparticles. This system was tested for swelling behaviour, degradation kinetics, mechanical properties and *in vitro* drug release. The surface morphology was studied by scanning electron microscopy. The possible mechanisms underlying the hydration and polymer relaxation kinetics of the composite system which were thought to have been responsible for modulating the release of MTX from the device are discussed. The device was capable of releasing MTX in a modulated and sustained manner and demonstrated to be suitable for long term delivery of methotrexate. The device was able to release MTX for the required time period in the brain parenchyma of rat models. Histological studies conducted on brain tissue samples recovered 30 days post-

implantation demonstrated that he device was biocompatible with the brain tissue since it only elicited mild to moderate inflammation with no signs of toxicity. The plasma concentration-time profile, CSF concentration-time profiles and brain tissue concentration-time profile of MTX after bolus intravenous administration of MTX and surgical implantation of the device were constructed and studied.

Chapter Seven is a concluding chapter and summarises the results obtained in this study. Recommendations for future research in this area are made with the aim of addressing any potential formulation shortfalls that may have been encountered.

CHAPTER TWO

DESIGN AND DEVELOPMENT OF POLYMERIC MEMBRANES AND SCAFFOLDS FOR CONTROLLED DELIVERY OF BIOACTIVE MOLECULES AND DRUG COMPOUNDS

2.1 Introduction

Polymer scaffolds have found wide application in various medical domains such as biomaterial science (novel smart biomaterials able to provide both physical and chemical cues), biology (cell proliferation and differentiation, biomolecules acting as molecular signals), engineering design aspects (2D cell expansion, 3D tissue growth, bioreactors, vuscularization, cell and tissue storage and shipping-biological packaging), biomedical chemical aspects of design (properties of native tissues, identification of minimum properties required of engineered tissues, mechanical signals regulating engineered tissues, and efficacy and safety of engineered tissues), informatics (gene and protein sequencing, gene expression analysis, protein expression and interaction analysis, quantitative cellular analysis and tissue analysis, *in silico* tissue and cell modelling, digital tissue manufacturing, automated quality assurance systems, data mining tools and clinical informatics and interfaces) (Fabiana, 2004).

In tissue engineering, polymer scaffolds are required to possess good mechanical and structural support, the scaffold should have a well defined microstructure with an interconnected network, mechanical properties similar to those of natural tissues, be biocompatible and bio-resorbable at a controllable degradation and resorption rate as well as provide the control over the sequestration and delivery of specific bioactive factors to enhance and guide the regeneration process (Niklason and Langer, 2001; Goldberg et al., 2007). Scaffolds are prepared by using synthetic or natural polymers and they are tailored according to the body site because the platform must bear mechanical stresses after implantation. Polymers used for fabrication

ofscaffolds can either be synthetic or naturally occurring and examples are listed in Table 2.1. Synthetic polymers have been regarded as essential materials for preparing scaffolds due to their biocompatibility and biodegradability. In addition, they have predictable and reproducible mechanical and physical properties (tensile strength, elastic modulus and degradation rate), excellent processing characteristics and they can be manufactured with great precision (Chen et al., 2008).

Table 2.1. Biopolymers used for preparing scaffolds

Biomaterial	Abbreviation
1. Synthetic polymers	
Bulk biodegradable polymers	
Aliphatic polyesters	
Poly(lactic acid)	PLA
Poly (D-lactic acid)	PDLA
Poly(L-lactic acid)	PLLA
Poly(D,L-lactic acid)	PDLLA
Poly(glycolic acid)	PGA
Poly(lactic-co-glycolic acid)	PLGA
Poly(ε-caprolactone)	PCL
Poly(hydroxyalkanoate)	PHA
Poly(3 or 4-hydroxybutarate)	PHB
Poly(3-hydroxyoctoate)	PHO
Poly(3-hydroxyvalerate)	PHV
Poy(*p*-dioxanone)	PPD or PDS
Poly(propylene fumarate)	PPF
Poly(1,3-trimethylene carbonate)	PTMC
Poly(glycerol-sebacate)	PGS
Poly(ester urethane)	PEU
Surface bioerodable polymers	POE
Poly(ortho ester)	PA
Poly(anhydride)	PPHOS
Poly(phosphazene)	PA
Polyurethane	PU
Nondegradable polymers	
Poly(tetrafluoroethylene)	PTFE
Poly(ethylene terephthalate)	PET
Poly(propylene)	PP
Poly(methyl methacrylate)	PMMA
Poly(N-isopropyl acrylamide)	PNIPAAm
2. Natural degradable polymers	
Polysacchaides	
Hyluronan	HyA
Alginate	
Chitosan	
Starch	
Proteins	
Collagen	
Gelatin	
Fibrin	

(Source: Cheng et al., 2008)

2.2 Design and Preparation of Polymeric Scaffolds

2.2.1 Solid phase separation

There are various phase separation techniques that can be used to fabricate polymer scaffolds and these are, thermally induced phase separation (TIPS), air casting of polymer solution and immersion precipitation (IP). The differences in the techniques emanates from the differences in desolvation mechanisms. Phase diagrams are constructed in order to predict whether or not a solution of a certain polymer in a certain solvent is suitable for scaffold formation. In particular, binary phase diagrams are used to predict transitions that occur during TIPS(Fig. 2.1) (van denWitte et al., 1996).Researches have also employed NMR spectroscopy to investigate phase transitions in aqueous solutions of thermoresponsive polymers (Spěváček et al., 2009). Only TIPS will be considered in our discussion since it is a phase separation technique that is commonly used for fabrication of polymer scaffolds.

TIPS operates on the principle of freeze drying binary polymer solutions. The technique is based on either liquid-liquid TIPS or solid-liquid TIPS. Liquid-liquid demixing processes play an important role in most TIPS process, however a combination of transitions may take place in a system.The morphology of the scaffolds fabricated by TIPS is thought to be dependant on the thermodynamic state of the solution to be quenched. A nucleation and growth mechanism in TIPS results in poorly connected structure while spinodal phase separation produces highly interconnected structure. The pore size of the scaffold is influenced by the concentration fluctuations in response to quenching, polymer concentration and flactuations associated with thermal flow. Therefore, scaffolds of desired morphology can be tailored by varying processing parameters such quenching rate, quench temperature and quench period or by varying formulation parameters such as polymer concentration, solvent composition, crystalline and molecular (Hua et al., 2003).

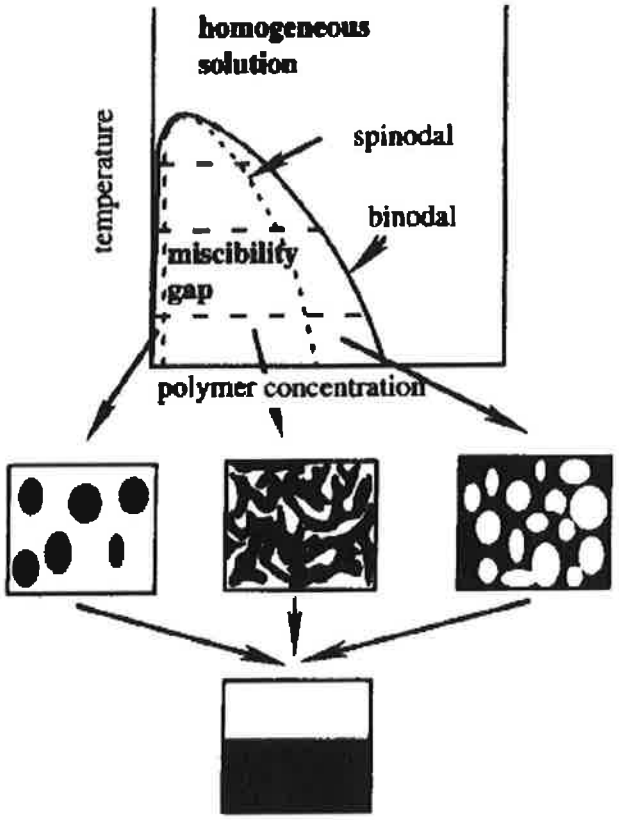

Figure 2.1 A schematic of a binary phase diagram of a polymer solution showing liquid-liquid demixing gap and possible structure formation in different part of the liquid-liquid demixing gap: nucleation and growth of polymer rich phase (left picture), bicontinuos morphology due to spinodal decomposition (middle picture), nucleation and growth of polymer poor phase (right picture). (Source: van de Witte et al., 1996).

2.2.2 Electrospinning technology

Electrospinning has found wide application in the preparation of fibrous scaffold with nanoscale dimensions due its relative simplicity. This scaffold fabrication technique utilizes electrostatic forces to spin polymer solutions or melts into whipped jets producing continuous fibers with diameters from nanometers to micrometer after solvent evaporation in the spinning process (Pham et al., 2006). Blend electrospinning involves emulsification of aqueous protein solution by ultra-sonication followed by mixing with polymer solution for electrospinning. In coaxial electrospinning, the polymer solution and the biological solution are coaxially and

simultaneously electrospun through different feeding capillary channels into one nozzle to generate composite nanofibers. In order to improve the fiber forming properties of low viscosity biological solutions, hydrophilic polymers such as poly(ethylene glycol), poly(ethylene oxide and dextran are usually blended with the biological solution. The addition of hydrophilic polymers has shown to have protein release modulating effects (Jiang et al., 2006 and Li et al.,2008).

Polycaprolactone-based nanofibrous scaffolds with incorporated protein via either the blend or coaxial electrospinning technique were fabricated. Both techniques were compared with respect to processing set-up and scaffold characteristics as well as release kinetics and biological activity of the loaded protein. Coaxial electrospinning resulted in uniform fiber morphology with core-shell structure, and a homogenous protein distribution throughout the core of fibers. In contrast, blend electrospinning formed bead-like fibers with a heterogenous protein distribution in the fibers. The coaxial scaffold exhibited more sustained release profiles than the comparative blend scaffold (Wei et al., 2010).

Electrospinning has been shown to be suitable for preparing polymeric membranes for biomedical applications such as tissue engineering, drug delivery and wound healing (Huang et al., 2000; Zong et al., 2000; Boland et al., 2001;Kenaeway et al., 2002; Li et al., 2002; Yoshimotoa et al., 2002). Electrospun scaffolds have been regarded as effective delivery systems due to stereological porous structure and high specific surface area (Jiang et al., 2006; Li et al., 2006). The close resemblance of the electrospun structures to the three-dimensional (3D) fibrous network found in the extracellular matrix (ECM) facilitates integration into biological tissues (Matthews et al., 2002;Li et al.,2006;Lee et al., 2008; Sill and Recum, 2008).Electrospum membranes (generally composed of nano-sized fibers) have high porosity, very compliant and can conform to motions (Reneker and Chun, 1996). In addition, they also have a high surface to volume ratio that facilitates cell attachment and drug sorption (Sisson et

al., 2009).Electrospun membranes have been prepared from hydrophilic and hydrophobic polymers such as poly(lactide-co-glycolide) (PLGA) (Boland et al., 2001; Yoshimotoa et al., 2002), poly(ε-caprolactone (PCL) and cellulose acetate (Liu, 2002).

2.2.3 Foaming using supercritical carbon dioxide (CO_2)/ Supercritical fluid technology

Supercritical fluid (SCF) gas foaming has an advantage over other techniques used for scaffold fabrication in that it does not require large volumes of potentially harmful organic solvents and can operate at relatively low temperatures (Hutmacher, 2000; Coombes et al., 2004). This technology takes advantage of the peculiar features dense gases such as high compressibility and diffusivity, very high evaporation rate and the possibility of fine tuning the solvent power through density modulation (temperature and/or pressure variation)(Pasquali and Bettini,2008). Supercritical fluid processing has been applied to the production of polymer scaffolds and composites, encapsulation and release of growth factors and cells for tissue engineering, extraction of residual solvents and other deleterious compounds from prefabricated scaffolds and sterilisation of implantable materials (Davies et al., 2008).

The SCF processes can be classified into four groups, (i) operation where SCF acts as a solvent, (ii) operations where SCF acts as a antisolvent, (iii) particles from a gas-saturated solutions and (iv) CO_2-assisted spray drying. Polymer scaffold formed by supercritical fluid technology are also known as polymer foams and are formed when a polymer is plasticised by saturation in supercritical fluid and rapidly depressurised at a constant temperature. As pressure is released, pockets of gas nucleate and grow in the polymer. As the supercritical fluid leaves the polymer, the *Tg* increases. At the point where the *Tg*for the polymer is higher than the than the foaming temperature, the porous structure is set (Goel and Beckman, 1993; Mooney et al., 1996). Reseachers have demonstrated that the degree of porosity and interconnectivity of the scaffolds could be tuned by modifying formulation variables such as blend composition and

process parameters such as processing temperature (Barry et al., 2004). Supercritical fluid technology has demonstrated significant advantages in addressing limitations that occur during the formation of polymer membranes by solvent induced phase separation (SIPS). Supercritical fluid replaces the liquid non-solvent used in SIPS which commonly require removal by expensive post-treatments.The residual solvents are known tocause problems in biomedical applications due to their toxicity. Compared to SIPS, supercritical CO_2 induced phase separation (SC-IPS) process can have several advantages, (i) SC-CO_2 can form and dry the polymer membrane rapidly, without the collapse of structure due to the absence of liquid-vapour interphase when the supercritical solvent-nonsolvent mixture is formed, (ii) the membrane can be obtained without additional post treatments because the polymer solvents is completely extracted and (iii) SC-CO_2allows one to generate symmetric membranes and to modulate the membrane morphology, cells and pore sizes by changing process parameters such as pressure, temperature and depressurization rate. Formulation variables such as polymer concentration and addition of another polymer in solution can equally be used to vary the properties of the membranes (Lee et al., 2004; Reverchon et al., 2008; Temtem et al., 2009). The role of the interactions in systems containing polymers for the definition of operative conditions in the supercritical processing has been reviewed elsewhere (Kikic, 2009).

2.2.4 Melt molding particulate leaching technology/ Injection molding/Micromolding

Micromolding involves the formation of micropatterns obtained by evaporation inducedself-assembly of diblock copolymer miscells and using the obtained microstructures as templates or moulds for micromolding scaffolds (Figure 2.2). The formation of templates for microfabrication of polymeric scaffolds is based on the cracking phenomenon which has been investigated by mathematical and experimental studies (Groisman et al., 1994; Allain et al., 1995;Shorlin et al., 2000; Jagla et al., 2002; Pauchard et al., 2003).

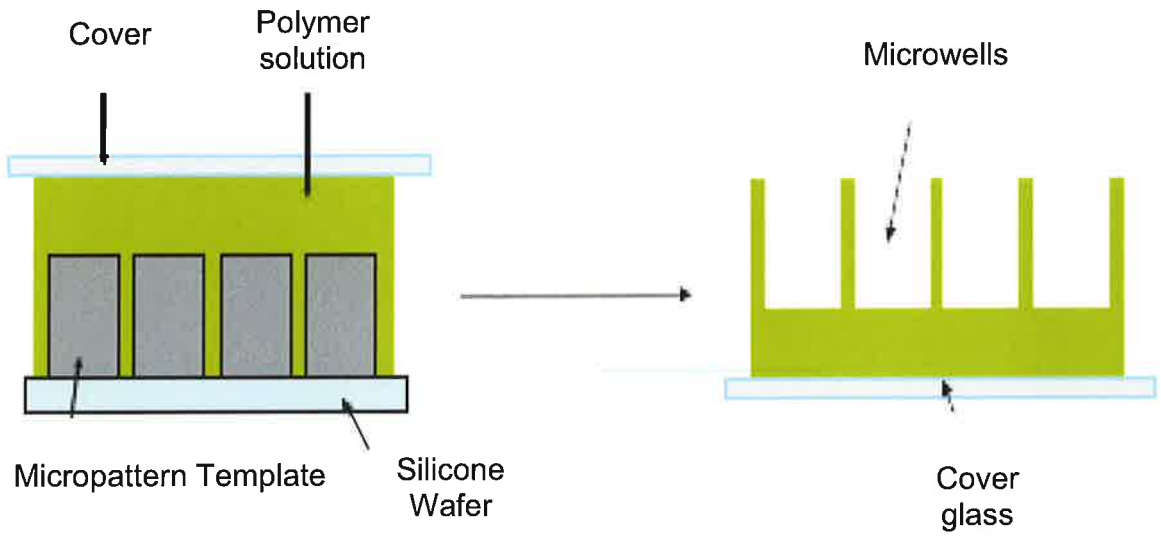

Figure 2.2 A schematic diagram showing a micromolding technique. (Adapted: Mi et al., 2006)

Injection molding is one of the most widely used methods for manufacturing polymeric products. Three main steps are involved in injection molding: filling, packing/holding and cooling. During the filling stage, ahot polymer melt rapidly fills a cold mold reproducing a cavity of desired product shape. During the packing or holding stage, the pressure is raised and extra material is forced into the mold to compensate for the effect that both temperature decrease and crystallinity development determine on density during solidification (Pantani et al., 2005). Ghosh and co-workers proposed a novel fabrication technique based on conventional injection molding

for preparation of unidirectionally oriented, porous scaffolds by selective polymer leaching. In their paper, injection molding was described asa versatile, efficient and highly reproducible process capable of fast production of complex geometric shapes with tight dimensional tolerances. Different layered structures were obtained by varying the injection molding processing conditions of a 50/50 w/w% PLLA/PEO blend. The effect of melt processing temperature and injection flow rate on the morphology of the porous structures was also investigated by scanning electron microscopy (Ghosh et al., 2008). Gomes and co-workers conducted a preliminary study on the development of a new method to produce biodegradable scaffolds from blends of corn starch with ethylene vinyl alcohol and corn starch with cellulose acetate. The developed methodology consisted of a conventional injection molding process, on which a solid blowing agent based on carboxylic acid is used to generate the foaming of the bulk of the moulded part (Gomes et al., 2001).

2.2.5 Selective laser sintering (SLS)

Selective laser sintering (SLS) is a heat intensive manufacturing process and involves thermally induced densification of powder particles by sintering and/or melting. For any given material, the choice of the SLS processing parameters will determine whether or not the material can be formed into structurally strong and dimensionally accurate shapes corresponding to the digital design for that shape. SLS processing parameters (laser power, scan speed, can spacing, part bed temperature and powder layer delay time) must be optimised in order to avoid thermal growth and bonding of surrounding powder to a parts boundaries, dimensional inaccuracies, manufacturing induced porosity in the designed solid regions of a part due to incomplete densification of the powder particles (Eshraghi and Das, 2010).

2.2.6 Solid free form fabrication (SFF)

The solid free-form fabrication (SFF), also known as rapid prototyping (RP) technology enables the use of three dimensional computed tomography (3D CT) data to design anatomically shaped scaffolds with varying internal architectures thereby allowing precise control over pore size, porosity, permeability and stiffness(Humacher 2000;Landers et. al., 2002; Sachlos and Czersnuka 2003).There are several RP techniques that have been employed for the fabrication of polymer scaffolds and these include three dimensional printing (3DP), fused deposition modelling (FDM), multi phase jet solidification (MPJS) and shape deposition manufacturing (SDM). 3DP has been reported as the most common technique used for scaffold preparation using poly(lactic acid) and poly(lactic-co-glycolic acid) and the method is based on using organic solvents as a binder for powder based aliphatic polyesters (Giordano et. al., 1996; Kim et. al., 1998; Park et. al., 1998).

FDM forms three-dimensional objects from computer generated solid or surface models. Models can also be derived from computer tomography scans or model data created from 3D object digitizing systems. FDM uses a small temperature-controlled extruder to force out a thermoplastic filament material and deposit a semi-molten polymer onto a platform in a layer by layer process. The mono filament is moved by two rollers and acts as a piston to drive the semi-molten extrude. At the end of each finished layer, the base platform is lowered and the next layer is deposited (Figure 2.3).

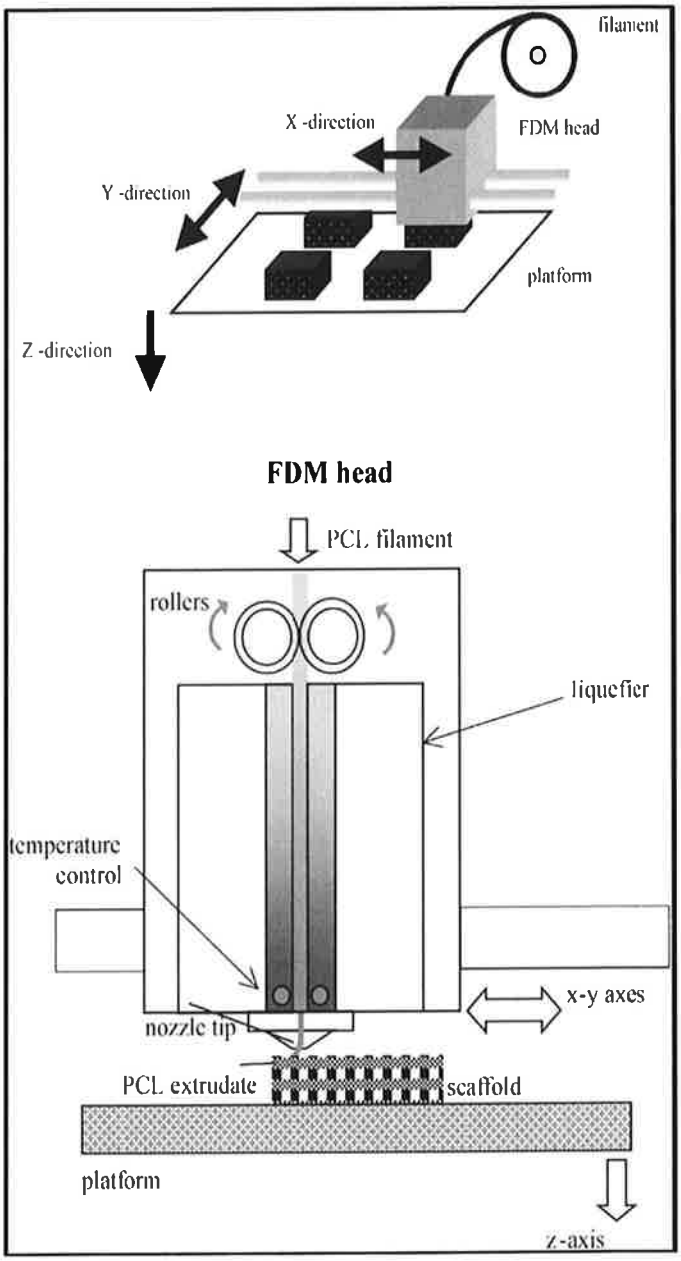

Figure 2.3 A schematic diagram of PCL FDM extrusion and deposition process (Source: Zein et al., 2002).

The designed scaffold is fabricated as a three-dimensional part based solely on the precise deposition of thin layers of extrude. The deposition path and parameters for every layer are designated depending on the material used, the fabrication conditions, the application of the designed scaffold and the preferences of the designer. The processing parameters of filling

each layer depend on the earlier inputs into the slicing software. These include FDM head speed, roller speed, slice interval and the direction of deposition within each layer. Each layer is made of "roads" deposited in x- and y-direction, in a raster, a contour or a combination of both. The direction of deposition is known as the "raster angle" for raster filling and this can be specified for each layer between 0° and 180° with respect to x-axis. The road width is controlled by both the flow parameters at a set temperature above the melting temperature of the thermoplastic material and also by the size of the nozzle tip (Zein et al., 2002).

2.2.7 Computer aided design (CAD) and computer aided manufacturing (CAM) of polymer scaffolds

Computer-aided-design (CAD) and computer aided manufacturing (CAM) allows the conceptualization and predetermination of scaffold morphological characteristics and mechanical properties. This technology has also been used for defining scaffolds that can be used as perfect-bone fitting substitutes (Ciocca et. al., 2009).

2.3 Processing Techniques for Control and Optimisation of Pore Size, Mechanical Properties and Morphology

2.3.1 Particulate seeding

Solid lipid templating has been used to control the porosity of scaffolds. This technique involves the use of solid lipid microparticles as porogens and non-halogenated polymer solvents to induce the precipitation of polymer scaffolds into scaffolds with interconnected pore structure. Hacker 2007, fabricated macroporous scaffolds with high inter-pore connectivity from different biodegradable polymers using solid lipid templating technique. It was demonstrated that pore size can be controlled by porogen particle size and adaptation of the viscosity of the polymer solution. Porosity could be modified by changing the ratio of porogen to polymer ratio (Hacker et

al., 2007). In another study, researchers improved the pore interconnectivity of PLA scaffolds produced by foaming using supercritical CO_2 by adding microparticulate silica to the polymer during processing. Scaffolds comprising of PLA and a range of silica contents (0-50wt/%) were produced and the scaffolds structure, pore size distribution and interconnectivity were assessed. It was found that incorporation of increasing quantities of silica microparticles increased the interconnectivity of the scaffold pore structure. The pore size distribution was also reduced through the addition of silica, while total porosity was found to be largely independed of silica content (Collins et al., 2010).

2.3.2 Thermal treatments

The biomechanical properties of electrospun nanofiber PCL scaffolds could be improved by performing thermal fiber bonding in Pluronic F127 solution at a range of temperatures from 54°C to 60°C. It was observed that the biochemical properties of the thermally bonded electrospun PCL scaffolds were significantly increased without any gross observable and ultrastructural changes when compared to the untreated PCL scaffolds (Lee et al., 2008).

2.3.3. Coating of polymer scaffolds

Wei-Wen and co-workers employed a chemical vapour deposition (CVD) polymerization technique to modify the surface of polycarprolactone (PCL) scaffold. Poly [(4-amino-xylylne)-co-(p-xylylene)] (PPX-NH_2) was deposited onto the surface of the scaffold to provide a reactive amine layer. The results showed that the performance of the scaffold was improved, cells continually proliferated on the surface of the modified scaffold with high survival rate (Wei-Wen et al., 2009). This technique can also be used to coat polymer scaffolds with polymer drug-solutions in order to attain a modulated drug release profiles.

2.3.4 Topological optimisation

Topological optimisation is a novel computer based technique for scaffold design. It is a form of shape optimisation, usually referred to as layout optimisation. The goal of topological optimisation is to find the best use of a material for body that is subjected to either single load or multiple load distribution. Researchers have proposed a topological optimisation scheme that could be employed to obtain the ideal topological architectures of scaffolds, maximising its mechanical behaviour (Almeida and Bártolo, 2010). In order to increase the interfacial connection of hydroxyapetite (HAP) to poly-L-lactic acid (PLLA),*y*-methacryloxypropyltrimethoxysilone (*y*-MPS) was used as a coupling agent to modify the surface of nano-HAP (NHAP) particles. Silane modified nano-HAP (MNHAP) and PLLA were fabricated to a nano-composite scaffold by a thermally induced phase separation method. Results showed that incorporating MNHAP into PLLA network buffered the pH reduction and reduced the weight loss in vitro degradation significantly (Wang et al., 2010).

2.3.5 Crosslinking of polymer scaffolds (photocrosslinking and chemical crosslinking)

Nuttelman and co-workers developed a degradable and photocrosslinkable poly(lactic acid)-g-PVA multifunctional macromers that could be reacted in solution to form degradable scaffolds. The mass loss profiles, bulk properties and the resulting properties of the scaffolds could be easily tailored by modifying the structure of the starting macromers including altering the number of lactide repeat unit per crosslinking side chain (Nuttelman et al., 2002). Jiang (2010), used citric acid as a non toxic crosslinker for cross-linking electrospun zein fibers. As a result, the water stability and the cytocompatibility of the zein fibers for medical applications were enhanced (Jiang et al., 2010).

2.4 Drug Delivery (protein, DNA and drug compounds) from Polymer Scaffolds

2.4.1 Matrix-mediated drug delivery

Incorporation of growth factors (GFs) in polymeric scaffolds used for tissue engineering applications prevents them from diffusing from the target site and being enzymatically deactivated or degraded. In addition, the bioactive molecules are localized to the target site and their release to non-target site is minimized (Chen and Mooney, 2003). The integration of controlled release strategies within polymer matrices has led to novel multifunctional platforms able to control and guide the tissue regeneration process (Saltzman and Olbricht, 2002;Kretlow et al., 2007;Lee and Shin,2007;Tessmar and Gopferich, 2007; Zhang and Suggs, 2007). The association between the polymer and the bioactive molecule can either be reversible (binding/de-binding kinetics) or irreversible. The release of the bioactive molecule from the scaffold is determined by factors such as the degradation rate of the scaffold, amount of bound bioactive molecule and the number of binding sites which ultimately determines the release profile (Salvay and Shea, 2006).

Jiang 2004, prepared and ibuprofen-loaded poly(lactide-co-glycolide)-g-chitosan electrospun membrane for application in post-operation atrial fibrillation (PoAF). The membrane was capable of sustained drug release and covered the atrium entirety. The device was suitable for this application since it possessed proper mechanical strength that could conform to constantly deforming atrium (Jiang et al., 2004). Antibiotics, tetracycline and mefoxin have been physically incorporated/dispersed into the electrospun PLGA membranes and their release behaviours were evaluated (Zong et al., 2000; Kenaway et al., 2002). Prabaharan and Jayakumar 2009,developed a porous biodegradable chitosan-graft-ß-cyclodextrin scaffolds which demonstrated controlled release of ketoprofen when used as a model drug. Drug loading into the scaffold was increased by increasing the chitosan-graft-ß-cyclodextrin or by decreasing

crosslinking densities. The highest drug loading (16.89wt%) was achieved at the scaffold was prepared from 3% chitosan-graft-ß-cyclodextrin initial concentration and 0.01M gluteraldehyde concentration. Ketoprofen release from the scaffold was slow and steady and equilibrium was reached after 23 hours.

Zhang and co-workers prepared a scaffold with an ionically crosslinked hydrogel coating layer containing vancomycin via novel drug loading method for sustained drug delivery. The poly(D,L-lactic acid)(PDLLA)/biphasic calcium phosphate (BCP) scaffold, fabricated by a particle-leaching/thermally induced phase separation method demonstrated a highly inter-connected porous structure and an average drug loading efficiency of 82.7±1.3%. Vancomycin was released in a slow sustained manner over a period of 18 days from the scaffolds and the release rate varied with varying concentration of the ionically crosslinked alginate coating solution (Zhang et al., 2008). Polymer scaffold have been used as reservoirs for sustained release of entrapped plasmid DNA (pDNA) molecules. Plamid DNA have been delivered to cells so as to facilitate *in situ* production of growth factors, signaling molecules and insoluble bioactive molecules of interest.

Tailored release of transforming growth factor-ß1 (TGF- ß1) from porous scaffolds was achieved by means of an emulsion coating method. Poly(ether-ester) multiblok copolymers were used to prepare emulsions containing TGF- ß1 which were subsequently applied onto prefabricated scaffolds. The scaffolds were effectively associated with TGF-ß1 and allowed to tailor precisely the release of the growth factor from 12 days to more than 50 days by varying the copolymer composition of the coating solution (Sohier et al., 2007). The release of vancomycin from ß-tricalcium phosphate (ß-TCP)/agarose scaffolds was tailored by including poly(ethylene glycol)(PEG) in the formulation and by varying the conditions of the drying procedures (freeze drying or desiccation). The modifications resulted in the generation of

different pore architectures and certain chemical interactions such as the formation of the argarose-PEG-vancomycin complex that yielded different drug release profiles (Cabañas et al., 2009). Dual drug release of an anaesthetic lidocaine and an antibiotic mupirocin was achieved from an electrospun scaffold. The two drugs were electrospun from a poly-L-lactic acid (PLLA) solution with a dual spinneret electrospinning apparatus into a single scaffold. The release of the drugs from the scaffold showed different profiles for the two drugs. Lidocaine hydrochloride exhibited an initial burst release (80% release within an hour)followed by a plateau after the first few hours. Mupirocin exhibited only 5% release in the first hour before experiencing a more sustained release for over 72 hours (Thakur et al., 2008). Saraf 2010,employed coaxial electrospinning as a means for the fabrication of PCL/PEG fiber mesh scaffolds and encapsulation and subsequent release of a non-viral gene delivery vector over a period of 60 days (Saraf et al., 2010).

2.4.2 Microsphere-mediated drug delivery

Wang and co-workers prepared a system consisting of growth factor (bone morphogenic protein 2 and insulin-like growth factor I) loaded microspheres incorporated in a scaffold and studied the delivery efficiency of the microsphere/scaffold system. The growth factors were encapsulated in either PLGA or silk microspheres and further incorporated in alginate and silk scaffolds to form concentration gradients. Depending on the nature of the carrier matrices and the microencapsulation process, the systems had distinguished growth factor release properties (Wang et. al., 2009). In another study, protein loaded PCL microspheres were successfully included within a scaffold and provided a sustained delivery of a model protein, bovine serum albumin (BSA) (Luciani et. al., 2008).

A novel system based on chitosan microspheres interspersed within a PLA scaffold (PLA/CMs) was prepared by thermally induced phase separation method. FT-IR analysis revealed that

there were strong hydrogen bond interactions between the PLA and the chitosan component. *In vitro* degradability investigation indicated that the dissolution of chitosan component was preferential than PLA matrix and the inclusion of CM could neutralize the acidity of the PLA degradation products. Compared with the rapid release from the CM, the BMP-2- derived synthetic peptide was released from the PLA/CMs scaffold in a temporally controlled manner, mainly depending on the degradation of the PLA matrix. (Niu etal., 2009).

2.5 Concluding Remarks

Polymer scaffolds have found wide applications in various medical domains. The techniques for preparing polymer scaffolds have improved over the years in order to avoid the use of organic solvents that may render the material toxic. Melt molding techniques and foaming by supercritical fluid do not require the use of organic solvents and thus have been favoured over phase separation techniques. The ability to control the morphological evolution and shape of the scaffold using computer technology coupled with melt molding techniques has allowed researchers to develop scaffolds according to pre-determined specific requirements.For example, CAD/CAM can be employed for the construction of implantable polymer based drug delivery scaffolds with anatomy specific architecture and suitable mechanical properties for sustained drug release in tumor resection cavities. Modifications of the scaffolds by crosslinking, coating with polymer solution, thermal treatment and particulate seeding can be made to improve the performance and properties. Specific drug and protein release requirements from polymer scaffolds and membranes can be obtained by preparing scaffolds capable controlled release or by incorporating drug-loaded nano or micro-structures into the scaffolds.

CHAPTER 3

COMPUTATIONAL AND MOLECULAR MODELING AND STRUCTURAL RATIONALIZATION FOR THE DESIGN OF A DRUG-LOADED PLLA/PVA BIOPOLYMERIC MEMBRANE

3.1. Introduction

Advances in biomaterials research has provided solutions for combating numerous challenges posed by various disease conditions (Karp and Langer, 2007). The amalgamation of polymeric science with the pharmaceutical sciences and medicine has led to the development of novel biomaterials for specific applications (Popovic and Brundin, 2006; Ponce et al., 2005; Whittlery and Shea, 2004; Ramehandan and Robinson, 1998). Despite the progress in the development of such biomaterials a large number of biomaterial-based devices are currently used clinically with unsatisfactory clinical performance (Joachim et al., 2007). Furthermore, very few synthetic devices are approved by the US Food and Drug Administration (FDA) due to the fact that the time, complexities and attempts to tailor the properties of polymers to complement specific applications are mostly based on trial and error (Eisenberg, 1995). Therefore there is a need to extend and focus biomaterials research toward economical approaches that may overcome the challenges of designing new biomaterials. Refined approaches such as combinatorial methods, high-throughput experimentation and computational molecular modeling for the development of biomaterials are able to significantly contribute to this area of research by creating opportunities to simulate, investigate, model and predict the structure and properties of newly synthesized biomaterials (Eksterowics et al.,2002; Kirkpatrick et al., 1999; Stanton et al., 2000).

Computational molecular modeling and structural rationalization techniques are becoming fundamental for the innovative development of biomaterials that were initially unexploited due to

the complex nature of biological and pharmacological domains and the expertise and interdisciplinary commitments required to formulate computational models of various phenomena (Ironi and Tentoni, 2003; Brocchine et al., 1997) However, the fusion of polymer and pharmaceutical science with computational chemistry has resulted in the incorporation of theoretical chemistry into efficient computer software to gain further insight into the complexity and behaviour of newly synthesized biomaterials in order to justify theoretical concepts when conclusive postulations correlate well with experimental results (Selvam et al.,2005; Tuzun et al., 1998). Computational chemistry employs molecular mechanics and quantum mechanics such as semi-empirical, *ab initio* and Density Functional Theory (DFT) to predict the molecular structure of biomaterials and compute different molecular descriptors. Computational modeling can be regarded as a third element in the research triad complementing experiment and theory (Smith et al.,2004; Gao, 2001)

Ironi and Tentonis (2003) employed a computational framework to explore the mucoadhesive potential of sodium carboxymethylcellulose. Polymer-mucin mixtures at varying concentrations underwent standard creep testing and accurate ordinary differential equation models were obtained from the data (Ironi and Tentonis, 2003).Computational modeling functions are best supported by techniques that facilitate the development of predictive models and reveal the molecular structure and underlying physical phenomena governing performance of a biomaterial that would not otherwise be revealed by laboratory experiments (Abramson et al., 2005; Gubskaya et al., 2007; Duce et al., 2006).

Biocompatible and biodegradable polymers in particular have been regarded as suitable materials for developing optimized drug delivery systems with improved therapeutic efficacies, better patient compliance and reduced side-effects (Stanton et al., 2000). Polymers are a versatile class of materials with well-defined physicochemical and physicomechanical properties

(Holder and Kilway, 2005; Omathanu et al., 2001; Esperon et al., 2008; Jose et al., 2008). Depending on the requirements placed upon a certain material, polymeric drug carriers can be fabricated into various geometries by employing processing methods ranging from implants, stents, grafts, microparticles or nanoparticles or membranes. The approach of combining different polymers leads to the formation of a modified polymer and provides a broader spectrum for fulfilling the needs of a drug delivery system. Aliphatic polyesters, such as poly(lactic acid) and their copolymers have been widely used for fabrication of drug delivery devices (Dorothee et al., 2006; Foernkier et al., 2003; Rajeev, 2000). In addition, formulations tend to show polyphasic drug release profiles which deviates from the ideal 'infusion-like' profile generated by zero-order release formulations (Anderson and Shive, 1997; Singh at al., 1997; Cui and Schwendenman 2001).

Grafting of polyester chains onto hydrophilic backbones would alter the degradation and release properties of the carrier system (Burrem et al., 1993). Kissel and coworkers successfully formulated a drug delivery system based on a modified polyester fabricated by grafting poly(lactic-*co*-glycolic acid) onto poly(vinyl alcohol) (PVA-PLGA) or amine modified poly(vinyl alcohol) or sulfobutylated poly(vinyl alcohol) to yield PVA-g-PLGA, DEAPA-PVA-g-PLGA and SB-PVA-g-PLGA respectively. Microparticles prepared from PVA-grafted PLGA also displayed superior encapsulation efficiencies for proteins ranging from 70-90% with yields of approximately 60-85%. Drug release modulation and erosion could be adjusted to meet specific applications when formulated into various drug delivery vehicles such as microparticles, nanoparticles, tablets, implants and membranes with erosion times ranging from hours to weeks (Kiesel et al., 2000 and 2005).

Therefore this study focused on applying computational chemistry as a modeling tool for the rational design of a biopolymeric membrane system for the delivery of methotrexate (MTX). The

information obtained from virtual molecular structures and computer models was used to formulate theoretical postulations on factors such as drug entrapment efficiency and the mechanisms of drug release. MTX was selected as the model drug due to the potential of employing the biopolymeric membrane as an intracranial implant for the treatment of Primary Central Nervous System Lymphoma (Mohile and Abrey, 2007).

3.2 Materials and Methods

Methotrexate (MTX) (model drug) and stannous octoate (catalyst) (Tin (II) 2- ethylhexanoate) were purchased from Sigma Aldrich (St Louis, MO, USA). Poly(vinyl alcohol) (PVA; grade 8/88, M_w=49,000g/mol) and triethanolamine (TEA) (plasticizer) was purchased from Saarchem (Krugersdorp, South Africa) a division of Merck chemicals. Poly (L-lactic acid) (PLLA; Resomer® grade R203H) was purchased from Boehringer Ingelheim (Ingelheim, Germany) and the dimethyl-sulphoxide (DMSO) (solvent), reagent grade acetone and methanol (non-solvent blend) were purchased from Rochelle Chemicals (Johannesburg, South Africa).

3.2.1 Preparation of the biopolymeric membrane

MTX-loaded biopolymeric membranes were fabricated by layered hydrophile-lipophile conjugation and graft co-polymerization of the lactone poly(L-lactic acid) (PLLA) and the polyol poly(vinyl alcohol) (PVA) with and without the addition of the amphiphile TEA (PLLA-PVA and TEA-PLLA-PVA) employing stannous octoate as a catalyst at a reaction temperature of 150°C. TEA was added due to it's relatively balance interphase absorption and was reacted with the modified co-polymer to induce backbone activation for the addition of model drug methotrexate (MTX). Phase separation was achieved by an immersion precipitation technique. Briefly, homogenous solutions of PLLA and PVA (10%$^{w}/_{v}$) were blended after solubilization in DMSO. The polymers were reacted in a ratio of 1:1.75 (15:20mL) PLLA/PVA in the presence of

stannous octoate at 150°C for 1 hour. Thereafter, 2.5mL TEA was added to the polymeric solution and the reaction was allowed to proceed for a further 1 hour. MTX (15mg) dissolved in 0.5mL DMSO was added to 2.5mL of the composite polymeric solutions and casted on a glass petri dish (15mm in diameter) and then immersed in a mixed non-solvent system comprising acetone:methanol in a ratio of 1:1. The resultant biopolymeric membranes were recovered after 24 hours from the coagulation bath and allowed to dry at room temperature (21±0.5°C) prior to further characterization. All reactions were performed with purified core molecules and monomers.

3.2.2 Computational and molecular structural modeling of the biopolymeric membrane formation

Computational and molecular structural modeling was performed to deduce a hypothesized chemical structure and potential inter-polymeric interaction during membrane balance and layering. Semi-empirical, *ab initio* and Density Functional Theories (DFT) of molecular and quantum mechanics was used to generate predictions of the molecular structure of the materials and compute various molecular attributes based on the inherent interfacial phenomena underlying the formation of the biopolymeric membranes prepared by the immersion precipitation technique. Models and graphics based on the step-wise molecular mechanism of membrane formation, polymer interconversion and grafting and drug chelation as envisioned by the chemical behavior and stability were generated on ACD/I-Lab, V5.11 (Add-on) software (Advanced Chemistry Development Inc., Toronto, Canada, 2000).

3.2.3 Analysis of the biopolymeric membrane swelling potential

Swelling of the biopolymeric membrane was determined by immersing a known mass of membrane samples in 10mL phosphate buffered saline (PBS) (pH 7.4; 37°C) in petri dishes (90mm in diameter) and allowed hydration to take place for 30 minutes. The membranes were

allowed to reach the maximum hydration potential and thereafter the swollen mass of the membranes was determined by gravimetric analysis using an electronic analytical mass balance (Mettler Toledo, Inc., Columbus, OH, USA) after removing the samples from the PBS solution and blotted with filter paper to adsorb water on the membrane surface. The degree of swelling was calculated as a difference between the mass of the non-hydrated and hydrated membranes (%) employing the following equation:

$$S_D = \frac{(W_s - W_i)}{W_i} \times 100 \qquad \text{Equation 3.1}$$

Where, S_D is the degree of swelling in PBS, and W_i and W_s are the masses of the biopolymeric membranes before and after hydration, respectively.

3.2.4 Assessment of biopolymeric membrane surface morphology

Scanning electron microscopy (SEM) was employed for assessing the membrane surface morphology on gold-platinum sputter-coated samples employing a Joel JSM-840 (Tokyo, Japan) scanning electron microscope. Various photomicrographs were attained under an electrical potential of 15kV by scanning fields selected at different magnifications.

3.2.5 Determination of membrane toughness and bi-axial extensibility

Textural profile analysis was employed for all physicomechanical investigations. The bi-axial extensibility was determined from Force-Distance profiles generated on a TA.XT*plus* Texture Analyzer (Stable Microsystems, Surrey, UK) equipped with a 2mm flat cylindrical probe, a 5kg loadcell and Texture Exponent V3.2 software for data processing. The method involved securing the biopolymeric membranes on a ring assembly with a 5mm diameter central hole using a secure raised platform (Figure 3.1). The centralized test probe was then lowered and embedded onto the membrane surface according to the relevant test parameter settings for

determining the biopolymeric membrane toughness and bi-axial extensibility as specified in Table 3.1.

Table 3.1 Test parameter settings employed for bi-axial extensibility testing of the biopolymeric membrane

Parameter	Setting
Test mode	Compression
Pre-test speed	1.00mm/sec
Test speed	1.00mm/sec
Post test speed	1.00mm/sec
Trigger mode	Distance
Distance	10mm
Trigger force	0.5000N

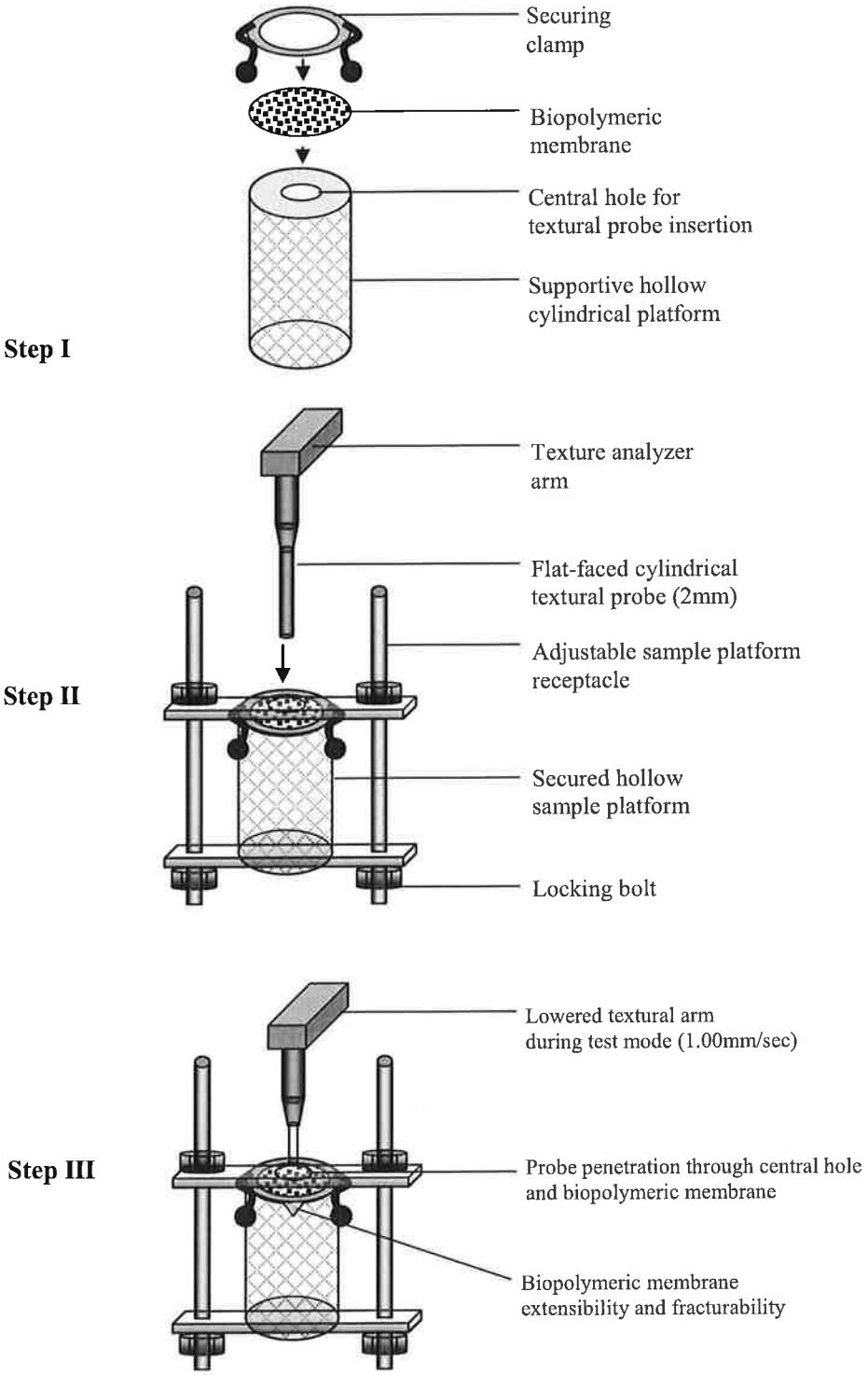

Figure 3.1. A schematic depicting the experimental configuration for assessing the toughness and bi-axial extensibility of the biopolymeric membrane employing textural profile analysis. Step I, involves securing of the sample; Step II, securing of sample platform to textural stage and Step III, lowering the textural probe during test mode for biopolymeric membrane analysis.

3.2.6 Determination of the drug entrapment efficiency within the biopolymeric membrane

Drug entrapment efficiency (DEE) analysis of the biopolymeric membrane was performed by re-dissolving membrane samples in 100mL PBS (pH 7.4; 37°C) and subsequently determining the quantity of MTX entrapped using a previously constructed standard linear curve generated at the maximum UV wavelength of λ303nm for MTX (CECIL 3021 Spectrophotometer, Cecil Instruments, Cambridge, England). The DEE value was calculated employing the following eqution:

$$DEE = \frac{(M_i - M_d)}{M_i} \times 100 \qquad \text{Equation 3.2}$$

Where, M_i is the initial mass of MTX dissolved in the casting polymer solution and M_d is the mass of MTX quantified in the media after membrane samples were completely dissolved.

3.2.7 *In vitro* release of MTX from the biopolymeric membranes

In vitro release studies were performed in PBS (pH7.4; 37°C). The biopolymeric membranes were placed in closed 150mL glass vessels containing 100mL of the release medium. The membranes were incubated at 37±0.5°C in an oscillating incubator set at 20rpm. At predetermined time intervals 5mL samples of the release medium were removed. Drug-free buffer was replaced into the vessel after sample removal in order to maintain sink conditions. The concentration of MTX was assayed by UV spectroscopy (CECIL 3021 Spectrophotometer, Cecil Instruments, Cambridge, England) at the maximum drug wavelength (λ max) of 303nm using a standard calibration curve of known concentrations range from 0.005-0.025mg/mL with a correlation coefficient R^2=0.99.

3.3 Results and Discussion

3.3.1. Formation of the MTX-PLLA-TEA-PVA biopolymeric membrane

The immersion precipitation reaction of PLLA and PVA in the presence of the catalyst stannous octoate and triethanolamine (TEA) at 150°C resulted in the formation of a modified co-polymer with a branched structure. The biopolymeric membranes revealed various consistencies ranging from non-opaque coarse MTX-loaded membranes (Figures 3.2a and c) to opaque smooth membranes (Figures 3.2b and d). The hydrophobic PLLA polymeric chains were conjugated in a graft-like manner onto the hydrophilic PVA backbone via esterification of the hydroxyl groups to form an amphiphilic polymer. The drug (MTX) was subsequently bonded to the PLLA segment as shown in (Figure 3.3a). The resultant membrane was shaped through structural polymeric layering to form a porous crystalline hydrogel-based drug delivery matrix (Figure 3.3b). The hydration and swelling kinetics of the system were mainly governed by the presence of the hydrophilic PVA backbone that controlled the quantity of water sorption and the extent of swelling of the polymeric matrix. A distinction was the insolubility of the adsorbate in the liquid sub-phase that resulted in the formation of a stable absolute conformation of the biopolymeric membrane that was dependant on the associated surface tension, the surface excess of TEA in comparison to the bulk phase and the concentration of TEA in the bulk phase (Figure 3c).

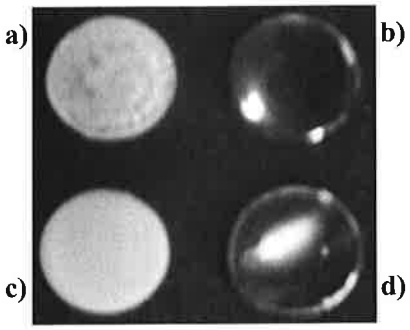

Figure 3.2. Digital images of the a) MTX-PLLA-PVA; b) PLLA-PVA; c) MTX-TEA-PLLA-PVA and d)TEA-PLLA-PVA biopolymeric membranes, where MTX=methotrexate; TEA=triethanolamine; PLLA=poly(L-lactic acid) and PVA=poly(vinyl alcohol).

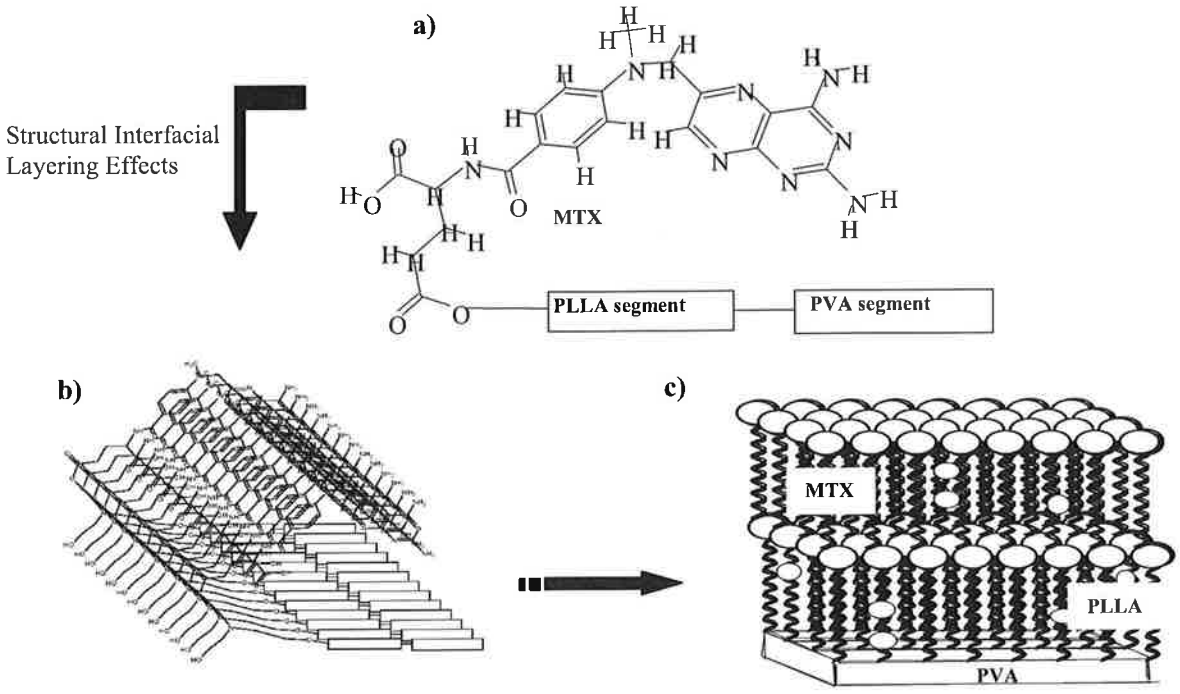

Figure 3.3. Schematics of a) A 1D representation of a MTX-loaded biopolymeric membrane entity conjugating MTX-PLLA-PVA, b) initial induction of structural layering and c) A 3D representation of the conformationally evolved biopolymeric membrane showing inter-layering of PLLA and MTX conjugated to the PVA backbone.

Steric hindrance may have shielded MTX binding sites and thus prevented MTX molecules from attaching at every PLLA monomer available along the entire modified polymer backbone accounting for the DEE values attained as discussed later. Thus, MTX binding to the PLLA segment was dependant on the extent of PLLA grafting onto the PVA backbone. To a lesser extent MTX molecules may also undergo further direct conjugation with free PVA monomers or assemble as freely dispersible entities within the modified polymeric complex.

3.3.2 The effect of the addition of amphiphilic triethanolamine (TEA)

TEA molecules inherently possess dendrimeric properties due to the large number of nitrogen atoms in the entity. A single TEA entity has the capacity of bearing two MTX molecules and may be regarded as a nodal point for drug attachment and drug release. In contrast to the MTX-PLLA-PVA matrices, TEA molecules in the MTX-TEA-PLLA-PVA matrices afforded the system with additional sites for drug attachment (Figure 3.4a). The layered structure led to the formation of a multi-layered matrix (Figure 3.4b) possessing unique hydration and swelling dynamics and MTX release kinetics. The sparse branching of polymeric chains in the MTX-TEA-PLLA-PVA matrix system afforded greater flexibility due to reduced steric hindrance. The average free volume per molecule available for MTX was increased in contrast to the MTX-PLLA-PVA membrane system.

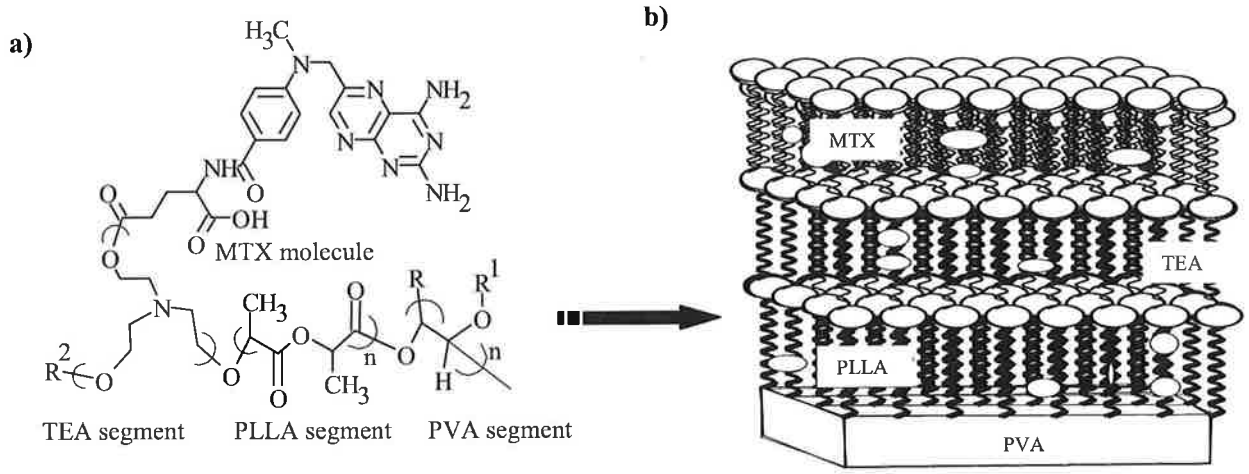

Figure 3.4. Schematic of a) MTX molecules bound to a PLLA-TEA-PVA backbone of the biopolymeric membrane where R=PVA polymeric chain, R1=PLLA-TEA-MTX linkage and R2= a MTX molecule; and b) A 3D structural model of the biopolymeric membrane depicting the multi-layers representing PLLA, TEA and MTX conjugated onto a PVA backbone.

PLLA co-polymeric conjugate blends with PVA can be modified significantly robust structures by the addition of amphiphilic TEA as a discrete plasticizing and drug binding entity within the matrix. TEA molecules are able to act as stress concentrators, which reduce the overall yield stress of the biopolymeric membrane, allowing plastic deformation, enhanced extensibility and ductile fracture during physicomechanical analysis and drug release studies in PBS (pH 7.4; 37°C). Crystallized PLLA has significantly reduced impact strength and therefore could be toughened by the addition of TEA as a separate immiscible rubbery phase in conjunction with PVA. Since the biopolymeric membrane is to be used in biomedical applications as a potential drug delivery device, the plasticizer TEA was chosen due to its ability to degrade into substances that are absorbable in the body that are hydrophilic and non-toxic.

3.3.3 Computational molecular structural modeling of the proposed mechanism of biopolymeric membrane layering

To develop a mechanistic structural molecular model for the effectual layering of the biopolymeric membrane a mono-layered membranous fusion approach was employed, which has been previously attempted as an effective approach for the formation of supported lipid bi-layered membranes that are able to describe biological cellular membranes with one or more components (Dufrene and Lee, 2000, Rinia et al., 2006).The conjugated MTX-TEA-PLLA-PVA-TEA-MTX membrane can be represented by a diverse contoured model in various spatial conformations due to the inherent stereo-electronic factors at the matrix site (Figure 3.5a). The formation of a layer is induced by self assembly of conjugated MTX, TEA, PLLA and PVA entities in different ordered orientations (Figure 3.5b). Chirality is able to induce activation at one end of the optically active molecules through linking, binding and association of the conjugated entities that ultimately lead to the formation of a multi-layered membrane structure (Figure 3.5c). The process of membrane multi-layering is based primarily on stereochemical factors and the weighted fusion of mono-layers to eventually form a multi-layered structure (Figure 3.5d).

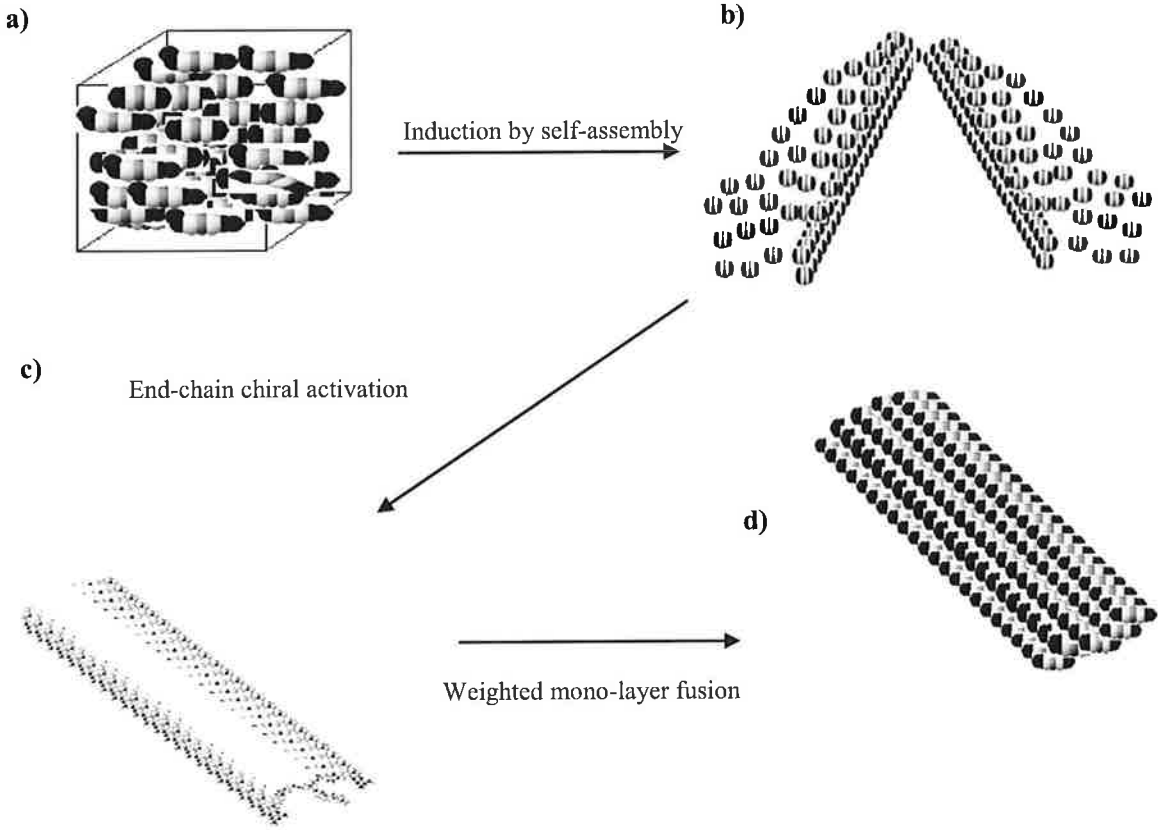

Figure 3.5. Schematic depicting a) a cube representing the diverse model contours of the conjugated MTX-TEA-PLLA-PVA-PLLA-TEA-MTX entity due to matrix stereo-electronic factors, b) formation of self-assembled mono-layered isomers, c) end-chain activation of fusion based on chirality of mono-layers and d) isomeric conjugation into an ordered multi-layered biopolymeric membrane

Preliminary factors that are required for multi-layered membrane formation is to obtain an even surface following PLLA deposition to ensure the fusion of subsequent layers incorporating MTX molecules. As depicted in the computational structural model generated in Figure 5 TEA linkage provided an even molecular surface, with a refractivity value of 38.78A^3 for the modeling area (Table 2). The subsequent MTX layer provided a central platform region for structural layering between the isomeric mono-layers (Figure 5b). Since TEA is amphiphilic the deposition of the tri-branched polyelectrolyte on the membrane surface improved the fusion process due to electrostatic interaction and allowed uniform supported multi-layering to occur.

Furthermore, DFT (6-31G) and *ab initio* computational results of the molecular characteristics employing HyperChem® V7.5 software (Hypercube Inc., Gainesville, FL, USA) indicated that the addition of TEA dramatically improved the layering effect (Table 2). Approximate surface area values obtained were $0.12A^2$ and $16.17A^2$for the MTX-PLLA-PVA and MTX-0TEA-PLLA-PVA membranes respectively.

The acetone:methanol blend was a strong non-solvent for PLLA and PVA. For this approach, compositions with high volume fractions of PLLA at the tri-nodal TEA were in equilibrium with the continuous solvent phase. Due to the strong non-solvent character of the acetone:methanol blend the miscibility gap proved to be sufficient for the immersion precipitation process to occur. Polarizability values of $65.49A^3$ and $80.09A^3$ were obtained for the MTX-PLLA-PVA and MTX-0TEA-PLLA-PVA membranes respectively. The difference in the polarizability values between the membrane formulations was aligned with the initial difference of $7.54A^3$ and $9.39A^3$ for native PLLA and PVA respectively (Table 3.2).

Formation of the biopolymeric membranes were a combination of thermodynamic and diffusion kinetic phenomena. In order to induce phase separation by a diffusion-driven process thermodynamic and kinetic conditions were fulfilled. The membrane formation process was governed by diffusion over the interface between the PLLA/PVA solution within the petri dish and the coagulation bath. Although two polymeric components were present in the casting solution only solvent and non-solvent diffused outward. The differences in hydration energy potentials (-11.81Kcal/mol and 6.86Kcal/mol for PLLA and PVA respectively) and Log P values (0.47 and 0.12 for PLLA and PVA respectively) conferred the induction of a diffusion flux that was sufficient to compensate for the energy needed to create a new insoluble surface during phase separation resulting in membrane formation at the interface (Table 3.2). A semi-porous

membrane structure was formed and the polymeric solution was in equilibrium with the coagulation bath creating a new structure.

Table 3.2. HyperChem® V7.5 (Hypercube Inc., Gainesville, FL, USA) computational molecular attributes at *ab initio* and Density Functional Theory (DFT) (6-31G)

	PLLA	PVA	P-P[2]	M-P-P[2]	T-P-P[3]	M-T-P-P[4]	TEA
Mass[a]	89.0	-	232.23	-	-	-	-
Polaribility[b]	7.54	9.39	21.65	65.49	32.17	80.09	15.05
Refractivity[c]	15.27	38.87	47.15	170.80	84.33	208.97	38.87
Log P	0.47	0.12	1.31	0.81	1.14	0.10	1.17
Hydration Energy[d]	-11.81	6.86	7.02	0.12	1.32	16.75	13.85
Volume[e]	309.6	A^3	77.63	398.04	358.56	1807.91	166.36
Surface Area (approx)[f]	38.88	159.45	393.82	16.85	160.23	823.71	242.22
Surface Area (grid)[g]	228.02	178.90	422.80	245.72	243.86	980.00	143.11
Partial Charges[h]	0.00	0.00	0.00	0.00	0.00	0.00	0.00

a- amu (atomic mass unit)
b, c and e-A^3 (Angstrom cube)
d-Kcal/mol
f and g-A^2 (Angstrom square)
h and e (net)

1-PLLA-PVA
2-MTX-PLLA-PVA
3-TEA-PLLA-PVA
4-MTX-TEA-PLLA-PVA

3.3.4 Assessment of the surface morphology of the biopolymeric membranes

High magnification SEM revealed distinct continuous layers of the biopolymeric membrane with macro-porous mosaic morphologies (Figure 3.6a). The high level of crystallinity is evident from the randomly shaped macro-pores with very sharp distinct borders (Figure 3.6b). Following the immersion step, the top surface of the membrane (Figure 3.6c) is formed spontaneously by the non-solvent-solvent diffusion process which occurs immediately at the polymer-non-solvent interphase. The bottom surface of the membrane (Figure 3.6d) is formed gradually as the non-solvent penetrates into deeper membrane depths and this result in the formation of more consistent mosaic morphology.

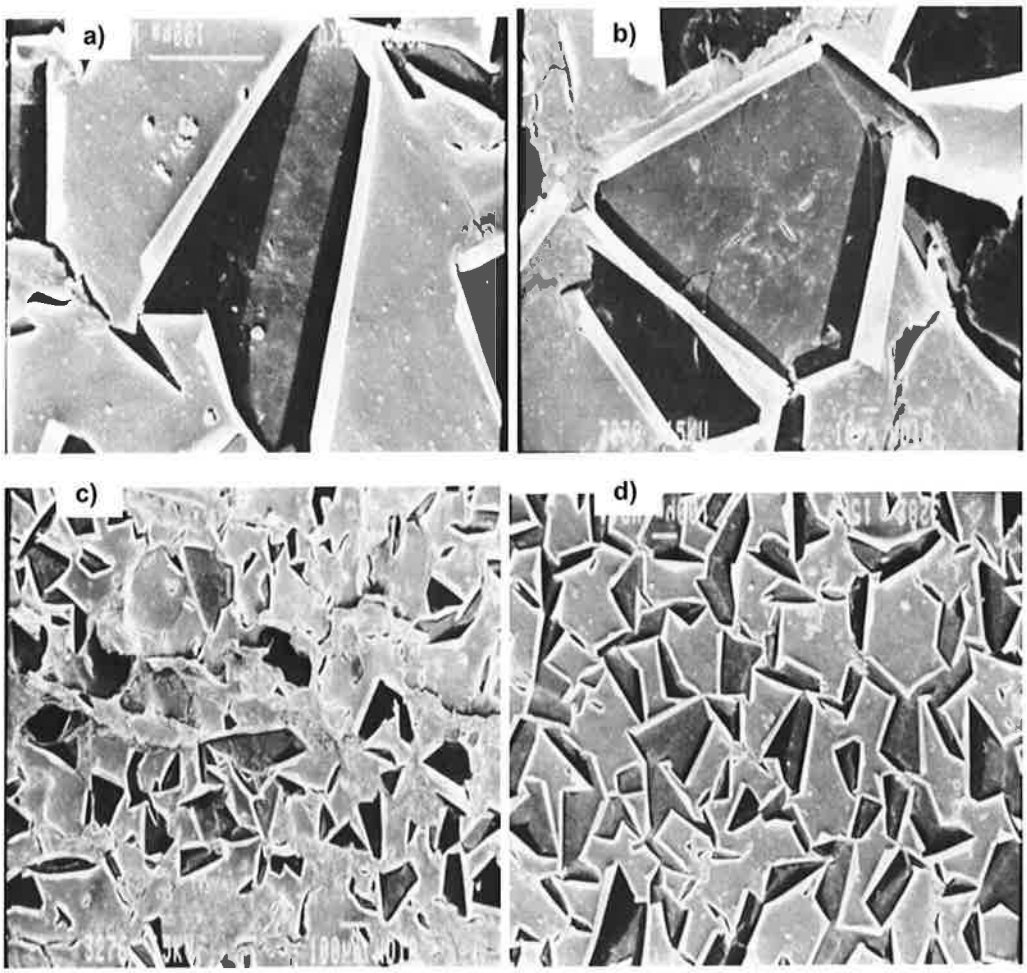

Figure 3.6. SEM photomicrographs of the biopolymeric membrane depicting a) and b) layered architecture and crystalline structure, c) the aerial surface and d) the bottom surface morphology of the membrane.

The formation of pores within the membrane depended on the sequence of the phase transition events in the immersion precipitation process (Rahimpour et al., 2008; Zeni et al., 2008). Numerous parameters, such as the compositions of the polymeric solution the precipitation bath and the temperature during preparation influenced the morphology and surface area of the formed membranes (Table3.2).

Membrane preparation is a non-equilibrium process, therefore a change in membrane structure was attributed to the arrangement of PLLA and PVA chains during membrane formation. A high polymer concentration region was formed at the interface between the polymer solution and the

coagulation bath. High polymer concentration at this interface acted as a diffusion barrier to mass transport. Phase separation at this stage will have no influence on the asymmetry of the process, which explains the symmetry in structure of the biopolymeric membranes. Fine particles were noted under high SEM magnification (Figure 3.6a and 3.6b). These particles may have been generated due to crystallization of polymer during the membrane formation process.

3.3.5. Membrane toughness and bi-axial extensibility

The physicomechanical strength of the biopolymeric membranes depended profoundly upon the polymer linkages. Dissimilar and unique degrees of extensibility were observed for the various biopolymeric membranes (Figures 3.7a and b). Extensibility can be defined as the degree to which a material can be extended /stretched prior to fracture and is related to the elasticity of the material. The inclusion of TEA in the membrane formulation resulted in a significant transition of the physicomechanical properties of the membranes. The MTX-TEA-PLLA-PVA membrane was superiorly robust with a considerably higher extensibility compared to the MTX-PLLA-PVA membrane as a greater force of extension and larger fracture distance was required (Figure 3.7a). When the elastic limit of the MTX-TEA-PLLA-PVA membranes was reached a greater resistance to structural deformation was noted (region *p* in Figure 3.7b). The variation in the textural properties may be related to the computational structural models that proposed the mechanism of membrane formation for the two formulations (MTX-TEA-PLLA-PVA and MTX-PLLA-PVA) leads to the different layered structural architectures.

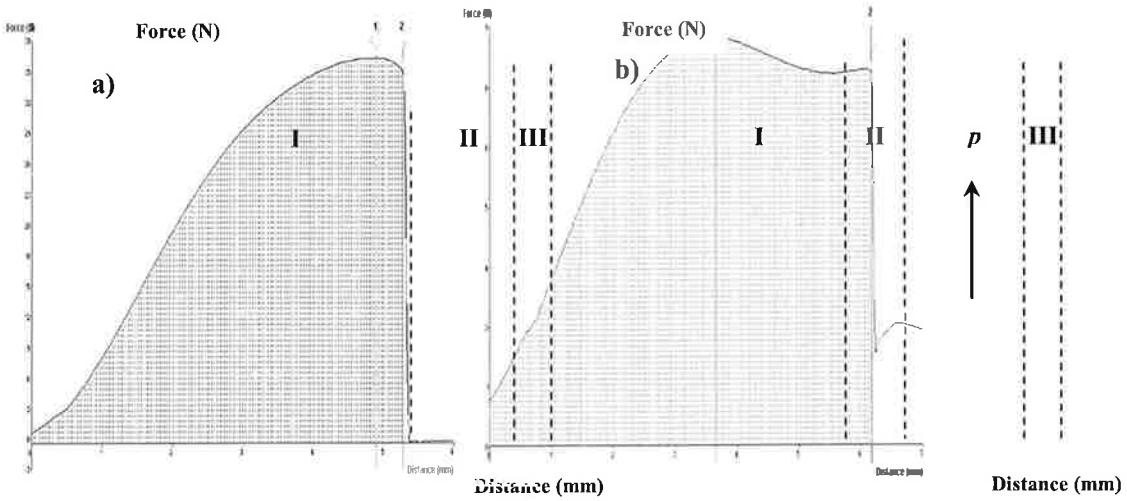

Figure 3.7. Typical biaxial extensibility profiles generated for a) a MTX-PLLA-PVA membrane and b) a MTX-TEA-PLLA-PVA membrane system. I=phase of linear extensibility; II=maximum extensibility; III=membrane fracture; *p*=region of extended membrane plasticity due to the addition of TEA

Textural profile analysis revealed that the biopolymeric membrane was significantly toughened by the introduction of TEA as a discrete rubbery phase within the co-polymer matrix. The MTX-TEA-PLLA-PVA biopolymeric membrane system was tougher (F=89N) and considerably more extensible (D=8.79mm) compared to MTX-PLLA-PVA (F=35N, D= 3.7mm) membranes since a greater force of extension and fracture distance was required. The MTX-TEA-PLLA-PVA membrane showed superior resistance to structural deformation. TEA molecules acted as a stress concentrator that reduced the overall yield stress of the membrane, allowing plastic deformation and ductile fracture to occur prior to membrane fracture (Figure 3.7b; region *p*). The grafted TEA molecules lowered the force required for fracture and therefore considerably increased the quantity of dissipated energy during fracture. PLLA quenched from the melt or non-crystallizable L- and D-lactide has a low impact strength. Thus the reduced strain to break during bi-axial extensibility testing was sensitive to minute surface imperfections. PLLA was therefore significantly toughened by blending with TEA as a separate, immiscible rubbery phase. The strength of the MTX-PLLA interface bond was a significant parameter for not only toughening of the biopolymeric membrane but also MTX entrapment and subsequent release.

The strength of this interface was modified by the use of TEA as a compatibilizer, graft and block co-polymer.

3.3.6 Drug entrapment efficiency and swelling studies

Relatively high MTX-loading capacities were achieved for both membrane formulations (Figure 3.8a). A significant difference in the swelling potential of the two formulations was also observed (Figure 3.8b).

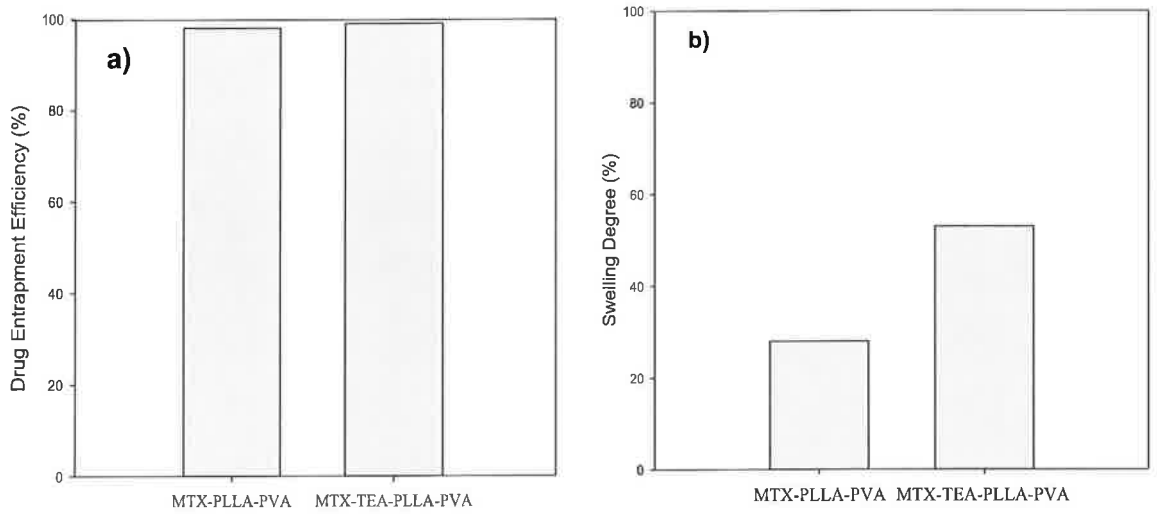

Figure 3.8. Histograms comparing a) the drug entrapment efficiency and b) the dynamic swelling potential of MTX-PLLA-PVA and MTX-TEA-PLLA-PVA biopolymeric membranes

Biopolymeric membranes that are formed by immersion precipitation of polymeric solutions in coagulation baths with a high solvent concentration, variations in the casting solution and the coagulation bath may have significant consequences on the DEE and swelling behavior of the membranes. The MTX-TEA-PLLA-PVA membranes showed a higher degree of swelling (53±0.5%) compared to the MTX-PLLA-PVA membranes (28±0.5%) (Figure 3.8b). This was due to the ability of the MTX-TEA-PLLA-PVA system to imbibe a larger quantity of water molecules due to its multi-layered conformational structure. The high MTX entrapment values indicated that the energy gain of de-mixing MTX was probably larger than the energy needed to form a

new interface for membrane formation. The extent of phase separation and further MTX entrapment can be enhanced by varying the molecular mass of the polymers, adjusting the blending procedures, and annealing the blended materials.

3.3.7. *In vitro* MTX release studies

The release of MTX from the biopolymeric system followed tri-phasic kinetics. An initial burst in MTX release was obs erved due to unbound MTX molecules entrapped within the polymer matrix. The initial burst phase of MTX release (Phase I) (unbounded MTX) was followed by steady state kinetics (Phase II) (TEA-bound MTX) presumably due to the gradual hydration and swelling of the biopolymeric membrane. A final controlled up-curving MTX release phase (Phase III) was observed due to a combination of surface and bulk erosion of the membrane (Figures 3.9a and b). The quantity of MTX released from the MTX-PLLA-PVA system (Figure 3.9a) at a particular time-point was greater than that released by MTX-TEA-PLLA-PVA system (Figure 3.9b) since more energy was required to break the TEA-MTX bond by hydrolytic cleavage. Therefore, confirming the function of TEA to act as a drug binding motif that was able to modulate MTX release.

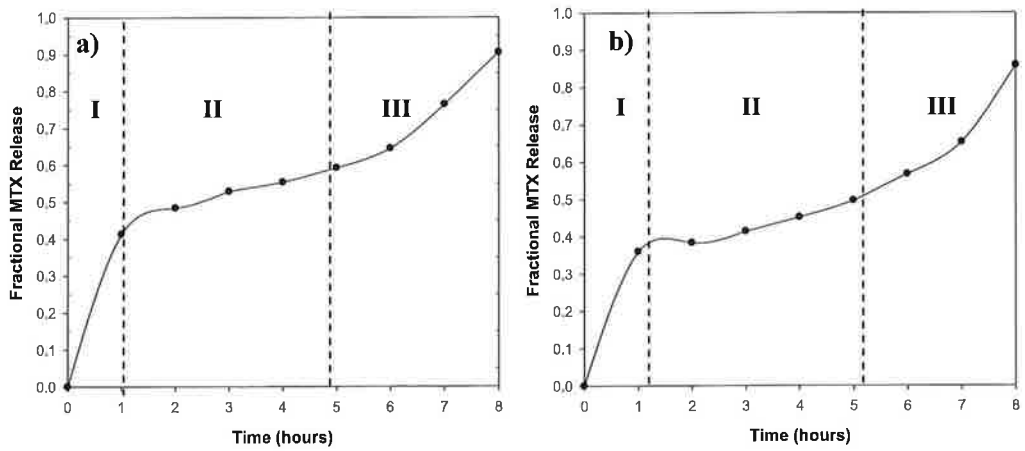

Figure 3.9. MTX release profiles from a) the MTX-PLLA-PVA and b) MTX-TEA-PLLA-PVA biopolymeric membrane formulations showing tri-phasic release kinetics with I-initial burst effect; II-a diffusional phase of MTX release; and III- a final controlled MTX release phase.

3.3.8 Hypothetical drug release mechanism

The biopolymeric membrane formulations, MTX-PLLA-PVA and MTX-TEA-PLLA-PVA, are amphiphilic structures with a thin planar geometry. The amphiphilic character is attributed to the hydrophobic characteristics of the PLLA branches and the hydrophilic characteristics of the PVA backbone. The degradation kinetics of the membranes will therefore deviate from those of a hydrophobic polymeric networks fabricated from native PLLA or PVA based hydrophilic hydrogels. The limited water sorption capabilities of PLLA are improved by conjugation onto the PVA backbone and the resultant modified polymer will thus possess the favourable properties of hydrogels. The computational structural molecular models depicted evidence of *in situ* MTX loading and therefore the biopolymeric membranes are highly likely to adopt a chemically-controlled mechanism of MTX release. However MTX release profiles from the two formulations (with and without TEA) differed owing to the presence of the MTX-binding motif TEA in the MTX-TEA-PLLA-PVA membrane. A purely kinetic-controlled release mechanism which occurs via bond cleavage and mediated by surface erosion may be responsible for MTX release modulation. The hydrolytic cleavage of the MTX-polymer covalent bond in the MTX-PLLA-PVA membrane is the rate limiting step with regard to MTX release. However, a different situation prevails with the MTX-TEA-PLLA-PVA membranes where TEA is tethered to MTX molecules, the kinetics and thermodynamics of which will determine the release kinetics of MTX from the membrane. The structural integrity of the membranes will be maintained since they would obey surface eroding phenomena.

3.4 Concluding Remarks

The use of intricate computational models and structural rationalization techniques played a critical role in predicting the structural conformation of the synthesized biopolymeric membrane. Computational modeling has provided a mechanistic insight to further comprehend the formation, molecular structural characteristics, physicomechanical properties and the ability to

entrap and modulate the release of MTX from the biopolymeric membrane. The stupendous physicomechanical properties of the membrane resulted from a superior balance of the polymeric phases employed and the addition of TEA which provided a synergistic approach in improving the biaxial extensibility, toughness of the membrane and the ability to modulate the drug release in a tri-phasic manner suitable for the novel delivery of MTX.

CHAPTER FOUR

PREPARATION, CHARACTERIZATION AND OPTIMISATION OF POLY(VINYL ALCOHOL)/POLY(LACTIC ACID) BIOPOLYMERIC MEMBRANES FOR DRUG DELIVERY APPLICATIONS

4.1. Introduction

Polymeric membranes can be prepared by different techniques that have been well researched in the field of Membrane Technology (Mulder, 1992). Immersion precipitation technique is one of the techniques that has been used extensively to prepare most of the commercially available membranes. The principle steps of this method involve casting of a polymer solution onto an inert support followed by the immersion of the support with the cast film into a bath filled with a nonsolvent for the polymer. The subsequent exchange of solvent for nonsolvent induces phase separation of the polymer solution. Phase separation occurs via liquid-liquid demixing by nucleation and growth of a polymer poor phase. The demixed solution solidified when the gel transition is passed in the course of the demixing process (van de Witte et al., 1996). Polymers have a unique combination of physical and chemical properties coupled with biocompatibility and have been successfully employed in many fields including the production of membranes (Burkoth et al., 2000).

The selection of polymers for a specific application depends on many factors such as mechanical characteristics, surface properties (hydrophilicity/hydrophobicity, lubricity, smoothness, surface energy), that determine biocompatibility, durability, permeability and water sorption capacity, bulk properties (molecular weight, adhesion, solubility, thermal properties), which influence the release mechanism, site of action, thermal stability, glass transition temperature (*Tg*) and melting temperature (*Tm*), structural properties (micro-morphology, pore size) that determine drug transport of water into and drug out of the polymer (Vaidya and

Chaudhury, 2002). Poly(vinyl alcohol) (PVA) is an attractive non-toxic polymer with wide industrial applications due to its high hydrophilic properties, water solubility, and most importantly good film forming by solution casting (Alla et.al., 2004). It is of interest because of its strength, processibility, low fouling potential, and long term temperature and pH stability (Gudemann and Peppas, 1995). PVA is biocompatible, non toxic and exhibits minimal cell adhesion and protein absorption, as desired in biomedical applications requiring contact with bodily fluids (Korsmeyer et al., 1983). It is also widely used in cosmetics, packaging and construction of pervaporation membranes. Polylactic acid (PLA) is an aliphatic polyester that has gained wide application in various medical fields such as tissue fixation, drug delivery, wound dressing and wound closure (Chen et al., 2003). It is a thermoplastic material derived from lactic acid and its increased usage is prompted by its biocompatibility, mechanical properties, and biodegradability. PLA degrades to lactic acid via hydrolytic desterification, and lactic forms pyruvate by lactate dehydrogenase. Pyruvate is an intermediate product in metabolic pathways, and it can generate glucose via gluconeogenesis or be metabolised to form CO_2 and water by the citric acid cycle (Mainil et al., 1997).

In most research studies involving the design and development of 3-dimensional scaffolds, polymers like PVA and PLA are used in combination with other polymers to yield a material which is suitably tailored for specific biomedical applications. The art, science and the availability of polymer engineering techniques for reacting or blending different polymers continues to expand the borders for the discovery of smart and intelligent biomaterials. Hydrogels have been reported to have high biocompatibility and are good candidates for use as matrices for controlled delivery of pharmaceuticals such as vitamins and peptides (Kwon et al., 1992; Nakatsuka and Andrady, 1992). PVA and PEG have been reported to be of limited compatibility over a range of 0-30%. Thus, some researchers have exposed PVA/PEG blends composed of PEG ratio of up to 30% to γradiation to doses of up to 100kGy to improve the mechanical properties of pure PVA (Alla et al., 2004). Oh and co-workers (2003) fabricated

PVA/PLGA scaffolds by blending poly (lactic-*co*-glycolic acid) and poly(vinyl alcohol) to improve the hydrophilicity and cell compatibility of the scaffolds with different PVA compositions of up to 20wt% by a melt-molding particulate leaching method (Oh et al., 2003). In another study, binary of alginate (ALG) with PVA as cast, formed a thermodynamically miscible phase in the amorphous state. Treatment of cast samples with calcium tertraborate solution resulted in the formation of an (interpenetrating)'IPN' structure. There are many more studies in the literature that substantiate the advantages of blending polymers. The purpose of the present study was to prepare and optimize a PVA/PLA biopolymeric membrane drug delivery system for modulated release of methotrexate (MTX) by employing a Box-Behnken experimental design. The desired release profile was zero-order over an extended period of time (± 30 days).

4.2 Materials and Methods

4.2.1. Materials

Folic acid (FA) (model drug) and stannous octoate (catalyst) (Tin (II) 2- ethylhexanoate) were purchased from Sigma Aldrich (St Louis, MO, USA). Poly(vinyl alcohol) (PVA; grade 8/88, M_w=49,000g/mol) and triethanolamine (TEC) (plasticizer) was purchased from Saarchem (Krugersdorp, South Africa) a division of Merck chemicals. Poly (L-lactic acid) (PLLA; Resomer® grade R203H) was purchased from Boehringer Ingelheim (Ingelheim, Germany). Dimethyl-sulphoxide (DMSO) (solvent), reagent grade acetone and methanol (non-solvent blend) were purchased from Rochelle Chemicals (Johannesburg, South Africa).

4.2.2. Preliminary studies

Preliminary studies were conducted in order to determine the lower and upper formulation variables as well as process variables (Table 4.1). PLA concentrations less than 6%w/v and greater than 8%w/v could not be phase separated to form membranes. PVA solutions greater consisting of concentrations greater than 10%w/v were partially phase separated after

immersion in the coagulation bath. Biopolymeric membranes could not be formed with PVA solutions that were less than 6%w/v.

Table 4.1 Independent formulation factors selected for biopolymeric membrane preparation and optimization

Independent Variables	Levels		
	Lower	Middle	Upper
PVA ($\%^{w}/_{v}$)	6	8	10
PVA volume (mL)	20	35	50
TEC volume (mL)	0.5	1.5	4.5

The maximum amount of triethanolamine (TEC) a plasticizer that could be added into the formulation was 2.5mL otherwise excess TEC would be trapped in the matrices and delay phase separation. The process variables, reaction temperature and time (150°C, 1 hour) were optimised and kept constant during the preparation of all biopolymeric membrane formulations. The maximum drug loading capacity of the biopolymeric membrane device was determined to be 15mg. Rapid drug release was observed when the drug loading capacity of the biopolymeric membrane was less than 15mg while a pronounced burst effect resulted from drug loading capacities that were greater than 15mg.

4.2.3 Preparation of the PLA/PVA drug loaded biopolymeric membranes

The method for preparing PLA/PVA biopolymeric membranes was described in detail in Chapter 3, section 3.2.1. Briefly, solutions of PVA (6, 8 and 10%w/v) and PLA (8%w/v) were prepared separately. Different concentrations of the two polymer solutions were reacted for 1 hour at 150°C in the presence of stannous octoate (SnOct). Triethanolamine (TEC) was then added to the resultant composite polymer solution and the reaction was allowed to proceed for another hour. Folic acid (FA) 15mg was added to 2mL of the composite polymer solution, cast onto 5mm diameter petri dish and immersed in a coagulation bath consisting of a mixture of methanol:

acetone in a 1:1 ratio. The resultant biopolymeric membranes were removed after 24 hours from the coagulation bath and vaporization of solvent took place at room temperature (25°C).

4.2.4 Construction of a randomized Box-Behnken experimental design for biopolymeric membrane preparation and optimisation

A randomized Box-Behnken Design (Minitab® V15, Minitab Inc., PA, USA) was employed to construct the number of formulations required for optimization. Experimental trials were performed on 15 statistically derived formulations of various combinations. The influence of varying independent formulation variables (PVA concentration, PVA volume and TEC volume) and their interaction effects on the physicochemical and physicomechemical properties of the biopolymeric membrane formulations was studied. The selected depended variables were swellability (S*w*), elastic modulus (*E*) and drug entrapment efficiency (DEE). A statistical model incorporating interactive and polynomial terms was utilized to evaluate the responses and the constituents of the biopolymeric membranes were optimised under pre-determined constraints. Response surface plots were constructed to visually represent the influence of independent variables on the selected formulation responses.

Table 4.2 Formulation of PLA/PVA biopolymeric membranes using a 3-Factor Box-Bhenken design with values of variables

Formulation number	PVA[a] (%,w/v)	PVA volume[b] (mL)	TEC volume[c] (mL)
1	6	50	2.5
2	10	35	4.5
3	6	35	4.5
4	8	35	2.5
5	8	50	0.5
6	10	50	2.5
7	6	35	0.5
8	8	35	2.5
9	8	20	0.5
10	10	20	2.5
11	8	20	4.5
12	8	35	2.5
13	8	50	4.5
14	6	20	2.5
15	10	35	0.5

a = concentration of PVA
b = quantity of PVA
c = quantity of triethanolamine

4. 2.5 Assessment of *in vitro* degradation of the PLA/PVA biopolymeric membranes

Degradation studies were carried out by placing pre-weighed biopolymeric membrane samples in 10mL phosphate buffered saline (PBS, pH 7.4). The samples were then kept in an orbital shaking incubator set at 20 rpm and maintained at 37°C. The membrane samples were removed from the buffer at a 24 hour intervals, dried to constant weight at 40°C in an oven and weighed. The degradation rate was determined as the percentage loss in weight over time. The experiment was continued by placing the membranes in fresh buffer solution until severe cracking or disintegration of the polymer was observed.

4.2.6 Analysis of membrane swellability

Swelling studies were conducted by immersing a known weight of biopolymeric membrane sample in 10mL phosphate buffer saline (PBS, pH 7.4) and allowing the membrane to achieve maximum hydration potential. The membranes were removed from the PBS and blotted with filter paper to adsorb excess water on the surface. The swollen weight of the membranes was determined gravimetrically by weighing on an electronic balance. The swellability of the

biopolymeric membrane formulations in PBS was calculated by employing the following equation:

$$Sw = \frac{(W_s - W_i)}{W_i} \times 100 \qquad \text{Equation 3.1}$$

Where, S_w is the swellability in PBS, and *Wi* and *Ws* are the weights of the membranes before and after hydration, respectively.

4.2.7 Analysis of drug entrapment efficiency

The drug entrapment efficiency (DEE) of the membranes was determined by completely dissolving the membrane samples in PBS, pH 7.4. The amount of FA entrapped in the membrane samples was determined by measuring the absorbance of the medium at a maximum UV wavelength of λ280nm and drug entrapment efficiency was calculated by employing the following equation:

$$DEE = \frac{(M_i - M_d)}{M_i} \times 100 \qquad \text{Equation 3.2}$$

Where, DEE is the drug entrapment efficiency, *Mi* is the initial mass of the drug dissolved in the casting polymer solution and *Md* is the mass of FA quantified in the media after the membranes were completely dissolved.

4.2.8 *In vitro* drug release studies

In vitro release studies were performed in PBS, pH7.4. The membranes were placed in jars containing 100mL of the release medium. The membranes were incubated in a shaking orbital incubator set at 20rpm with the temperature maintained at 37°C. Samples of 5mL were collected from the release medium on a 24 hour interval and were replaced with fresh buffer solution of equal volume. The drug concentration in the solution was assayed by UV spectroscopy (CECIL 3021 spectrophotometer, Cecil Instruments, Cambridge, England) at a wavelength of 280 nm.

4.2.9 Tensile mechanical testing

The mechanical properties of the biopolymeric membranes were determined by textural profiling. Biaxial extensibility force-distance profiles were constructed by employing a 2mm flat probe attached to the TA.XTplus Texture Analyser (Stable Microsystems, Surrey, UK) controlled via a 5kg load cell and Texture Exponent V3.2 software. The method involves securing the membranes between two rings with 5-mm diameter hole on a raised platform. The centralised probe was then lowered and embedded onto the membrane surface according to the specified test parameters. The elastic modulus of each membrane formulation was determined and expressed as the ratio of stress exerted on the membrane sample to the amount of deformation. The data obtained from the resultant force-distance profiles was used to calculate the elastic modulus according to the following equation:

$$E = \frac{\text{tensile stress}}{\text{tensile strain}} = \frac{F}{A_o \Delta D} \qquad \text{Equation 4.1}$$

Where,

E is the elastic modulus

F is the force applied to the membrane

A_0 is the original cross-sectional area through which the force is applied

ΔD is the amount by which the membrane is extended

A factor change in modulus due to swelling and incorporation of the drug into the polymer matrix was determined for each membrane formulation according to the following equations:

$$\Delta E_{sw} = \frac{E\,\text{hydrated membrane}}{E\,\text{unhydrated membrane}} \qquad \text{Equation 4.2}$$

$$\Delta E_{drug} = \frac{E\,\text{drug loaded membrane}}{E\,\text{drug} - \text{free membrane}} \qquad \text{Equation 4.3}$$

Where,

ΔE_{sw} is a factor change in modulus due to swelling of the matrix and,

ΔE_{drug} is a factor change in modulus due to incorporaration of the drug into the polymer matrix.

Table 4.3 Test parameter settings employed for textural profiling

Test Parameter	Biaxial extensibility
Test mode	Compression
Pre-test speed	0.50mm/sec
Test speed	0.50mm/sec
Post test speed	0.50mm/sec
Trigger mode	Distance
Distance	10mm
Trigger type	Auto force
Trigger force	0.5000N
Stop plot at	Target distance

4.2.10 Analysis of the membrane surface morphology

The surface morphology and microphase organisation was investigated by scanning electron microscopy (SEM). The SEM was obtained on gold-platinum sputter coated samples using Joel JSM 840 (Tokyo, Japan). The photomicrographs were attained under an electrical potential of 15 kV by scanning fields selected at different magnifications.

4.2.11 Surface plots and constrained optimisation

Formulation constrained optimization was performed by employing a statistical model (Minitab V15®, Minitab Inc, PA, USA). Response surface plots were constructed to visually represent the influence of independent variables (PVA concentration, PVA volume and TEC volume) on the response parameters (DEE, elastic modulus and swellability). The quantities of the independent formulation variables required for preparing an optimised formulation were determined by analysing the results obtained from the *in vitro* studies performed on each formulation.

4.3 Results and Discussion

The biopolymeric formulations with varying combination of independent variables were successfully prepared according to the experimental design (Table 4.3). The formation of a PVA/PLA composite polymer may be explained on the basis that the stannous octoate in the reaction mixture induced the formation of radicals on the macromolecules of PVA and PLA.The radicals eventually initiated the formation of covalent bonds between polymer chains to forma a PLA/PVA composite polymer. Subsequent to immersion of the PLA/PVA polymer in the coagulation bath, the exchange of solvent and non-solvent occurred followed by liquid-liquid demixing by nucleation and growth of the polymer poor phase leading to the formation of the biopolymeric membranes.

Biopolymeric membranes prepared from 8%w/v PLA solution formed membranes with better mechanical properties than membranes prepared from solutions of lower or higher concentration. Phase separation in the coagulation bath occurred over a period of 24 hours. Poorly phase separated membranes characterised by a robust collapsed structure were formed when the cast solution was kept for more than 24 hours in the coagulation bath. It was observed that biopolymeric membranes with an intact organised structure were formed by using a casting solution comprising of intermediate PLA concentration and high PVA concentration. All the formulations of the experimental design yielded biopolymeric membrane formulations with similar dimensions, 1mm in thickness and 10±2mm in diameter. The membranes maintained a consistent shape (did not fold or curl) upon solvent evaporation during the drying step.

4.3.1. Mechanical properties of the membranes

Textural profiling can be regarded as a structural parameter that is related to matrix density. The elastic modulus (E) and a factor change in modulus (ΔE) for the biopolymeric membrane formulations are listed in Table 4.4. Mechanical properties of polymer solids exhibited non-linear

viscoelastic behaviour at small strains (Ward,1993). It was observed that most of the PLA/PVA biopolymeric membrane formulations from the experimental design were crystalline in nature and this meant that their mechanical behaviour would be more complicated compared to amorphous polymeric material (Tanaka et al., 1993; Lai and Bakker, 1993). The gradual and consistent application of strain or stress on the membranes via the probe mayhave eventually caused plastic deformation which could be expressed as dislocation, formation of microvoids or the slippage of crystallites (Lai and Bakker, 1995; Lin 1994).

Table 4.4 Elastic modulus and factor change in modulus for various PLA/PVA biopolymeric membranes

Formulation	E^a(Nmm^2)	E^b(Nmm^2)	E^c(Nmm^2)	ΔE_{Sw}	ΔE_{drug}
F2	1.8	-	3.1	-	1.7
F3	0.5	-	0.4	-	0.8
F4	1.5	0.8	2.4	1.9	1.6
F5	0.8	0.4	0.7	2.0	0.9
F6	5.3	1.0	8.5	5.3	1.6
F7	0.4	0.4	0.6	0.0	1.5
F8	1.5	0.8	2.4	1.9	1.6
F9	0.4	0.4	1.0	0.0	2.5
F10	2.7	0.6	4.1	4.5	1.5
F11	0.5	-	0.7	-	1.4
F12	1.5	0.8	2.4	1.9	1.6
F14	0.4	0.4	0.5	0.0	1.3
F15	0.7	0.3	1.0	2.3	1.4
F16	1.9	1.4	2.2	1.4	1.2

E^a = modulus of drug-loaded membrane
E^b = modulus of hydrated membrane
E^c = modulus of plain membrane
ΔE_{Sw}= factor change in modulus due to hydration
ΔE_{drug}= factor change in modulus due to drug loading

The backbone of the biopolymeric membranes was based on rubbery host polymer PVA onto which rigid PLLA branches were grafted possibly acting as reinforcement structures. Differences in starting material quantities as per experimental design yielded membranes of varying crystalline matrix architecture and density. As a result, the membranes demonstrated varying strength of resistance to deformation when the probe was embedded onto their surfaces. The force of resistance encountered by the penetrating probe was unique for each biopolymeric membrane formulation and this force gave information about the mechanical structure and

matrix density. Some membrane formulations showed morphing mechanical behaviour which was characterised by a drop in modulus upon hydration. This behaviour could be explained by considering that swelling may have induced phase transitions in the membranes which ultimately led to a plasticising effect. As a result there was a decrease in tensile strength and/or increased extensibility with a reduction in modulus(Jeffrrey et.al., 2008). Figure 4.1 shows the elastic modulus of different formulations upon hydration and after drug loading.

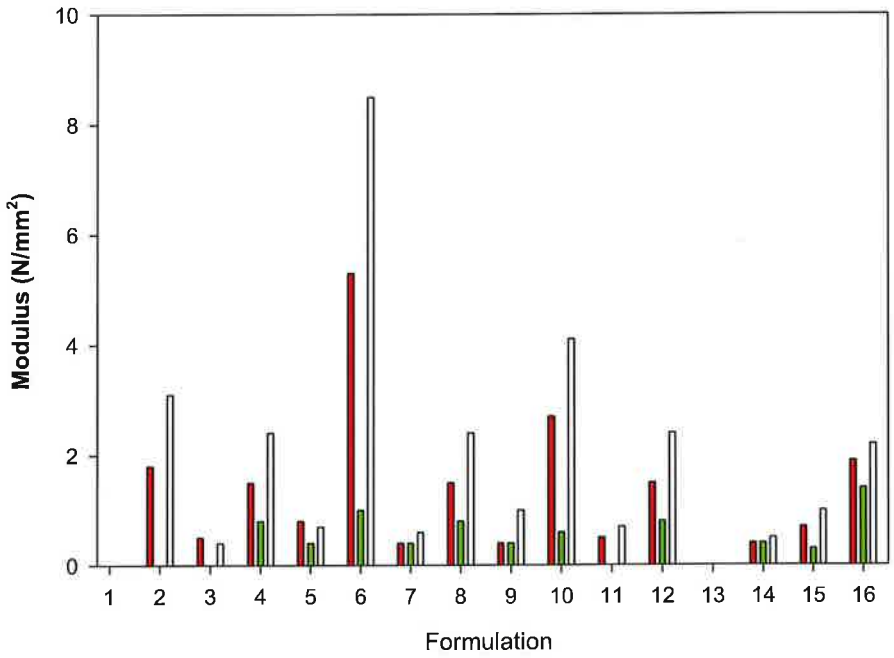

Figure 4.1 Bar graph depicting the elastic modulus for various biopolymeric membranes formulations at different physicochemical states: drug-loaded (red), hydrated (green) and drug-free (grey)

A change in modulus induced by hydration and drug loading was quantified as a factor change in modulus, which varied within different biopolymeric formulations Figure 4.2.The swollen membranes were resistant to fouling since they did not tear or break at peak forces and thus demonstrated the ability to maintain their physical structure in their hydrated state. It was also observed that there was no change in modulus upon hydration and drug loading for formulation F7 and F14 and this could have been due to delayed phase transitions. Drug loading resulted in either a reduction or increase in elastic modulus.

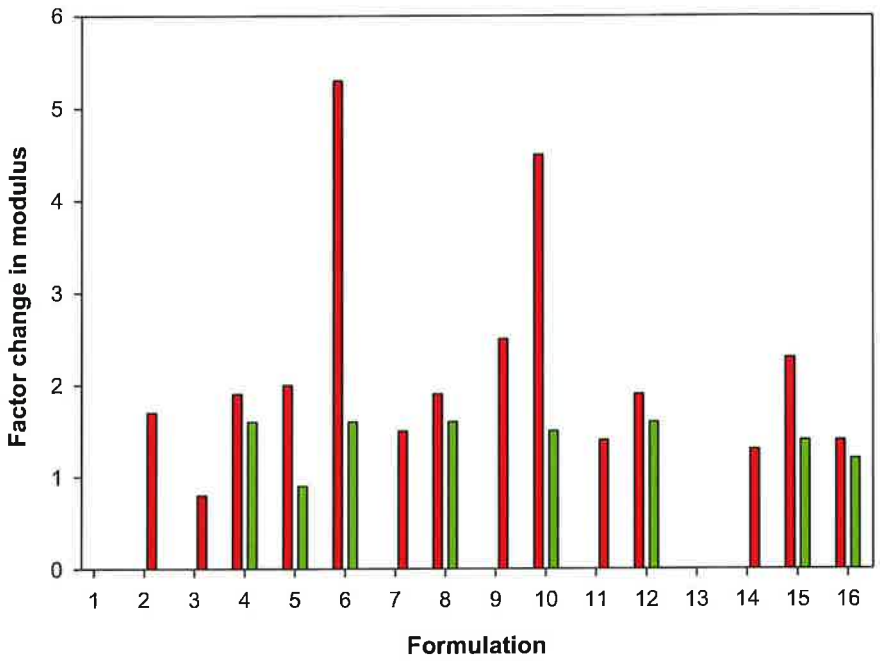

Figure 4. 2 Bar graph depicting a factor change in modulus for various biopolymeric membranes upon hydration (red) and drug loading (green).

In vitro assessment of the mechanical properties of an implantable polymer based drug delivery device is critical because it gives information on the mechanical adaptability and fouling potential. Chronic inflammation and trauma are a common result of a stiff and rigid material implanted into the brain tissue (Rutten, 2002).The inflammatory response elicited by the brain in response to the implanted material can be minimised by designing materials which closely mimic the viscoelastic mechanical properties of the brain tissue. Thus, textural profiling enabled the screening of an adaptive drug delivery device which could display an initial high degree of stiffness to allow implantation into the brain parenchyma but then soften slowly overtime and without excessive swelling upon implantation in response to the physiological environment (Szarowski et al., 2003). During pre-formulation studies, an effort must be made to identify the formulation and process parameters that would yield a device that would suite the intended site of implantation. The final formulation must be capable of temporarily bearing the mechanical stresses after implantation and eliminating any potential stress discontinuities at tissue-implant

interphase until the entire drug has been released over the required period. Most of the biopolymeric membrane formulations obtained from the experimental design demonstrated the desired viscoelastic mechanical behaviour (extensible and elastic) which would enable them to integrate well into the neural tissue without inducing undue mechanical pressure (Tian et al., 2005).

4.3.2. Swelling behaviour of the biopolymeric membranes

The biopolymeric membrane formulations demonstrated a wide array of swelling behaviour in buffer (PBS, pH 7.4) Figure 4.3. The swellability may have been mainly governed by the concentration of PVA which controlled water uptake into the matrix. Biopolymeric membrane formulations prepared from 10%w/v PVA showed enhanced swelling (25-50%) and membrane formulations prepared from 6%w/v PVA showed minimal swelling (~20%). A biopolymeric membrane prepared with highest TEC quantity (F11) showed enhanced swelling (> 50%) while F9 showed minimal swelling (~10%). From the results, it could be deduced that a low PVA concentration, low PVA volume ratio and low to intermediate TEC may be required to prepare biopolymeric membranes with low swellability.

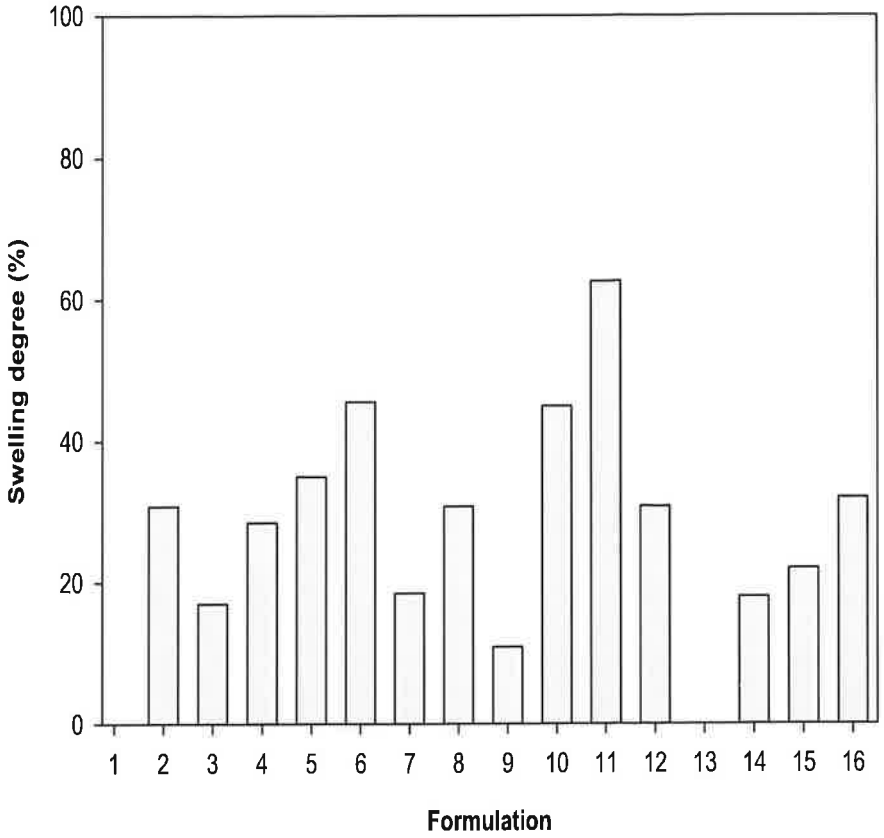

Figure 4.3 Bar graph depicting swelling potential (Sw) of various biopolymeric membrane formulations obtained from the experimental design (n=3, SD±7.2).

4.3.3. Drug entrapment efficiency (DEE) studies

The biopolymeric membrane formulations from the experimental design demonstrated good drug entrapment efficiencies which ranged between 30-97% (Figure 4.4). The low solubility of FA in the coagulation bath may have contributed to improved drug entrapment efficiencies. The strong molecular interactions between the polymer and the drug molecules may have also ensured that the drug remains conjugated within the polymer matrix. The difference in DEE within various biopolymericmembrane formulations may have been due to the differences in matrix densities and differences in initial reaction stoichiometry. Dense matrices had a greater capacity of entrapping drug molecules in their network structure, thereby significantly delaying

the diffusion of unconjugated drug molecules into the coagulation bath. During preliminary studies, it is crucial to investigate the solubility of the drug in various non-solvent bath and select the coagulation bath into which a drug is least soluble since this may have an effect on the ultimate DEE of the system. The existence molecular interactions of sufficient bond strength between the polymer and drug molecules may to some extent to improve DEE. In order to gain deeper understanding into the molecular interactions, computational chemistry tools may be employed to elucidate the type and to evaluate the bond strength of various molecular interactions that exist in a particular system.

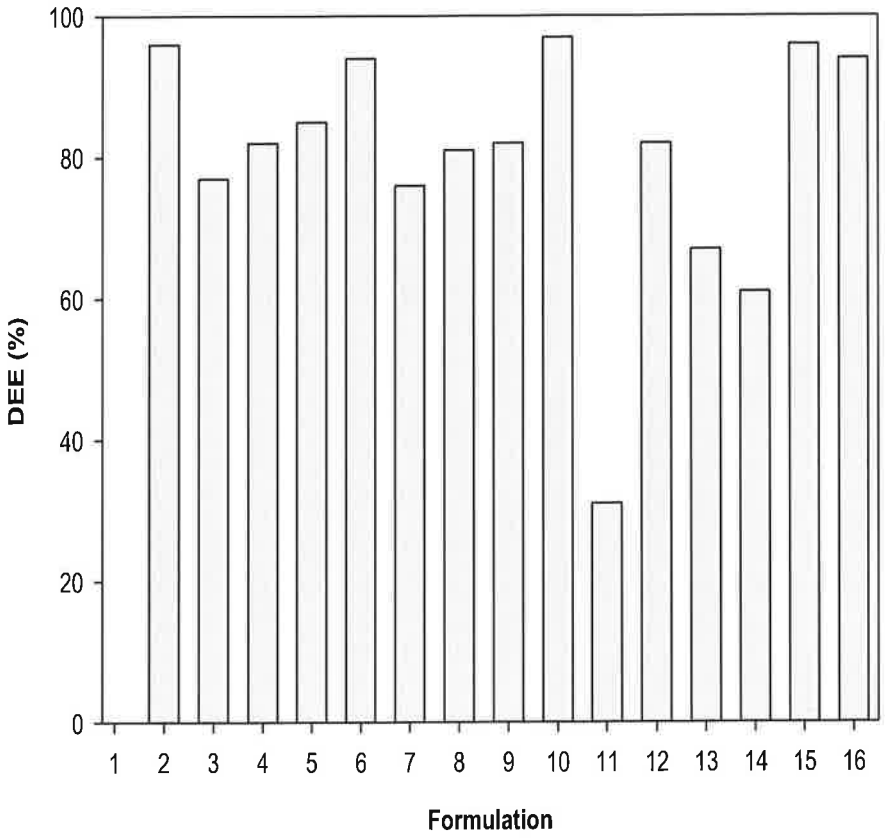

Figure 4.4 Bar graph depicting drug entrapment efficiency (DEE) of various biopolymeric membrane formulations obtained from the experimental design (n=3, SD±20.4).

4.3.4. Degradation behaviour of the PLA/PVA biopolymeric membranes

The biopolymeric membrane formulations showed biphasic degradation kinetics. The initial phase was characterized by a steep slope indicating a rapid loss in weight due to diffusion and dissolution of unreacted polymer fractions from the matrices. The second phase was characterized by a lag phase due to cleavage of hydrolytically sensitive bonds in the amphiphilic polymer structure which lead to surface erosion (Figure 4.5).

Efficient grafting of PLA chains onto the PVA backbone was achieved by increasing the PVA concentration and PVA volume ratio. The hydrophobic PLA chains may have been perpendicularly aligned onto the PVA backbone, retarding water penetration into the biopolymeric membrane. As a result, degradation at the surface was greater that the rate of water penetration. It was observed that degradation rate decreased with increasing PVA concentration. The membranes maintained a constant geometry during degradation, and this showed that the mechanism of degradation was via surface erosion.Other factors that may have contributed to differences in the degradation rate include matrix density, porosity and crystallinity.

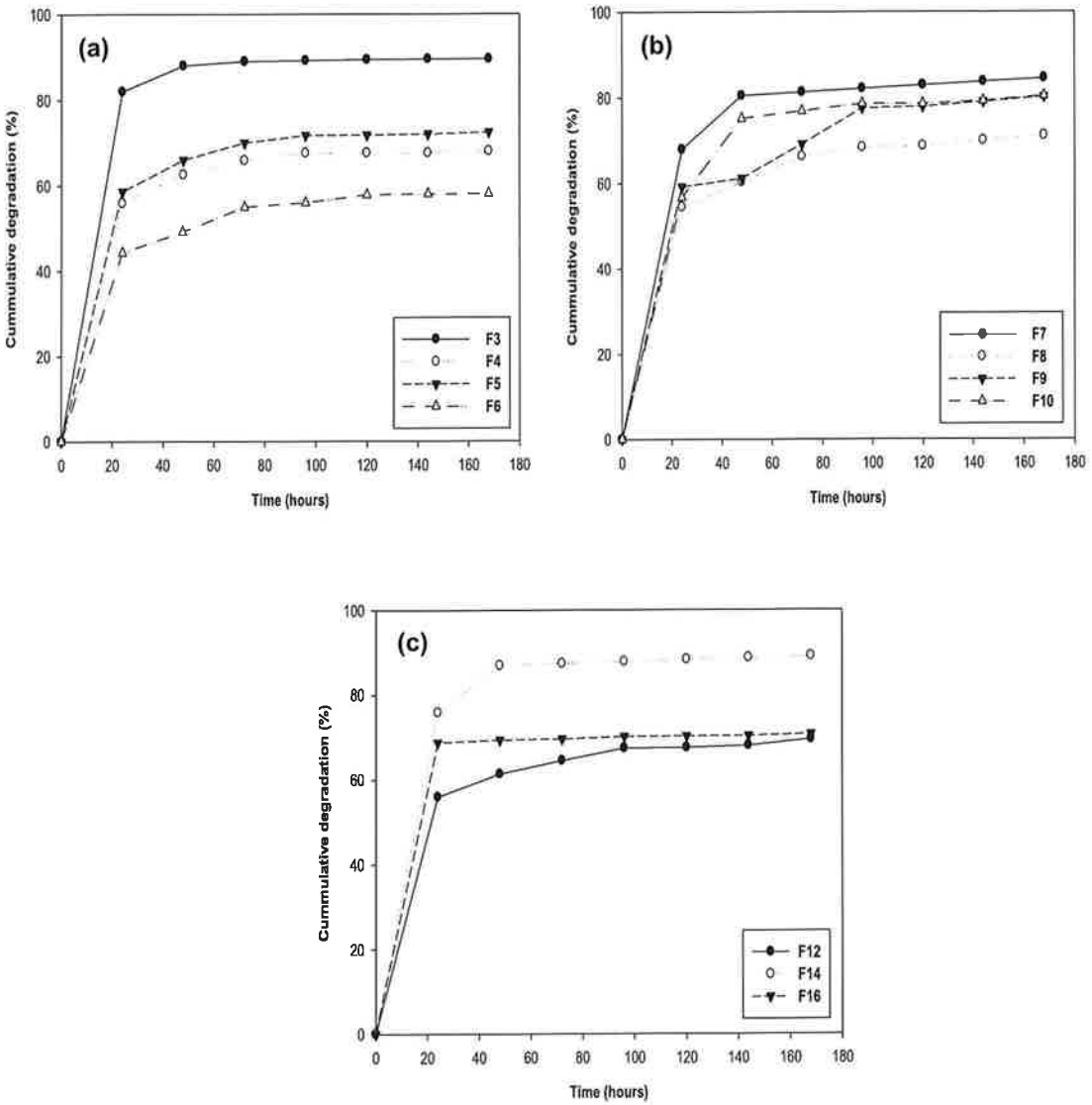

Figure 4.5 Degradation profiles for various biopolymeric membrane formulations in PBS (pH 7,4; 37°C) (a) Formulation 3-6, (b) Formulation 7-10 and (c) Formulation 12,14 and 16.

4.3.5 *In vitro* drug release studies

Drug release modulation was achieved by incorporating the FA into the matrices during formulation. Depending on the internal microstructure formed during phase separation, drug release patterns varied from one membrane to the other (Figure 4.6). In order to gain more insight into microstructure evolution which was based on interactions between drug, polymer and solvent species some researchers have developed the diffuse-interphase theory (Saylor et al., 2007). Calculations based on this theory have demonstrated that for a characteristic delivery system, variations in microstructure arising due to changes in either drug loading or processing variables could have significant impact on both bulk release kinetics and uniformity of the release across the system. The membranes displayed a wide array of drug release rates owing the evolution of various internal microstructures. Since the processing variables were kept constant, a wide array of drug release profiles could have been as a result of variations in quantities of the independent formulation variables used for preparing each biopolymeric membrane formulation. All the biopolymeric membrane formulations showed a burst release due to desorption of surface bound drug. The release of FA from formulations fabricated with 10%w/v PVA followed zero-order release kinetics. A reduction in PVA concentration resulted in the reduction in FA release with the release profiles adopting biphasicrelease kinetics. The second phase of drug release was thought to have been mainly influenced by degradation which resulted in zero order release profiles. It was observed that drug release from formulations fabricated with 10%w/v PVA was by diffusion with more than 80% of the drug released in 8 hours. Surface erosion resulting from slow hydrolysis of drug-polymer bonds controlled drug release from biopolymeric formulations fabricated with lower PVA concentrations. Some formulations (F3 and F4) fabricated with low PVA concentration, intermediate PVA volume and intermediate to high TEC showed retardation in FA release, with approximately 40% of the drug released in 12 hours. The drug binding avidity of TEC was more pronounced when the independent variables were used in this combination (low PVA concentration and intermediate PVA volume ratio).

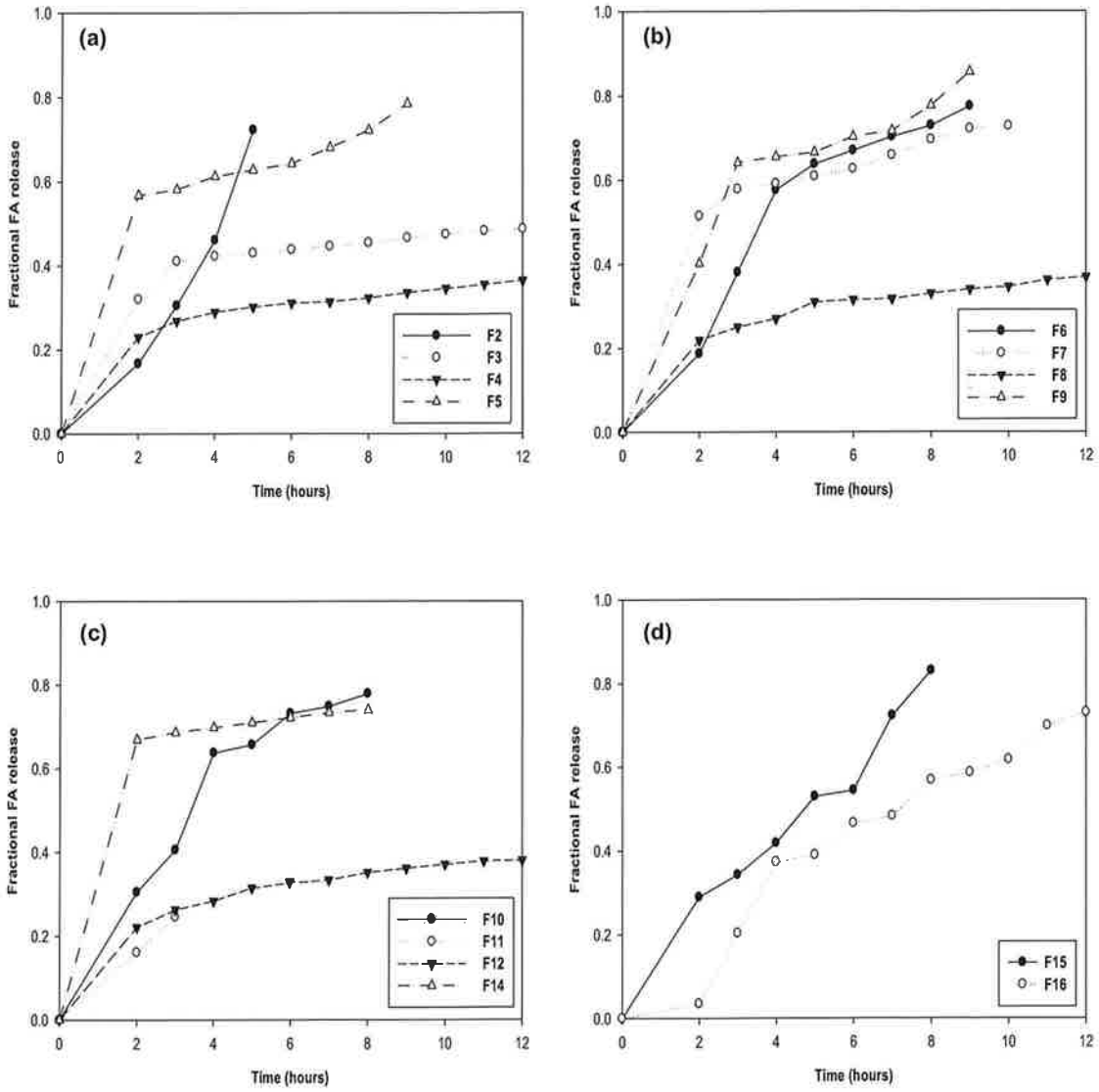

Figure 4.6 Drug release profiles for various biopolymeric membrane formulations in PBS (pH 7,4; 37°C) (a) Formulation 2-5, (b) Formulation 6-9, (c) Formulation 10-12 and 14 and (c) Formulation 15 and 16.

4.3.6. Analysis of membrane surface morphology

During immersion precipitation, liquid-liquid demixing processes are largely responsible for membrane morphology (Lim and Kim, 2002). Scanning electron micrographs showed polymeric membranes with interconnected porous cellular surface structures. Differences in morphology between the top side (Figure 4.7a) and the bottom side (Figure 4.7b) of the biopolymeric membranes were observed. The top surface showed less porosity and interconnectivity compared to the bottom side due to delay time to demixing as the diffusion of non-solvent molecules changes the composition of the polymer solution (van de Witte et al., 1996).

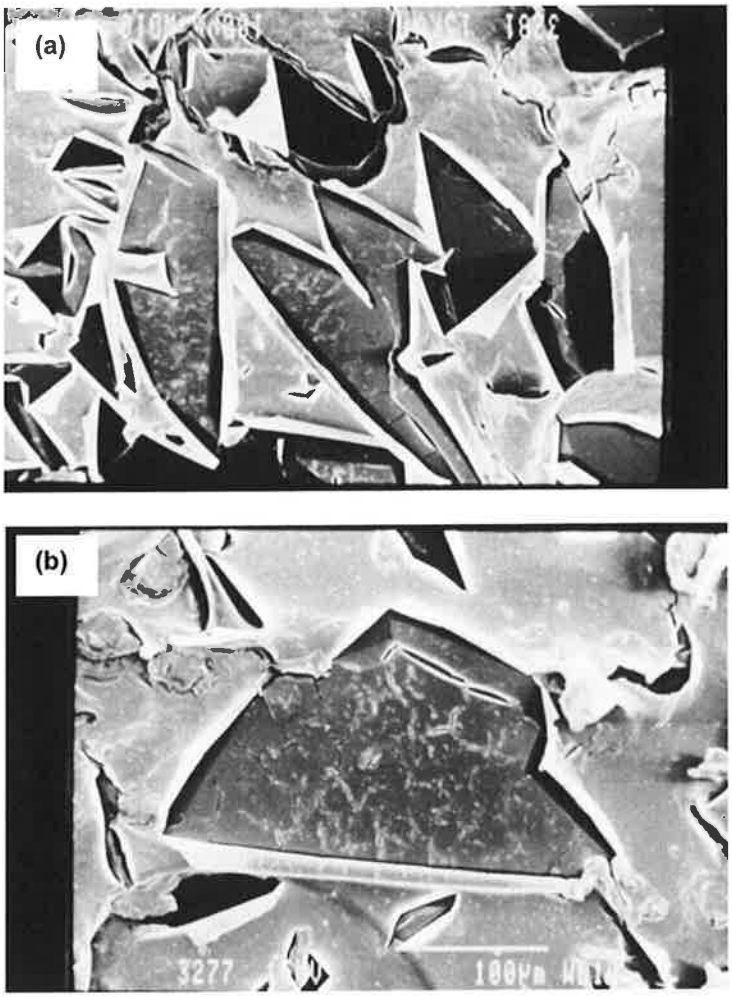

Figure 4.7 Scanning electron micrographs (SEM) depicting (a) the surface of the biopolymeric membrane that was directly in contact with the non-solvent and (b) the surface of the membrane that was in contact with the support.

4.3.7 Surface plots for drug entrapment efficiency

Drug entrapment efficiency (DEE) increased with increasing PVA concentration. A significant increase in DEE was observed at PVA concentrations greater than 8%w/v (Figure 4.8a and b). At high PVA concentrations (10%w/v), biopolymeric membranes with highly dense matrices were formed. These highly dense matrices had a greater capacity to counter act the diffusion of drug molecules into the coagulation bath. An increase in TEC concentration decreased DEE (Figure 4.8b and c). As a plasticizer, TEC increased the elasticity of the biopolymeric membranes which decreased the matrix density. At high amounts, TEC molecules may have prevented the formation of polymer-drug bonds by competing with drug molecules for the bonding site. High TEC (>2.5mL) quantities delayed phase separation resulting in biopolymeric membranes with poorly formed matrices. A combination of these factors facilitated diffusion of drug molecules into the coagulation bath. Volume ratio (PVA) had no significant influence on DEE (Figure 4.8a and c).

(a)

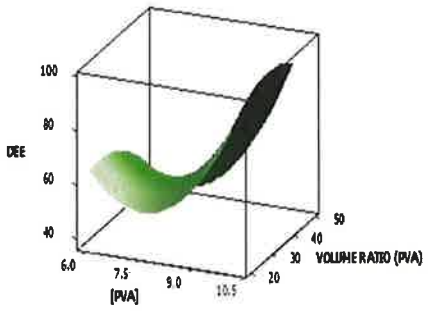

(b)

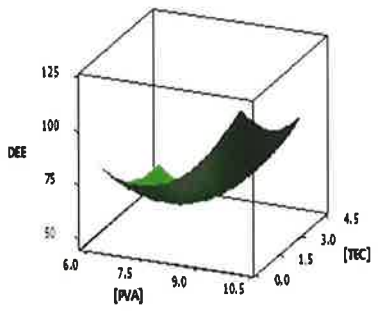

(c)

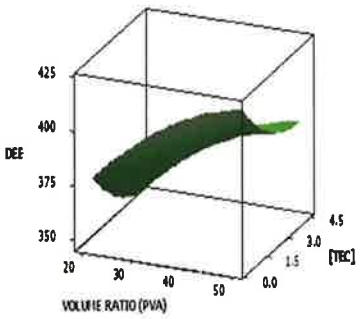

Figure 4.8 Response surface plots depicting the effect of (a) PVA concentration and PVA volume ratio, (b) the effect of PVA concentration and quantity of TEC and (c) the effect of PVA volume ratio and quantity of TEC on DEE.

4.3.8 Surface plots for matrix erosion

Matrix erosion increased with increasing PVA concentration (Figure 4.9a and b). This effect was significant at PVA concentrations greater the 8%w/v. An increase in PVA concentration increased the hydrophilic component of the composite biopolymeric membranes. As a result, the biopolymeric membranes had greater water imbibing capacity. Thus, matrix erosion was accelerated by high influx of water molecules into the system followed by hydrolytic cleavage of the highly strained bonds holding the network structure. Matrix erosion decreased with increasing PVA volume ratio (Figure 4.9a and c). Matrix erosion increased with increasing quantities TEC (Figure 4.9b and c).

(a)

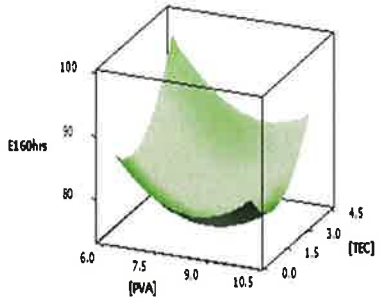

(b)

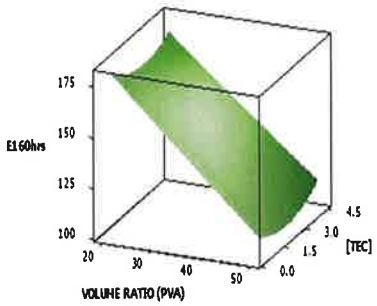

(c)

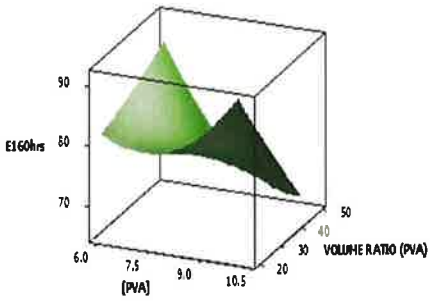

Figure 4.9 Response surface plots depicting the effect of (a) PVA concentration and quantity of TEC, (b) PVA volume ratio and quantity of TEC and (c) PVA concentration and PVA volume ratio on biopolymeric membrane erosion.

4.3.9 Surface plots for swellability of the biopolymeric membranes

The swellability (Sw) of the biopolymeric membranes increased with increasing PVA concentration (Figure 4.10a and b). An increase in PVA concentration increased the hydrophilicity and water imbibing capacity of the biopolymeric membranes. The swellability also increased with increasing PVA volume ratio and this effect was significant at intermediate (8%w/v) and higher (10%w/v) PVA quantities (Figure 4.10 a and c). An increase in the quantity of TEC increased the swellability of the membranes (Figure 4.10b and c). The plasticizing effect of TEC may have afforded the polymer chains with greater structural flexibility. As the water molecules diffused into the matrix, the chains conformed to spatial positions which reduced strains on the intermolecular bonds. Structural flexibility increased with increasing amount of TEC. Furthermore, high quantities of TEC may have lead to the formation of membranes with a poor structure and as a result, water molecules were able to freely diffuse into the matrix.

(a)

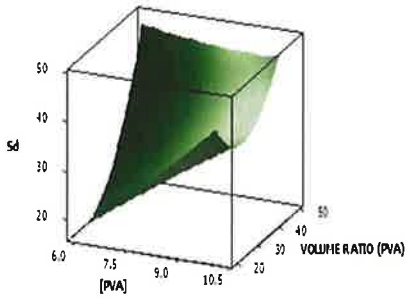

(b)

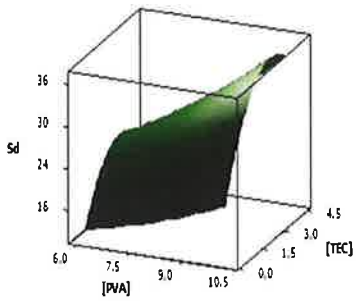

(c)

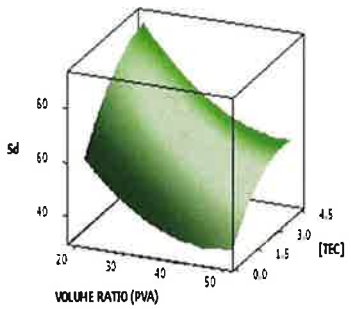

Figure 4.10 Response surface plots depicting the effect of (a) PVA concentration and PVA volume ratio, PVA concentration and quantity of TEC and (c) PVA volume ratio and quantity of TEC on the swellability of the biopolymeric membranes.

4.3.10 Constrained optimisation

Based on the results obtained from the experimental design, a desirability plot was constructed to determine the requisite formulation variables for producing an optimised PLA/PVA biopolymeric membrane (Figure 4.11). The desirability plot was carefully adjusted by varying the formulation variables in order to achieve a biopolymeric formulation with a swellability of 30%, achieving 45% matrix erosion in 160 hours and with a drug entrapment efficiency of 90%.

In order to prepare a biopolymeric membrane with the above mentioned properties, the following quantities of independent variables were as follows: PVA concentration of 8.78%w/v, PVA volume ratio of 35.15v/v and the quantity of TEC must be 0.7mL. The optimised formulation obtained demonstrated a maximum swelling of 32% and lost 65% of the weight in 160 hours and had a DEE of 94%. The results obtained for the optimised formulation were satisfactory, considering the complexity of the phase separation process especially with the lack of phase diagrams to give insight into the dynamics and boundaries involved in the system to ascertain its reproducibility.

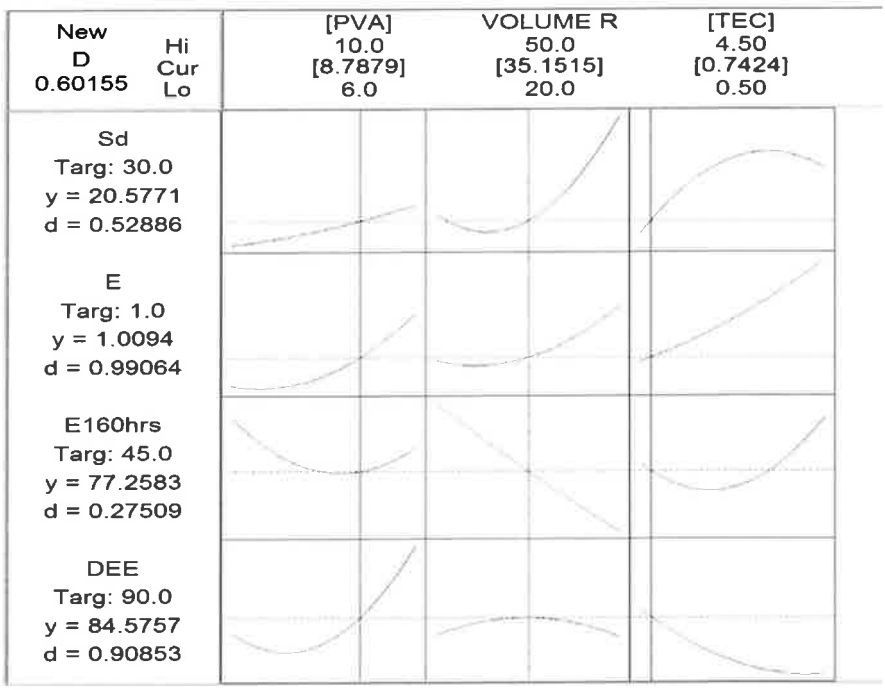

Figure 4.11 Desirability plots depicting the requisite variables for producing PVA/PLA biopolymeric membrane with desired target responses.

4.4 Concluding Remarks

PLA and PVA have been widely employed for preparing biomaterials for various medical applications. In this study, we prepared a composite polymer by reacting PLA and PVA in the presence of stannous octoate. The composite polymer was phase separated by immersion precipitation technique to form biopolymeric membranes. An experimental design was employed for preparing various formulations and in order to study the effects of formulation variables on the properties of the membranes. A desired biopolymeric membrane formulation was obtained through an optimization process. The optimised biopolymeric membrane formulation showed a desirably high degree of stiffness that would allow for handling during the surgical procedure. Once implanted, its morphing mechanical behaviour would then allow mechanical adaptability into the viscoelastic environment of the brain tissue. The viscoelastic mechanical properties resembled that of the brain tissue and thus the device demonstrated minimal potential for inducing tissue inflammation at the site of implantation. A unique balance of hydrophilicity and hydrophobicity of the composite PLA/PVA polymer prevented excessive swelling. Minimal swellability was crucial in order to ensure that that the device would not exert undue pressure to the surrounding tissue once implanted. The PLA component was responsible for the prolonging degradation while the PVA component was responsible for the elastic mechanical properties. In contrast to the bulk degrading mechanism observed with most PLA based drug delivery devices, the biopolymeric membrane degraded by surface erosion. The biopolymeric membrane demonstrated a high drug entrapment efficiency and the drug was released in a biphasic manner. Drug release was characterized by a burst effect followed by a gradual release over a period of 12 hours. The drug release form the device was induced by matrix hydration followed by the diffusion of the drug molecules across the concentration gradient. Drug release modulation was mainly due to gradual surface erosion.

CHAPTER FIVE

A COMPOSITE METHOTREXATE-LOADED NANOCARRIER FOR THE LOCALISED TREATMENT OF PRIMARY CENTRAL NERVOUS SYSTEM LYMPHOMA

5.1 Introduction

Much research has shown that for the optimal drug action, the most efficient mechanism is to deliver the drug to the desired site of action in the body while attempting to decrease or avoid the side-effects at non-target site (Li et al., 2005; Hu et al., 2008). Various drug delivery systems (DDS) such as liposomes (Hou et al., 2003), micelles (Gupta et al., 2000) and polymer micro/nanoparticles (Pignatello et al., 2002) have thus far shown much promise in controlled release and targeted drug delivery. To date, biocompatible and biodegradable polymer nanoparticles are the most preferred candidates for DDS (Soppimath et al., 2002).

Polymer based nano-drug delivery systems have had a significant impact on medical technology, greatly enhancing the efficacy of many existing drugs and enabling the construction of entirely new therapeutic modalities (Yi et al., 2005). Nano-drug delivery systems have demonstrated the ability to protect and target therapeutic compounds to the site of action and reduce the toxicity or side effects (Knight, 1981). Biodegradable polymeric nanoparticles have attracted considerable attention due to their ability to target particular organs/tissues and as potential carriers of DNA, proteins, peptides and genes (Lanza et al., 1997; Langer, 2000;). Umezwa and Eto 1998,prepared mannose-liposomes from *p*-aminophenyl-α mannoside which were able to cross the blood-brain barrier (BBB) via the glucose transporter to finally reach the mouse brain. Fenart and co-workers (1999) prepared 1, 2-dipalmitoyl-sn-glycero-3-phosphatidylcholine (DMPC)-coated maltodextrin nanoparticles which were able to cross an *in vitro* model of the BBB and this suggested an interaction of the coating with the BBB choline transporter. The physicochemical properties of nanoparticles are important parameters in

determining the physiological functions and stability of drug-loaded nanoparticles. Various reports are found in the literature on how to control the fabrication parameters so as to modulate the physicochemical aspects of drug-loaded nanoparticles for the delivery of macromolecules such as genes and proteins in therapeutics (Gan et al., 2005; Gan and Wang, 2007, Tsai et al., 2008).

So far, polymeric nanoparticles ranging in size from 10 to 1000 nm have been made from various biodegradable polymers such as polylactic acid (PLA), poly (lactic-co-glycolic acid, (PLGA), chitosan and poly (alkylcyanoacrylate) (PACA) (Gasper, 1991;Calvo et al., 1997; Gref et al., 2003). The particle size of nanoparticles is one of the most significant determinants of mucosal and epithelial tissue uptake including intracellular trafficking (Prabha, 2002). Surface charge is another important determinant in not only playing a key role in stability, mucoadhesiveness, and permeation enhancing effect of the nanoparticles (Smith et al., 2004); but also the ability of nanoparticles to escape from the endolysosomes (Panyam et al, 2002). The subcellular and submicrometer size of nanoparticles makes it possible for them to penetrate deep into tissues through fine capillaries and cross the fenestration present in the epithelial lining. This allows efficient delivery of therapeutic agents to target sites in the body (Gan et al., 2005).

PLA and PLGA have been used to prepare a great number of polymeric nanoparticles due to their biodegradability and biocompatibility (Hayes et al., 1996; Tushar et al., 2008). Nano-formulations can be administered by alternate routes such as ocular, intravenous and oral (Allemann et al., 1993; Couvreur et al., 1979; Das et al., 1995; Kumaresh et al., 2001; LaVan DA et al., 2003; Vauthier et al., 1991). Conventionally, nanoparticles (NP's) have been prepared mainly by dispersion of the preformed polymers or by polymerization of monomers (Couvreur et al., 1979; Jalil and Nixon, 1990; Kwon and Okano, 1996; Rosa, 2000). However, with years of experience into nano-fabrication, formulation of nanostructures from biodegradable polymers

still remains a challenge (Rosa, 2000; Hu et al., 2008). Some of the methods that have been proposed for the preparation of polymer nanoparticles are: solvent evaporation, nano-precipitation, crosslinking and salting-out (Fessi et al., 1989; Allemann et al., 1993;Gorner et al., 1999). Drug loading into the NP's can be achieved by incorporating the drug at the time of NP production or by adsorbing the drug after the formation of NP's by incubating them in the drug solution (Tushar et al., 2008). Couvreur and co-workers (1997), studied the adsorption of dactinimycin and methotrexate on the surface of poly(methylcyanoacrylate) and poly (ethylcyanoacrylate) and it was observed that methotrexate bound the NP's to a lesser extent.

The aim of this study was to prepare methotrexate (MTX)-loaded NP's from biodegradable polymers poly(DL-lactide) (PLA) and methacrylic acid copolymer (MAA), ensued by characterization and optimization of the formulation.

5.2. Materials and Methods

5.2.1 Materials

Poly (DL-lactide) (PLA) Resomer R203H was purchased from Boehringer Ingelheim Pharma GmbH (Germany). Methacrylic acid copolymer (MAA) Eudragit® S 100) was purchased from Degussa, Rohm GmbH, Pharma Polymers (Germany). Poly(ethylene glycol) (PEG) was purchased from Merck (Schuchardt OHG, Hohenbrunn, Germany). Sodium hydroxide (NaOH), dimethyl sulphoxide (DMSO), isopropyl alcohol and dichloromethane were purchased from Rochelle Chemicals (Johannesburg, South Africa). Methotrexate was purchase from Sigma Aldrich (St Louis, MO). All other reagents used were of analytical grade and were employed as purchased.

5.2.2 Preparation of the MTX-PLA/MAA-loaded nanoparticles

A 3-Factor Box Behnken design was applied for generating various NP formulations (Table 5.2). The NP's were prepared by double emulsion solvent evaporation technique. The internal aqueous-phase *(W1)* was prepared by dissolving 5mg of methotrexate in a 1mL solution of 0.1M NaOH. The organic phase *(O)* was prepared by co-dissolving the polymers PLA and MAA in a mixed solvent system comprising of dichloromethane and isopropyl alcohol in a ratio of 1:1. The internal aqueous-phase and the organic phase were homogenized (Polytron, PT 2000, KINEMATIKA, AG LITTAU, Switzerland) for 3min at room temperature (25±0.5°C) to form a primary emulsion *(W1/O)*. The external aqueous-phase *(W2)* was prepared by dissolving PEG in an acidic buffer (pH 2.0) to form a 2.5%w/v polymer solution. The primary emulsion *(W1/O)* was added drop wise to the external aqueous-phase *(W2)* and emulsification was continued for 10min using to form nanoparticles. The formed emulsion was centrifuged (Nison Instrument (Shangai) Limited, Shangai, China) at 15,000rpm for 10 minutes at 25°C, washed two times with deionized water and then lyophilized (LABCONCO, Kansas City, Missouri, USA) for 24 hours.

Table 5.1 Arrangement of the 3-Factor Box-Behnken Design for the PLA/MAA nanoparticle formulations.

Formulation Number	Quantity of PLA (mg)	Quantity of MAA (mg)	Ratio *W1: O* (mL)
1	2	30.0	1:5
2	6	17.5	1:6
3	2	17.5	1:6
4	4	17.5	1:5
5	4	30.0	1:4
6	6	30.0	1:5
7	2	17.5	1:4
8	4	17.5	1:5
9	4	5.0	1:4
10	6	5.0	1:5
11	4	5.0	1:6
12	4	17.5	1:5
13	4	30.0	1:6
14	2	5.0	1:5
15	6	17.5	1:4

5.2.3 Determination of size distribution, zeta potential and polydispersity index of all formulations

Particle size was measured by firstly dispersing a small quantity of nanoparticles in deionized water. The nanoparticle suspension was then filtered through a 0.22µm filter (Millipore, Billerica, USA) to remove dust particles and polymer agglomerates. The size of the nanoparticles was measured by dynamic laser scattering on a Zetasizer (Nano-ZS series, Malvern Instruments, Worcestershire, UK). For zeta potential and polydispersity index (PdI) determination,a nanoparticle formulation sample was immersed in deionized water and agitated thoroughly to facilitate nanoparticle suspension. The zeta potential and polydispersity index were then determined using a ZetaSizer Nano ZS instrument (Malvern Instruments Ltd., Malvern, Worcestershire, UK).

5.2.4 Enhancement of the drug-loading capacity of the optimised nanoparticle formulation

The optimised NP's were prepared by following the same method outlined in section 5.2.2. However it was observed that the drug loading capacity was very poor when the drug was added during preparation. In an attempt to enhance drug loading capacity, the drug was added after the preparation of the NP's. This was achieved by incubating the NP's in a concentrated drug solution. Briefly, MTX 10mg was dissolved in 0.7mL of 50% methanol containing 1% DMSO. The formed NP's were accurately weighed (80mg) and mixed with the drug solution. The resultant suspension was then placed in an oven maintained at 30°C for 24 hours. The nanoparticles were removed from the oven and dried at room temperature (25°C) for 24 hours.

5.2.5 Determination of drug entrapment efficiency of all formulations

The amount of MTX in the formulations was determined by adding the nanoparticles to 10mL phosphate buffer saline (PBS, pH 7.4) and centrifuging at 3,000 rpmfor 1 hour. The supernatant was analyzed for MTX content by UV spectrophotometry (CECIL 3021 Spectrophotometer, Cecil Instruments, Cambridge, England) at 307 nm. Drug entrapment was expressed both as drug loading (%) and drug content (%w/v) by employing equation 5.1 and 5.2.

$$\text{Drug loading}(\%) = \frac{\text{mass of the drug in the nanoparticles}}{\text{mass of the drug used in the formulation}} \times 100 \qquad \text{Equation 5.1}$$

$$\text{Drug loading}(\%) = \frac{\text{mass of the drug in the nanoparticles}}{\text{mass of nanoparticles recovered}} \times 100 \qquad \text{Equation 5.2}$$

5.2.6 *In vitro* drug release studies

In vitro release of MTX from the nanoparticles was evaluated in phosphate buffer (PBS, pH 7.4). Nanoparticles were added directly into the dissolution medium and placed in an orbital shaking incubator set at 20rpm with the temperature maintained at 37°C. At specified times, 5mL samples of the release media were withdrawn and analyzed by UV spectrophotometry (CECIL 3021 Spectrophotometer, Cecil Instruments, Cambridge, England) at 307 nm. After sampling, the media was replaced with fresh buffer (PBS, pH 7.4) solution of equal volume.It was reported in one study that this method was not very sensitive for studying rapid release formulations, but can only be used for release of formulations having the release time longer than 1 hour (Panyam and Labhasetwar, 2003)

5.2.7 Fourier-Transform Infrared Spectroscopic Investigations

The samples were scanned over a wave number range of 4000 to 650cm^{-1} in Perkin Elmer Spectrum 100 Series (PerkinElmer Life and Analytical Sciences, Inc. Waltham, Massachusetts, USA). Samples were placed on diamond crystals and processed by universal ATR polarization accessory for the FT-IR spectrum series.

5.2.8 Asessment of the size and shape of the nanoparticles

Nanoparticle size and shape was also explored using transmission electron microscopy (TEM) (JEOL 1200 EX, 120keV). Samples were prepared by placing a dispersion of nanoparticles in ethanol on a copper grid with a perforated carbon film, followed by evaporation and viewing at room temperature at various magnifications.

5.2.9 Temperature modulated differential scanning calorimetry on poly(lactic acid)/methacrylic acid copolymer nanoparticles.

Thermal analysis was performed on the constituent polymers, PLA/MAA nanoparticles using a Temperature Modulated Differential Scanning Calorimeter (TMDSC) (Mettler Toledo, DSC1, STAR^e System, Swchwerzenback, Switzerland) to assess the thermal behavioral transitions. These transitions were determined in terms of the glass transition (T_g) temperature, measured as the reversible heat flow due to changes in the magnitude of the C_p-complex values (ΔC_p) melting (T_m) and crystallization (T_c) temperature peaks which are consequences of irreversible and reversible heat flow corresponding to the total heat flow. The temperature calibration was accomplished with the melting transition of indium. The transitions of the individual polymers were compared with the transition of the composite MTX-PLA/MAA nanoparticles. Samples were weighed (5mg) on perforated 40µl aluminum pans, crimed and then ramped from −35 to 230°C on TMDSC under nitrogen atmosphere in order to diminish oxidation at a rate of 1°C /min.The instrument parameters were as shown in Table 5.2.

Table 5.2 Temperature modulated differential scanning calorimetry settings employed for thermal analysis

Segment Type	Parameter Setting
SINE PHASE[a]	
Start	-35°C
Heating rate	1°C /min
Amplitude	0.8°C
Period	0.8°C
LOOP PHASE[b]	
To segment	1
Increment	0.8°C
End	230°C
Count	436

[a] *Sinusoidal Oscillations*
[b] *Oscillation period*

5.2.10 Molecular simulation of the potential mechanisms of polymeric nanoparticle formation

Molecular Mechanics Computations in vacuum were performed using the HyperChem™ 8.0.8 Molecular Modeling System (Hypercube Inc., Gainesville, Florida, USA) and ChemBio3D Ultra 11.0 (CambridgeSoft Corporation,Cambridge, UK) on an HP Pavilion dv5 Pentium Dual CPU T3200 workstation. The decamer of Polylactic acid (PLA) and nonamer of Methacrylic acid copolymer (MAA) were generated from standard bond lengths and angles employing polymer builder tools using ChemBio3D Ultra in their syndiotactic stereochemistry as 3D models whereas the structure of Methotrexate (MTX) was built up with natural bond angles as defined in the Hyperchem software. The models were initially energy-minimized using MM+ force field and the resulting structures were again energy-minimized using the Amber 3 (AssistedModelBuilding and Energy Refinements) force field. The conformer having the lowest energy was used to create the polymer-drug complexes. A complex of one molecule with another was assembled by disposing them in a parallel way, and the same procedure of energy-minimization was repeated to generate the final models: PLA-MTX and MAA-MTX. Full geometry optimizations were carried out in vacuum employing the Polak–Ribiere conjugate gradient method until an RMS gradient of 0.001kcal/mol was reached. Force field options in the AMBER (with all hydrogen

atoms explicitly included) and MM+ (extended to incorporate non-bonded cut-offs, restraints, and periodic boundary conditions) methods were the HyperChem 8.0.8 defaults. Computational and molecular structural modeling was performed to deduce a hypothesized mechanism of nanoparticle formation and potential inter-polymeric interaction during particle formation. Semi-empirical molecular theories were used to generate predictions of the molecular structure of the materials and compute various molecular attributes on ACD/I-Lab, V5.11software (Advanced Chemistry Development Inc., Toronto, Canada, 2000)based on the inherent interfacial phenomena underlying the formation of the nanoparticles that were prepared by double emulsion solvent evaporation technique. Models and graphics based on the step-wise molecular mechanism of nanoparticle formation and polymeric transitions as envisioned by the chemical behavior and stability were generated on ACD/I-Lab, V5.11 (Add-on) software (Advanced Chemistry Development Inc., Toronto, Canada, 2000).

5.3 Results and Discussion

5.3.1 Preparation and constrained optimisation of the nanoparticles

MTX-loaded nanoparticle formulations with varying parameters were obtained by using different preparative variables of the 3-Factor Box-Behnken design (Table 5.3). The organic solvents were selected based on the influenced by the solubility characteristics of PLA, MAA and MTX. The double emulsion-evaporation technique was usedfor preparing the nanosystems (Tabata et al., 1993). Upon adding the primary emulsion *(W1/O)* to the external aqueous phase *(W2)*, the mixture *(W1/O/W2)* became turbid indicating spontaneous formation of the nanoparticles. Nanoprecipitation was induced during solvent and non-solvent exchange which occurred simultaneously with organic solvent evaporation leading to the formation of the nanoparticles. The addition of PEG in the external-aqueous phase enhanced the stability of the nanoparticle formulations. Slow addition of the primary emulsion into the external aqueous phase was crucial in order avoid the formation of polymer aggregates. In general, nanoparticle formation was

satisfactory (small particles and better yields) when polymer solution was semi-dilute at intermediate phase volume ratios. The aggregation tendency was pronounced when the formulation variables were stretched beyond the lower and upper selected limits (Table 5.4) leading to the formation of robust nanoparticles. The response parameters selected for optimising the nanoparticle formulation were size, drug entrapment/loading efficiency and the yield.The formulation variables required for preparing the desired optimized nanoparticle formulation (particle size of 313nm, yield of 85.5mg and DEE of 9.45%) were determined by computer optimisation process (Figure 5.1).

Table 5.3 Response obtained for the studied formulation variables from the 3-Factor Box-Behnken design

Formulation Number	Size (nm)	PdI	DEE (%)	Yield (mg)
1	258.2	0.255	5	69.65
2	309.8	0.371	6.6	70.45
3	211.1	0.237	5.1	54.6
4	238.2	0.365	4	63.8
5	239.5	0.289	8.9	84.0
6	286.3	0.277	8.8	86.2
7	308.4	0.413	7	67.5
8	227.3	0.297	4.0	64.2
9	274.8	0.388	5.6	56.85
10	1012	0.971	7.3	57.1
11	263.8	0.197	4.9	55.7
12	242.1	0.354	4.2	61.8
13	378.3	0.250	7.6	74.4
14	222.1	0.682	1.5	38.6
15	241.1	0.281	6	59.9
O	331	0.289	12	82.4
O1	211	0.284	98	82.4

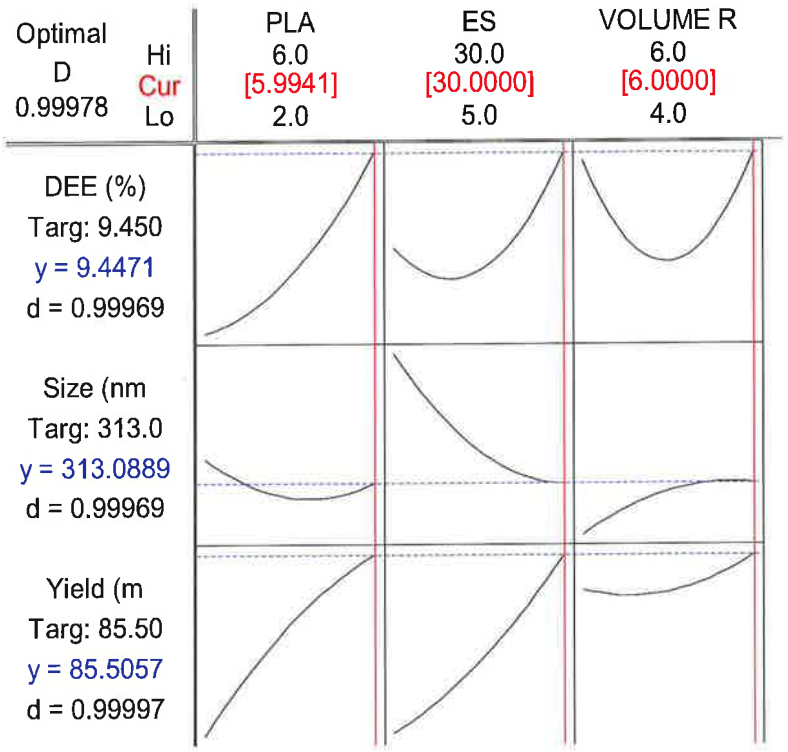

Figure 5.1 Desirability plots depicting the requisite variables for producing PLA/MAA nanoparticles with the desired targeted responses.

Table 5.4 Formulation constraints employed for the response optimization

Variables	**Limits**
Quantity of PLA	2-6 mg
Quantity of MAA	5-30mg
Ratio *(W1/O)*	1:4 – 1:6

5.3.2 Effects of formulation variables on the size of the nanoparticles

Particle size is an important parameter of the nanoparticles since it affects drug loading and drug release (Legrand et al., 2007). The size of the nanoparticles from the design varied from 211nm and 378.3nm (Figure 5.2a). The formulations displayed poly dispersity index (PdI) values of less than 0.5 which was an indication of homogenous nanoparticle size distribution. The size distribution measurement showed that the size of the optimized nanoparticles was 331nm which deviated slightly from the target (Figure 5.2b). It was observed that the size of the optimized nanoparticles was reduced to 211nm upon incubating the nanoparticles in a

concentrated MTX solution in an attempt to improve the drug loading (Figure 5.2c). This effect was thought to be caused by the insolubilities of the native polymers in 50% methanol which resulted in the shrinkage of the nanoparticles. The reduction in size could have further been enhanced by the evaporation of the volatile solvent from the surface of the nanoparticles during the drying phase.

Response surface plots showed that an increase in the amount of PLA resulted in an increase in the size of the nanoparticles (Figure 5.3a and b). An increase in the amount of MAA had an antagonistic effect and resulted in a decrease in the size of the nanoparticles (Figure 5.3a andc). The phase volume ratio had no significant influence on the size of the nanoparticles (Figure5.3b and c). This was further evidenced by the size distribution residual plots (Figure 5.3d).

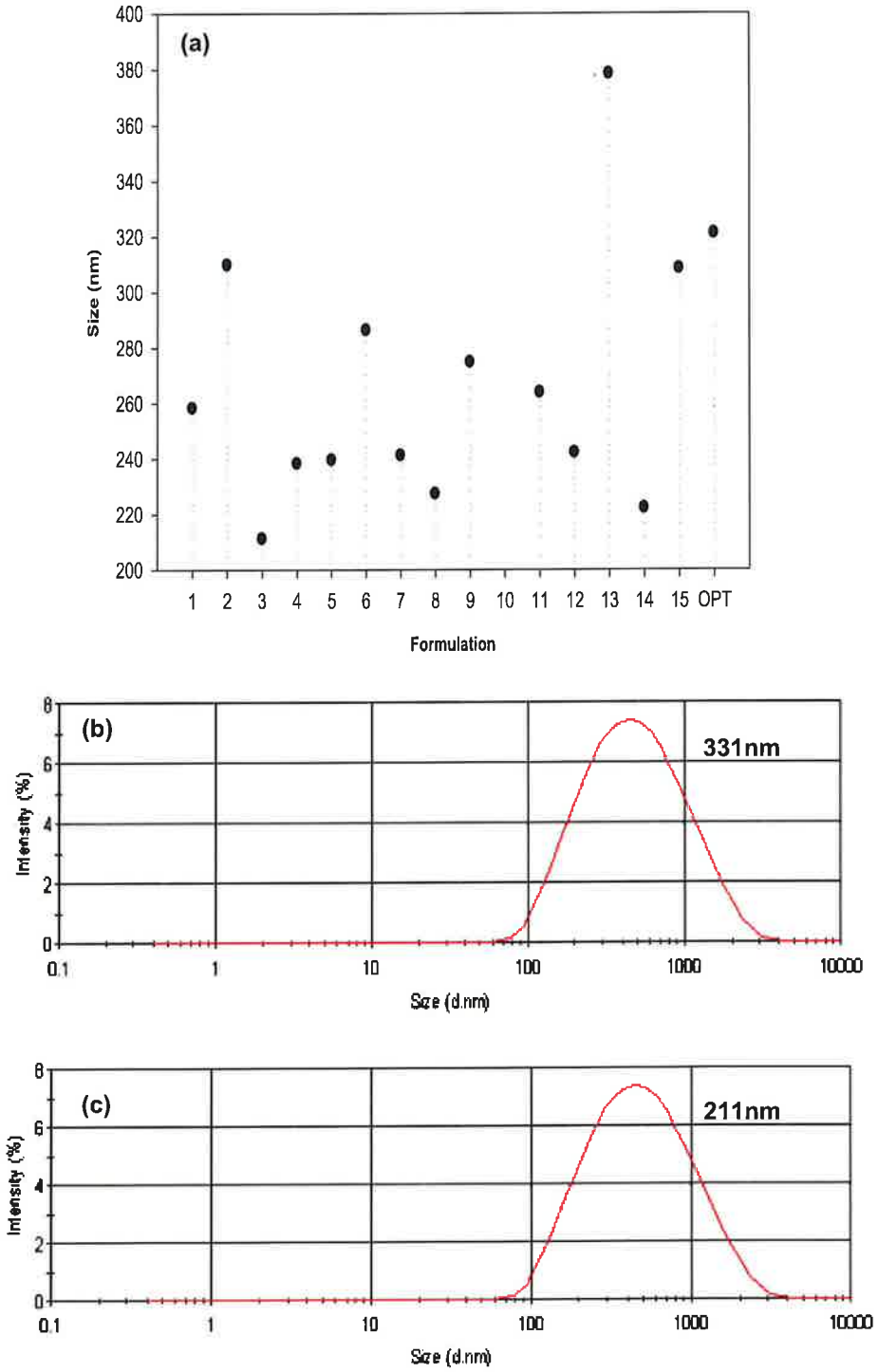

Figure 5.2 (a) Size-plot depicting the sizes of different PLA/MAA nanoparticle formulations, (b) monomodal size distribution for the optimized PLA/MAA nanoparticle formulation (n=3, SD≤1.53) and (c) monomodal size distribution for the final PLA/MAA formulation (n=3, SD≤1.0).

(a)

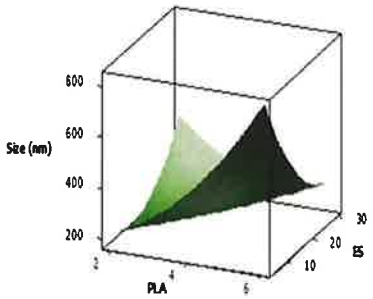

(b)

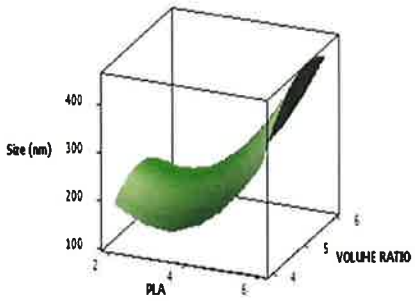

(c)

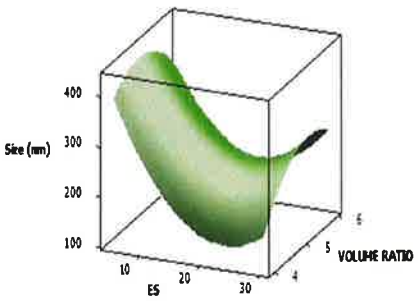

Figure 5.3 Response surface plots depicting the effect of (a) quantity of PLA and quantity of ES (MAA), (b) quantity of PLA and phase volume ratio and (c) quantity of ES (MAA) and phase volume ratio on the size of the nanoparticles.

5.3.3 Effect of formulation variables on the zeta potential of the nanoparticles

The zeta potential values ranged from -0.048 to -1.07. These relatively low values of zeta potential indicate that the PLA/MAA NP's were not stabilized by electrostatic repulsion forces which might be one of the reasons for the aggregation tendency of the particles. However, this was not a problem of major concern since the NP's were meant to be incorporated into a matrix for implantation as opposed to intravenous administration.

5.3.4 Effect of formulation variables on the drug entrapment efficiency of the nanoparticles

All formulations from the experimental design showed poor drug entrapment efficiency (DEE) (Figure 5.4). Efforts to improve DEE by optimization process proved futile with only 12% of MTX entrapped in the optimized formulation. The possible reason for poor DEE was that, blending of PLA and MAA did not lead to the formation of an amphiphilic polymer which self-assembles into spherical nano-systems of core-shell structure during homogenization (Kwon and Okano, 1996). As a result, a high amount of drug molecules remained in solution during phase separation. Thus, an alternative approach aimed at improving the drug entrapment efficiency was investigated. Huafang and co-workers (2005) have shown that drugs can be loaded onto the particles and become more stable through adsorption on the surface of PLA nanoparticles. In this view, this method was adopted to improve the drug entrapment efficiency of the optimized formulation by incubating the nanoparticles into a concentrated MTX solution and allowing them to cure in an oven at 30°C for 24 hours. By so doing, the drug loading capacity of the final formulation was significantly improved to 98%. Surface plots showed that an increase in the quantity of the polymers in the formulation increased DEE (Figure 5.5a and b) and (Figure 5.5c). Drug entrapment efficiency decreased when the formulations were prepared with a primary emulsion consisting of an intermediate phase volume ratio (1:5) and increased when the primary emulsion consisting of a lower (1:4) or higher (1:6) phase volume ratio was used (Figure 5.5b and c). Residual plots for DEE are shown in Figure 5.5d.

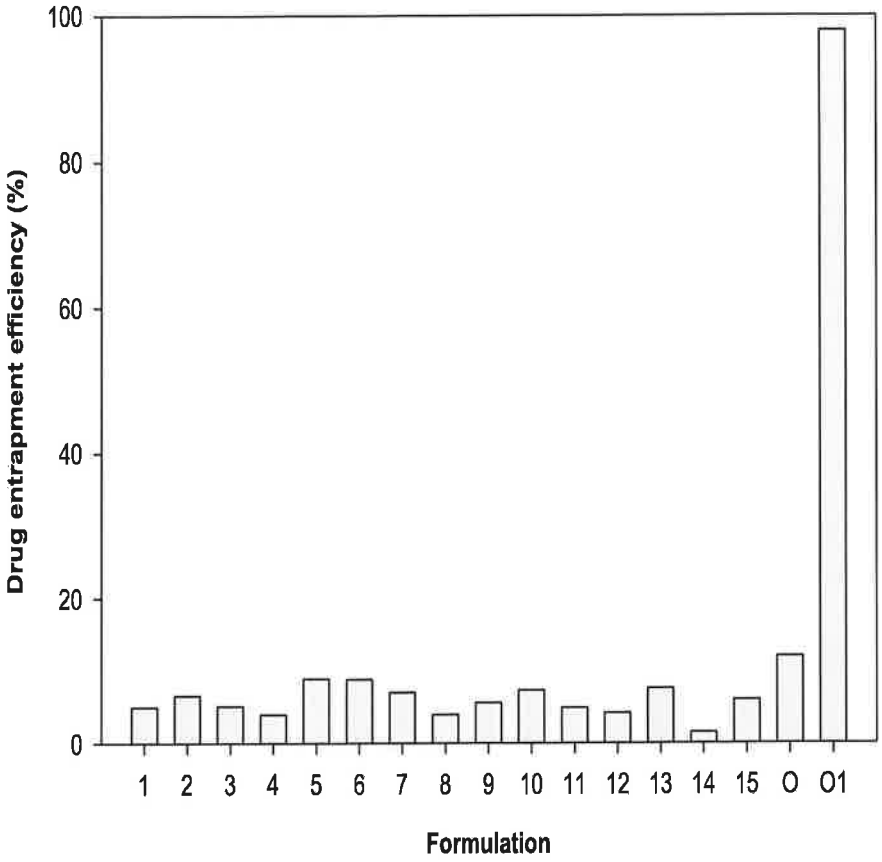

Figure 5.4 Bar-plots depicting differences in DEE within various PLA/MAA nanoparticle formulations.

(a)

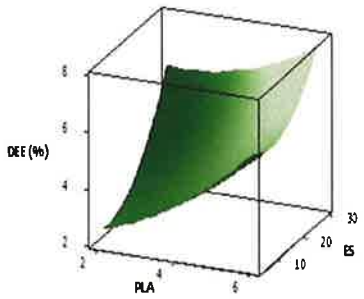

(b)

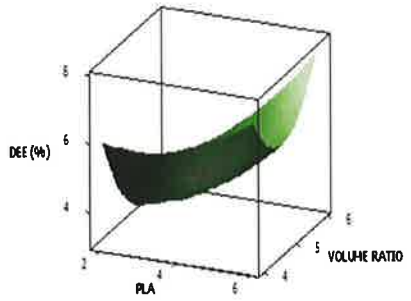

(c)

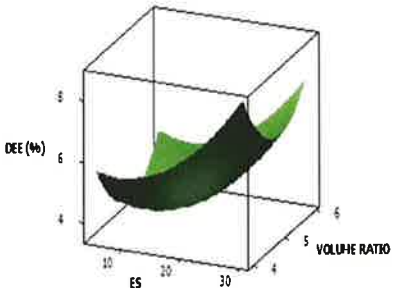

Figure 5.5 Response surface plots depicting the effect of (a) quantity of PLA and quantity of ES (MAA), (b) quantity of PLA and phase volume ratio and (c) quantity of ES (MAA) and phase volume ratio on theDEE of the nanoparticles.

5.3.5 Effect of formulation variables on the yield of nanoparticles

The yield of the nanoparticles from the experimental design was directly proportional to the amounts of starting polymer material used and ranged between 36.8mg and 86.2 mg (Figure 5.6). The yield for the optimized formulation was 82.4mg, and very close to the target of 85.5mg. Response surface plots showed that an increase in the amount of PLA had a slight increase in the yield of the nanoparticles (Figure 5.7a). Increase in MAA resulted in a significant increase in

the yield of the nanoparticles (Figure 5.7a and c), while the phase volume ratio had no significant influence on the yield of the nanoparticles (Figure 5.7b and c). Residual plots for the yield are displayed in Figure 5.7d.

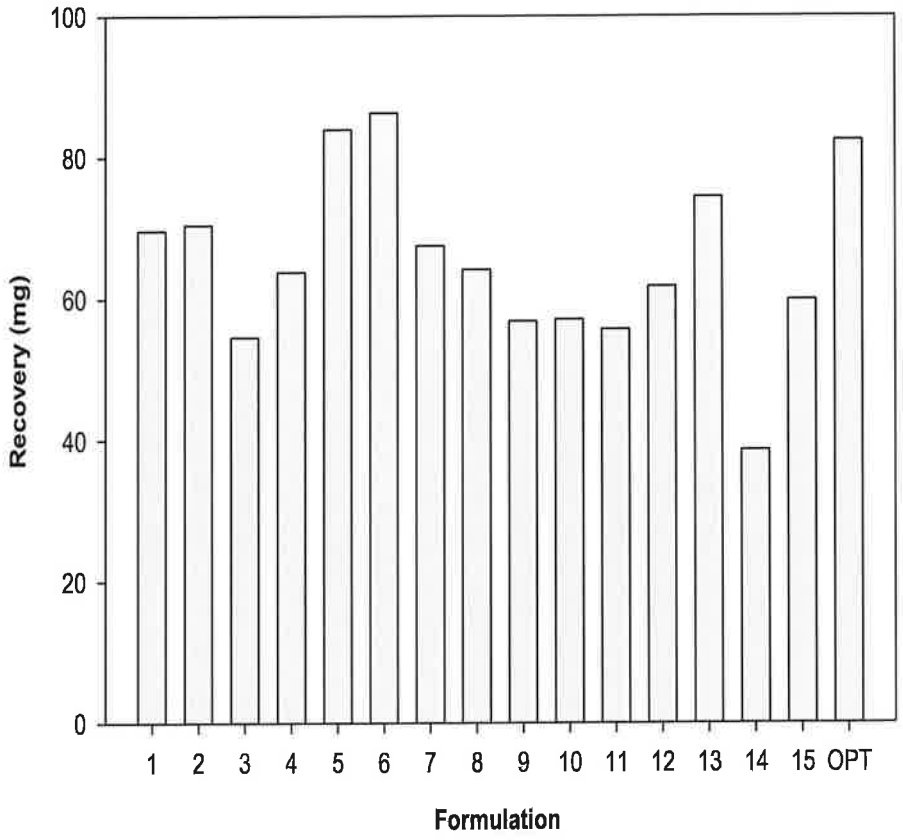

Figure 5.6 Bar chart plots depicting differences in the yield within various PLA/MAA nanoparticle formulations.

(a)

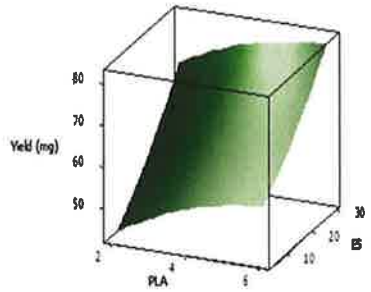

(b)

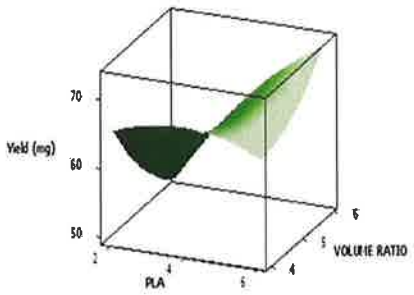

(c)

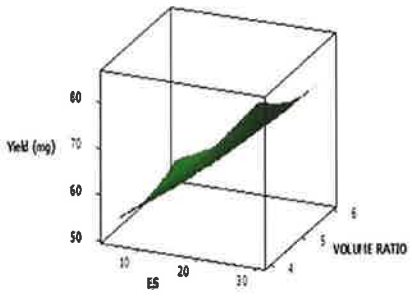

Figure 5.7 Response surface plots depicting the effect of (a) amount of PLA and amount of ES (MAA), (b) amount of PLA and phase volume ratio and (c)amount of ES (MAA) and phase volume ratio on the yield of nanoparticles.

5.3.6 Fourier Transform Infrared Spectroscopic Investigations

The spectra of the drug-free and MTX-loaded optimized nanoparticle formulations corresponded to those of the native polymers (Figure 5.8 and 5.9). This observation showed that the polymers underwent minimal chemical change during processing. Therefore, we expected the NP's to display chemical properties which were representative of the individual native polymers. Differences were noted in FT-IR spectra between the drug-free and the MTX-loaded nanoparticle formulations (Figure 5.9c). The extra peaks that were observed in the drug-loaded formulation were attributable to the presence of a 1, 3 substituted compound (1509.36-1466.67 cm^{-1}) and a phenyl amino compound (1633.22-1604.09cm^{-1}). Thus this showed that MTX was adsorbed to the nanoparticles either by weak H-bonds formed between the carboxylic groups of MTX and the hydroxyl groups of MAA, or by ionic bonds formed between the amine groups of MTX and the carboxylic groups found in both polymers. It was thought MTX was dispersed in the polymeric matrix in its microcrystalline form without polymorph change or transition into an amorphous form.

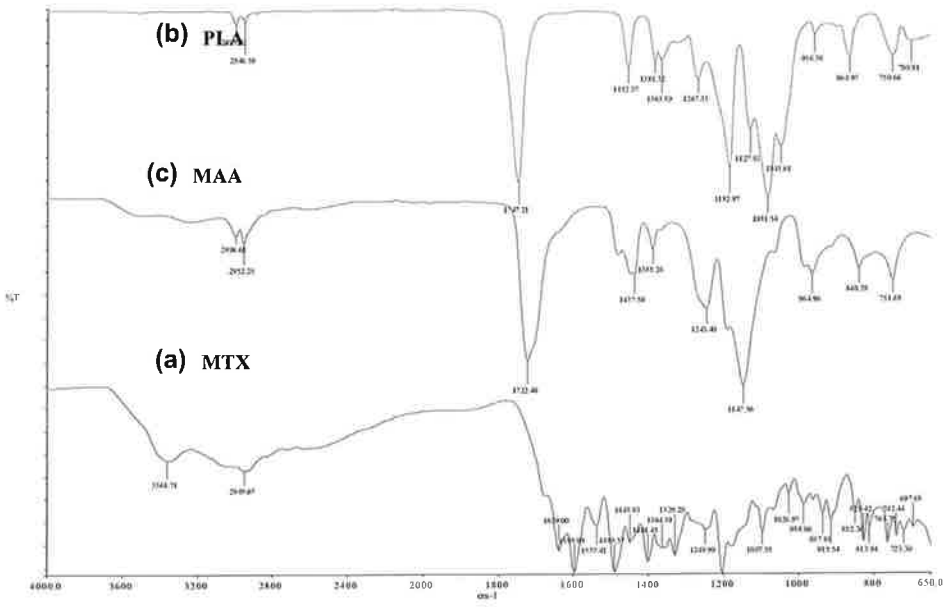

Figure 5.8 FT-IR spectra of (a) methotrexate (MTX), (b) poly(DL-lactide) (PLA) and (c) methacrylic acid copolymer (1:2) (MAA).

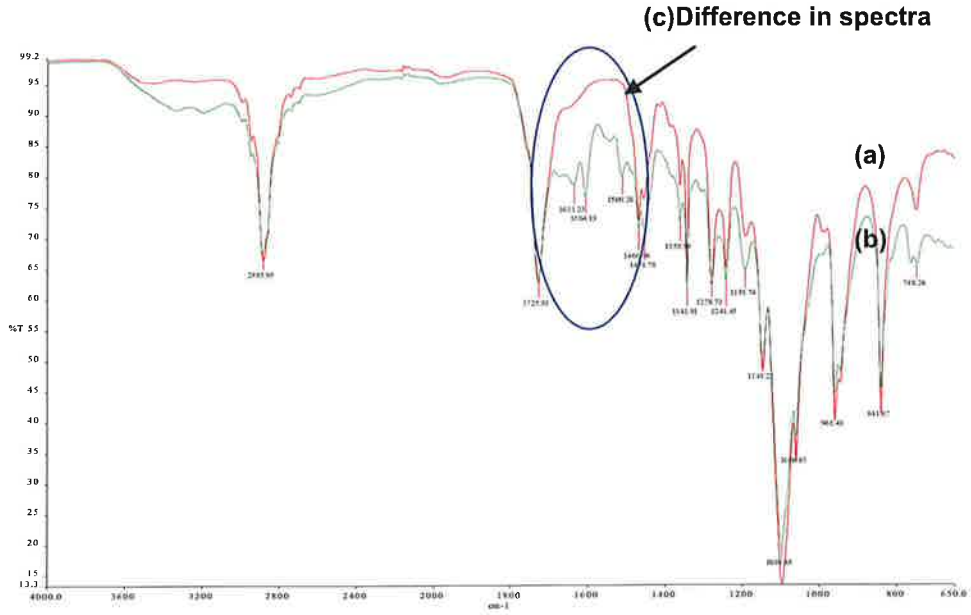

Figure 5.9 FT-IR spectra of (a) drug-free PLA/MAA nanoparticles, (b) MTX-loaded PLA/MAA nanoparticles and (c) the difference in the spectra.

5.3.7 *In vitro* drug release studies

In vitro dissolution test indicated a controlled release profile of MTX from the final nanoparticle formulation. As discussed earlier in FT-IR studies, the polymers underwent minimal chemical or no chemical transformation during the preparation of the nanoparticles. Therefore, the drug release mechanism was to some extent governed by unique behavior of the constituent polymers in the release media. MAA is an ionic polymer that is slowly soluble in neutral to weakly alkaline media. (Jain et al., 2005). PLA is a pH independent polymer that degrades very slowly in weakly alkaline media. Drug release occurred by diffusion of drug molecules from the polymer matrix and followed a biphasic pattern (Figure 5.10). The first phase was attributed to the diffusion of drug molecules that were weakly adsorbed onto the surface of the nanoparticles accounting for 50% of the drug released in 24 hours. Modulation in drug release occurred during the second phase as a result of bond hydrolysis for which the subsequent release of MTX molecules dispersed in the inner matrix (Figure 5.10). The insolubility of MAA in the media prevented rapid matrix hydration and complete polymer chain relaxation. As a result, the polymer matrix maintained a tight interconnected network structure and retarded the diffusion of

drug molecules. PLA imparted the nanoparticles with a certain degree of hydrophobicity and its presence reduced the rate of matrix hydration by delaying the penetration of water molecules. The slow rate of hydration, relaxation and degradation of the polymers in the dissolution media resulted in prolonged drug release for over 84 hours (Figure 5.10).

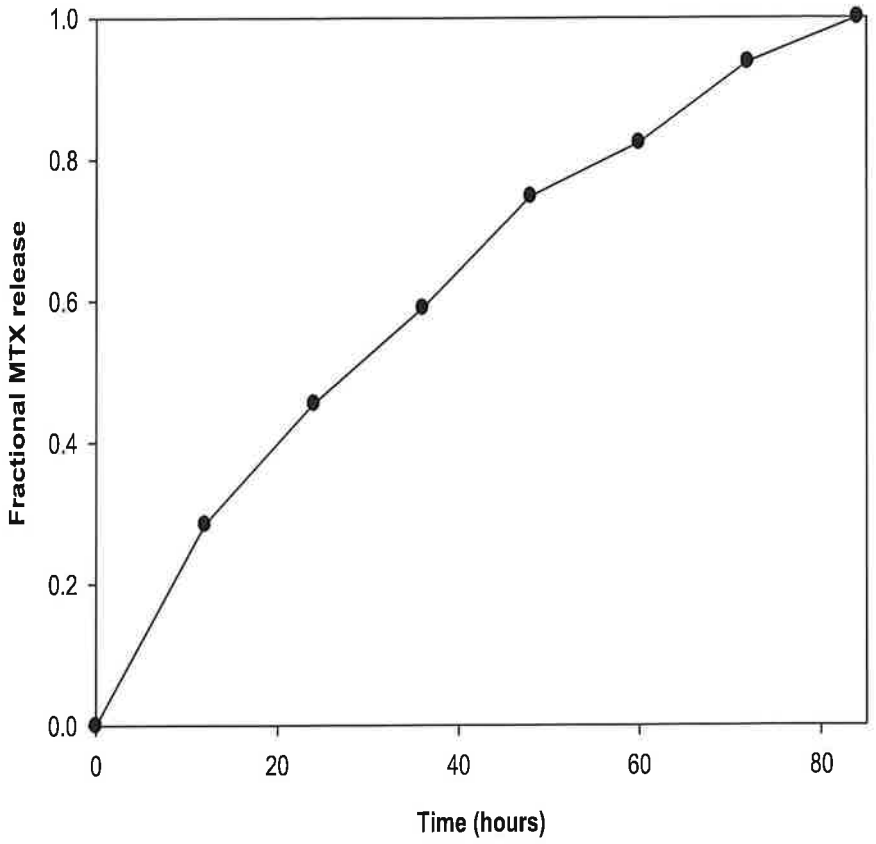

Figure 5.10 Release profile of MTX from an optimized PLA/MAA nanoparticle with highest drug incorporation efficiency (n=3, SD≤0,34).

5.3.8 Morphological characterization of the nanoparticles

Transmission electron micrographs revealed the presence of nanoparticles with almost spherical shape. The micrographs also confirmed the formation of matrix-type nanoparticles with isolated areas of core and shell structure which appearerdas clear areas in the micrograph (Figure 5.11).

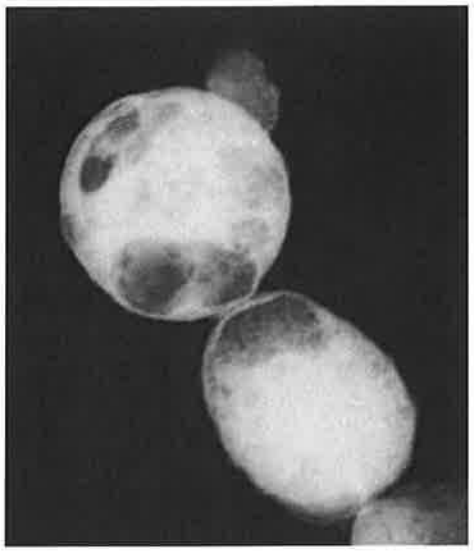

Figure 5.11 Transmission electron micrograph (TEM) of the PLA/MAA nanoparticles (Scale: 10mm=100nm).

5.3.9 Temperature modulated differential scanning calorimetry on poly(lactic acid)/Methacrylic acid copolymer nanoparticles

The thermal stability of PLA/MAA NP's was investigated by temperature modulated DSC (TMDSC), in the temperature range of 35-230°C. With TMDSC, the effects of baseline slope and curvature for the analysed samples became reduced thereby increasing the sensitivity of the system. Overlapping events such as molecular relaxation and glass transitions could be easily separated. With TMDSC it was also possible to directly measure the *Cp*. TMDSC utilizes sinusoidal temperature modulations with constant heating and cooling rates typified by short small amplitudes that were able to unveil and distinguish important hidden, overlapping thermal events which the conventional DSC would not show.

The theoretical T_g for PLA lies between 50-80°C while T_m lies between 173-178°C (Narladkar et al., 2008). MAA has a theoretical T_m of 100°C and a T_g that ranges ranges from 85-165°C (Goh et al., 1990). The signals for glass transition and for the melting of PLA/MAA composite appear in the reversing heat flow signal of the MDSC thermograms (Figure 5.12). As seen clearly, The TMDSC resulted into a *Tg*of 40°C(Figure 5.12) (i.e. lower than for both PLA and MAA indicating

a shift to lower temperatures which is typical of PLA (Lucke et al., 2000), due to being a relatively stiff and brittle polymer with low deformation at break (Krishnamachari et al., 2009).
It is also possible that the deconvolution of the total TMDSC signals for the PLA/MAA nanoparticles in reversing and non-reversing events were lower than either of the two polymers. This is an indication that the melting component could have been predominantly reversing, which could have resulted from the concurrent re-crystallization and melting phenomena offsetting each other due to solid-to-solid phase transition during heating. The total heat flow, reversing, non-reversing, *Cp* inphase and *Cp* outphase curves showed a very close association with the glass transition and relaxation phenomena of the amorphous PLA region.

The exothermic and endothermic non-reversible events occurred simultaneously. This thermal behavior might have contributed to the controlled drug release effect that was obtained since the permeability of the adsorbed drug decreases as the polymer changes from amorphous or glassy solid state to crystalline state. The controlled rate of drug release would have most certainly been due to subsequent formation of dense polymer matrix after mixing PLA and MAA polymers.

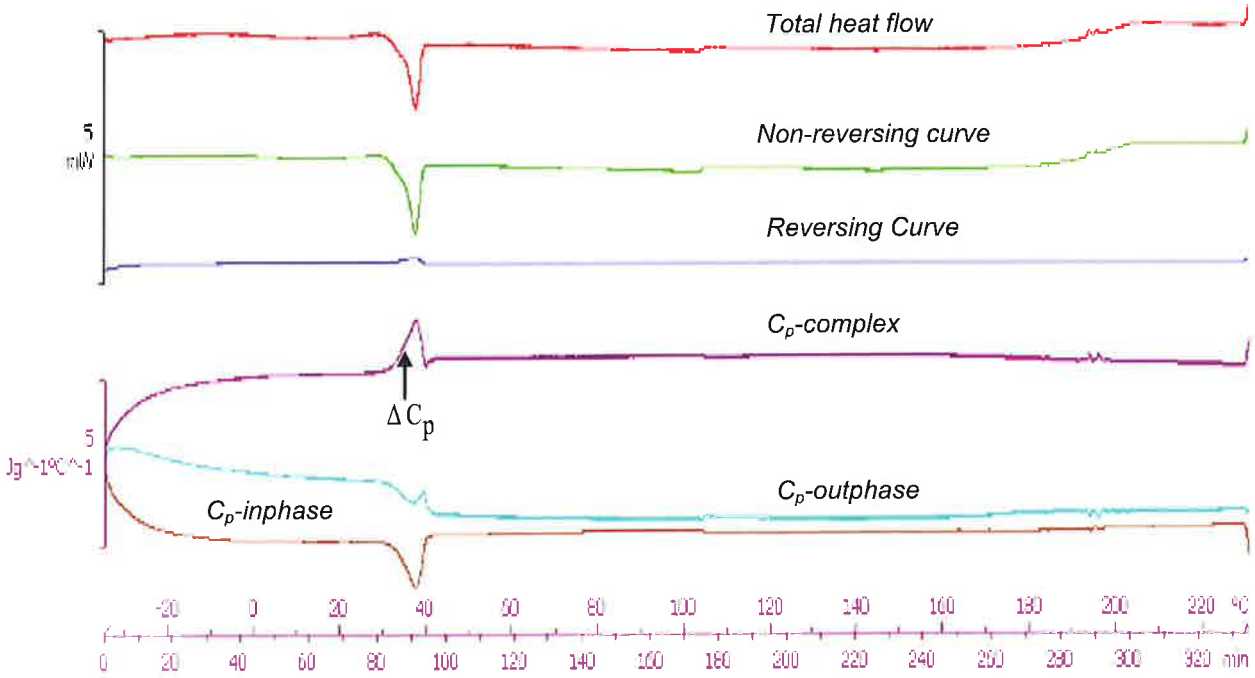

Figure 5.12 Temperature modulated DSC thermograms of PLA/MAA nanoparticles showing the endothermic and exothermic peaks generated from the reversible, non-reversible, total heat flow curves, and the *Cp*-complex, outphase and inphase profiles that generated the reversible curves.

5.3.10 Molecular simulation of the potential mechanisms of polymeric nanoparticle formation and characterization thereof

Computational modeling methods were used for the prediction of preferred molecular conformations of the drug-polymer complexes using force field minimizations and the modes of interaction were envisaged in relation to the increase in drug loading/encapsulation efficiency by adsorption and FT-IR investigations. The monomer length for the polymer chain depicting molecular structures of PLA and MAA were determined on the basis of equivalent grid surface area (Table 5.6) covered by the polymers so that the inherent stereo-electronic factors at the interaction site can be perfectly optimized. The set of low-energy conformers that were in equilibrium with each other was identified and portrayed as lowest energy conformational model. The low-energy conformers of the PLA-MTX and MAA-MTX, that were in equilibrium with each other following molecular mechanics simulations, are depicted in Figure 5.13 and the possible component binding energies, and the intrinsic molecular attributes to which they would

be responsive, are listed in Table 5.5. Invariant factors common to mathematical description of binding energy and substituent characteristics have been ignored. It is evident from the energy values that the MAA-MTX complex is stabilized by a binding energy of 13.753 kcal/mol as compared to 5.192 kcal/mol in case if PLA-MTX. These energy optimizations were supported mainly by the van der waals interactions between the drug and the polymer molecule. Here, the MAA-MTX was stabilized with van der waals forces by a magnitude of 14.488kcal/mol as against of 6.954kcal/mol in PLA-MTX. This spatial preference of MAA over PLA is also depicted in the Figure 5.13a where a deeper inspection revealed the close proximity of the MTX and MAA molecules. This was further confirmed by the surface-to-volume ratios (SVR) of the complexes (Table 5.6) with MAA-MTX having lower SVR than PLA-MTX. The lower the SVR, the more stable is the structure. Furthermore, a significant contribution was also provided by the strong H-bonding in MAA-MTX with a bond length (Figure 5.13a) of 2.6454A° and the energy value exceeding by almost 50 times as compared to PLA-MTX. These interactions involving the non-bonded attractive forces may induce dipoles in the complex where the binding energy changes may be proportional to the polarizability of the substituents, which are in turn proportional to molar refractivity values where the structure with lower index of refraction is more stable. MAA-MTX was hence highly stabilized in comparison to the PLA-MTX (Table 5.6) with reference to refractivity.

The above findings corroborated with the drug loading/entrapment efficiency which indicated that drugs can be loaded onto the particles and become more stable through adsorption on the surface of PLA nanoparticles as depicted in Figure 5.13c. Furthermore, the predicted FTIR results were confirmed via the formation of amide linkage between C-O and N-H group of MTX and MAA or PLA respectively. Although, PLA-MTX complex is less stable, the energy values, molecular attributes and geometrical orientation are quite comparable with of that of MAA-MTX. The molecule of MTX displaying an energy minimized extended conformation was found to be lying over the top of a folded PLA molecule (Figure 5.13c). Deeper inspection of the system

revealed that the nitrogen atoms of MTX were in close interaction with the oxygen atoms of the carboxylic groups of PLA oligomer. These findings support the hypothesis of charge–dipole and dipole–dipole interactions between the drug and the polymers. This could also explain the high propensity of PLA-MAA to adsorb methotrexate.

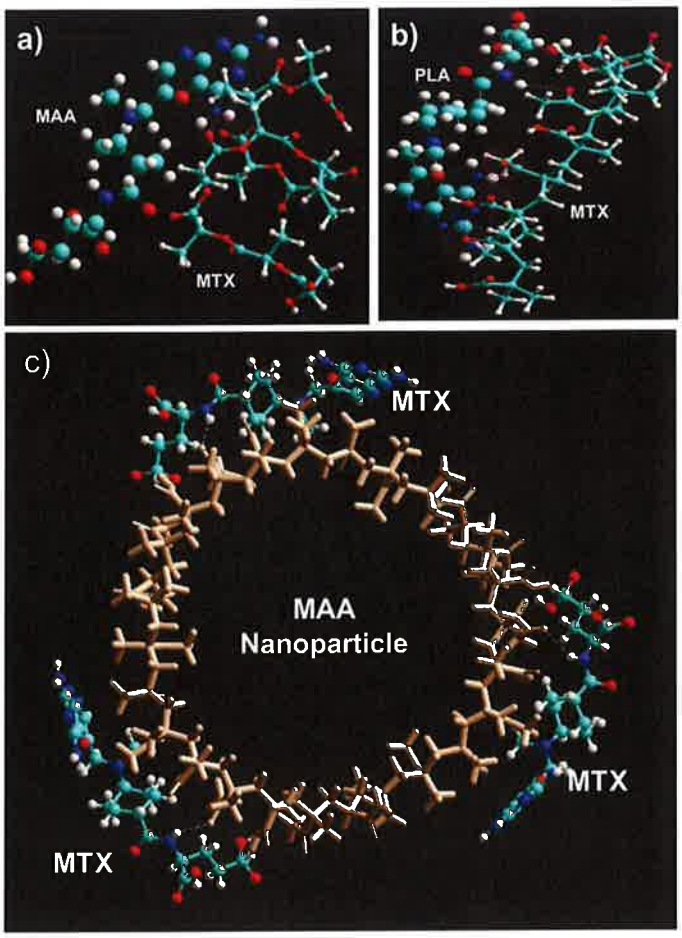

Figure 5.13 Energy minimized geometrical preferences of the drug-polymer complexes derived from molecular mechanics calculations: (a) MAA-MTX, (b) PLA-MTX and (c) depiction of adsorption of MTX on MAA nanoparticle (brown colored-tube rendered). MTX is rendered in spheres and polymers are in ball/cylinder rendering. Color codes for elements are-Carbon:cyan, Nitrogen:blue, Oxygen:red and Hydrogen:white.

Table 5.5 Calculated energy parameters (kcal/mol) and molecular attributes of the complexes involving PLA, MAA and MTX

Structure	Energy (kcal/mol)				
	Total	$\Delta E_{binding}$	VDW	ΔE_{vdw}	H bond
PLA	1.713	-	-8.776	-	-0.006
MAA	62.382	-	16.84	-	-0.01
MTX	9.457	-	4.845	-	0
PLA–MTX	5.978	-5.192	-10.885	-6.954	-0.009
MAA–MTX	58.086	-13.753	7.197	-14.488	-0.456

$\Delta E_{binding} = E_{(Host.Guest)} - E_{(Host)} - E_{(Guest)}$
$\Delta E_{vdw} = Vdw_{(HostGuest)} - VdW_{(Host)} - VdW_{(Guest)}$

Table 5.6 Calculated molecular attributes of the complexes involving PLA, MAA and MTX

Structure	Molecular attributes				
	Surface area (grid)	Volume	Surface-to-volume ratio	Refractivity	ΔRef
PLA	922.53	1828.26	0.5046	156.96	-
MAA	987.05	1954.76	0.5049	195.59	-
MTX	726.43	1255.51	0.5786	114.6	-
PLA–MTX	1373.47	2855.1	0.4811	270.67	-0.89
MAA–MTX	1315.76	2874.97	0.4577	307.21	-2.98

$\Delta Ref = Ref_{(HostGuest)} - Ref_{(Host)} - Ref_{(Guest)}$

The mechanistic elucidation of polymeric strand coalescence, chain interaction and exchange of reactant and product molecules during dispersion in the emulsification process have been molecularly simulated as shown in Figure 5.14a-d. When the coalesced polymeric strands disperse within the crosslinking medium both excess reactant and newly transitioned sol-gel polymeric molecules are re-distributed into daughter strands. Nucleation of the nanoparticle from the liquid-phase product during solvent evaporation process is depicted in Figure 5.14a. Growth of the nanoparticle by further sol-gel polymer molecule interactions is mediated by coalescence-exchange of strands and complete sphericalization. Coagulation of a multitude of sol-gel polymeric molecules during coalescence of nucleated strands results in further particle size growth (Figure 5.14b and c). The ion-balance, ion exchange, hydration and interaction

between hydrophilic sites in the PLA/MAA polymers and MTX were important parameters that facilitated the adsorption of the drug to the polymer composite (Figure 5.14d).

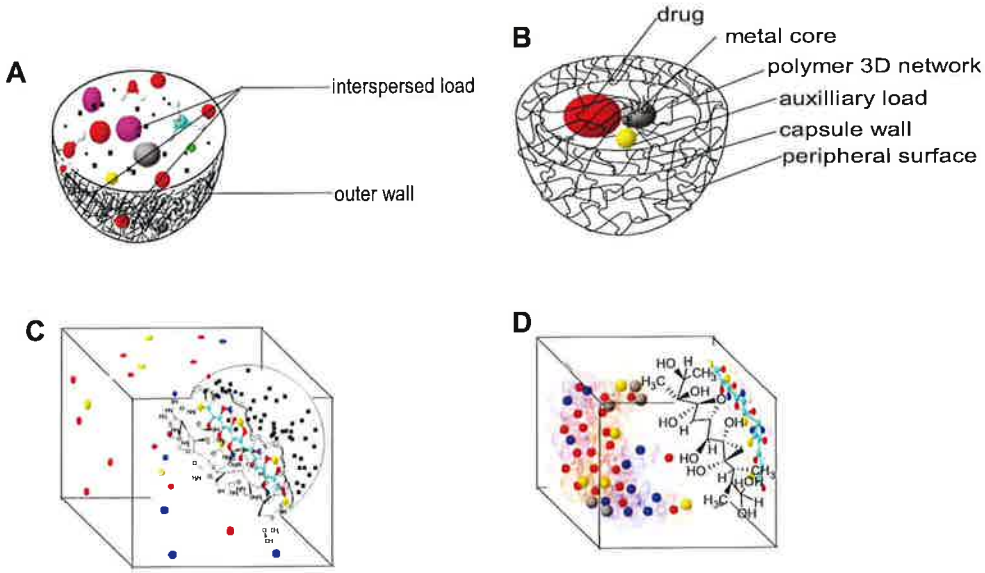

Figure 5.14 a) Polymer-drug composite showing the interspersed load and the polymer outer wall, b) MTX-PLA/MAA linkage depicted in a stereo-orientation pattern, c) the 3D sketch depicting the polymer surface embedded the MTX-PLA/MAA, and d) surrounding medium in an un-hydrated condition.

The molecular models revealing the mechanisms of PLA/MAA nanoparticle formation employing the three top-down sol-gel emulsification chemical strategies demonstrated the simplicity, potential reproducibility and stability of the nano-emulsions formed for PLA/MAA nanoparticle isolation (Figure 5.15a-f). In hydrodynamic cavitation processing, nanoparticles are generated through the formation and release of gas bubbles within the sol-gel solution that is rapidly pressurized within a supercritical drying chamber and exposed to cavitational disturbances and high temperature heating (Sunstrom et al., 1996). The erupted hydrodynamic bubbles are responsible for nucleation, growth, and quenching of the nanoparticles with the particle size controlled by adjusting the pressure and the solution retention time in the cavitation chamber. This process is highly complex and most polymers are susceptible to cavitation and high temperature and this may result in premature degradation of the polymer. Thus, the top-down

sol-gel double emulsion-evaporation technique detailed in this study (Figure 5.15a-f) offers superior nanoparticle processing approaches.

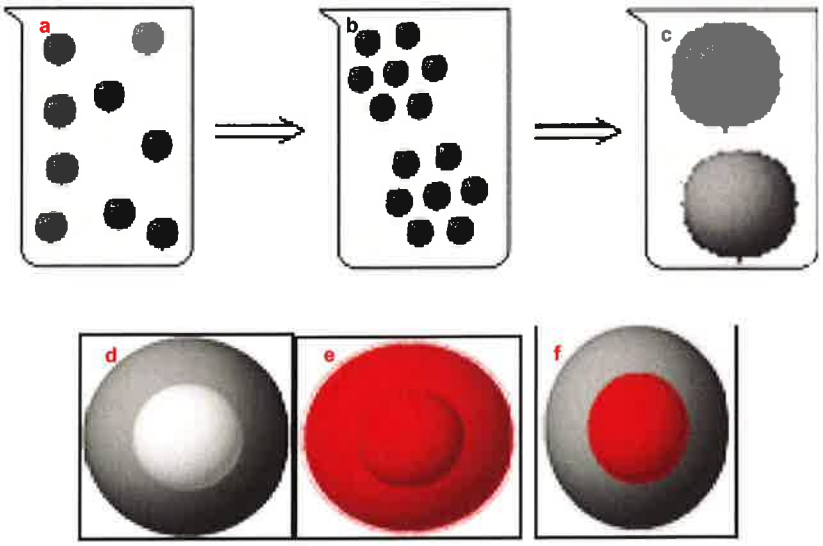

Figure 5.15 A computographic representation depicting a) formation of uniform nanoparticles molecules, b) cluster or grouping of molecules, c) nanoparticles, d) ion fill with synthetic PLA/MAA coating, e) MTX-PLA/MAA fill with MTX coating/wrapping, f) Heterogeneous fill depicting the adsorption of MTX onto thePLA/MAA composite.

5.4 Concluding Remarks

Different formulations of PLA/MAA nanoparticles were successfully prepared by double emulsion solvent evaporation technique on a randomized Box-Behnken statistical design template. The requisite variables required for producing an optimized PLA/MAA nanoparticle formulation with the targeted response parameters was elucidated by desirability plots. The difference between the actual and targeted response values was minimal. Constrained optimization studied elucidated information on the interaction effects of the independent variables (amount of PLA, amount of MAA and phase volume ratio) on the response parameters (size, DEE and yield). In general, the amounts of polymers had a significant influence on the response parameters while variations in the phase volume ratio showed minimal influence. The ideal DEE could not be achieved by optimization, a large amount of drug remained in solution

during the formation of nanoparticles. SEM and TEM confirmed the formation of matrix type nanoparticles and thus the approach of incubating the nanoparticles in a concentrated MTX solution with subsequent curing significantly improved drug loading. Modulation and prolongation of drug release from the nanoparticles was achieved as a result of careful selection of polymers and method of nanoparticles preparation. Further studies aimed at improving the zeta potential of the nanoparticles needs to be performed. In conclusion, the drug adsorbed nanoparticles in this study were better stabilized by higher binding energies, higher van der waals forces, shorter H-bond length, low surface-to-volume ratios and low indices of refraction.

CHAPTER 6

IN VITRO AND *IN VIVO* EVALUATION OF THE MAA/PLA MTX-LOADED NANOPARTICLE BASED PLA/PVA BIOPOLYMERIC MEMBRANE DEVICE

6.1 Introduction

Different polymer based drug delivery systems can be combined with the primary objective of improving and addressing therapeutic hurdles that are related to chemical, pharmacokinetic and physiological aspects of conventional dosage forms. Brain tumours represent a perfect example of a disease condition that can benefit from tailored polymer based drug delivery system where effective therapeutic management is dependent on various factors such as schedule of drug administration, lipophilicity of the anticancer compound, protein binding and the sensitivity of the tumor to the delivered compound. The extent to which a chemotherapeutic agent penetrates the tumor is primarily governed by the physiological blood-brain-barrier (BBB). Lipophilic compounds such as procarbazine and nitrsoureas possess a very high therapeutic index compared to hydrophilic compounds such as methotrexate (Zunkeleret al.,1996). However, in spite of their greater penetrability into tumor cells and preferential partitioning in lipid membranes and cellular structures, clinical use of these drugs permitted modest gains in terms of therapeutic efficacy due to large clearance and the inactivation constants (Manjour et.al., 1995; Hoang-Xuang and Delattre, 1996). As a result, hydrophilic molecules have become the focus of research.

Hydrophilic molecules have small transfer, clearance and inactivation constant values and are therefore capable of diffusing into deeper brain areas (Ushio et al., 1984). Comprehensive pharmacokinetic studies focusing on methotraxate (MTX), a hydrophilic anticancer compound primarily used for the treatment of primary central nervous system lymphoma (PCNSL), primary and metastatic brain tumors have been conducted by researchers (Chatelu et al., 1991; Pech et

al., 1998). Dukic et al (2000) studied the influence of schedule of administration on MTX penetration in brain tumors using rat models. By using doses of MTX corresponding to those used in clinical practice (50mg/kg), it was shown that intravenous bolus administration schedules promote MTX delivery in brain tumour tissue compared to intravenous infusion over four hours. The mode of drug administration (intrathecal vs. intracisternal) affects drug distribution. Intrathecally administered drugs are affected by factors such as bulk flow of the cerebrospinal fluid (CSF), diffusion into and through the extracellular space and the blood vessels, binding, uptake or metabolism by cells, molecular weight (MW) of the chemotherapeutic agent and capillary permeability (Blasberg et al., 1975; Levin et al., 1976). In another pharmacokinetic study it was shown that hydrophilic compounds such as MTX with low capillary permeability can achieve significant distribution in brain parenchyma when delivered intrathecally (Tzuu-Yuang et al.,1999).

MTX has been in clinical use for five decades and as a result has become substrate for certain members of the ABC transporter family located on the blood-brain-barrier (BBB) and blood-cerebrospinal fluid-barrier (BCSFB) which serve as drug efflux pumps that can alter MTX pharmacokinetic properties and the associated sensitivity of tumor cells (Shah and DeAngelis, 2000; Volk et al., 2000). The aim of this study was to fabricate and evaluate the *in vitro* and *invivo* performance of a drug delivery system based on MTX-loaded methacrylic acid/poly(lactide)(MAA/PLA)nanoparticles embedded within a poly(lactide)/poly(vinyl alcohol) (PLA/PVA) biopolymeric membrane for the treatment of primary brain tumors.

6.2 Materials and Methods

6.2.1 Materials

Solvents used for the chromatographic separation were of UPLC grade, and all other reagents were of analytical grade. Double deionised water was obtained from a Milli-Q system (Milli-Q, Millipore, Johannesburg). Human plasma was obtained from the South African National Blood Services (SANBS). Abitrex®, a commercial intravenous formulation containing 50mg/ml of MTX was purchased from a local Hospital pharmacy. Healthy adult Sprague Dawley rats were used for *in vivo* biocompatibility and biodistribution studies.

6.2.2 Preparation of the PLA/PVA composite polymer

The first step in the fabrication of the NBBM involved preparing a solution of PVA 8.79%w/v and PLA 10%w/v separately in dimethyl sulphoxide (DMSO). The polymer solutions were reacted at 150°C in the presence of stannous octoate (SnOct) for 1 hour. The reaction was allowed to proceed for a further 1 hour after adding 0.7mL of triethanolamine (TEC).

6.2.3 Preparation of MTX-loaded MAA/PLA nanoparticles

A primary emulsion was formed from an aqueous phase of 0.1M NaOH (*W1*) and an organic phase (*O*) which was prepared by dissolving PLA 5.99mg and MAA 30mg in 10mL mixture of dichloromethane and isopropyl alcohol in a 1:1 ratio. The external aqueous phase (*W2*) was prepared by forming a solution of polyethylene glycol (PEG) 2.5%w/v in acid buffer pH 2.0. The primary emulsion (*W1*) was then added drop wise to the external aqueous phase (*W2*) and the mixture was homogenised for 10min. The resultant nanoparticles were collected by centrifuge, washed twice with deionised water followed by freeze drying for 24 hours. Accurately weighed nanoparticles (80mg) were incubated in a concentrated solution comprising of MTX dissolved in 0.7mL 80% methanol containing 1% DMSO. The nanoparticles were then placed in an oven maintained at 30°C for 24 hours.

6.2.4 Preparation of the MTX-loaded PLA/MAA nanoparticle based PLA/PVA biopolymeric membrane

A homogenous suspension was formed by blending MTX–loaded MAA/PLA nanoparticles with 2,5mL PLA/PVA composite polymer. The suspension was then cast onto a 5mm diameter petri dish and immersed in a coagulation bath comprising of methanol: acetone mixture in a 1:1 ratio. A phase separated MTX-loaded MAA/PLA nanoparticle based PLA/PVA biopolymeric membrane (NBBM) was recovered after 24 hours. The residual solvent was allowed to evaporate at room temperature ± 25°C.

6.2.5 Analysis of the swellability

Swelling studies were conducted by immersing a known weight NBBM in 10mL phosphate buffer saline (PBS, pH 7.4) and allowing the device to reach maximum hydration potential. The device was then removed from the PBS and blotted with filter paper to adsorb excess water on the surface. The weight of the device before and after hydration was determined gravimetrically by weighing the on an electronic balance. The swelling potential was calculated from Equation 3.1 (Chapter 3, section 3.2.3).

6.2.6 Tensile mechanical testing

The mechanical properties of the NBBM were determined by textural profiling. Biaxial extensibility force-distance profiles were generated by employing a 2mm flat probe attached to the TA.XTplus Texture Analyser (Stable Microsystems, Surrey, UK) controlled via a 5kg load cell and Texture Exponent V3.2 software. The method involves securing the device between two rings with 5mm diameter hole on a raised platform. The centralised probe was then lowered and embedded onto the surface of the device. The elastic modulus (E) of the drug delivery system before and after hydration was determined and expressed as the ratio of stress exerted on the system to the amount of deformation. The data obtained from the resultant force-distance profiles was used to determine E using the Equation 4.1 (Chapter 4, section 4.2.9).

Table6.1 Test parameters employed for Bi-axial Extensibility testing of the NBBM device

Parameter	Setting
Test mode	Compression
Pre-test speed	1.00mm/sec
Test speed	1.00mm/sec
Post test speed	1.00mm/sec
Trigger mode	Distance
Distance	10mm
Trigger force	0.5000N

6.2.7 Assessment of the degradation behavior

Degradation studies were carried out by placing the NBBM in 10mL phosphate buffered saline (PBS, pH 7.4) in an orbital shaking incubator maintained at 37°C. The system was removed from the buffer on a 24 hour interval, dried to constant weight at 40°C in an oven and weighed.The experiment was continued by placing the system in fresh PBS solution. The degradation rate was determined as the percentage weight loss over 30 days.

6.2.8 *In vitro* drug release studies

In vitro drug release studies were performed in PBS, pH7.4. The device was placed in 100mL of the dissolution medium and incubated at 37°C under constant shaking at 20rpm in the shaking orbital incubator. Samples of 5mL were collected from the release medium on a 24 hour interval and were replaced with fresh buffer solution of equal volume. The drug concentration in the sample was assayed by UV spectroscopy (CECIL 3021 spectrophotometer, Cecil Instruments, Cambridge, England) at 312 nm.

6.2.9 Animal Preparation

Male Sprague Dawley rats weighing 400-500g were housed in groups of three per cage under controlled environment (temperature: 20±°C and humidity: 65±15%) and maintained under 12:12 hour light: dark cycle. They were allowed to adapt to the housing environment for four weeks during which they were weighed and monitored twice weekly prior to the study. The

animals had access to food and tap water. All animal handling procedures were according to the Central Animal Services (CAS) standard operating procedures (Animal Ethics no. 2006/09/04').

6.2.10 Intravenous bolus administration of MTX

Each rat was given a dose of MTX (50mg/kg) according to the individual weight. The rats were placed in a restrainer and MTX was given by bolus intravenous administration via a No 1 catheter inserted into the tail vein. The administered dose corresponded to that used in clinical practice for the treatment of patients with Primary Central Lymphomas or Metastatic Brain Tumors (Chatelut et al., 199; Pech et al., 1998; Pignon et al., 1994).

6.2.11 Surgical implantation of the NBBM device into the brain parenchyma

The rats were anaesthetised with a mixture of Ketamine (65mg/kg) and xylazine (7.5mg/kg) for the duration of the procedure which was performed in an aseptic manner. Their heads were placed and secured in a stereotaxic frame and shaved. A small (0.5-1cm) para-midline right sided scalp skin incision was made and the scalp periosteum reflected. An electric twist drill was used to make a controlled perforation of the skull approximately 0.5mm in diameter. The skull opening was followed by sharp incision of the dural lining. The cylindrical shaped implant which was less than 20% of the rat brain volume (0.865± 0.026 cm^3) was inserted into the brain parenchyma. Post-implantation, the skull defect was sealed with wax and the scalp insertion closed with a single layer of appropriately sized non-absorbable suture. The rats received Temgesic (0.1mL diluted to 1mL with ultra purified water), at a dose of 1mL post-operatively for pain relief with a rehydration treatment of 5% glucose in 0.9% saline. One group of rats was implanted with a placebo device while the other group was implanted with a drug-loaded device.

6.2.12 Plasma and CSF sampling

Rats were anaesthetised with a mixture of ketamine (20mg/kg) and xylazine (7.5mg/kg) and blood samples (4mL) were collected by cardiac puncture using a 5mL syringe and a 23G

needle flushed with heparin-saline solution (25 000 UI). The rats were then euthanized with sodium pentobarbitone and the skin overlapping the neck was shaven. A needle attached to the polyethylene tubing connected to a 1 mL syringe was then inserted at the occipital crest through the skin and muscles towards the cisterna magma to obtain the CSF (100- 150µL). The blood samples were centrifuged at 3000rpm for 20min and the plasma was collected. The plasma and CSF samples were collected on day 1,7,14, 21 and 30 and stored in a refrigerator at -70°C for further analysis.

6.2.13 Brain tissue harvesting

The brain tissue was exposed by carefully removing the skull using surgical forceps. The intact brain tissue was removed from the cranial cavity and collected into a container filled with 10%w/v neutral buffered formalin. Brain tissue samples were collected on day 1, 7, 14, 21, and 30.

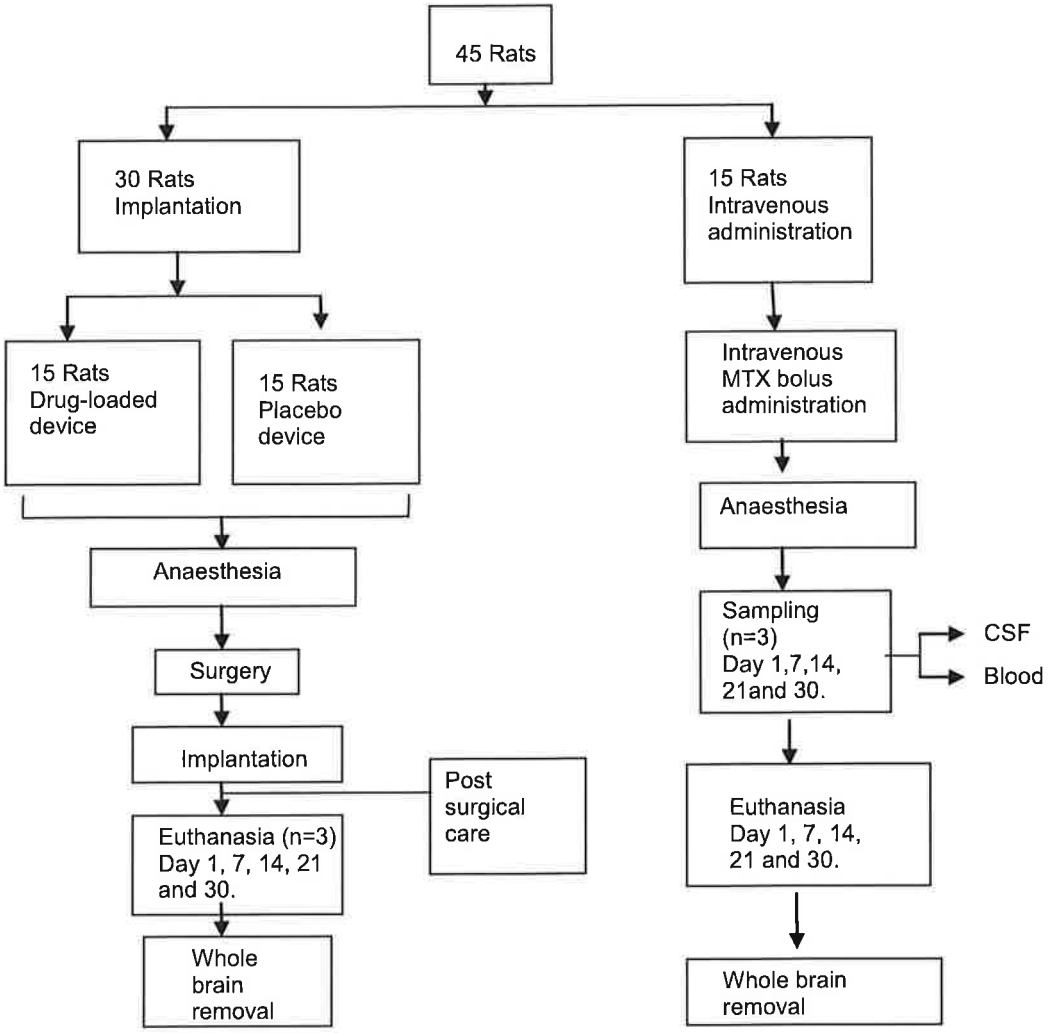

Figure 6.1 Flow diagram showing the layout of the *in vivo* studies

6.2.14 Histological evaluation

Histological evaluation was performed brains tissue samples (implanted with the placebo device and drug-loaded device) recovered at day 30 post implantation. Cross sections were selected from:

A: mid-section of the anterior half of the cerebrum including the tissue implant on the dorsal aspect of the right cerebral hemisphere.

B: a cross section from the middle of the posterior half of the cerebrum

C: a cross section in the middle of the cerebellum

D: a cross section from the medulla oblongata

From the abovementioned cross section tissue blocks specific sections were produced after routine histological processing and stained with Haematoxylin and Eosin stain in an automated strainer.

6.2.15 Ultra Performance Liquid Chromatographic (UPLC) separations

Waters Acquity UPLC (Waters Corporation, Milford, Massachusetts, USA) was employed for computing calibration curves and determining MTX levels in physiological samples. All samples were injected in a UPLC system where separation was achieved on a Acquity UPLC BEH C18column (50 x 2.1mm, i.d.,1.7µm particle size, Interchim, Montlucon, France) maintained at 25°C. Separations were achieved by using a mobile phase consisting of methanol:PBS (45: 55) running at a flow rate of 0.2ml/min). The run time was set at 3min and the injection volume was 5.0µl. The eluent was monitored on a Photodiode Array detector set at a wavelength range of 300nm to 312nm.

6.2.16 Preparation of aCSF, standard solutions andcalibration curve

Artificial cerebrospinal fluid (aCSF) was prepared by making up solutions A and B. Solution A was prepared by dissolving sodium chloride 8.66g, potassium chloride 0.224g, magnesium chloride 0.163g and calcium chloride 0.206g in 500mL of deionised water. Solution B was prepared by dissolving disodium hydrogen phosphate 0.214g and sodium hydrogen phosphate 0.027g in 500mL of deionised water. Solution A and B were combined in 1:1 ratio to make up the aCSF. A standard stock solution of MTX 120µg/mL was prepared by dissolving MTX in methanol: PBS, pH 7.4 (1:4) mixture. Working standard solutions were prepared in the range of 7.5-120µg/mL by performing serial dilutions of the standard stock solution. An internal standard solution (IS) 0.25mg/mL was prepared by dissolving AZT in methanol: PBS, pH 7.4 (1:4) mixture. To 400µL of working standard solutions, 400µL of aCSF and 150µL of IS was added. The calibration curve fitted by weighted (1/ x^2) linear regration was determined via UPLC

analysis by plotting the ratio of Area Under the Curve (AUC) of AZT and MTX peaks versus the concentration of the working standard solutions.

6.2.17 Preparation of plasma standard stock solutions and calibration curve

The human plasma was first pre-treated by adding 10mL acetonitrile to 20mL of plasma. The mixture was vortex-mixed for 3minutes and centrifuged at 3000rpm for 5minutes. The supernatant was collected by filtering through a 0.22µm filter. A standard solution 600µg/mL was prepared by dissolving MTX in methanol: PBS, pH 7.4 (1:4) mixture. An internal standard solution 0.25mg/mL was prepared by dissolving AZT in methanol:PBS (1:4) mixture. Working standard solutions were prepared in the range of 120-600µg/mL by performing serial dilutions of the standard stock solution. To each 400µL of working standard solutions, 400µL of plasma and 150µl AZT was added. A calibration curve fitted by weighted ($1/ x^2$) linear regration was determined via UPLC analysis by plotting the ratio of AUC of AZT and MTX versus the concentration of the working solutions.

6.2.18 Determining optimal conditions for Solid Phase Extraction (SPE)

Solid phase extraction was conducted on a single use Water Oasis®HLB 3cc (60mg) extraction cartridge (Waters Corporation, Milford, Massachusetts, USA). The cartridge was pre-conditioned with 1mL methanol followed by 1mL ultra pure water MilliQ. To 1mL of plasma was added 1mL of acetonitrile. The mixture was vortex-mixed for 3 minutes and centrifuged for 5 minutes at 3000rpm.The supernatant 400µL was collected and 400µL of 7.5µg/mL of MTX solution and 150µL of IS was added to it. The mixture was vortex-mixed for 1 minute and the samples were loaded onto the cartridges and washed with 1mL mixture of varying PBS: methanol (90:10, 80:20, 70:30 and 60:40) mixtures. The analyte was finally eluted by washing with 500µL of PBS and 2mL methanol.

6.2.19 Analysis of MTX levels in plasma and CSF samples

Analyte plasma samples were prepared by adding 1mL acetonitrile to 1mL of plasma. The mixture was vortex-mixed for 3 minutes and then centrifuged for 3 minutes at 3000rpm. The supernatant 900µL was collected and to it was added 150µL of IS. The mixture was processed by SPE and then injected into the column. CSF analyte samples were injected directly into the column after adding 150µL of IS.

6.2.20 Assay of MTX in rat brain regions

The rat brains were removed from the 10% neutral buffered formalin and the implant was carefully removed from the brain tissue. Regions (4-5mg) around the area of implantation were dissected on ice. The regions were then placed in 1.5mm cornical test tubes and a solution (1mL) 0.1M perchloric acid and 4 $x10^{-5}$ sodium bisulfite was added into the tube. The mixture was sonicated at 200W for 1 minute and the homogenate was centrifuged at 3000rpm for 3 minutes. The IS (150µL) was pipetted into 750µL aliquot of the supernatant. The solution was then injected onto the chromatographic column.

6.3 Results and Discussion

6.3.1 Description and dimension of the NBBM

The NBBM device was opaquely transparent and dark orange in colour. The elastic device was 1mm thick, 7.5mm in diameter and weighed approximately 0.25g. The surface was visibly smooth and with a rubbery texture.

6.3.2 Surgical procedure and wellbeing of the animals

Following the surgical procedure, the rats recovered well from anaesthesia and all animals resumed normal life for the duration of the study. However, a slight loss in weight was observed

during the first week of the study in both study groups. During the course of the study, no gross behavioural disorders or neurological signs were observed.

6.3.3 Swellability and tensile mechanical testing

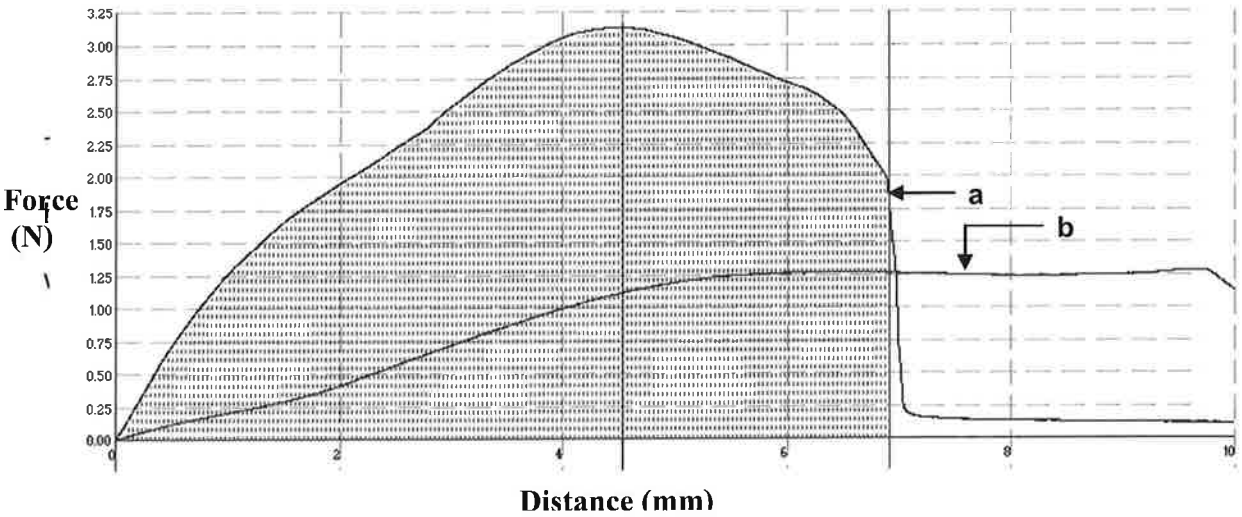

Figure 6.2 Textural profile for the (a) unhydrated NBBM and the (b) hydrated NBBM

The NBBM device demonstrated viscoelastic mechanical behaviour and showed a low swelling potential of 26.5%.The matrix of the unhydrated device (Figure 6.2a) was tough (Peak Force: 3.30N) and rigid (Distance: 7.0mm). However, a significant transition in the mechanical properties was observed upon hydration (Figure 6.2b). As water molecules penetrated the matrix, the elasticity of the device increased with subsequent increase in chain mobility. The toughness of the device was reduced by more than 50% (Peak Force: 1.30N) and the elasticity increased by over 20% (Distance: 9.64mm). The embedded MTX-loaded nanoparticles increased the density of the matrix and therefore may have contributed to the toughness of the unhydrated device.

The robust and elatic nature of the device prevented structural collapse due to hydration during and after implantion. The elastic modulus (*E*) was 0.03N.mm^2 before hydration and 0.02N.mm^2 after hydration. This observation indicated that the device had low fowling potential and therefore dose dumping would not occur once the device is implanted into the brain parenchyma. The results also showed that the device possessed sufficient mechanical strength require for handling during surgery and during storage. Upon implantation, the transition in the mechanical properties would transform the device into a soft material and this would aid integration into the viscoelastic brain tissue. Thus, the trauma and severe inflammation associated with implantation of hard and rigid materials into the brain parenchyma would be avoided.

6.3.4 Evaluation of the degradation behavior

Degradation of the NBBM device occurred via surface erosion and followed a bi-phasic pattern (Figure 6.3). The initial phase (Phase I) was characterized by rapid degradation where 60% weight loss occurred in 5 days. The second phase (Phase II) was characterized by slow constant surface erosion. The initial phase may have been due to the diffusion of unreacted polymer material from the polymer matrix resulting in rapid loss in weight. The second phase could only be initiated one the device had reached hydration equilibrium and this phase was characterized by slow and constant surface erosion. The synergistic water repelling effect of the PLA chains and the MTX-loaded nanoparticles delayed water penetration into the system. The device degraded for a prolonged period of over 30 days and the surface erosion mechanism was thought to have been induced by the perpendicularly aligned PLA chains extending towards the dissolution medium from the PVA backbone.

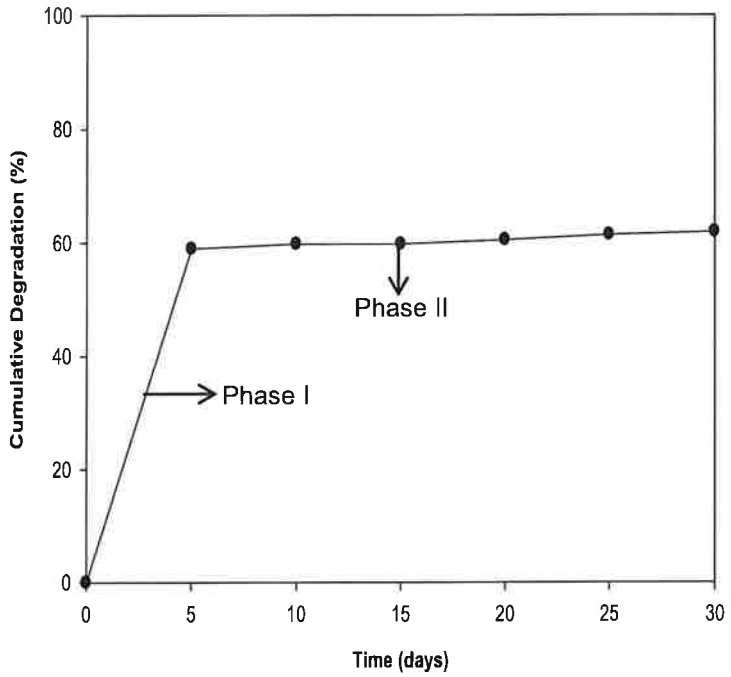

Figure 6.3 Degradation profile of the NBBM device in PBS (pH 7.4; 37°C), (n=3, SD≤0.36).

6.3.5 *In vitro* drug release

Drug release from the NBBM device was controlled by the rate of hydration, presence of two diffusion layers (nanoparticles and biopolymeric membrane), rate of drug hydrolysis in the nanoparticles and surface erosion. The hydration of the device was delayed by hydrophobic PLA chains and the embedded nanoparticles. Once the device had reached the state of hydration equilibrium, the loosely bound drug on the surface of the nanoparticles and the drug dispersed within the biopolymeric membrane during fabrication was released first. The drug molecules diffused through the biopolymeric membrane layer which controlled the rate of drug diffusion. Drug molecules that were conjugated within the matrix of the nanoparticles followed a different path. The drug-polymer bonds had to be hydrolysed first to render the drug molecules free. The free drug molecule diffused through the layer of the diffusion layer of the nanoparticles first and then through diffusion layer of the biopolymeric membrane. The rate of dug diffusion at the level of each layer was different due to a difference in the structural composition of the nanoparticles and the biopolymeric membrane. Drug release from the NBBM device followed

zero-order kinetics and controlled drug release was maintained by the slow and constantly eroding surface (Figure 6.4).

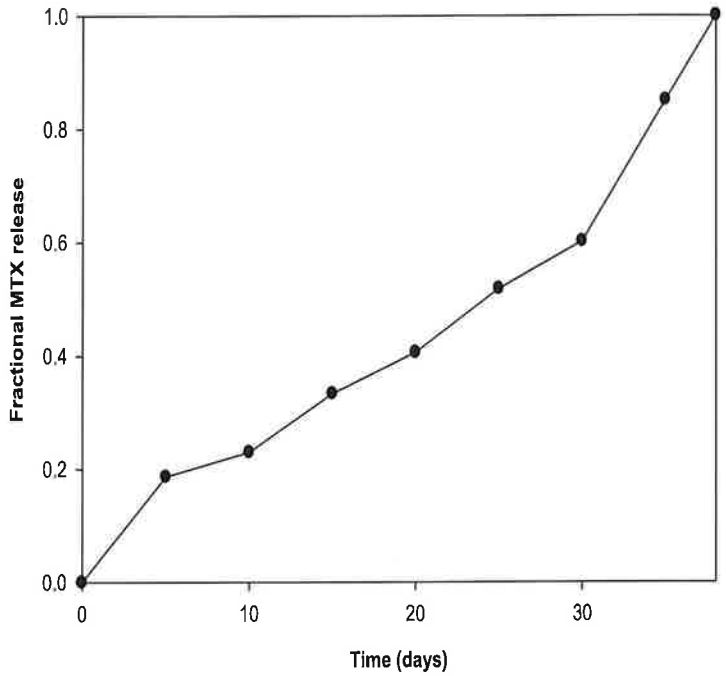

Figure 6.4 MTX release profile from the NBBM device in PBS (pH 7.4; 37°C), (n=3, SD≤0.74)

6.3.6 Histological findings

6.3.6.1 *Drug-loaded implant*

A: Mid-anterior cerebral section

In the dorsal part of the mid-anterior right cerebral hemisphere a surgical defect of the dura mater and leptomeninges measuring 2.05mm on the dorsal aspect of the cerebrum was detected. The surgical implant measuring 1.0 x 2.0mm could be identified in the cerebral cortex and penetrated up to the corpus callosum above the right lateral ventricle which was distorted by the implant. The implant revealed a homogenous mild basophilic staining in the H/E stained section and there was no inflammation present within the implant. The neuroparenchyma directly next to the implant showed mild inflammatory infiltrates with mainly macrophages (microglia) and gitter cells visible in the cerebral cortex. Few perivascular lymphocytes were present in the inflamed brain tissue. A mild spongiosis was also evident. Similar spongiosis

could be demonstrated in the underlying corpus callusum. The rest of the cross section at this level showed no significant neuropathology.

B: Mid-posterior cerebral section

At this level the hippocampus was clearly visible but no diagnostic neuropathology could be demonstrated in the cerebral cortex as well as the underlying white matter of the brain. The aqueduct of Sylvius appeared normal.

C: Mid-cerebellar section

The cerebellar grey matter as well as the cerebellar peduncle, white matter and fourth ventricle were morphologically normal.

D: Medulla oblongata section

In the section from the medulla oblongata posterior to the fourth ventricle no pathology was present in the leptomeninges and neuroparenchyma. The central canal and white matter of the medulla oblongata appeared morphologically normal.

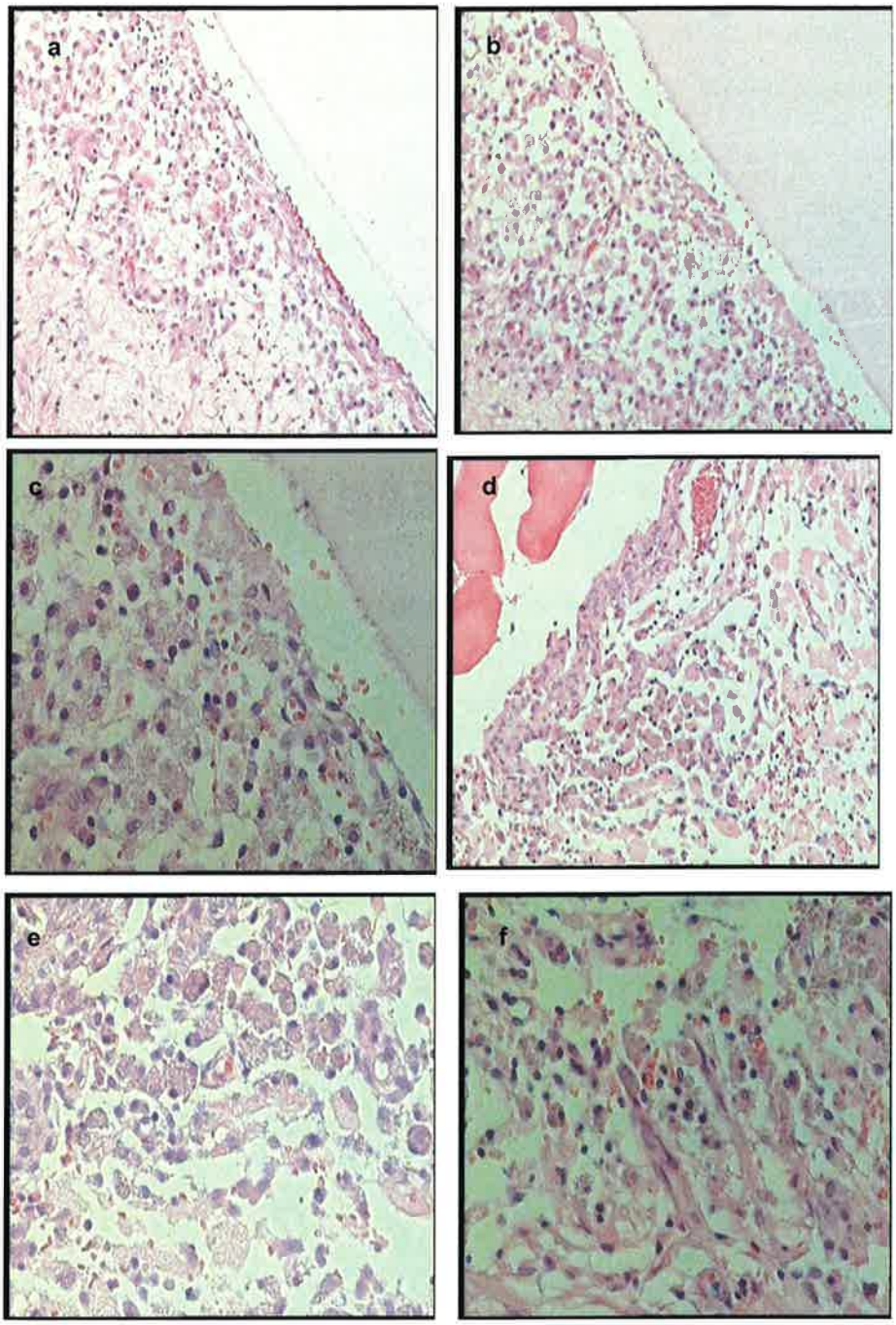

Figure 6.5 (a) the homogenous implant is present in the one part of the section, while the inflammatory process could be demonstrated in the neurocortex of the cerebrum, (b)mild inflammation observed in the neurocortex associated with the drug-loaded polymeric implant, (c) edge of the implant and neuroparenchyma with microglia as well as gitter cells visible (d), bright eisinophilic material at the edge of the surface with mild granulomatous inflammation in the neuroparenchyma,(e) gitter cells and microglia in the inflammatory region adjacent to the drug-loaded polymeric implant and (f) mild inflammatory process in the leptomeninges and neuroparenchyma with microglia visible.

6.3.6.2 *Placebo implant*

A: Mid-anterior cerebral section

In the dorsal aspect of the right cerebral hemisphere a defect in the dura mater measuring 2.00mm could be demonstrated. In the underlying mid-dorsal cerebrum the surgical implant measured 1.10 x 2.3mm. There were no morphological differences in the appearance of the placebo implant when compared with similar drug-loaded implant. The surgical defect extended in the cortex up to the corpus callosum above the right lateral ventricle. Minimal inflammation was present in the brain tissue along the surgical implantation site. A few microglia and gitter cells were identified in the cerebral cortex at the junction with the implant. Minimal status spongiosis was visible.

B: Mid-posterior cerebral section

No neuropathology was present at this level of the brain.

C: Mid-cerebellar section:

The cerebellar grey matter as well as the underlying cerebellar peduncle and white matter appeared morphologically normal. The section includes the fourth ventricle.

D: Medulla oblongata section:

No lesions were detected in the section of the medulla oblongata posterior to the fourth ventricle.

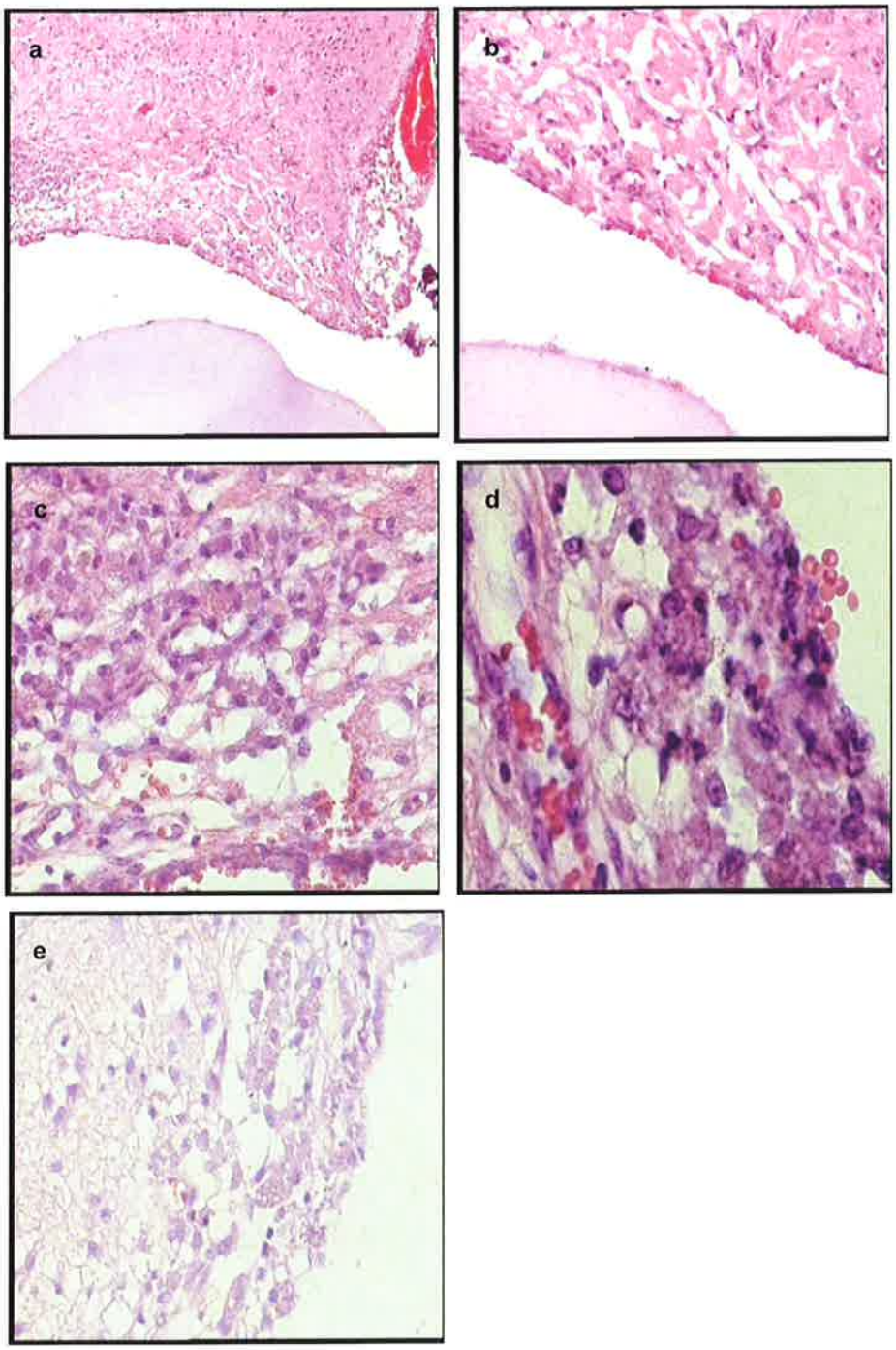

Figure 6.6 (a) the edge between the polymeric placebo implant and the brain tissue showing minimal inflammation, (b) at higher magnification, (c) minimal inflammation in the neuroparenchyma, (d) inflammatory area with few glitter cells in the neuroparenchyma and (e) minimal inflammation in cortical neuroparenchyma.

The morphological evaluation confirmed in the dorsal parts of the mid-anterior cerebral sections from the drug-loaded as well as the placebo implants a surgical-induced defect and the implanted material. Thirty days post implantation, organization was visible where microglia were clearing the damaged tissue in both the anterior cerebral cortical sections (drug-loaded implant and placebo implant). The inflammatory reaction in the neuroparenchyma along the implant was graded mild in the drug-loaded implantation site and minimal in the placebo site. At the other levels of the cerebrum, cerebellum and medulla oblongata no neuropathology could be detected in the H/E stained sections from the drug-loaded and placebo specimens.

6.3.7 MTX and AZT chromatographic separation and calibration in aCSF and plasma

MTX was eluted at first at 2.7 min and AZT was eluted at 4.00 min in aCSF. However, the eluting times of the compounds were shorter in plasma. MTX was eluted at 1.6 min and AZT at 2.5 min. The CSF calibration curve ($y = 0.0248x + 0.05$, $r^2 = 0.99$) and the plasma calibration curve ($y=0.0009x$, $r^2= 0.99$) were linear in the concentration range studied. The optimal methanol: PBS composition required for achieving efficient conditions for SPE was 90:10.

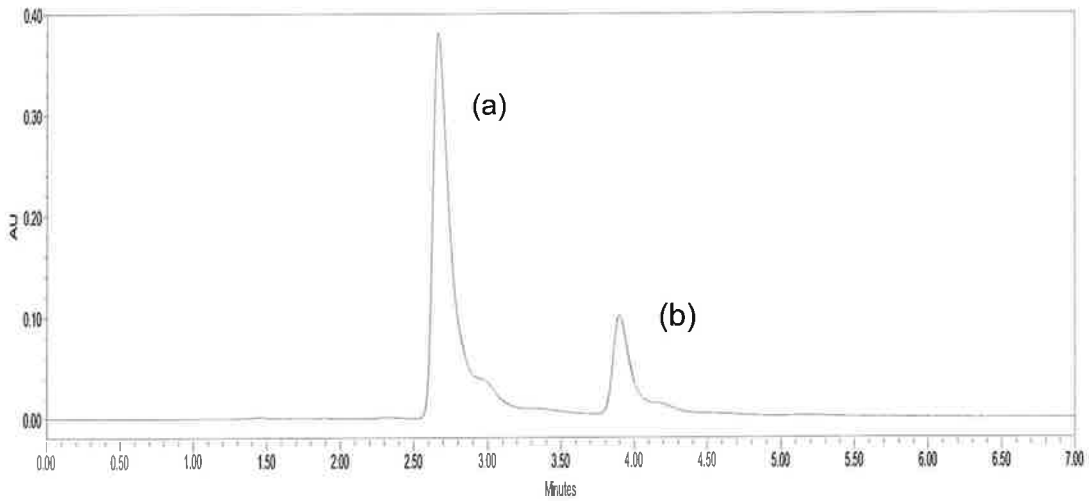

Figure 6.7 Chromatogram showing separation and eluting times for (a) MTX and (b) AZT in aCSF (n=3, SD≤0.62).

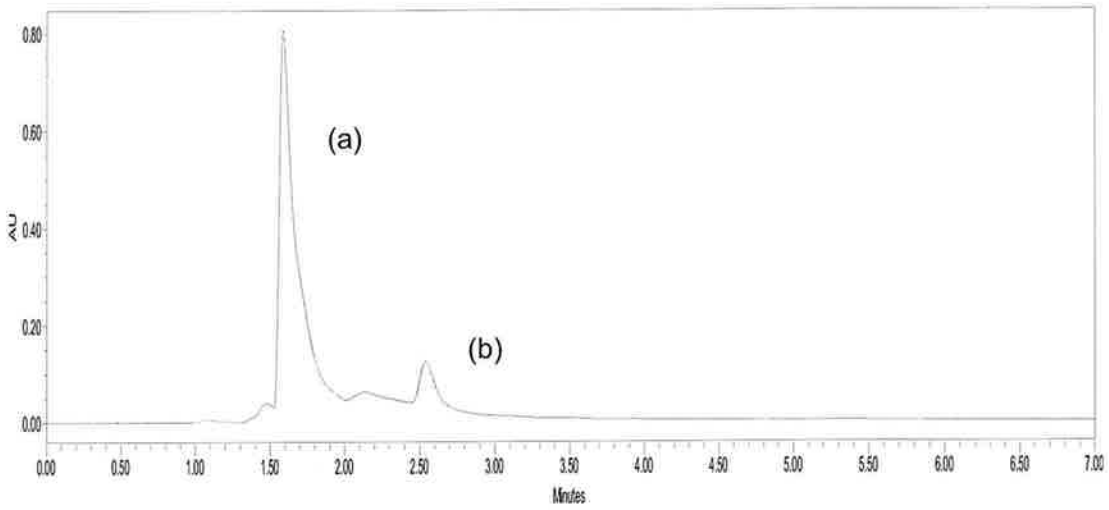

Figure 6.8 Chromatogram showing separation and eluting times for (a) MTX and (b) AZT in plasma (n=3, SD≤0.73)

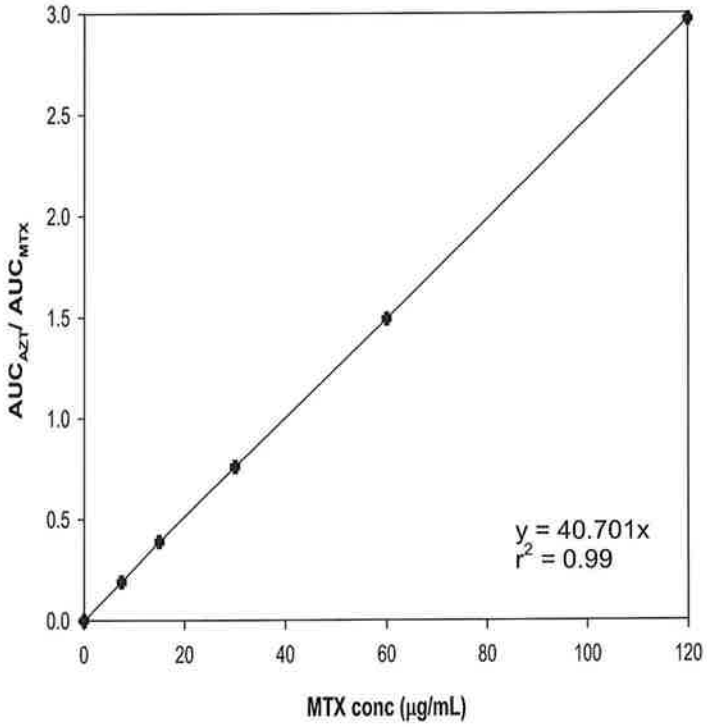

Figure 6.9 MTX calibration curve in aCSF.

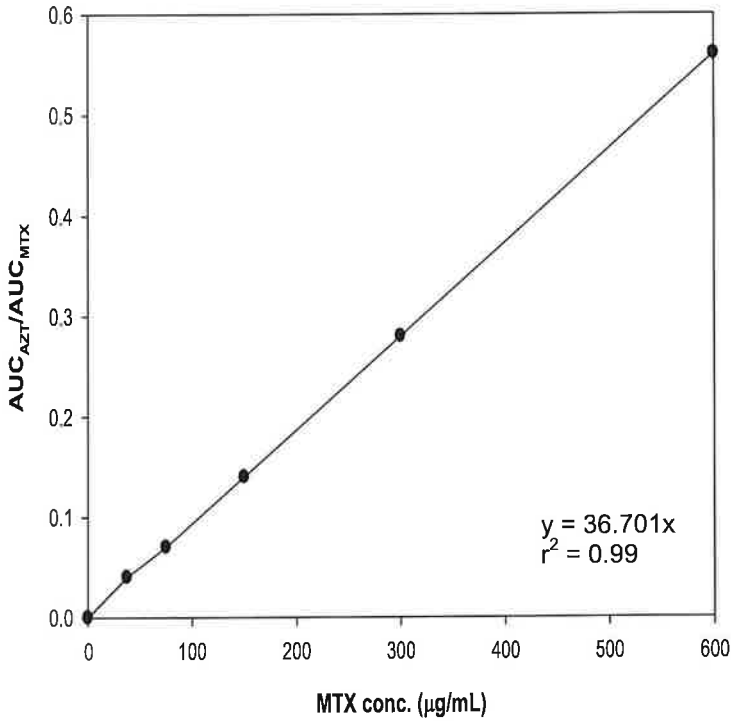

Figure 6.10 MTX calibration curve in plasma.

6.3.8 CSF, plasma and brain tissue concentration profiles following intravenous administration of MTX and surgical implantation of MTX-loaded NBBM

The plasma concentration-time profile of MTX is shown in Figure 6.11. On day 1 after intravenous infusion, plasma concentration reached a maximum of 37, 5µg/mL then there was a rapid decline. High protein binding of MTX may have slightly delayed clearance of MTX from the blood. The concentration-time profile of MTX in the CSF following bolus administration is shown in Figure 6.12. CSF concentrations reached a maximum of 2.4µg/mL which indicated that a small proportion of the administered dose was able to reach the brain tissue. MTX was rapidly cleared from the CSF following intravenous administration and this further reduced the bioavailability of MTX. In contrast to the intravenous route of MTX administration, MTX was released in a gradual manner from the NBBM device (Figure 6.13). The results showed that the brain tissue concentration of MTX increased steadily over an extended period and concentration

reached a maximum of 36.72µg/mL on day 14. MTX was slowly cleared from the brain tissue and this may have been attributed to high tissue binding affinity of MTX due to the targeted delivery strategy. On day 30 post implantation, MTX concentrations of 20µg/mL could still be detected in the brain tissue. No traces of MTX released from the device were detected in the plasma after 30 days.

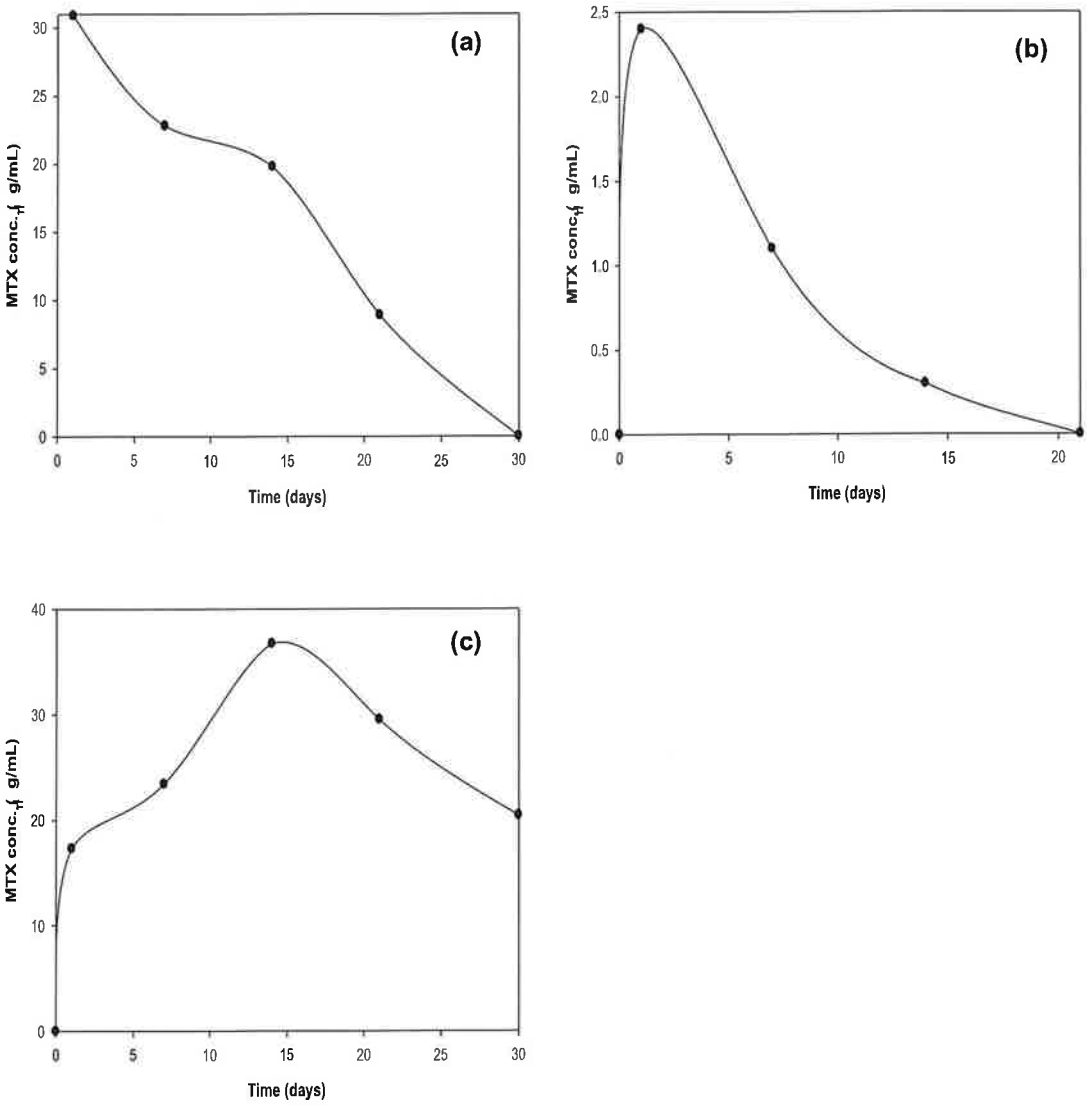

Figure 6.11 (a) Plasma concentration-time profile following bolus intravenous administration of MTX (n=3, SD≤0.53), (b) CSF concentration-time profile following bolus intravenous administration of MTX (n=3, SD≤0.62) and (c) Brain tissue concentration-time profile following implantation with MTX-loaded NBBM device (n=3, SD≤0.67).

6.3.9 Concluding Remarks

A drug delivery system based on MAA/PLA nanoparticles embedded in PLA/PVA biopolymeric membrane was fabricated by phase separation. The device showed minimal swelling and degraded slowly via surface erosion over a period of more than 30 days in PBS. Textural profiling showed that the mechanical properties of the unhydrated device would be suitable for handling during surgical procedure and storage. The device demonstrated the capability to translate into a viscoelastic material upon hydration. The morphing behaviour would allow the device to integrate well into the brain tissue and without inducing trauma. The inherent strength of the NBBM device was preserved upon hydration and indicated that the device had a low fouling potential and this would prevent dose dumping once the device was implanted into the brain. Histological findings showed that the implant was biocompatible with the brain tissue since it only elicited mild inflammatory response in both the placebo and the drug study group. The NBBM device demonstrated superior drug release profile and bioavailability when compared to its intravenous counterpart. MTX was released via zero-order kinetic from the NBBM device implanted in the brain tissue of rats. MTX concentration of up to 20ug/mL could still be traced in the brain tissue 30 day post implantation. This NBBM was able to release MTX in a sustained manner in the brain parenchyma. Thus, the NBBM holds the potential for targeted delivery of MTX for the treatment of primary brain tumors such as primary central nervous system lymphoma (PCNSL).

CHAPTER SEVEN

CONCLUSIONS AND RECOMMENDATIONS

7.1 Conclusions

This research was focused on designing and fabricating a polymer based implantable device for local and extended release of MTX in the treatment and management of PCNSL. A nanoparticle based biopolymeric membrane (NBBM) device was fabricated by incorporating PLA/MAA nanoparticles into a PLA/PVA biopolymeric membrane. The biopolymeric membranes were prepared by immersion precipitation technique (phase separation) and the nanoparticles were prepared by double emulsion evaporation technique. The two drug delivery systems (DDS) were optimised separately after a carrying out extensive experiments which were designed by a 3-Factor Box-Behnken design and carefully studying the resultant data. The interaction of formulation variables was explained by means of constructed surface plots. Computational modeling was carried out on the biopolymeric membrane in order to elucidate and understand the fundamental molecular interactions that lead to its formation. Similarly, molecular simulations of potential mechanisms of polymeric nanoparticle formation were constructed.

The physicochemical and mechanical properties of the optimised DDS were evaluated independently by conducting various experiments. The surface morphology of the DDS were characterized by SEM (biopolymeric membrane) and TEM (nanoparticle) and drug release from each system was studied in simulated physiological conditions (pH 7.4, 37°C). The biopolymeric membrane was analysed for *in vitro* degradation, S_w and DEE. The mechanical properties (elastic modulus) were evaluated by tensile mechanical testing. The nanoparticles were analysed for size distribution, yield and drug DEE. Molecular interactions and thermal properties of the nanoparticles were studied by FT-IR spectroscopic and DSC investigations respectively.

The optimised biopolymeric membrane degraded by surface erosion over a prolonged period (65% weight loss in 160 hours) and demonstrated a low S_w of 32%. DEE was high (94%) and the drug was released in a biphasic manner with a typical profile characterized by an initial burst effect followed by gradual release. The difference between the predicted experimental results (S_w: 30%, % weight loss: 45% in 160 hours and DEE: 90%) and actual experimental results were not significant. The membrane demonstrated tough and elastic mechanical properties. The formulation attributes demonstrated by the optimised biopolymeric membrane were acceptable except for the drug release duration.

The optimised nanoparticles showed a size distribution of 331nm and a yield of 84.4 mg. DEE was poor (12%) and an alternative fabrication approach of adsorbing the drug onto the surface of the nanoparticle was adopted to improve the drug loading. This was achieved by incubating the nanoparticles into a concentrated MTX solution. By so doing, drug loading increased to 98% and the size decreased to 211 nm. The difference between the predicted experimental results (size: 313 nm and yield: 85.5 mg) and the actual results was not significant, thus the formulation attributes demonstrated by the nanoparticles were satisfactory. FT-IR spectroscopy results showed that the chemical composition of the initial starting material did not change during fabrication. The results of the DSC investigations suggested that the PLA/MAA nanoparticles had a lower *Tg* (40°C) than its individual constituent polymers, PLA (50°C – 80°C) and MAA (85°C – 165°C).

NBBM device was produced by incorporating optimised nanoparticles into an optimised biopolymeric membrane which was thin (1mm), round (7.5mm diameter), elastic with a smooth surface. The device demonstrated low S_w (26%) and degraded by surface erosion over 30 days. In contrast to the individual drug delivery systems (biopolymeric membrane and nanoparticles), drug release from the NBBM followed zero-order kinetics and drug release modulation was

achieved over a prolonged period (>30 days). The burst effect that was observed with the nanoparticle and biopolymeric membrane was eliminated.

Histological studies conducted in rat models showed that the NBBM was biocompatible with the brain tissue. Surgical implantation in the brain resulted in mild inflammation either from the device or surgical procedure itself. MTX could be traced at the site of implantation 30 days post implantation and this showed that the device was capable of releasing the drug *in vivo* for an extended period. Based on the results of this research, the NBBM device would be a suitable candidate for delivering therapeutic concentrations of MTX in the brain parenchyma of patients diagnosed with PCNSL.

7.2 Recommendations

The limitation of the immersion precipitation is that it requires the use of organic solvents which may increase the risk of toxicity. Other techniques such as melt molding, foaming and particulate leaching method can be employed for preparing scaffolds and these do not require the use of organic solvents. The performance of the scaffolds and polymer membranes can further be improved by crosslinking, coating with polymer solutions or incorporation of nano or micro structures. The time spent in the lab and the cost of research can be significantly reduced by employing computational modeling tools in the early stages of formulation development. The data obtained from computer models can be collated and used to accurately determine the formulation variables required to realise the desired device. Future research may focus on ways of addressing the rapid initial degradation phase which was thought to be due to leaching of unreacted polymer material from the biopolymeric membrane. This can be achieved by determining the optimal stoichiometric requirements and reaction conditions for preparing the PLA/PVA composite polymer. The next stage of research can be focused on assessing the

therapeutic efficacy of the NBBM device on higher animal models such as rabbits with a pre-induced primary brain tumor.

8. REFERENCES

Abramson S.D., Alexe G., Hammer P.L., Kohn J,A., Computational approach to predicting cell growth on polymeric biomaterials, J Biomed Mater Res **73**, (2005), 116-124.

Alla S.G.A., Said H.M., El-Nagger A.W., Structural Properties of y-irradiated Poly(vinyl alcohol)/ Poly(ethylene glycol) Polymer Blends, J Appl Polm Sci **94**, (2004), 167-176.

Allain C., Limat L., Regular patterns of cracks formed by directional drying of colloid suspensions, Phys Rev Lett **74** (15), (1995), 2981-4.

Allemann E., Gurnay R., Doelker E., Drug-loaded nanoparticles: Preparation methods and drug targeting issues, Eur J Pharm Sci **39**, (1993), 173-191.

Almeida H., Bártolo P.,Virtual topological optimisation of scaffolds for rapid prototyping, Med Eng Phys **32**, (2010), 775-782.

Anderson J.M., Shive M.S., Biodegradation and biocompatibility of PLA and PLGA microspheres, Adv Drug Deliver Rev **28**, (1997), 5-24.

Benoit J., Faisant N., Venier-Julienne M., and Menei P., Development of microspheres for neurological disorders: From basics to clinical applications, J Controlled Release, **65**, (2000), 285-296.

Beral V., Peterman T., Berkelman R., Jaffe H., AIDS-associated non-Hodgkin's lymphoma (see comments), Lancet **337**, (1991), 805-9.

Bodor N., Simpkins J.W., Brain-specific sustained release of dopamine with a redox delivery system, Science **221**, (1983), 61-67.

Boland E.D., Wnek G.E., Simpson D.G., Pawlowski K.J., Bowlin G.L., J Macromol Sci Pure, **A38**, (2001), 1321.

Boland E.D., Wnek G.E., Simpson D.G., Pawlowski K.J., Bowlin G.L., J Macromol Sci Pure **A38**, (2001), 1321.

Brem H., Piantadosi S., Burger P., et al., Placebo-controlled trial of safety and efficacy of intraoperative controlled delivery by biodegradable polymers of chemotherapy for recurrent gliomas, Lancet **345**, (1995),1008-1012.

Brocchini S., James K., Tangpasuthadol V., Khon J., A combinatorial approach for polymer design, J Am Chem Soc, **119**, (1997), 4553-4554.

Burkoth A.K., Anseth K.S., A review of photocrosslinked polyanhydrides: in situ forming degradable networks, Biomaterials, **21**, (2000), 2395-2404.

Burrem D.A., Zylsta E., Lonsburg P.T., Langer R., Synthesis and RDG peptide modification of a new biodegradable copolymer poly(lactic acid)-co-lysine, J Am Chem Soc **115**, (1993), 11011-11011.

Cabañas M.V., Román P.J., Valle-Regi M., Tailoring vancomycin release from ß-TCP/argarose scaffolds, Eur J Pharm Sci **37**, (2009), 249-256.

Calvo P., Remunan-Lopez C., Vila-Jato J.L., Alonso M.J., Development of positively charged colloidal drug carriers: chitosan-coated polyester nanoparticles and submicron-emulsions, Colloid Polym Sci, **275**, (1997), 46-53.

Chen Q., Harding S.E., Ali N.N., Lyon A., Boccaccini A., Biomaterials in cardiac tissue engineering: Ten years of research survey, **R59**, (2008), 1-37.

Chen R.R., Mooney D.J., Polymeric growth factor delivery strategies for tissue engineering, Pharm Res, **20**, (2003), 1103-1112.

Ciocca L., De Crescoenzio F., Fantini M., Scotti R., CAD /CAM and rapid prototyped scaffold construction for bone regenerative medicine and surgical transfer of virtual planning : A pilot study, Computerized Medical Imaging and Graphics, **33**, (2009), 58-62.

Cocidglio M., Hukkaire-Buys D., Alric CJ., Determination of schizandrin in human plasma by gas chromatography-mass spectroscopy, Chromatography and Biomedical Applications, **674**, (1995), 101-110.

Collins N.J., Bridson R.H., Leeke G.A., Grover L.M., Particulate seeding enhances interconnectiviy in polymeric scaffold foamed using supercritical CO_2, Acta Biom, **6**, (2010), 1055-1060.

Coombes A.G.A, Rizzi S.C., Williamson M., Barralet J.E., Downes S., Wallace W.A., Precipitation castion of polycaprolactone for applications in tissue engineering and drug delivery, Biomaterials, **25**, (2004), 4185-94.

Courvreur P., Kante B., Roland M., Speiser P., Adsorption of antineoplastic drugs to polyalkylcyanoacrylate nanoparticles and their release in calf serum, J Pharm Sci, **68**, (1979),1521-1523.

Couvreur P., Kante B., Roland M., Goit P., Bauduin P., Speiser P., Polycyanoacrylate nanocapsules as potential lysosomotropic carriers : preaparation, morphology and sorptive properties, J Pharm Pharmacol **31**, (1979), 331-332.

Crone C., Olesen S.E., Dielectrically resistance of brain microvuscular endothelium, Brain Res, **241**, (1982), 49-55.

Cui C., Schwendenman S.P., Surface entrapment of polylysine in biodegradable poly(DL-lactide-co-glycolide) microparticles, Macromolecules, **34**, (2001), 8426-8433.0

Dan W., Daviau T., Ying P., Zhao Z., Nowotnik D., Clow C.S., Tyler B., Brem H., Effects of GLIADEL® wafer initial molecular weight on the erosion of wafer and release of BCNU, J Control Release, **42**, (1996), 83-92.

Das K.S., Tucker I.G., Hill D.J.T., Ganguly N., Evaluation of poly (isobutylcyanoacrylate) nanoparticle for mucoadhesive ocular drug delivery. I. Effect of formulation variables on physicochemical characteristics of nanoparticles, Pharmaceut Res, **12** (4), (1995), 534-540.

Dorothee R., Andreas L., Ilka P., Marsha A.M., Ralf-Peter F., Biocompatibility testing of novel multifunctional biomaterials for tissue engineering applications in head and neck surgery: an overview, Eur Arch Oto-Rhino-L, **263** (2006), 215-222.

Duce C., Micheli A., Solaro R., Starita A., Tine M.R., Prediction of chemical-physical properties by neural networks for structures, Macromol Symp, **234**, (2006), 13-19.

Dufrene Y.F., Lee G.U., Advances in the characterization of supported lipid films with the atomic force microscope, Biochimica et Biophysica Acta (BBA)-Biomembranes **1509**, (2000), 14-41.

Dukic SF., Heurtaux T., Kaltenbach M.L., Hoizey G., Lallemand A., Vistelle R., Influence of administration on methotrexate penetration in brain tumours, Eur J Cancer, **36**, (2000), 1578-84.

Eisenberg P., Executive summary of NIH workshop on biomaterials and medical implants (1995), 16-17 October, Bethesda MD: National Institutes of Health.

Eksterowics J.E., Evensen E., Lemmen C., Brady G.P., Lanctot J.K., Bradley E.K., et al., Coupling structure-based design with combinatorial chemistry: application of active site derived pharmacophores with informative library design, J Mol Graph Model, **20**, (2002), 469-77.

Eshraghi S., Das S., Mechanical and microstructural properties of polycaprolactone scaffolds with one-dimensional, two dimensional and three-dimensional orthogonally oriented porous architectures produced by selective laser sintering, Acta Biom, **6**, (2010), 2467-76.

Esperon S., Bossy-Nobs L., Petropolous L.K., Gurny R., Guex-Crosier Y.A., Biodegradable drug delivery system for the treatment of postoperative inflammation, Int J Pharm, **352**, (2008), 240-247.

Fabiana Q., The great promise of protein delivery technologies, Int J Pham, (2008), 1-17.

Hutmacher D.W., Sittinger M., Risbud M.V., Scaffold based tissue engineering: rationale for computer aided design and solid free form fabrication systems, Trends Biotechnol, **22**, (2004), 354 - 362.

Fenart L., Casanova A., Dehouck B., Duhem C., Slupek S., Cecchelli R., et al., Evaluation of the effect of charge and lipid coating on the ability of 60 nm nanoparticles to cross an *in vitro* model of the blood-brain barrier, J Pharmacol Exp Ther, **291**(3), (1999),1017-22.

Feng S., Chien S., Chemotherapeutic engineering: Application and further development of chemical engineering principles for chemotherapy of cancer and other diseases, Chem Eng Sci, **58**, (2003), 408 - 4114.

Foernkier E., Passirani C., Montero-Menei C.N., Benoit J.P., Biocompatibility of implantable synthetic polymeric drug carriers: focus on brain biocompatibility, Biomaterials, **24**, (2003), 3311-3331.

Fung L.K., Shin M., Tyler B., Brem H., Saltzman M., Chemotherapeutic drugs released from polymers: distribution of 1,3 bis(2-chloroethyl)-1-nitrosourea in the rat brain, Pharm Res **13**, (1996), 671-682.

Fung K.L., Ewend M.G., Sills A., Sipos E.P., Thompson R., Watts M., et al., Pharmacokinetics of interstitial delivery of carmustine 4-hydroperoxycyclophosphamide, and paclitaxel from biodegradable polymer implant in the monkey brain, Cancer Res, **58**, (1998), 672-684.

Furuse M., Hirase T., Ito M., Occludin: a novel integral membrane protein localizing at tight junctions, J. Cell Biol., **123**, (2003), 1777-1788.

Gan Q., Wang T., Chchrane C., McCarron P., Modulation of surface charge, particle size and morphological properties of chitosan-TPP nanoparticles intended for gene delivery, Colloid Surface B, **44**, (2005), 65-73.

Gan Q., Wang T., Chitosan nanoparticle as protein delivery carrier: Systematic examination of fabrication conditions for efficient loading and release, Colloid Surface B, **59**, (2007), 24 - 34.

Gaspar R., Polyalkylcyanoacrylate nanoparticles in drug targeting, Rev Port Farmacia, **41**, (1991), 36-45.

Ghosh S., Viana J.C., Reis R.L., Mano J.F., Development of porous lamellar poly(L-lactic acid) scaffolds by conventional injection molding process, Acta Biom, **4**, (2008), 887-896.

Giordano R.A., Wu B.M., Borland S.W.,Cima L.G., Sachs E.M., Cima M.J., Mechanical properties of dens poly lactic acid structures fabricated by three dimensional printing, J Biomat Sci-Pol E, **8** (1), (1996), 63-75.

Goldberg M., Langer R., Jia X., Nanostructured materials for applications in drug delivery and tissue engineering, J Biomat Sci-Pol E, **18**, (2007), 241-268.

Lee Y.M., Kim D.S., Lee C., Park H.B., Rhim J., Crosslinked poly(vinyl alcohol) membranes containing sulfonic acid group: proton and methanol transport through membranes, J Membrane Sci, **238**, (2004),143-151.

Gref R., Couvreur P., Barratt G., Mysiakine E., Surface engineered nanoparticles for multiple ligand coupling, Biomaterials, **24** (24), (2003), 4529-37.

Groisman A., Kaplan E., An experimental study of cracking induced by desiccation, Europhys Lett, **25**, (1994), 415-20.

Gubskaya A.V., Kholodovych V., Knight D., Kohn J., Welsh W.J., Prediction of fibrinogen adsorption for biodegradable polymers: Integration of molecular dynamics and surrogate modeling, Polymer, **48**, (2007), 5788-5801.

Gudeman L.F., Peppas N.A., pH-Sensitive membranes from poly(vinyl alcohol)/poly(acrylic acid) interpenetrating networks, J Membrane Sci, **107**, (1995), 239-248.

Guerin C., Olivi A., Weingart J.D., Lawson C., Brem H., Recent advances in brain tumor therapy: local intracerebral drug delivery by polymers, Invest New Drugs, **22**, (2004), 27-37.

Gupta K., Madan S., Majumdar D.K., Maitra A., Ketorolac entrapped polymeric micelles: preparation, characterization and ocular anti-inflammatory studies, Int J Pharm, **209**, (2000), 1-14.

Hacker M., Ringhofer M., Appel B., Neubauer M., Vogel T., Young S., Mikos A.G., Blunk T.,Göpferich A., Schulz M.B., Solid lipid templating of macroporous tissue engineering scaffolds, Biomaterials, **28**, (2007), 3497-3507.

Hayes M.D., Hallihan M.J, Love B.J, Aning A.O., Habenschuss A., Theiss T., PGA and PLA as biodegradable polymers, Transactions of the annual meeting of the society for biomaterials in conjunction with the international biomaterials symposium, 1996, pp. 400.

Hirshi K., D'Armore P., Control of angiogenesis by pericytes: molecular mechanisms and significance, ESX, **79**, (2007), 419-428.

Hoang-Xuang K., Delattre JY., Chimiotherapie des temeurs cerebrales malignes primitives de l'adulte, Rev Prat, **46**, (1996), 450-6.

Holder A.J., Kilway K.V., Rational design of dental materials using computational chemistry, Dent Mater, **21**, (2005), 47-55.

Hou D., Xie C.S., Huang K.J., Zhu C.H., The production and characteristics of lipid nanoparticles (SLNs), Biomaterials, **24**, (2003), 1781-1785.

Hu-Lin J., Kwon J., Kim E., Kim Y., Arote R., Jere D., Jeong H., Jang M., Nah J., Xu C., Park I., Cho M., Cho C., Galactosylated poly(ethylene glycol)-chitosan-graft-polyethylenimine as gene carrier for hepatocyte-targeting, J Control Release, **131**, (2008), 150-157.

Hua F.J., Park T.G., Lee D.S., A facile preparation of highly interconnected macroporous poly(D,L-lactic acid-co-glycolic acid) (PLGA) scaffolds by liquid-liquid separation of a PLGA-dioxane-water-ternary system, Polymer, **44**, (2003), 1911-1920.

Huang L., McMillan R.A., Apkarian R.P., Pourdeyhimi B., Conticello V.P., Chaikof E.L., Generation of synthetic elastin-mimetic small diameter fibers and fiber networks, Macromolecules, **33**, (2000), 2989.

Humacher D.W., Scaffolds in tissue engineering and cartilage, Biomaterials, **21**, (2000), 2529-43.

Hutmacher D.W., Sittinger M., Risbud M.V., Scaffold based tissue engineering: rationale for computer aided design and solid free form fabrication systems, Trends Biotechnol, **22**, (2004), 354-362.

Ironi L., Tentoni S., A model based approach to the assessment of physicochemical properties of drug delivery materials, Comput Chem Eng, **27**, (2003), 803-812.

Jagla E.A., Stable propagation of an ordered array of cracks during directional drying, Phys Rev E, **65** (046147), (2002).

Jalil R., Nixon J.R., Biodegradable poly(lactic acid) and poly(lactide-co-glycolide) microcapsules: problems associated with preparative techniques and release properties, J Microencapsul, **7**, (1990), 297-325.

Jiang H., Fang D., Hsiao B., Chu B., Chen W., Preparation and characterization of ibuprofen-loaded poly(lactide-co-glycolide)/poly(ethylene glycol)-g-chitosan electrospun membranes, J Biomat Sci-Polm E, **15**, (2004), 279-296.

Jiang H., Hu Y., Zhao P., Li Y., Zhu K., Modulation of protein release from biodegradable core-shell structured fibers prepared by coaxial electrospinning, J Biomed Mater Res-A, **79**, (2006), 50-7.

Jiang Q., Reddy N., Yang Y., Cytocompatible cross-linking of electrospun zein fibers for the development of water-stable tissue engineering scaffolds, Acta Biom 2010.

Johanson C., Pearmeability and vuscularity of the developing brain: cerebellum vs. cerebral cortex, Brain Res., **190**, (1980), 3-16.

Joachim K., Welsh W.J., Knight D., A new approach to the rationale discovery of polymeric biomaterials, Biomaterials, **28**, (2007), Pages 4171-4177.

Jose L., Arias M., Aldofina R., Margarita L., Delgado A.V., Poly(alkylcyanoacrylate) colloidal particles as vehicles for antitumor drug delivery: a comparative study, Colloid Surface B, **62**, (2008), 64-70.

Karp M. and Langer R., Development and therapeutic application of advanced biomaterials, Curr Opin Biotech, **18**, (2007), 454-459.

Kenaway E., Bowlin G.L., Mansfield K., Layman J., Simpson D.G., Sanders E.H., Wnek G.E., Release of tetracycline hydrochloride from electrospun poly(ethylene-co-vinylacetate), poly(lactic acid), and a blend, J Control Release, **81**, (2002), 57.

Kikicl., Polymer-supercritical fluid interactions, J Supercrit Fluids, **47**, (2009), 458-465.

Kim S.S., Utsunomiya H., Koski J.A., Wu B.M., Cima M.J., Sohn J., Mukai K., Griffith L.G., Vacanti J.P., Survival and function of hepatocytes on novel three dimensional synthetic biodegradable polymer scaffold with intrinsic network of channels, Ann Surg, **228** (1), (1998), 8-13.

Kim S.W., Feijen J., Cremers H., Bae Y.H., Kwon G.S., Release of macromolecules from albumin-heparin microspheres, Int J Pharm, **79**, (1992), 191-198.

Kirkpatrick D.L., Watson S., Ulhaq S., Structure-based drug design: combinatorial chemistry and molecular modeling, Comb Chem High T Scr, **2**,(1999), 211-221.

Kissel T., Breitenbach A.,Pistel K.F., Biodegradable comb polyesters. Part II. Erosion and release properties of poly(vinyl alcohol)-g-poly(lactic-co-glycolic acid), Polymer, **41**, (2000), 4781-4792.

Kissel T., Lea A.D., Wittmar M., The role of branched polyesters and their modifications in the development of modern drug delivery vehicles, J Control Release, **101**, (2005), 137- 149.

Knight C.G., (Ed.), Liposomes from physical structure to therapeutic applications, Elsevier, Amsterdam, 1981.

Kretlow J.D., Klouda L., Mikos A.G., Injectable matrices and scaffolds for drug delivery tissue engineering, Adv Drug Deliv Rev, **59**, (2007), 263-273.

Kumaresh S., Soppimath S., Aminabhavi T.M., Kulkarni A.R., Rudzinski W.E., Biodegradable polymeric nanoparticles as drug delivery devices, J Control Release, **70**, (2001), 1-20.

Kwon G.S., Okano T., Polymeric micelles as new drug carriers, Adv Drug Deliver Rev, **21**, (1996), 107-16.

Lai J., Bakker A., Non-linear creep and recovery behaviour of high-density polyethylene Scripta Metallurgicaet Materialia, **28**, (1993), 1447-1452.

Landers R., Pfister A., Hubner U., John H., Schmelzeisen R., Mülhaupt R., Fabrication of tissue engineering scaffolds by means of rapid prototyping techniques, J Mater Sci, **37**, (2002), 3017-16.

Langer R., Biomaterials in drug delivery and tissue engineering: One laboratory experience, Account Chem Res, **33**, (2000), 94-101.

Lanza R.P., Langer R., Chick W.L., Principles of Tissue Engineering: Academic Press, Austin, TX, 1997, 405-427.

LaVan D.A., et al., Small scale systems for *in vivo* drug delivery, Nat Biotechnol, **21**, (2003), 1184-1191.

Lee J.S., Oh S.H., Liu J., Soker S., Atala A., Yoo J.J., The use of thermal treatments to enhance the mechanical properties of electrospun poly(ε-caprolactone) scaffolds, Biomaterilas , **29**, (2008), 1422-30.

Lee J., Cuddihy M.J., Kotov N.A., Three-dimensional cell structure matrices: state of the art, Tissue Eng, **16** B, (2008), 61.

Lee S.H., Shin H., Matrices and scaffolds for the delivery of bioactive molecules in bone and cartilage tissue engineering, Adv Drug Deliver Rev, **59**, (2007), 339-359.

Lee Y.M., Kim D.S., Lee C., Park H.B., Rhim J., Crosslinked poly(vinyl alcohol) membranes containing sulfonic acid group: proton and methanol transport through membranes, J Membrane Sci, **238**, (2004),143-151.

Legrand P., Lesieur S., Bochot A., Gref R., Raatjes W., Barratt G., Vauthier C., Influence of polymer behaviour in organic solution on the production of polylactides nanoparticles by nanoprecipitation, Int J Pharm, **344**, (2007), 33-43.

Levin V.A., Landahl H.D., Freeman-Done M.A., The application of brain capillary permeability co-efficient measurement to pathological condition and the section of agents which cross the blood-brain barrier, J Pharmacokinet Biop, **4**, (1976), 499-519.

Li C., Jin C., Kim H.J., Kaplan D.L., Electrospun silk-bmp-2 scaffolds for bone tissue engineering, Biomaterials, **3** (27), (2006), 115-24.

Li W.J., Laurencin C.T., Caterson E.J., Taun R.S., Ko F.K., Nanofibers and nanoparticles for orthopaedic surgery applications, J Biomed Mater Res, **60**, (2002), 613.

Li W.C., Cooper J.A., Mauck R.L., Fabrication and characterization of six electrospun poly (alpha-hydroxy ester)-based fibrous scaffold for tissue engineering applications, Acta Biom **2**, (2006), 377.

Li Y., Jiang H.,Zhu K., Encapsulation and controlled release of lysozyme from electrospun poly(epsilon-caprolactone)/poly(ethylene glycol) non woven membranes by formation of lysosome-oleate complexes, J Mater Sci-Mater M, **19**, (2008), 827-32.

Li C., Liu Z., Zhuo R., Synthesis and properties of degradable hydrogels of konjacglucomannan grafted acrylic acid for colon-specific drug delivery, Polymer, **46**, (2005),6274-6281.

Lim B., Kim S., Morphology of crosslinked poly(butyl methacrylate-co-methyl methacrylate) porous membranes, J Membrane Sci, **209**, (2002), 293-307.

Lin Q., Yee A.F., Mechanical properties of in situ composites based on polycarbonate and liquid crystalline polymer, Polymer, **35**, (1994), 3463-3469.

Liu H.Q., Hsieh Y.L., Single-step protein surface-attachment to electrospun fibers, J Polym Sci Pol Phys, **40**, (2002), 2119.

Luciani A., Coccoli V., Orsi S., Ambrocio L., Netti P.A., PCL microspheres based functional scaffolds by bottom-up approach with predefined microstructural properties and release profiles, Biomaterials, **29**, (2008), 4800-7.

Lutz J.M., Coleman M.P., Trends in primary cerebral lymphoma, Brit J Cancer, **70**, (1994), 716-18.

Mailin-Varlet P., Rahn B., Gogolewski S., Long-term *in vivo* degradation and bone reaction to various polylactides: 1. One-year results, Biomaterials, **18**, (1997), 257-266.

Manjour A., Poisson M., Delattre J.Y., Chimiotherapie des tumeurs cerebrales primitives malignes, La Lettre Cancerologue, **4**, (1995), 49-67.

Martin-Padura I., Lostaglio S., Schneemann M., Junctional adhesion molecule, a novel member of the immunoglobulin superfamily that distributes at intercellular junctions and modulates monocyte transmigration, J Cell Biol, **142**, (1998), 117-127.

Matthews J.A., Wnek G.E., Simpson D.G., Bowlin G.L., Electrospinning of collagen nanofibers, Biomacromolecules, **3**, (2002), 232.

Menei P., Boisdron-Celle M., Croue A., Guy G., Benoit J.P., Effect of stereotactic implantation of biodegradable 5-fluorouracil-loaded microspheres in healthy and C6 glioma-bearing rats, Neurosurgery, **39**, (1996), 117-124.

Millar J.R., Interpenetrating polymer networks-styrene-divinylbenzene copolymers with 2 or 3 interpenetrating networks, and their sulphonates, J Chem Soc (1960), 1311.

Mitte L., Anderson J., Mollecular architecture of tight junctions, Annu Rev Physiol, **60,** (1998), 121-142.

Mitie L., Itallie C.V., Anderson J., Molecular physiology and pathophysiology of tight junctions, Am. J. Physiol: Gastr Liver Phys, **279**, (2000), G250-G254.

Mohile N.A., Abrey L.E.,Primary central nervous system lymphoma, Neurol Clin **25**, (2007), 1193-1207.

Mulder M., Basic principles of membrane technology, Dordrecht, The Netherlands: Kluwer, 1991.

Nag S., Morphology and Molecular Properties of Cellular Component growth factors of Normal Cerebral Vessels, Humana Press, Totowa, NJ, 2003.

Niu X., Feng Q., Wang M., Guo X., Zheng Q., *In vitro* and release behaviour of porous poly(lactic acid) scaffolds containing chitosan microspheres as a carrier for BMP-2-derived synthetic peptide, Polym Degrad Stabil, **94**, (2009), 176-82.

Neuwelt E.A., Goldman D.L., Dahlborg S.A., et al., Primary CNS lymphoma treated with osmotic blood- brain barrier disruption: Prolonged survival and preservation of cognitive function, J Clin Oncol, **9**, (2004), 1580- 90.

Omathanu P., Ramesh P., Polymers in drug delivery, Curr Opin Chem Biol, **5**, (2001), 447-451.

Pantani R., Coccurullo I., Speranza V., Titomanlio G., Modeling of morphology evolution in the injection molding process of thermoplastic polymers, Prog Polym Sci, **30**, (2005), 1185-1222.

Pignatello R., Bucolo C., Ferrara P., Maltese A., Puleo A., Puglisi G., RS100® nanosuspensions for the ophthalmic controlled delivery of ibuprofen, Eur J Pharm Sci, **16**, (2002), 53 – 61.

Oh H., Kang S.G., Kim E.S., Cho S.H., Lee J.H., Fabrication and characterization of hydrophilic poly(lactic-*co*-glycolic acid)/poly(vinyl alcohol) blend cell scaffolds by melt-molding particulate-leaching method, Biomaterials, **24**, (2003), 4011-4021.

Panyam J., Labhasetwar V., Size-dependency of nanoparticle-mediated gene transfection: studies with fractionated nanoparticles, Int J Pharm, **244**, (2002), 105 -115.

Park A., Wu B., Graffith L.G., Intergration of surface modification and 3D fabrication techniques to prepare patterned poly(L-lactide) substrates allowing regionally selective cell adhesion, J Biomat Sci-Polm E, **9**, (1998), 89-110.

Pasqualil., Bettini R., Are pharmaceuticals really going supercritical?, Int J Pharm, **364**, (2008), 176-187.

Pauchard L., Adda-Bedia M., Allain C., Couder Y., Morphologies resulting from directional propagation of fractures, Phys Rev E, **67** (027103), 2003.

Pech I.V., Peterson K., Cairncross J.G., Chemotherapy for brain tumors, Oncology, **12**, (1998), 537-53.

Peppas A.N., Korsmeyer R.W., Gurny R., Doelker E., Buri P., Mechanisms of solute release from porous hydrophilic polymers, Int J Pharm, **15**, (1983), 25-35.

Pham Q.P., Sharma U., Mikos A.G., Electrospinning of polymeric nanofibers Tissue Eng **12**, (2006), 1197-211.

Pollack I.F., Keating R., New deliveries for paediatric brain tumors, J Neuro-Oncol, **75**, (2005), 315-326.

Ponce S., Orive G., Gascon A.R., Hernandez R.M., Pedraz J.L., Nanoparticles prepared with different biomaterials to immobilize GDNF secreting fibroblasts, Int J Pharm, **293**, (2005), 1-10.

Popovic N. and Brundin P., Therapeutic potential of controlled drug delivery systems in neurodegenerative diseases, Int J Pharm, **34**, (2006), 120-126.

Prabaharan M., Jayakumar R., Chitosan-graft-ß-cyclodextrin scaffolds with controlled drug release for tissue engineering applications, Int J Biol Macr, **44**, (2009), 320-325.

Rahimpour A., Madaeni S.S., Mehdipour-Ataei S., Synthesis of a novel poly(amide-imide) (PAI) and preparation and characterization of PAI blended polyethersulfone (PES) membranes, J Membrane Sci, **311**, (2008), 349-359.

Rajeev A.J.,The manufacturing techniques of various drug loaded biodegradable poly(lactide-*co*-glycolide) (PLGA) devices, Biomaterials, **21**, (2000), 2475-2490.

Ramehandan M.,Robinson D., *In vitro* and *in vivo* release of ciprofloxacin from PLGA 50:50 implants, J Control Release, **45**,(1998), 167- 175.

Reneker D.H., Chun I., Spinning continous fibers for nanotechnology, Nanotechnology, **7**, (1996), 216.

Rosa G.D., Immelli R., Rotonda M.I.L., Miro A., Qualgia F., Influence of the co- encapsulation of different non-ionic surfctants on the properties of PLGA insulin-loaded microspheres, J Control Release, **69**, (2000), 283-295.

Rutten M.G., Victor P.M., Müller K.E., Soethout E.C., Neutrophil migration in the lung, general and bovine-specific aspects, Veterinary Immunology and Immunopathology, **87**, (2002), 277-285.

Sachlos E., Czersnuka J.T., Making tissue engineering scaffolds work, Review on the application solid free form fabrication technology to the production of tissue engineering scaffolds, Eur Cells Mater, **5**, (2003), 29-40.

Sahiner N., Pekel N., Güven, Radiation, synthesis, characterization and amidoximation of N-vinyl-2-pyrrolidone/acrylonitrile interpenetrating polymer networks, React Func Polym **39**, (1999), 139.

Saltzman W.M., Olbricht W.L., Building drug delivery into tissue engineering, Nat Rev Drug Discov, **1**, (2002), 177-186.

Salvay D.M., Shea L.D., Inductive tissue engineering with protein and DNA-releasing scaffolds, Mol Biosyst, **2**, (2006), 36-48.

Saylor D.M., Kim C., Patwardhan D.V., Warren J.A., Diffuse-interface theory for structure formation and release behavior in controlled drug release systems, Acta Biomaterialia, **3**, (2007), 851-864.

Selvam P., Tsuboi H., Kubo M., Koyaba M., Miyamoto A., Tight-binding quantum chemical molecular dynamics method: a novel approach to the understanding and design of new materials and catalysts, Catalysis Today, **100**, (2005), 11-25.

Shorlin K.A., Bruyn J.R., Graham M., Morris S.W., Development and geometry of isotropic and directional shrinkage-crack patterns, Phys Rev E, **61**(6), (2000), 6950-7.

Sill T.J., Recum H.Av., Electrospinning: applications in drug delivery, tissue engineering, Biomaterials, **29**, (2008), 1989.

Singh M., Briones M., Ott G., O Hagon D., Cationic microparticles: a potent delivery system for DNA vaccines, Proc Natl Acad Sci USA, (1997), 811-816.

Sipos E., Tyler B., Burger P., Brem H., Optimizing interstitial delivery of BCNU from controlled release polymers for the treatment of brain tumors, Cancer Chemoth Pharm, **39**, (1997), 383-389.

Sisson K., Zhang C., Farach-Carson M.C., Chase D.B., Rabolt J.F., Evaluation of cross-linking methods for electrospun gelatin on cell growth and viability, Biomacromolecules, **10**, (2009), 1675.

Smith R.J., Agnieszka S., Weber N., Knight D., Abramson S., Khon J., Integration of combinatorial synthesis, rapid screening, and computational modeling in biomaterials development, Macromol Rapid Comm, **25**, (2004), 27-40.

Sohier J., Hamann D., Koenders M., Cucchiarini M., Madry H., van Blitterswijk C., de Groot K., Bezemer J.M., Tailored release of TGF- ß1 from porous scaffolds for cartilage tissue engineering, Int J Pharm, **332**, (2007), 80-89.

Spěváček J., NMR investigations of phase transitions in aqueous polymer solutions and gels, Curr Opin Colloid In, **14**, (2009), 184-191.

Stanton R.V., MountJ., Miller J.L., Combinatorial library design: maximising model-fitting compounds within matrix synthesis constraints, J Chem Inf Comp Sci, **40**, (2000) 701-705.

Szarowski D.H., Anderson M.D., Retterer S., Spence A.J., Isaacson M., Craighead H.G., Turner J.N., Shain W.,Brain responses to micro-machined silicon devices, Brain Research, **983**, (2003), 23-35.

Tabata Y., Takebayashi, Y., Ueda, T., Ikada, Y., A formulation method using D,L-lactic acid oligomer for protein released with reduced initial burst, J Control Release, **23**, (1993) 55–64.

Tanaka K., Nishio S., Matsauura Y., YAmabe T., Preparation of organic semiconductive thin film by plasma-polymerization of aromatic compounds and their derivatives, Synthetic Metals, **55**,1993, 896-901.

Tai W., Cui F., Cai Q., Ma J., Lee I., Hou S., Xu Q., The repair of brain lesion by implantation of hyaluronic acid hydrogels modified with laminin, J Neurosci Meth, **148**, (2005), 60-70.

Tessmar J.K., Gopferich A.M., Matrices and scaffolds for protein delivery in tissue engineering, Adv Drug Deliver Rev, **59**, (2007), 360-373.

Thakur R.A., Florek C.A., Kohn J., Michnak B.B., Electrospun nanofibrous scaffold with targeted drug release profiles for potential application as wound dressing, Int J Pharm, **364**, (2008), 87-93.

Tsai M.L., Bai S W., Chen R., Cavitation effects versus stretch effects resulted in different size and polydispersity of ionotropic gelation chitosan-sodium tripolyphosphate nanoparticle, Carbohyd Polm, **71**, (2008), 448 -457.

Tushar K.V., Aliasgar S., Mansoor M.A., Improved oral bioavailability and brain transport of Saquinavir upon administration in novel nanoemulsion formulations, Int J Pharm, **347**, (2008), 93-101.

Tuzun R.E., Noid D.W.,Sumpter B.G., Computer simulation of complex strongly coupled nanometer-scale systems: breaking the billion atom barrier, Comput Method Appl M, **35**, (1998), 93-100.

Tzuu-Yuang H., Norio A., Toru H., YukitakaU., ACNU, MTX, and 5-FU penetration of rat brain tissue and tumors, J Neuro-Oncol, **45**, (1999), 9-17.

Umezwa F., Eto Y., Liposome targeting to mouse brain: mannose as a recognition marker, Biochem Bioph Res Co, **153** (3), (1988),1038-44.

Ushio Y., Hayakawa T., Hasegawa H., Yanmada K., Arita N., Chemotherapy of malignant gliomas, Neurosurgery Rev, **7**, (1984), 3-12.

Vaidya A., Chaudhury M.K., Synthesis and surface properties of environmentally responsive segmented polyurethanes, J Colloid Interf Sci, **249**, (2002), 235-245.

Van de Witte P., Dijkstra P.J., van den Berg J.W.A., Feijen J., Phase separation processes in polymer solutions in relation to membrane formation, J Membrane Sci, **117**(1996), 1-31.

Valtonen S., Timonen U., Toivanen P., et al., Interstitial chemotherapy with carmustine-loaded polymers for high grade gliomas: a randomized, double blind study, Neurosurgery, **1**, (1997), 44-49.

Vauthier C., Beananabbou S., Spenlehauer G., Veillard M., Couvreur P., Methodology of ultra-dispersed polymer system, STP Pharm Sci, **1**, (1991), 109-116.

Volk EL., Rohde K., Rhee M., McGuire J.J.,Doyle L.A., Ross D.D., Schneider E., Cancer Res, **60**, (2000), 3514-21.

Wang C., Li J., Teo Lee C.S. T., The delivery of BCNU to brain tumors, J Control Release, **61**, (1999), 21-41.

Wang X., Wenk E., Zhang X., Meinel L., Vunjak-Novakovic G., Kaplan D.L., Growth factor gradients via microsphere delivery in biopolymeric scaffolds for osteochondral tissue engineering, J Control Release, **134**, (2009), 81-90.

Wang X., Song G., Lou T., Fabrication and characterization of nano-composite scaffold of PLLA/silane modified hydroxypatite, Med Eng Phys, **32**, (2010), 391-397.

Ward I.M., Birly A.W., Harworth B., Verlag J.B., Physics of plastics: Processing, properties and materials engineering: Polymer, **34**, (1993), 246.

Wei-Wen H., Elkasabi Y., Chen H., Zhang Y., Lahann J., Holister S.J., Krebbsbach P.H., The use of reactive polymer coatings to facilitate gene delivery from poly(ε-caprolactone) scaffolds, Biomaterials, **30**, 2009, 5785-5792.

Werner M.H., Phuphanich S., Lyman G.H., The increasing incidence of malignant gliomas and primary central nervous system lymphoma in elderly, Cancer, **76** (1), (995),1634-42.

Wolburg H., Lippoldt A., Tight junctions of the blood-brain barrier: development, composition and regulation, Vasc Pharmacol, **38**, (2000), 323-337.

Wolburg H., Wolburg-Buscholz K., Krans J., Rascher-Eggstein G., Liebner S., Hamm S., Duffner F., Grote E.H., Risau W., Engelhardt B., Localization of claudin-3 in tight junctions of the blood-brain barrier is selectively lost during experimental autoimmune encephalomyelitis and human glioblastoma multiforme, Acta Neuropathol, **105**, (2003), 586-592.

Whittlerey K.J., Shea C.D., Delivery systems for small molecule drugs, proteins, and DNA: the neuroscience/biomaterials interface, Exp Neurol, **190**, (2004), 1-16.

Yi L., Carlos A.A., Shaoshen C., Shaping biodegradable polymers as nanostructures: Fabrication and applications, Drug Discovery Today Technologies, **2** (1), (2005), 97-102.

Yoshimotoa H., Shina M.Y., Teraira H., Vacanti J.P., A biodegradable nanofiber scaffold by electrospinning and its potential for bone tissue engineering, Biomaterials, **24**, (2003), 2077.

Zein I., Hutmacher D.W., Tan K.C., Teoh S.H., Fused deposition modeling of novel scaffold architectures for tissue engineering applications, Biomaterials, **23**, (2002), 1169-85.

Zeni M., Riveros R., de Souza J.F., Mello K., Meireles C., Filho G.R., Morphologic analysis of porous polyamide 6,6 membranes prepared by phase inversion, Desalination, **221**, (2008), 294-297.

Zhang G., Suggs L.J., Matrices and scaffolds for drug delivery in vascular tissue engineering, Adv Drug Deliver Rev, **59**, (2007), 360-373.

Zhang L.F., Yang D.J., Chen H.C., Sun R., Xu L., Xiong Z.C., Govender T., Xiong C.D., An ionically crosslinked hydrogel containing vancomycin coating on a porous scaffold for drug delivery and cell culture, Int J Pharm, **353**, (2008), 74-87.

Zong X.H., Kim K., Fang D.F., Ran S.F., Hsiao B.S., Chu B., Control of dimensional stability and degradation rate in electrospun composite scaffolds composed of poly(DL-lactide-co-glycolide) and poly(ε-caprolactone) Polymer, **43**, (2002), 4403.

9. APPENDICES

Appendix I

Computational and Molecular Modeling and Structural Rationalization for the Design of a Drug-loaded PLLA/PVA Biopolymeric Membrane. Bongani Sibeko, Viness Pillay, Yahya E. Choonara, Riaz A. Khan, Girish Modi, Sunny E. Iyuke, Dinesh Naidoo and Michael P. Danckwerts, Journal of Biomedical Materials, 2009, (4) 1:15014.

Appendix II

A poster entitled "Synthetic Approaches for Fabricating Biopolymeric Membranes for Rate-modulated Drug Delivery". Bongani Sibeko, Viness Pillay, Yahya E. Choonara, Girish Modi, Sunny E. Iyuke and Michael P. Danckwerts. Workshop on Structure and properties of Nanomaterials, University of Zululand, 2007.

Appendix III

A poster entitled "Influence of complex oxidizing agents on the physicochemical and physicomechanical properties of crosslinked co-blended polymeric membranes." Bongani Sibeko, Viness Pillay, Yahya E. Choonara, Girish Modi, Sunny E. Iyuke and Michael P. Danckwerts. 28th Annual Conference of the Academy of the Pharmaceutical Sciences, Athene Conference Centre, Club Mykonos, and Langerbaan, Cape Town, 2007.

Appendix IV

A podium presentation entitled "An implantable hydrogel drug delivery system for chemotherapeutic applications". Bongani Sibeko, Viness Pillay, Yahya E. Choonara, Girish

Modi, Sunny E. Iyuke and Michael P. Danckwerts. Research day and postgrad expo, University of the Witwatersrand, Faculty of Health Sciences, 2008.

Appendix VI

A podium presentation entitled "Fabrication and Characterization of MTX-loaded PLA/PVA biopolymeric membranous drug delivery device". Bongani Sibeko, Viness Pillay, Yahya E. Choonara, Girish Modi, Sunny E. Iyuke and Michael P. Danckwerts. 29th Annual Conference of the Academy of the Pharmaceutical Sciences, Hunters Rest, Rustenburg on the, 2008.

Appendix I

Computational and Molecular Modeling and Structural Rationalization for the Design of a Drug-loaded PLLA/PVA Biopolymeric Membrane. Bongani Sibeko, Viness Pillay, Yahya E. Choonara, Riaz A. Khan, Girish Modi, Sunny E. Iyuke, Dinesh Naidoo and Michael P. Danckwerts, Journal of Biomedical Materials, 2009, (4) 1:15014.

IOP PUBLISHING BIOMEDICAL MATERIALS

Biomed. Mater. 4 (2009) 015014 (11pp) doi:10.1088/1748-6041/4/1/015014

Computational molecular modeling and structural rationalization for the design of a drug-loaded PLLA/PVA biopolymeric membrane

B Sibeko[1], V Pillay[1,5], Y E Choonara[1], R A Khan[1], G Modi[2], S E Iyuke[3], D Naidoo[4] and M P Danckwerts[1]

[1] Department of Pharmacy and Pharmacology, University of the Witwatersrand, 7 York Road, Parktown, 2193 Johannesburg, South Africa
[2] Division of Neurosciences, Department of Neurology, University of the Witwatersrand, Johannesburg, South Africa
[3] School of Chemical and Metallurgical Engineering, University of the Witwatersrand, Johannesburg, South Africa
[4] Division of Neurosciences, Department of Neurosurgery, University of the Witwatersrand, Johannesburg, South Africa

E-mail: viness.pillay@wits.ac.za

Received 23 July 2008
Accepted for publication 7 November 2008
Published 12 December 2008
Online at stacks.iop.org/BMM/4/015014

Abstract

The purpose of this study was to design, characterize and assess the influence of triethanolamine (TEA) on the physicomechanical properties and release of methotrexate (MTX) from a composite biopolymeric membrane. Conjugated poly(L-lactic acid) (PLLA) and poly(vinyl alcohol) (PVA) membranes were prepared by immersion precipitation with and without the addition of TEA. Drug entrapment efficiency (DEE) and release studies were performed in phosphate buffered saline (pH 7.4, 37 °C). Scanning electron microscopy elucidated the membrane surface morphology. Computational and structural molecular modeling rationalized the potential mechanisms of membrane formation and MTX release. Bi-axial force–distance (*F–D*) extensibility profiles were generated to determine the membrane toughness, elasticity and fracturability. Membranes were significantly toughened by the addition of TEA as a discrete rubbery phase within the co-polymer matrix. MTX-TEA-PLLA-PVA membranes were tougher ($F = 89$ N) and more extensible ($D = 8.79$ mm) compared to MTX-PLLA-PVA ($F = 35$ N, $D = 3.7$ mm) membranes as a greater force of extension and fracture distance were required ($N = 10$). DEE values were relatively high (>80%, $N = 5$) for both formulations. Photomicrographs revealed distinct crystalline layered morphologies with macro-pores. MTX was released by tri-phasic kinetics with a lower fractional release of MTX from MTX-TEA-PLLA-PVA membranes compared to MTX-PLLA-PVA. TEA provided a synergistic approach to improving the membrane physicomechanical properties and modulation of MTX release. The composite biopolymeric membrane may therefore be suitable for the novel delivery of MTX in the treatment of chronic primary central nervous system lymphoma.

1. Introduction

Advances in biomaterials research have provided solutions for combating numerous challenges posed by various disease conditions [1]. The amalgamation of polymeric science with the pharmaceutical sciences and medicine has led to the development of novel biomaterials for specific applications [2–5]. Despite the progress in the development of such biomaterials, a large number of biomaterial-based devices

[5] Corresponding author.

 © 2009 IOP Publishing Ltd Printed in the UK

are currently used clinically with unsatisfactory clinical performance [6]. Furthermore, very few synthetic devices are approved by the US Food and Drug Administration (FDA) due to the fact that the time, complexities and attempts to tailor the properties of polymers to complement specific applications are mostly based on trial and error [7]. Therefore, there is a need to extend and focus biomaterials research toward economical approaches that may overcome the challenges of designing new biomaterials. Refined approaches such as combinatorial methods, high-throughput experimentation and computational molecular modeling for the development of biomaterials are able to significantly contribute to this area of research by creating opportunities to simulate, investigate, model and predict the structure and properties of newly synthesized biomaterials [8–10].

Computational molecular modeling and structural rationalization techniques are becoming fundamental to the innovative development of biomaterials that were initially unexploited due to the complex nature of biological and pharmacological domains and the expertise and interdisciplinary commitments required to formulate computational models of various phenomena [11, 12]. However, the fusion of polymer and pharmaceutical science with computational chemistry has resulted in the incorporation of theoretical chemistry into efficient computer software to gain further insight into the complexity and behavior of newly synthesized biomaterials in order to justify theoretical concepts when conclusive postulations correlate well with experimental results [13, 14]. Computational chemistry employs molecular mechanics and quantum mechanics such as semi-empirical, *ab initio* and density functional theory (DFT) to predict the molecular structure of biomaterials and compute different molecular descriptors. Computational modeling can be regarded as a third element in the research triad complementing experiment and theory [15, 16].

Ironi and Tentoni [11] employed a computational framework to explore the mucoadhesive potential of sodium carboxymethylcellulose. Polymer–mucin mixtures at varying concentrations underwent standard creep testing, and accurate ordinary differential equation models were obtained from the data [11]. Computational modeling functions are best supported by techniques that facilitate the development of predictive models and reveal the molecular structure and underlying physical phenomena governing the performance of a biomaterial that would not otherwise be revealed by laboratory experiments [17–19].

Biocompatible and biodegradable polymers in particular have been regarded as suitable materials for developing optimized drug delivery systems with improved therapeutic efficacies, better patient compliance and reduced side-effects [9]. Polymers are a versatile class of materials with well-defined physicochemical and physicomechanical properties [20–23]. Depending on the requirements placed upon a certain material, polymeric drug carriers can be fabricated into various geometries by employing processing methods ranging from implants, stents, grafts, microparticles or nanoparticles or membranes. The combination of different polymers is an approach that leads to the formation of a modified polymer that provides a broader spectrum for fulfilling the objectives of the drug delivery system. Aliphatic polyesters, such as poly (lactic acid), and their co-polymers have been widely used for fabrication of drug delivery devices [24–26]. In addition, formulations tend to show polyphasic drug release profiles which deviate from the ideal 'infusion-like' profile generated by zero-order release formulations [27–29].

Grafting of polyester chains onto hydrophilic backbones would alter the degradation and release properties of the carrier system [30]. Kissel *et al* [31, 32] successfully formulated a drug delivery system based on a modified polyester fabricated by grafting poly(lactic-co-glycolic acid) (PLGA) onto poly(vinyl alcohol) (PVA) or amine modified poly(vinyl alcohol) or sulfobutylated poly(vinyl alcohol) to yield PVA-g-PLGA, DEAPA-PVA-g-PLGA and SB-PVA-g-PLGA respectively. Microparticles prepared from PVA-grafted PLGA also displayed superior encapsulation efficiencies for proteins ranging from 70% to 90% with yields of approximately 60–85%. Drug release modulation and erosion could be adjusted to meet specific applications when formulated into various drug delivery vehicles such as microparticles, nanoparticles, tablets, implants and membranes with erosion times ranging from hours to weeks [31, 32].

Therefore, this study focused on applying computational chemistry as a modeling tool for the rational design of a biopolymeric membrane system for the delivery of methotrexate (MTX). The molecular structural predictions were performed using database fragments for predicting the design and evolution of the biopolymeric membrane with pre-defined physical property endpoints. The fragmental approach was the most appropriate with the measured physical properties decomposed into classes, substituent contributions and interaction corrections. Algorithms that were used such as the Gaussian interface fragmented the membrane according to the physical understanding of the phenomenon being modeled such as the principals of tautomerism as well as partition or distribution coefficients. The information obtained from virtual molecular structures and computer models will be used to formulate theoretical postulations on factors such as drug entrapment efficiency (DEE) and the mechanisms of drug release. MTX was selected as the model drug due to the potential of employing the biopolymeric membrane as an intracranial implant for the treatment of primary central nervous system lymphoma [33].

2. Materials and methods

2.1. Materials

Methotrexate (model drug) and stannous octoate (catalyst) (Tin (II) 2-ethylhexanoate) were purchased from Sigma Aldrich (St Louis, MO). Poly(vinyl alcohol) (grade 8/88, $M_w = 49\,000\ \mathrm{g\ mol^{-1}}$) and triethanolamine (TEA) (plasticizer) were purchased from Saarchem (Krugersdorp, South Africa), a division of Merck chemicals. Poly (L-lactic acid) (PLLA; Resomer® grade R203H) was purchased from Boehringer Ingelheim (Ingelheim, Germany) and dimethyl-sulfoxide

(DMSO) (solvent), reagent grade acetone and methanol (non-solvent blend) were purchased from Rochelle Chemicals (Johannesburg, South Africa).

2.2. *Preparation of the biopolymeric membrane*

MTX-loaded biopolymeric membranes were fabricated by layered hydrophile–lipophile conjugation and graft co-polymerization of the lactone PLLA and the polyol PVA with and without the addition of the amphiphile TEA (PLLA-PVA and TEA-PLLA-PVA) employing stannous octoate as a catalyst at a reaction temperature of 150 °C. TEA was added due to its relatively balanced interphase absorption and was reacted with the modified co-polymer to induce backbone activation for the addition of the model drug MTX. Phase separation was achieved by an immersion precipitation technique. Briefly, homogenous solutions of PLLA and PVA (10% w/v) were blended after solubilization in DMSO. The polymers were reacted in a ratio of 1:1.75 (15:20 mL) PLLA/PVA in the presence of stannous octoate at 150 °C for 1 h. Thereafter, 2.5 mL TEA was added to the polymeric solution and the reaction was allowed to proceed for a further 1 h. MTX (15 mg) dissolved in 0.5 mL DMSO was added to 2.5 mL of the composite polymeric solutions and casted on a glass petri dish (15 mm in diameter) and then immersed in a mixed non-solvent system comprising acetone:methanol in a ratio of 1:1. The resultant biopolymeric membranes were recovered after 24 h from the coagulation bath and allowed to dry at room temperature (21 ± 0.5 °C) prior to further characterization. All reactions were performed with purified core molecules and monomers.

2.3. *Computational and molecular structural modeling of biopolymeric membrane formation*

Computational and molecular structural modeling was performed to deduce a hypothesized chemical structure and potential inter-polymeric interaction during membrane balance and layering. Semi-empirical, *ab initio* and DFTs of molecular and quantum mechanics were used to generate predictions of the molecular structure of the materials and compute various molecular attributes based on the inherent interfacial phenomena underlying the formation of the biopolymeric membranes prepared by the immersion precipitation technique [34–36]. Models and graphics based on the step-wise molecular mechanism of membrane formation, polymer interconversion, grafting and drug chelation as envisioned by the chemical behavior and stability were generated on ACD/I-Lab, V5.11 (Add-on) software (Advanced Chemistry Development Inc., Toronto, Canada, 2000).

2.4. *Analysis of the biopolymeric membrane swelling potential*

Swelling of the biopolymeric membrane was determined by immersing a known mass of membrane samples in 10 mL phosphate buffered saline (PBS) (pH 7.4, 37 °C) in petri dishes (90 mm in diameter) and allowed hydration to take place for 30 min. The membranes were allowed to reach maximum hydration potential, and thereafter the swollen mass of the membranes was determined by gravimetric analysis using an electronic analytical mass balance (Mettler Toledo, Inc., Columbus, OH) after removing the samples from the PBS solution and blotted with filter paper to adsorb water on the membrane surface. The degree of swelling was calculated as a difference between the mass of the non-hydrated and hydrated membranes (%) employing equation (1):

$$S_D = \frac{(W_s - W_i)}{W_i} \times 100, \quad (1)$$

where S_D is the degree of swelling in PBS and W_i and W_s are the masses of the biopolymeric membranes before and after hydration, respectively.

Table 1. Test parameters employed bi-axial extensibility testing of the biopolymeric membrane.

Parameter	Setting
Test mode	Compression
Pre-test speed	1.00 mm s^{-1}
Test speed	1.00 mm s^{-1}
Post-test speed	1.00 mm s^{-1}
Trigger mode	Distance
Distance	10 mm
Trigger force	0.5000 N

2.5. *Assessment of biopolymeric membrane surface morphology*

Scanning electron microscopy (SEM) was employed for assessing the membrane surface morphology on gold–platinum sputter-coated samples employing a Joel JSM-840 (Tokyo, Japan) scanning electron microscope. Various photomicrographs were attained under an electrical potential of 15 kV by scanning fields selected at different magnifications.

2.6. *Determination of membrane toughness and bi-axial extensibility*

Textural profile analysis was employed for all physicomechanical investigations. The bi-axial extensibility was determined from force–distance profiles generated on a TA.XT*plus* Texture Analyzer (Stable Microsystems, Surrey, UK) equipped with a 2 mm flat cylindrical probe, a 5 kg loadcell and Texture Exponent V3.2 software for data processing. The method involved securing the biopolymeric membranes on a ring assembly with a 5 mm diameter central hole using a secure raised platform (figure 1). The centralized test probe was then lowered and embedded onto the membrane surface according to the relevant test parameter settings for determining the biopolymeric membrane toughness and bi-axial extensibility, as specified in table 1.

2.7. *Determination of the drug entrapment efficiency within the biopolymeric membrane*

Drug entrapment efficiency analysis of the biopolymeric membrane was performed by redissolving membrane samples

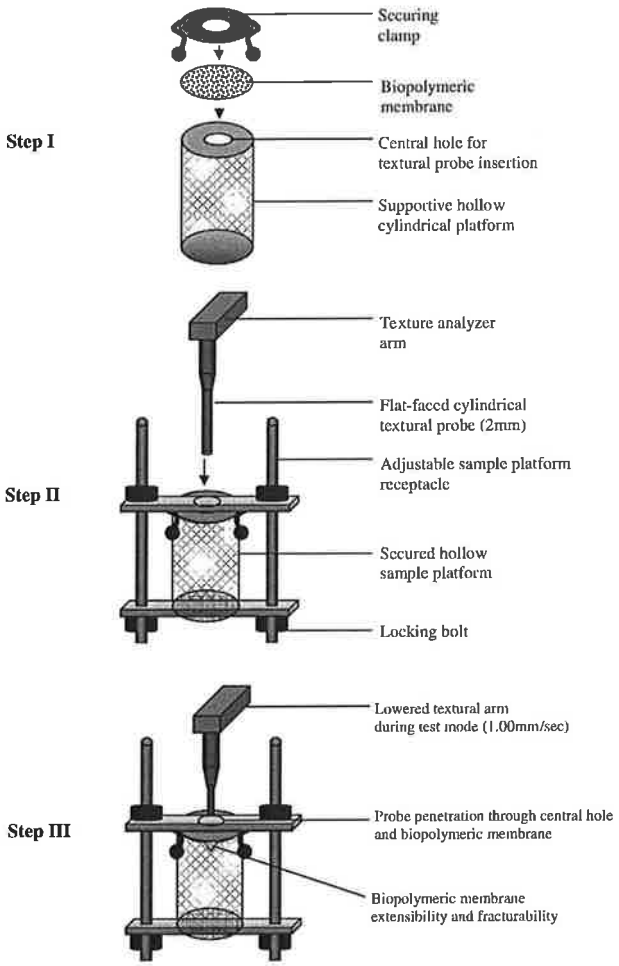

Figure 1. A schematic depicting the experimental configuration for assessing the toughness and bi-axial extensibility of the biopolymeric membrane employing textural profile analysis. Step I involves securing the sample, step II involves securing a sample platform to textural stage and step III involves lowering the textural probe during the test mode for biopolymeric membrane analysis.

in 100 mL PBS (pH 7.4, 37 °C) and subsequently determining the quantity of MTX entrapped using a previously constructed standard linear curve generated at the maximum UV wavelength of $\lambda_{303\,nm}$ for MTX (CECIL 3021 Spectrophotometer, Cecil Instruments, Cambridge, UK). The DEE value was calculated employing equation (2):

$$\mathrm{DEE} = \frac{(M_i - M_d)}{M_i} \times 100, \qquad (2)$$

where M_i is the initial mass of MTX dissolved in the casting polymer solution and M_d is the mass of MTX quantified in the media after membrane samples were completely dissolved.

2.8. In vitro release of MTX from the biopolymeric membranes

In vitro release studies were performed in PBS (pH 7.4, 37 °C). The biopolymeric membranes were placed in closed 150 mL glass vessels containing 100 mL of the release medium. The membranes were incubated at 37 ± 0.5 °C in an oscillating incubator set at 20 rpm. At predetermined time intervals, 5 mL samples of the release medium were removed. Drug-free buffer was replaced into the vessel after sample removal in order to maintain sink conditions. The concentration of MTX was assayed by UV spectroscopy (CECIL 3021 Spectrophotometer, Cecil Instruments, Cambridge, UK) at the maximum drug wavelength if $\lambda_{303\,nm}$ using a standard calibration curve of known concentrations ranging from 0.005 to 0.025 mg mL^{-1} with a correlation coefficient $R^2 = 0.99$. In order to assess any UV interference from both the TEA and formulation degradation products, release studies were also performed on placebo formulations at $\lambda_{303\,nm}$.

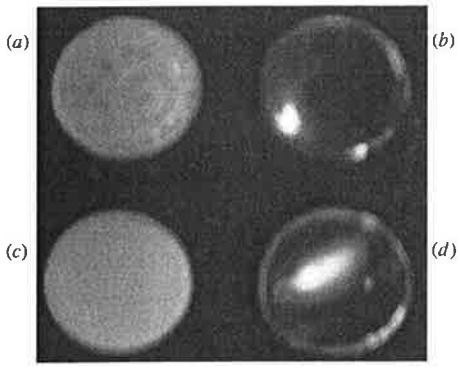

Figure 2. Digital images of the (*a*) MTX-PLLA-PVA, (*b*) PLLA-PVA, (*c*) MTX-TEA-PLLA-PVA and (*d*) TEA-PLLA-PVA biopolymeric membranes, where MTX = methotrexate, TEA = triethanolamine, PLLA = poly(L-lactic acid) and PVA = poly(vinyl alcohol).

3. Results and discussion

3.1. Formation of the MTX-PLLA-TEA-PVA biopolymeric membrane

The immersion precipitation reaction of PLLA and PVA in the presence of the catalyst stannous octoate and triethanolamine (TEA) at 150 °C resulted in the formation of a modified co-polymer with a branched structure. The biopolymeric membranes revealed various consistencies ranging from non-opaque coarse MTX-loaded membranes (figures 2(*a*) and (*c*)) to opaque smooth membranes (figures 2(*b*) and (*d*)). The hydrophobic PLLA polymeric chains were conjugated in a graft-like manner onto the hydrophilic PVA backbone via esterification of the hydroxyl groups to form an amphiphilic polymer. The drug (MTX) was subsequently bonded to the PLLA segment as shown in figure 3(*a*). The resultant membrane was shaped through structural polymeric layering to form a porous crystalline hydrogel-based drug delivery matrix (figure 3(*b*)). The hydration and swelling kinetics of the system were mainly governed by the presence of the hydrophilic PVA backbone that controlled the quantity of water sorption and the extent of swelling of the polymeric matrix. A distinction was the insolubility of the adsorbate in the liquid sub-phase that resulted in the formation of a stable

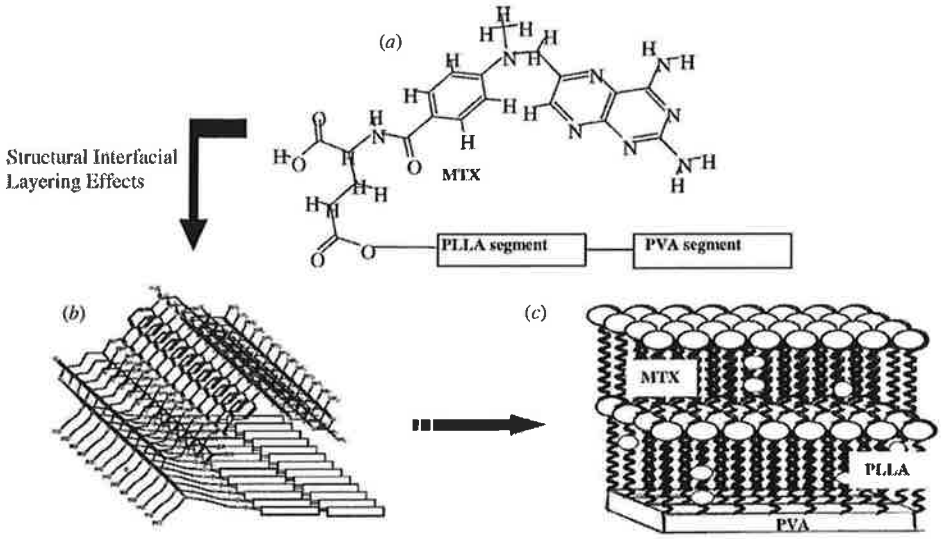

Figure 3. Schematics of (*a*) a 1D representation of a MTX-loaded biopolymeric membrane entity conjugating MTX-PLLA-PVA, (*b*) initial induction of structural layering and (*c*) a 3D representation of the conformationally evolved biopolymeric membrane showing inter-layering of PLLA and MTX conjugated to the PVA backbone.

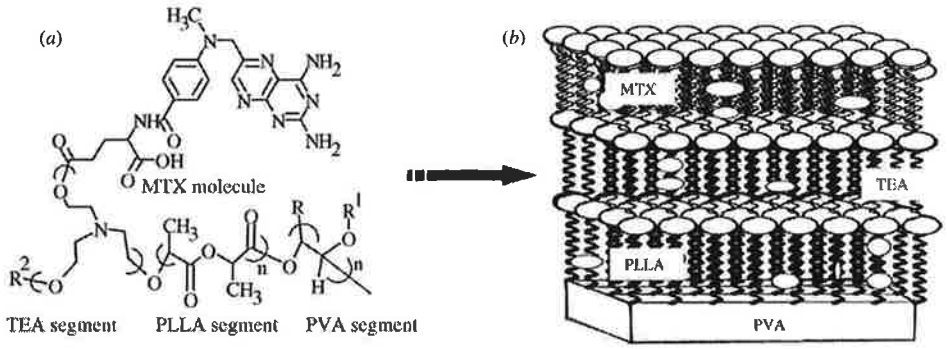

Figure 4. Schematic of (*a*) MTX molecules bound to a PLLA-TEA-PVA backbone of the biopolymeric membrane where R = PVA polymeric chain, R1 = PLLA-TEA-MTX linkage and R2 = a MTX molecule and (*b*) A 3D structural model of the biopolymeric membrane depicting the multi-layers representing PLLA, TEA and MTX conjugated onto a PVA backbone.

absolute conformation of the biopolymeric membrane that was dependent on the associated surface tension, the surface excess of TEA in comparison to the bulk phase and the concentration of TEA in the bulk phase (figure 3(*c*)).

Steric hindrance may have shielded MTX binding sites and thus prevented MTX molecules from attaching at every PLLA monomer available along the entire modified polymer backbone accounting for the DEE values attained as discussed later. Thus, MTX binding to the PLLA segment was dependent on the extent of PLLA grafting onto the PVA backbone. To a lesser extent, MTX molecules may also undergo further direct conjugation with free PVA monomers or assemble as freely dispersible entities within the modified polymeric complex.

3.2. The effect of the addition of amphiphilic TEA

TEA molecules inherently possess dendrimeric properties due to the large number of nitrogen atoms in the entity. A single TEA entity has the capacity of bearing two MTX molecules and may be regarded as a nodal point for drug attachment and drug release. In contrast to the MTX-PLLA-PVA matrices, TEA molecules in the MTX-TEA-PLLA-PVA matrices afforded the system with additional sites for drug attachment (figure 4(*a*)). The layered structure led to the formation of a multi-layered matrix (figure 4(*b*)) possessing unique hydration and swelling dynamics and MTX release kinetics. The sparse branching of polymeric chains in the MTX-TEA-PLLA-PVA matrix system afforded greater flexibility due to reduced steric hindrance. The average free volume per molecule available for MTX was increased in contrast to the MTX-PLLA-PVA membrane system.

Co-polymeric PLLA conjugate blends with PVA can be significantly modified as robust structures by the addition of amphiphilic TEA as a discrete plasticizing and drug binding entity within the matrix. TEA molecules are able to act as stress concentrators, which reduce the overall yield stress of the biopolymeric membrane, allowing plastic deformation, enhanced extensibility and ductile fracture during physicomechanical analysis and drug release studies

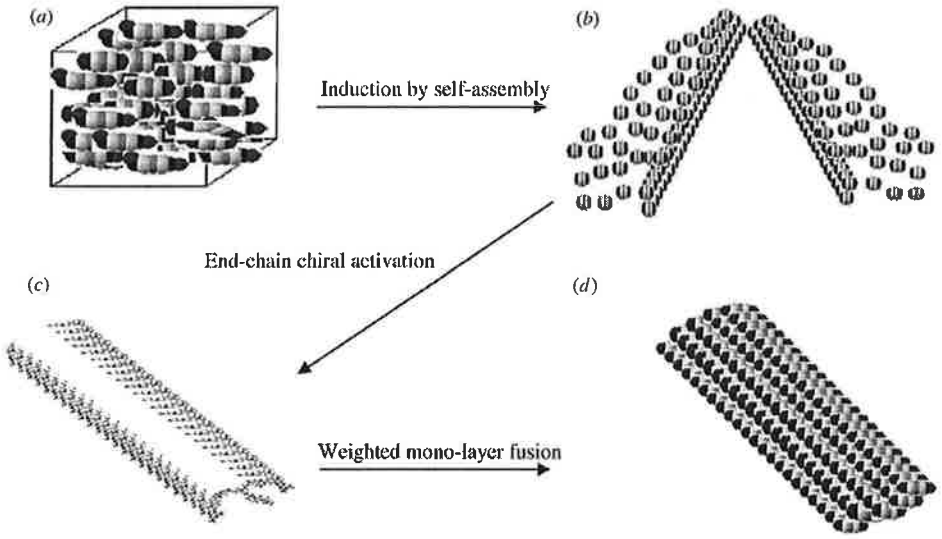

Figure 5. Schematic depicting (*a*) a cube representing the diverse model contours of the conjugated MTX-TEA-PLLA-PVA-PLLA-TEA-MTX entity due to matrix stereo-electronic factors, (*b*) formation of self-assembled mono-layered isomers, (*c*) end-chain activation of fusion based on chirality of mono-layers and (*d*) isomeric conjugation into an ordered multi-layered biopolymeric membrane

Table 2. HyperChem® V7.5 (Hypercube Inc., Gainesville, FL) computational molecular attributes at *ab initio* and DFT (6–31 G).

	PLLA	PVA	P-P [a]	M-P-P [b]	T-P-P [c]	M-T-P-P [d]	TEA
Mass (amu)	89.0	–	232.23	–	–	–	–
Polarizability (Å^3)	7.54	9.39	21.65	65.49	32.17	80.09	15.05
Refractivity (Å^3)	15.27	38.87	47.15	170.80	84.33	208.97	38.87
Log *P*	0.47	0.12	1.31	0.81	1.14	0.10	1.17
Hydration energy (kcal mol^{-3})	−11.81	6.86	7.02	0.12	1.32	16.75	13.85
Volume (Å^3)	309.6	A^3	77.63	398.04	358.56	1807.91	166.36
Surface area (approx.) (Å^2)	38.88	159.45	393.82	16.85	160.23	823.71	242.22
Surface area (grid) (Å^2)	228.02	178.90	422.80	245.72	243.86	980.00	143.11
Partial charges[e]	0.00	0.00	0.00	0.00	0.00	0.00	0.00

[a] PLLA-PVA.
[b] MTX-PLLA-PVA.
[c] TEA-PLLA-PVA.
[d] MTX-TEA-PLLA-PVA.
[e] net.

in PBS (pH 7.4, 37 °C). Crystallized PLLA has a significantly reduced impact strength and therefore could be toughened by the addition of TEA as a separate immiscible rubbery phase in conjunction with PVA. Since the biopolymeric membrane is to be used in biomedical applications as a potential drug delivery device, the plasticizer TEA was chosen due to its ability to degrade into substances that are absorbable in the body that are hydrophilic and non-toxic.

3.3. Computational molecular structural modeling of the proposed mechanism of biopolymeric membrane layering

To develop a mechanistic structural molecular model for the effectual layering of the biopolymeric membrane, a mono-layered membranous fusion approach was employed, which has been previously attempted as an effective approach to the formation of supported lipid bi-layered membranes that are able to describe biological cellular membranes with one or more components [37, 38]. The conjugated MTX-TEA-PLLA-PVA-TEA-MTX membrane can be represented by a diverse contoured model in various spatial conformations due to the inherent stereo-electronic factors at the matrix site (figure 5(*a*)). The formation of a layer is induced by self-assembly of conjugated MTX, TEA, PLLA and PVA entities in different ordered orientations (figure 5(*b*)). Chirality is able to induce activation at one end of the optically active molecules through linking, binding and association of the conjugated entities that ultimately lead to the formation of a multi-layered membrane structure (figure 5(*c*)). The process of membrane multi-layering is primarily based on stereochemical factors and the weighted fusion of mono-layers to eventually form a multi-layered structure (figure 5(*d*)).

Preliminary factors that are required for multi-layered membrane formation are to obtain an even surface following PLLA deposition to ensure the fusion of subsequent layers incorporating MTX molecules. As depicted in the computational structural model generated in figure 5, TEA linkage provided an even molecular surface, with a refractivity value of 38.78 Å^3 for the modeling area (table 2). The

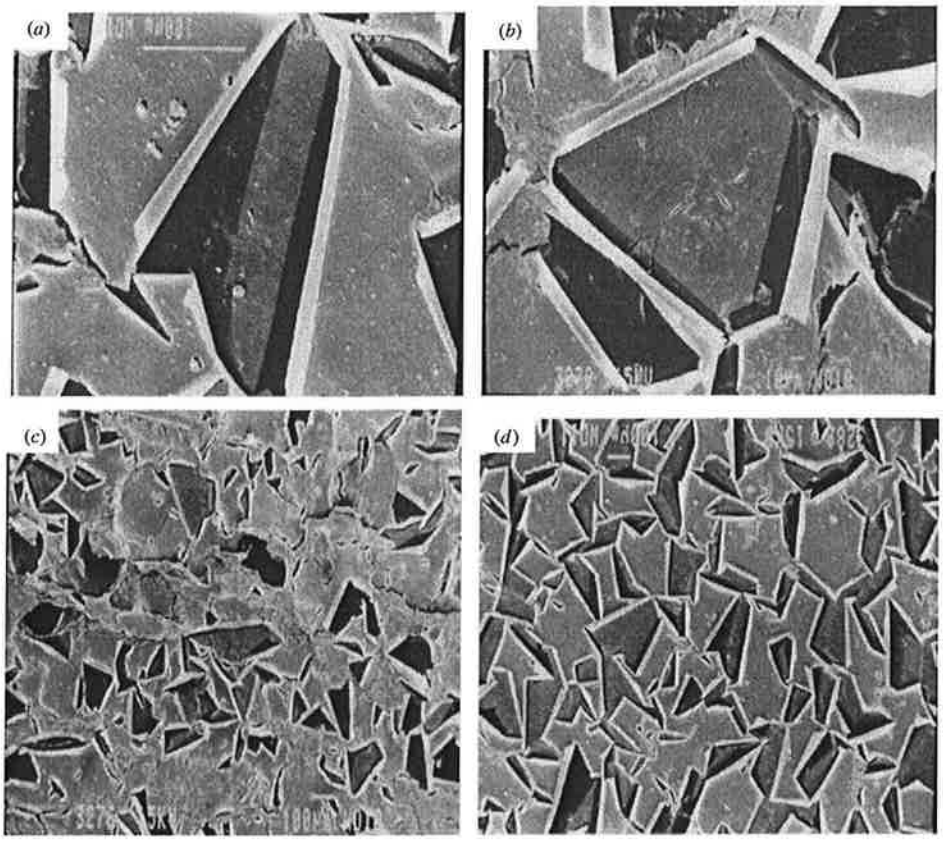

Figure 6. SEM photomicrographs of the biopolymeric membrane depicting (*a*) and (*b*) layered architecture and crystalline structure, (*c*) the aerial surface and (*d*) the bottom surface morphology of the membrane (magnification: 6000×, 15 keV; scale: 1 cm = 100 μm).

subsequent MTX layer provided a central platform region for structural layering between the isomeric mono-layers (figure 5(*b*)). Since TEA is amphiphilic, the deposition of the tri-branched polyelectrolyte on the membrane surface improved the fusion process due to electrostatic interaction and allowed uniform supported multi-layering to occur.

Furthermore, DFT (6–31 G) and *ab initio* computational results of the molecular characteristics employing HyperChem® V7.5 software (Hypercube Inc., Gainesville, FL, USA) indicated that the addition of TEA dramatically improved the layering effect (table 2). Approximate surface area values obtained were 0.12 Å^2 and 16.17 Å^2 for the MTX-PLLA-PVA and MTX-TEA-PLLA-PVA membranes, respectively.

The acetone:methanol blend was a strong non-solvent for PLLA and PVA. For this approach, compositions with high volume fractions of PLLA at the tri-nodal TEA were in equilibrium with the continuous solvent phase. Due to the strong non-solvent character of the acetone:methanol blend, the miscibility gap proved to be sufficient for the immersion precipitation process to occur. Polarizability values of 65.49 Å^3 and 80.09 Å^3 were obtained for the MTX-PLLA-PVA and MTX-TEA-PLLA-PVA membranes, respectively. The difference in the polarizability values between the membrane formulations was aligned with the initial difference of 7.54 Å^3 and 9.39 Å^3 for native PLLA and PVA, respectively (table 2).

Formation of the biopolymeric membranes occurred as a result of a combination of thermodynamic and diffusion kinetic phenomena. In order to induce phase separation, the diffusion of the polymeric phase and the rate of diffusion were thermodynamically fulfilled. The membrane formation process was governed by diffusion over the interface between the PLLA/PVA casting solution within the petri dish and the external coagulation bath. Although two polymeric components were present in the casting solution, only the solvent and non-solvent phases diffused outward. The differences in hydration energy potentials (-11.81 kcal mol^{-1} and 6.86 kcal mol^{-1} for PLLA and PVA respectively) and log *P* values (0.47 and 0.12 for PLLA and PVA respectively) of the polymeric phase conferred the induction of a diffusion flux that was sufficient to compensate for the residual energy needed to create a new insoluble surface during phase separation resulting in membrane formation at the interface (table 2). A semi-porous membrane structure was formed and the polymeric solution was in equilibrium with the coagulation bath creating a new structure.

3.4. Assessment of the surface morphology of the biopolymeric membranes

High magnification SEM revealed distinct continuous layers of the biopolymeric membrane with macro-porous mosaic

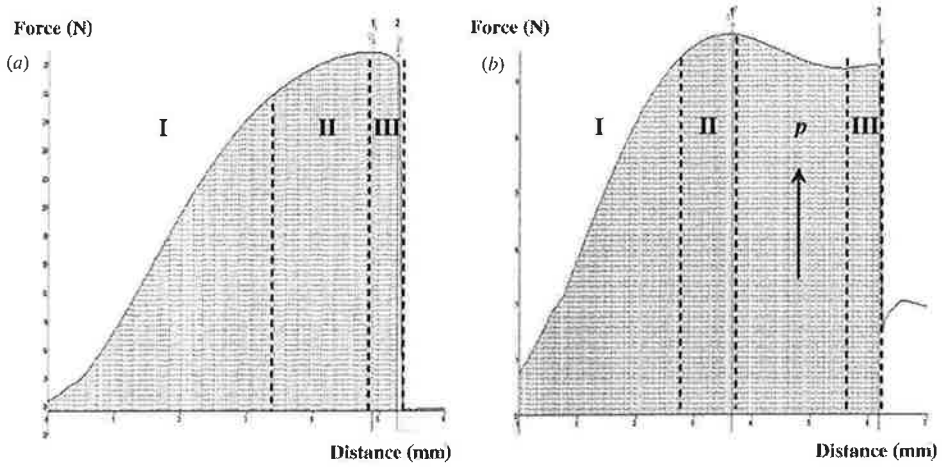

Figure 7. Typical bi-axial extensibility profiles generated for (*a*) a MTX-PLLA-PVA membrane and (*b*) a MTX-TEA-PLLA-PVA membrane system. I = phase of linear extensibility, II = maximum extensibility, III = membrane fracture, *p* = region of extended membrane plasticity due to the addition of TEA.

(This figure is in colour only in the electronic version)

morphologies (figure 6(*a*)). The high level of crystallinity is evident from the randomly shaped macro-pores with very sharp distinct borders (figure 6(*b*)). Following the immersion step, the top surface of the membrane (figure 6(*c*)) is formed spontaneously by the non-solvent–solvent diffusion process which occurs immediately at the polymer–non-solvent interphase. The bottom surface of the membrane (figure 6(*d*)) is formed gradually as the non-solvent penetrates into deeper membrane depths, and this results in the formation of more consistent mosaic morphology.

The formation of pores within the membrane depended on the sequence of the phase transition events in the immersion precipitation process [39, 40]. Numerous parameters, such as the compositions of the polymeric solution, the precipitation bath and the temperature during preparation, influenced the morphology and surface area of the formed membranes (table 2).

Since membrane preparation is a non-equilibrium process, this clearly implied that the change in the membrane structure was attributed to the arrangement of PLLA and PVA chains during membrane formation. A high polymer concentration region was formed at the interface between the polymer solution and the coagulation bath. High polymer concentration at this interface acted as a diffusion barrier to mass transport. Phase separation at this stage will have no influence on the asymmetry of the process, which explains the symmetry in the structure of the biopolymeric membranes. Fine particles were noted under high SEM magnification (figures 6(*a*) and (*b*)). These particles may have been generated due to crystallization of the polymer during the membrane formation process [23, 24].

3.5. Membrane toughness and bi-axial extensibility

The physicomechanical strength of the biopolymeric membranes profoundly depended upon the polymer linkages. Dissimilar and unique degrees of extensibility were observed for the various biopolymeric membranes (figures 7(*a*) and (*b*)). Extensibility can be defined as the degree to which a material can be extended/stretched prior to fracture and is related to the elasticity of the material. The inclusion of TEA in the membrane formulation resulted in a significant transition of the physicomechanical properties of the membranes. The MTX-TEA-PLLA-PVA membrane was superiorly robust with a considerably higher extensibility compared to the MTX-PLLA-PVA membrane as a greater force of extension and larger fracture distance were required (figure 7(*a*)). When the elastic limit of the MTX-TEA-PLLA-PVA membranes was reached, a greater resistance to structural deformation was noted (region *p* in figure 7(*b*)). The variation in the textural properties may be related to the computational structural models that proposed that the mechanism of membrane formation for the two formulations (MTX-TEA-PLLA-PVA and MTX-PLLA-PVA) leads to different layered structural architectures.

Textural profile analysis revealed that the biopolymeric membrane was significantly toughened by the introduction of TEA as a discrete rubbery phase within the co-polymer matrix. The MTX-TEA-PLLA-PVA biopolymeric membrane system was tougher (F = 89 N) and considerably more extensible (D = 8.79 mm) compared to MTX-PLLA-PVA (F = 35 N, D = 3.7 mm) membranes since a greater force of extension and fracture distance were required. The MTX-TEA-PLLA-PVA membrane showed resistance superior to structural deformation. TEA molecules acted as a stress concentrator that reduced the overall yield stress of the membrane, allowing plastic deformation and ductile fracture to occur prior to membrane fracture (figure 7(*b*), region *p*). The grafted TEA molecules lowered the force required for fracture and therefore considerably increased the quantity of dissipated energy during fracture. PLLA quenched from the melt or non-crystallizable L- and D-lactide has a low impact strength. Thus, the reduced strain to break during bi-axial extensibility testing was sensitive to minute surface imperfections. PLLA

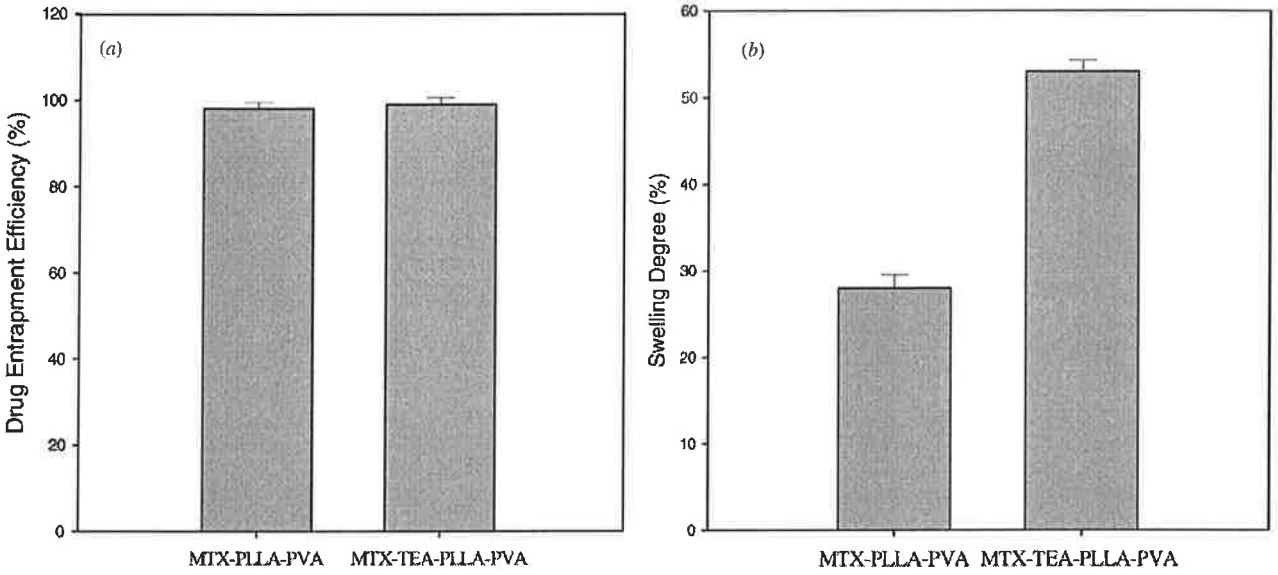

Figure 8. Histograms comparing (*a*) the drug entrapment efficiency and (*b*) the dynamic swelling potential of MTX-PLLA-PVA and MTX-TEA-PLLA-PVA biopolymeric membranes.

was therefore significantly toughened by blending with TEA as a separate, immiscible rubbery phase. The strength of the MTX-PLLA interface bond was a significant parameter for not only the toughening of the biopolymeric membrane but also MTX entrapment and subsequent release. The strength of this interface was modified by the use of TEA as a compatibilizer, graft and block co-polymer.

3.6. Drug entrapment efficiency and swelling studies

Relatively high MTX-loading capacities were achieved for both membrane formulations (figure 8(*a*)). A significant difference in the swelling potential of the two formulations was also observed (figure 8(*b*)).

Biopolymeric membranes that are formed by immersion precipitation of polymeric solutions in coagulation baths with a high solvent concentration, variations in the casting solution and the coagulation bath may have significant consequences on the DEE and swelling behavior of the membranes. The MTX-TEA-PLLA-PVA membranes showed a higher degree of swelling (53 $\pm$ 0.5%) compared to the MTX-PLLA-PVA membranes (28 $\pm$ 0.5%) (figure 8(*b*)). This was due to the ability of the MTX-TEA-PLLA-PVA system to imbibe a larger quantity of water molecules due to its multi-layered conformational structure. The high MTX entrapment values indicated that the energy gain of de-mixing MTX was probably larger than the energy needed to form a new interface for membrane formation. The extent of phase separation and further MTX entrapment can be enhanced by varying the molecular mass of the polymers, adjusting the blending procedures and annealing the blended materials.

3.7. In vitro MTX release studies

The release of MTX from the biopolymeric system followed tri-phasic kinetics. An initial burst in MTX release was observed due to unbound MTX molecules entrapped within the polymer matrix. The initial burst phase of MTX release (phase I) (unbounded MTX) was followed by steady-state kinetics (phase II) (TEA-bound MTX) presumably due to the gradual hydration and swelling of the biopolymeric membrane. A final controlled up-curving MTX release phase (phase III) was observed due to a combination of surface and bulk erosion of the membrane (figures 8(*a*) and (*b*)). The quantity of MTX released from the MTX-PLLA-PVA system (figure 9(*a*)) at a particular time point was greater than that released by the MTX-TEA-PLLA-PVA system (figure 9(*b*)) since more energy was required to break the TEA-MTX bond by hydrolytic cleavage, therefore confirming the function of TEA to act as a drug binding motif that was able to modulate MTX release.

An increase in TEA concentration between 2.5 and 4.5 mL resulted in a superiorly controlled and more prolonged MTX release in a bi-phasic manner (figure 10). The final burst/diffusional phase of MTX release was eliminated since more drug molecules were conjugated within the system owing to the increased presence and availability of TEA molecules.

3.8. Hypothetical drug release mechanism

The biopolymeric membrane formulations, MTX-PLLA-PVA and MTX-TEA-PLLA-PVA, are amphiphilic structures with a thin planar geometry. The amphiphilic character is attributed to the hydrophobic characteristics of the PLLA branches and the hydrophilic characteristics of the PVA backbone. The degradation kinetics of the membranes will therefore deviate from those of a hydrophobic polymeric network fabricated from native PLLA- or PVA-based hydrophilic hydrogels. The limited water sorption capabilities of PLLA are improved by conjugation onto the PVA backbone, and the resultant

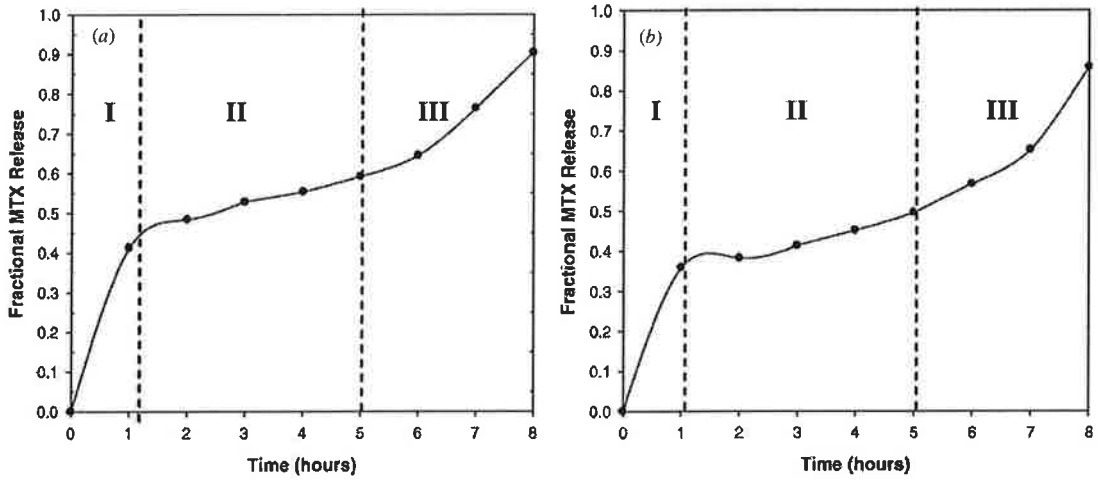

Figure 9. MTX release profiles from (*a*) the MTX-PLLA-PVA and (*b*) MTX-TEA-PLLA-PVA biopolymeric membrane formulations showing tri-phasic release kinetics with I—initial burst effect, II—a diffusional phase of MTX release and III—erosion-dependent MTX release with up-curving kinetics.

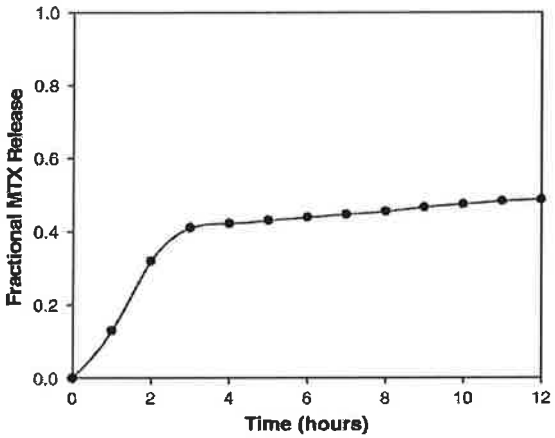

Figure 10. MTX release profile from MTX-TEA-PLLA-PVA biopolymeric membranes showing bi-phasic release kinetics due to an increase in TEA concentration (an initial burst effect followed by a diffusional phase of MTX release).

modified polymer will thus possess the favorable properties of hydrogels. The computational structural molecular models depicted evidence of *in situ* MTX loading, and therefore the biopolymeric membranes are highly likely to adopt a chemically controlled mechanism of MTX release. However, MTX release profiles from the two formulations (with and without TEA) differed owing to the presence of MTX-binding motif TEA in the MTX-TEA-PLLA-PVA membrane. A purely kinetic-controlled release mechanism which occurs via bond cleavage and mediated by surface erosion may be responsible for MTX release modulation. The hydrolytic cleavage of the MTX-polymer covalent bond in the MTX-PLLA-PVA membrane is the rate-limiting step with regard to MTX release. However, a different situation prevails with the MTX-TEA-PLLA-PVA membranes where TEA is tethered to MTX molecules, the kinetics and thermodynamics of which will determine the release kinetics of MTX from the membrane. The structural integrity of the membranes will be maintained since they would obey surface eroding phenomena.

4. Conclusions

The use of intricate computational models and structural rationalization techniques played a critical role in predicting the structural conformation of the synthesized biopolymeric membrane. Computational modeling has provided a mechanistic insight to further comprehend the formation, molecular structural characteristics, physicomechanical properties and the ability to entrap and modulate the release of MTX from the biopolymeric membrane. The stupendous physicomechanical properties of the membrane resulted from a superior balance of the polymeric phases employed and the addition of TEA which provided a synergistic approach to improving the bi-axial extensibility, toughness of the membrane and the ability to modulate the drug release in a tri-phasic manner suitable for the novel delivery of MTX.

References

[1] Karp M and Langer R 2007 Development and therapeutic application of advanced biomaterials *Curr. Opin. Biotechnol.* **18** 454–9

[2] Popovic N and Brundin P 2006 Therapeutic potential of controlled drug delivery systems in neurodegenerative diseases *Int. J. Pharm.* **34** 120–6

[3] Ponce S, Orive G, Gascon A R, Hernandez R M and Pedraz J L 2005 Nanoparticles prepared with different biomaterials to immobilize GDNF secreting fibroblasts *Int. J. Pharm.* **293** 1–10

[4] Whittlerey K J and Shea C D 2004 Delivery systems for small molecule drugs, proteins, and DNA: the neuroscience/biomaterials interface *Exp. Neurol.* **190** 1–16

[5] Ramehandan M and Robinson D 1998 *In vitro* and *in vivo* release of ciprofloxacin from PLGA 50:50 implants *J. Control. Rel.* **45** 167–75

[6] Kohn J, Wels W J and Knight D 2007 A new approach to the rationale discovery of biomaterials *Biomaterials* **28** 4171–7
[7] Eisenberg P 1995 *Executive Summery of NIH Workshop on Biomaterials and Medical Implants (16–17 Oct)* (Bethesda, MD: National Institutes of Health)
[8] Eksterowics J E *et al* 2002 Coupling structure-based design with combinatorial chemistry: application of active site derived pharmacophores with informative library design *J. Mol. Graph. Model* **20** 469–77
[9] Stanton R V, Mount J and Miller J L 2000 Combinatorial library design: maximising model-fitting compounds within matrix synthesis constraints *J. Chem. Inf. Comput. Sci.* **40** 701–5
[10] Kirkpatrick D L, Watson S and Ulhaq S 1999 Structure-based drug design: combinatorial chemistry and molecular modeling *Comb. Chem. High Throughput Screen* **2** 211–21
[11] Ironi L and Tentoni S 2003 A model based approach to the assessment of physicochemical properties of drug delivery materials *Comput. Chem. Eng.* **27** 803–12
[12] Brocchini S, James K, Tangpasuthadol V and Khon J 1997 A combinatorial approach for polymer design *J. Am. Chem. Soc.* **119** 4553–4
[13] Selvam P, Tsuboi H, Kubo M, Koyaba M and Miyamoto A 2005 Tight-binding quantum chemical molecular dynamics method: a novel approach to the understanding and design of new materials and catalysts *Catalysis Today* **100** 11–25
[14] Tuzun R E, Noid D W and Sumpter B G 1998 Computer simulation of complex strongly coupled nanometer-scale systems: breaking the billion atom barrier *Comput. Math. Appl.* **35** 93–100
[15] Smith R J, Agnieszka S, Weber N, Knight D, Abramson S and Khon J 2004 Integration of combinatorial synthesis, rapid screening, and computational modeling in biomaterials development *Macromol. Rapid Commun.* **25** 27–40
[16] Gao H 2001 Modeling strategies for nano- and biomaterials *European White Book on Fundamental Research in Material Science* ed M Ruhle, H Dosch, E J Mittemeijer and M H Van de Voorde (Stuttgart: Max-Planck-Gesellschaft) pp 144–8
[17] Abramson S D, Alexe G, Hammer P L and Kohn J A 2005 Computational approach to predicting cell growth on polymeric biomaterials *J. Biomed. Mater. Res.* **73** 116–24
[18] Gubskaya A V, Kholodovych V, Knight D, Kohn J and Welsh W J 2007 Prediction of fibrinogen adsorption for biodegradable polymers: integration of molecular dynamics and surrogate modeling *Polymer* **48** 5788–801
[19] Duce C, Micheli A, Solaro R, Starita A and Tine M R 2006 Prediction of chemical-physical properties by neural networks for structures *Macromol. Symp.* **234** 13–9
[20] Holder A J and Kilway K V 2005 Rational design of dental materials using computational chemistry *Dental Mater.* **21** 47–55
[21] Pillai O, Dhanikula A B and Pachagnula R 2001 Drug delivery: an odyssey of 100 years *Curr. Opin. Chem. Biol.* **5** 439–46
[22] Esperon S, Bossy-Nobs L, Petropolous L K, Gurny R and Guex-Crosier Y A 2008 Biodegradable drug delivery system for the treatment of postoperative inflammation *Int. J. Pharm.* **352** 240–7
[23] Jose L, Arias M, Aldofina R, Margarita L and Delgado A V 2008 Poly(alkylcyanoacrylate) colloidal particles as vehicles for antitumor drug delivery: a comparative study *Colloids Surf.* B **62** 64–70
[24] Dorothee R, Andreas L, Ilka P, Marsha A M and Ralf-Peter F 2006 Biocompatibility testing of novel multifunctional biomaterials for tissue engineering applications in head and neck surgery: an overview *Eur. Arch. Otorhinolaryngol.* **263** 215–22
[25] Foernkier E, Passirani C, Montero-Menei C N and Benoit J P 2003 Biocompatibility of implantable synthetic polymeric drug carriers: focus on brain biocompatibility *Biomaterials* **24** 3311–31
[26] Rajeev A J 2000 The manufacturing techniques of various drug loaded biodegradable poly(lactide-*co*-glycolide) (PLGA) devices *Biomaterials* **21** 2475–90
[27] Anderson J M and Shive M S 1997 Biodegradation and biocompatibility of PLA and PLGA microspheres *Adv. Drug Deliv. Rev.* **28** 5–24
[28] Singh M, Briones M, Ott G and Hagon O D 1997 Cationic microparticles: a potent delivery system for DNA vaccines *Proc. Natl Acad. Sci.* 811–6
[29] Cui C and Schwendenman S P 2001 Surface entrapment of polylysine in biodegradable poly(DL- lactide-co-glycolide) microparticles *Macromolecules* **34** 8426–33
[30] Burrem D A, Zylsta E, Lonsburg P T and Langer R 1993 Synthesis and RDG peptide modification of a new biodegradable copolymer poly(lactic acid)-co-lysine *J. Am. Chem. Soc.* **115** 11011
[31] Kissel T, Breitenbach A and Pistel K F 2000 Biodegradable comb polyesters: II. Erosion and release properties of poly(vinyl alcohol)-g-poly(lactic-co-glycolic acid) *Polymer* **41** 4781–92
[32] Kissel T, Lea A D and Wittmar M 2005 The role of branched polyesters and their modifications in the development of modern drug delivery vehicles *J. Control. Rel.* **101** 137–49
[33] Mohile N A and Abrey L E 2007 Primary central nervous system lymphoma *Neurol. Clin.* **25** 1193–207
[34] Hohenberg P and Kohn W 1964 Inhomogeneous electron gas *Phys. Rev.* **136** B864–71
[35] Kohn W and Sham L J 1965 Self-consistent equations including exchange and correlation effects *Phys. Rev.* **140** A1133–8
[36] Becke A D 1993 Density-functional thermochemistry: III. The role of exact exchange *Chem. Phys.* **98** 5648
[37] Dufrene Y F and Lee G U 2000 Advances in the characterization of supported lipid films with the atomic force microscope *Biochim. Biophys. Acta* **1509** 14–41
[38] Rinia H A, Wurpel G W H and Muller M 2006 Chapter 4 visualization and characterization of domains in supported model membranes *Adv. Planar Lipid Bilayers Liposomes* **3** 85–123
[39] Rahimpour A, Madaeni S S and Mehdipour-Ataei S 2008 Synthesis of a novel poly(amide-imide) (PAI) and preparation and characterization of PAI blended polyethersulfone (PES) membranes *J. Membr. Sci.* **311** 349–59
[40] Zeni M, Riveros R, de Souza J F, Mello K, Meireles C and Filho G R 2008 Morphologic analysis of porous polyamide 6,6 membranes prepared by phase inversion *Desalination* **221** 294–7

Appendix II

A poster entitled "Synthetic Approaches for Fabricating Biopolymeric Membranes for Rate-modulated Drug Delivery". Bongani Sibeko, Viness Pillay, Yahya E. Choonara, Girish Modi, Sunny E. Iyuke and Michael P. Danckwerts. Workshop on Structure and properties of Nanomaterials, University of Zululand, 2007.

SYNTHETIC APPROACHES FOR FABRICATING BIOPOLYMERIC MEMBRANES FOR RATE-MODULATED DRUG DELIVERY

Bongani Sibeko[1], Viness Pillay*[1], Yahya E. Choonara[1] Girish Modi[2], Sunny Iyuke[3] and Michael P. Danckwerts[1]

[1] University of the Witwatersrand, Department of Pharmacy and Pharmacology, 7 York Road, Parktown, 2193, Johannesburg, South Africa
[2] University of the Witwatersrand, Department of Neurology, Division of Neurosciences, 7 York Road, Parktown, 2193, Johannesburg, South Africa,
[3] University of the Witwatersrand, School of Chemical and Metallurgical Engineering, 7 York Road, Parktown, 2193, Johannesburg, South Africa,
***Correspondence: viness.pillay@wits.ac.za**

INTRODUCTION

Drug delivery approaches based on nanotechnology have been investigated for the treatment of problematic life long diseases such as brain tumors. In particular polymeric based nanoparticles have been considered as potential drug delivery systems that circumvent most therapeutic challenges in order to successfully carry chemotherapeutic agents safely into the targeted organ (brain). However, formulation of polymeric nanoparticles capable of steady state drug release for weeks can prove to be a very difficult challenge therefore in order to further retard drug release and prolong the degradation of potential drug delivery candidates, drug loaded polymeric nanoparticles can be embedded in suitable biopolymeric membrane systems which will serve as drug modulating matrices.

PURPOSE

To fabricate various biopolymeric membrane systems based on hydrophilic and amphiphilic polymer blends which will serve as drug modulating matrices when embedded with drug-loaded nanostructures.

METHODS

The membranes were prepared by the immersion-precipitation technique. In this process, a homogenous casting solution consisting of polymer and solvent is immersed in a nonsolvent coagulation bath. The exchange of solvent and nonsolvent causes the polymer to precipitate, by which membrane is formed.



Figure 1: Schematic depiction of the of the immersion-precipitation process: P, polymer; S, solvent; NS, nonsolvent

Membranes fabricated from amphiphilic polymer blends:
Solutions (10%$^{w}/_{w}$) of PVA and PLA were prepared by dissolving each polymer in dimethylsulphoxide at 21°C. Polymer solutions were blended in various ratios ranging from 20-80%$^{w}/_{w}$ and then cast on glass moulds and immersed in a methanol coagulation bath. The resultant membranes were left to dry at room temperature for 24 hours.

Membranes fabricated from hydrophilic polymer blends (PVA/PEG):
Aqueous solutions (15%$^{w}/_{w}$) of PVA and PEG were prepared by dissolving the polymers separately in deionised water. Polymer solutions were blended in 80/20, 60/40 ratio and then cast on glass moulds. The cast solutions were then immersed in an acetone: water coagulation bath and left to dry at room temperature for 24 hours.

RESULTS

Membranes fabricated from amphiphilic polymer blends:



Figure 2: PVA/PLA 80:20



(Surface morphology)



Figure 3: PVA/PLA 60:40



(Surface morphology)



Figure 4: PVA/PLA 40:60



Figure 5: PVAPLA 20:80

Membranes fabricated from hydrophilic polymer blends (PVA/PEG):



PVA/PEG 80:20

The 80/20 and 60/40 (PVA/PLA) ratio formed tough homogenous membranes with inherent elastic properties. Ratios of 40/60 (PVA/PLA) blends formed uneven membranes with irregular pore distribution and had poor mechanical properties. The 20/80 (PVA/PLA) blends precipitated into fragile interconnected polymeric strands that did not resemble a membranous structure. Membrane formation by phase separation of PVA/PLA blends was depended on the quantity of PVA in the blend. Reducing the quantity of PVA compromised the mechanical properties and resulted in the formation of poorly phase-separated polymeric structures. Both polymer blends 80/20 and 60/40 PVA/PEG formed robust non-homogenous membranes that lacked elasticity. The membranes displayed a highly porous surface which was attributed to spontaneous phase-separation. There were no significant differences in the morphology and mechanical properties of both blends. Polymer solutions could not be blended when the ratio of PEG exceeded 40%, hence this was the maximum quantity needed for membrane formation. Fabrication of biopolymeric membranes from hydrophilic or hydrophobic polymers provided desirable mechanical properties for various therapeutic applications. Based on the polymers employed, these matrices may provide an array of drug modulating effects when embedded with drug-loaded nanostructures.

Appendix III

A poster entitled "Influence of complex oxidizing agents on the physicochemical and physicomechanical properties of crosslinked co-blended polymeric membranes." Bongani Sibeko, Viness Pillay, Yahya E. Choonara, Girish Modi, Sunny E. Iyuke and Michael P. Danckwerts. 28th Annual Conference of the Academy of the Pharmaceutical Sciences, Athene Conference Centre, Club Mykonos, and Langerbaan, Cape Town, 2007.

Influence of complex oxidizing agents on the physicochemical and physicomechanical properties of crosslinked co-blended polymeric membranes

Bongani Sibeko[1], Viness Pillay*[1], Yahya E. Choonara,[1] Girish Modi[2], Sunny E. Iyuke[3] and Michael P. Danckwerts[1]

[1]*University of the Witwatersrand, Department of Pharmacy and Pharmacology, 7 York Road, Parktown, 2193, Johannesburg, South Africa*

[2]*University of the Witwatersrand, Department of Neurology, Division of Neurosciences, 7 York Road, Parktown, 2193, Johannesburg, South Africa*

[3]*University of the Witwatersrand, School of Chemical and Metallurgical Engineering, Johannesburg, South Africa*

**correspondence: viness.pillay@wits.ac.za*

Introduction

Hydrophilic polymers such as poly (vinyl alcohol) [PVA] and poly (ethylene glycol) [PEG] have been successfully employed in the formulation of novel drug delivery systems. Their ability to absorb water in their network structure has been the foundation for controlled drug delivery. In addition, these polymers are non-toxic, biodegradable, biocompatible and cost effective. With the ever increasing pressure for the development of novel drug delivery devices to address problematic diseases such as Primary Central Nervous System Lymphoma (PCNSL), novel drug delivery devices based on such polymers can provide us with solutions to the therapeutic hurdles associated with effective treatment.

PCNSL is an aggressive form of malignancy that arises in distinct anatomical sites within the brain. Radiotherapy (RT) has been the standard treatment producing a response rate of 60-65%, however relapse usually occurs within few months. Intravenous administration of single or a cocktail of chemotherapeutic agents has produced promising results in some cases however at the expense of detrimental side effects. Hence, the need for better therapeutic strategies for effective management of this disease is required.

Purpose

The purpose of this study was to fabricate PVA/PEG co-blend membranes and investigate the effects of varying concentrations of complex proxy salts (oxidising agent, CPS) on the physicomechanical and chemical properties and drug release behaviour of various membrane formulations. This study serves as the preliminary formulation stage towards the realization of a suitable implantable biopolymeric membrane system for the treatment of PCNSL.

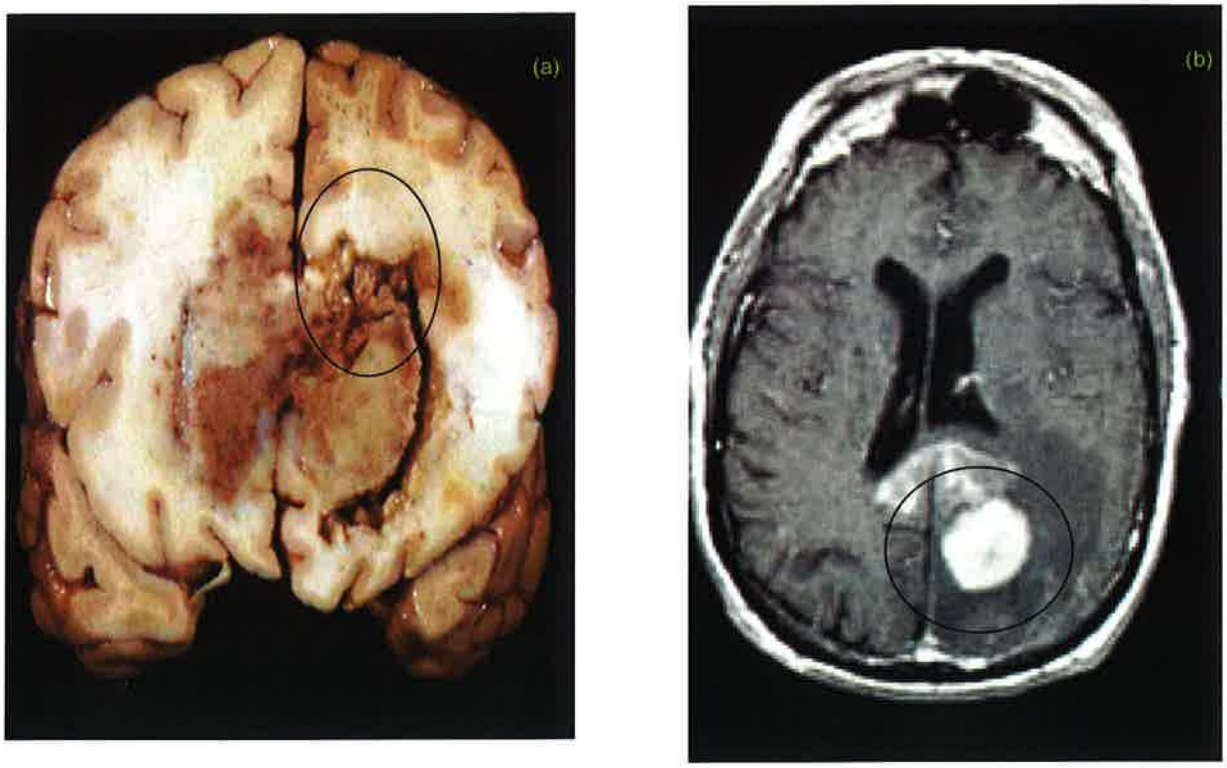

Figure1: A high resolution picture (a) and a Magnetic Resonance Image (MRI) revealing a brain of a patient with PCNSL.

Experimental Methods

Membranes were prepared by the immersion precipitation (wet phase separation) method. Aqueous solutions (15%$^{w}/_{w}$) of PVA and PEG were prepared in deionised water at 90^{0}C (PVA) and 21^{0}C (PEG). Polymers were blended in 80/20 ratio PVA: PEG until complete miscibility. Samples (20g) were weighed and a CPS was added in concentrations ranging from1-5%$^{w}/_{w}$ under agitation. A batch containing model drug theophylline was prepared in a similar manner. Samples (1mm×15mm) were cast on moulds at room temperature for 48 hours and subsequently evaluated for their physicomechanical properties and drug release behaviour.

Textural Profile Analysis: Uniaxial stress-strain profiles were generated by employing a TA.X*Tplus* Texture Analyser (Stable Microsystems, UK). Samples (70mm×2mm) were exposed to a predetermined stretch load of 1N and 100% strain.

In Vitro Drug Release Studies*:* Drug release studies were performed in 100mL PBS (pH 7.4; 37^{0}C) at 20rpm in a shaking incubator. Samples were removed at 1 hour intervals over 5 hours and analysed by UV spectrophotometry at 270nm.

Cumulative Degradation Studies*:* Degradation studies were performed in PBS (pH 7.4; 37^{0}C) at 20rpm in a shaking incubator. Membranes were removed at 24 hour intervals, dried to constant mass and compared to the initial membrane mass.

(a)

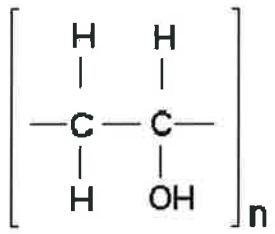

(a) PVA chemical structure, molecular weight of 124.000 – 186.000g/mol.

(b)

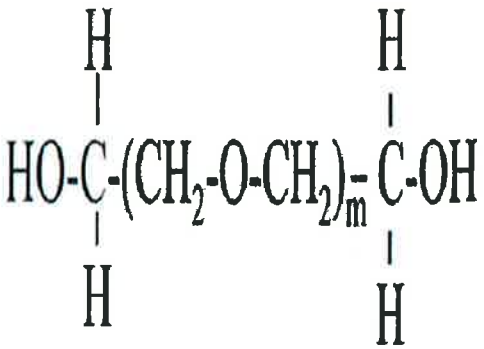

(b) PEG chemical structure, molecular weight of 4000g/mol.

(c)

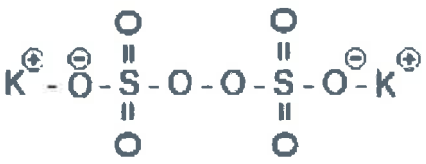

(c) Potassium peroxydisulphate chemical structure, molecular weight of 270.33g/mol.

Figure 2: Chemical structures

Results

Figure 3: *Textural Profile Analysis*

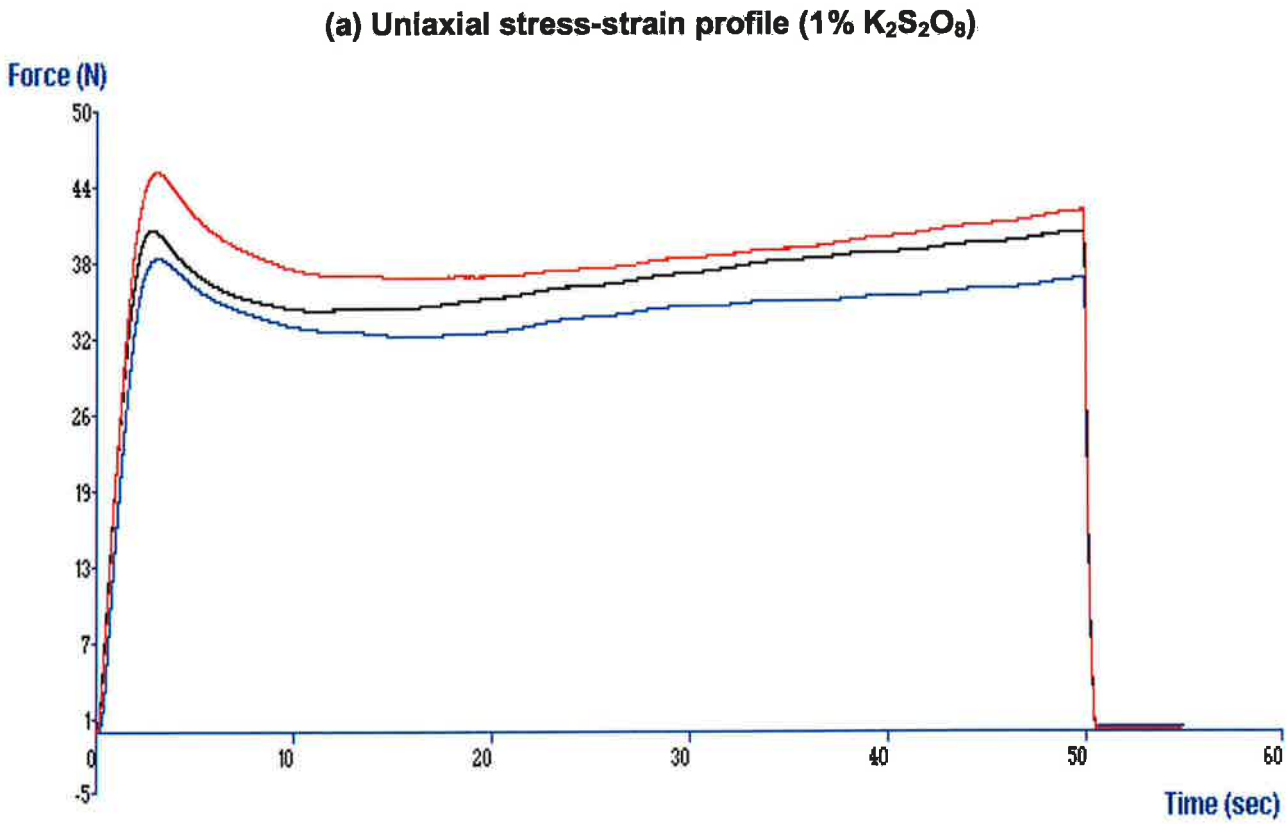

(b) Uniaxial stress-strain profile (3% $K_2S_2O_8$)

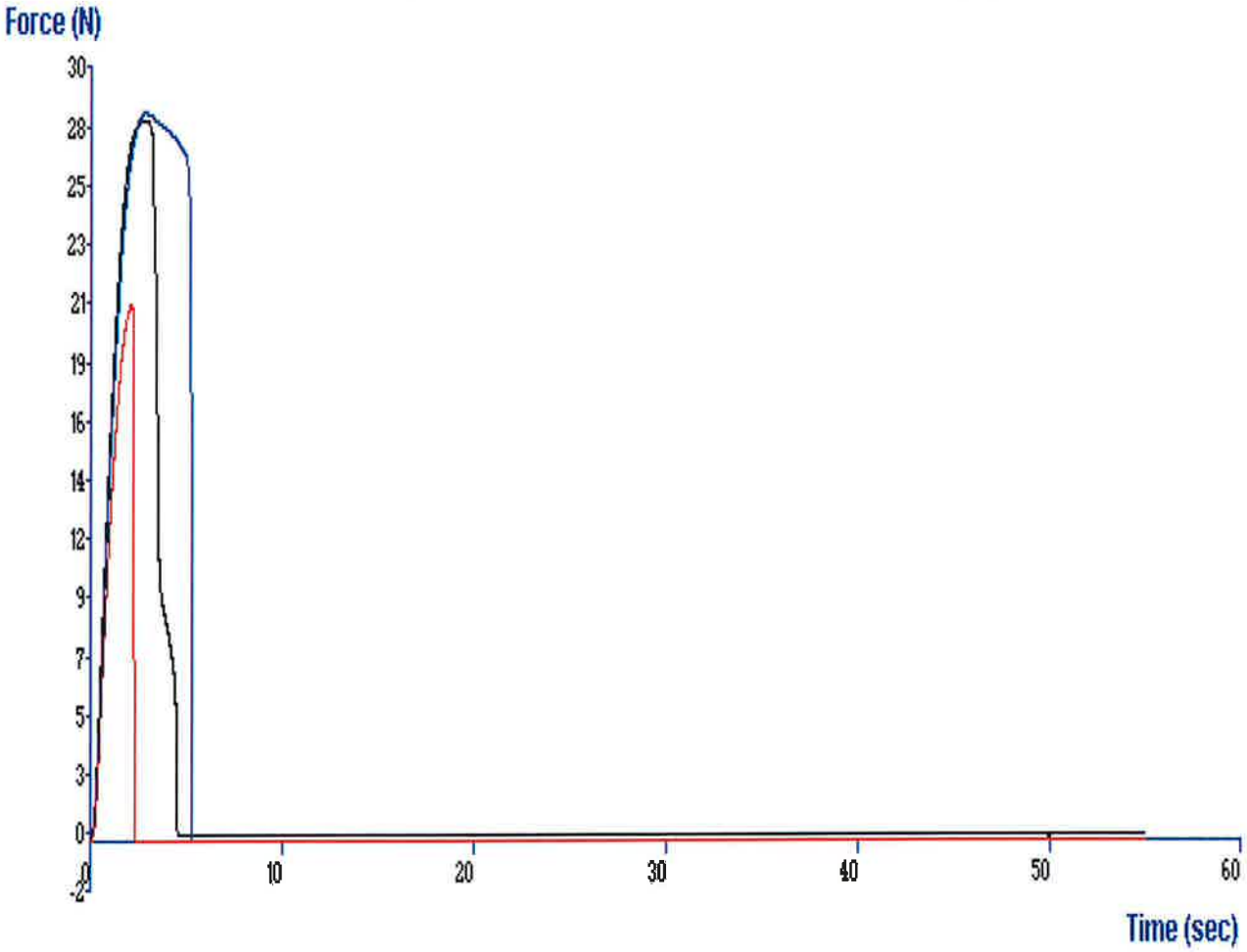

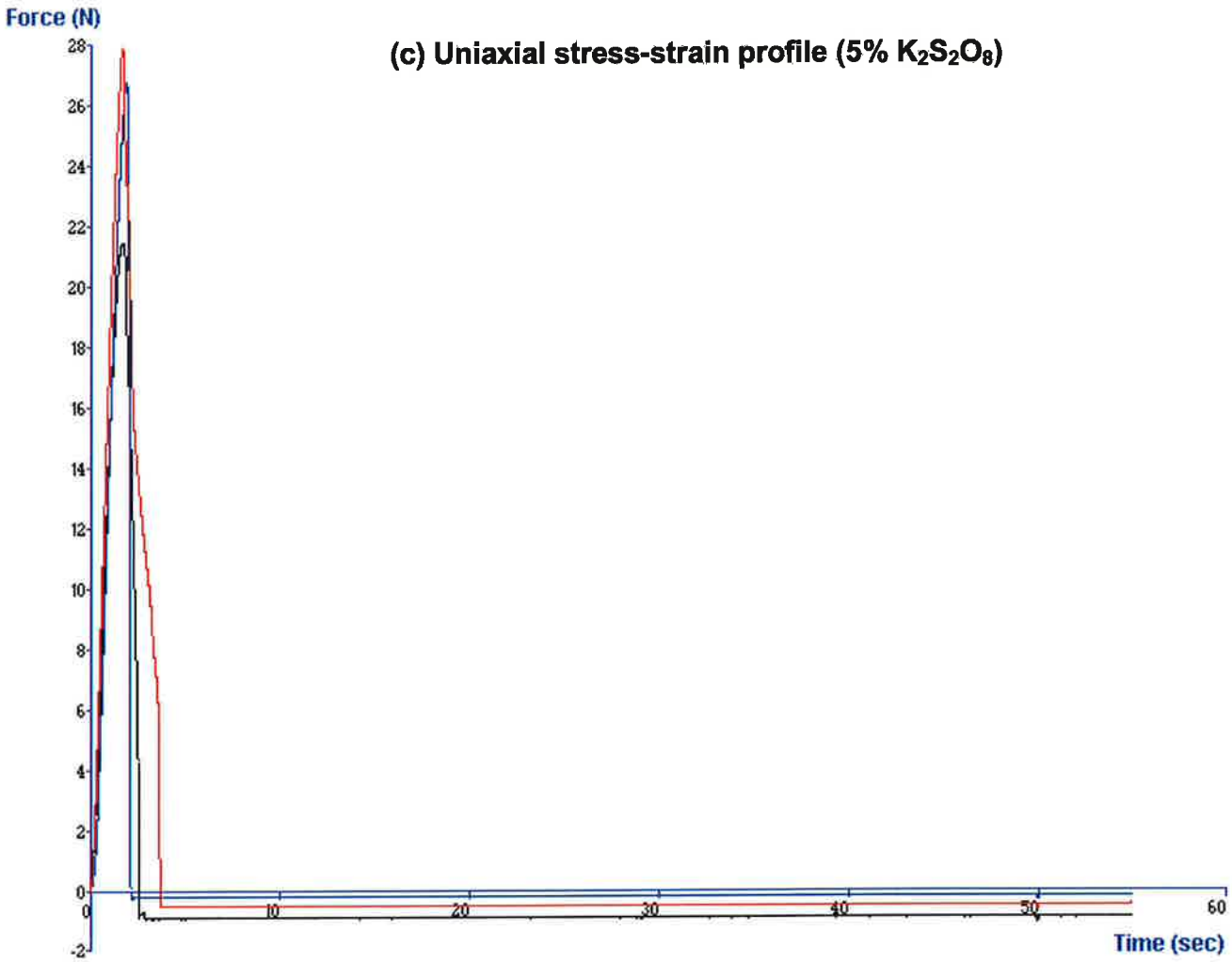

(c) Uniaxial stress-strain profile (5% $K_2S_2O_8$)

Figure 4: *Swelling Studies*

Degree of swelling = $\frac{Ws - Wi}{Wi} X\ 100$

Where *Ws* is the weight of the membranes in the swollen state a and *Wi* is the initial weight of the membranes.

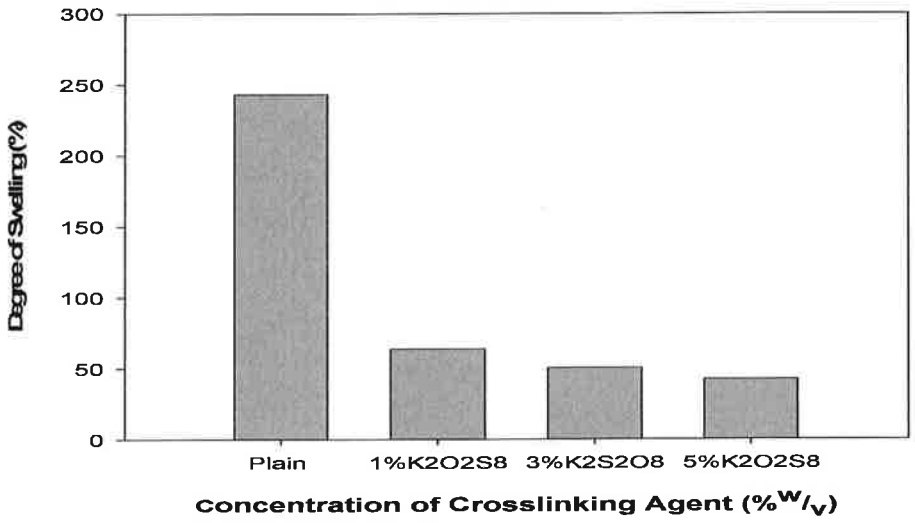

Figure 5: *Drug Release Studies*

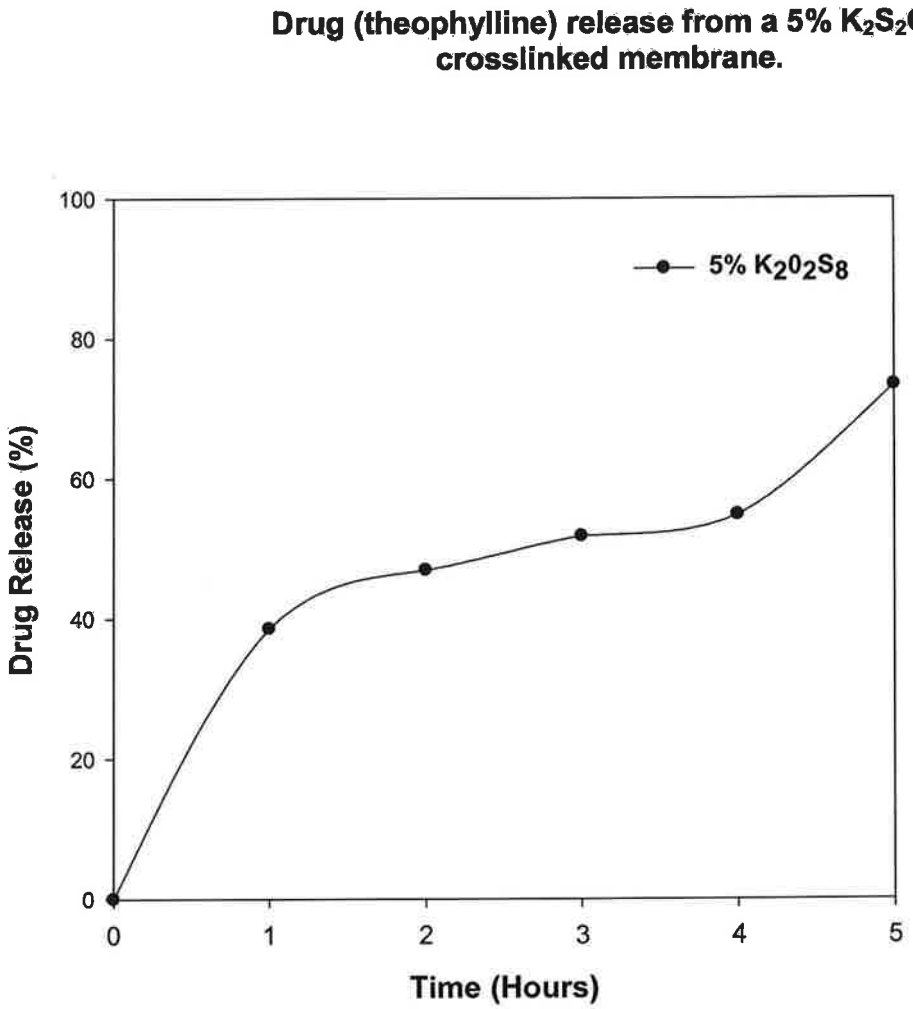

Discussions

The physicomechanical and chemical properties of the PVA/PEG co-blended polymeric membranes can be varied by varying the concentration of the CPS ($K_2S_2O_8$). The extensibility of the membranes decreased with increasing concentration of the crosslinking agent and the membranes exhibited non-linear stress-strain behaviour. The loss of extensibility as the concentration of the crosslinking agent increases may be due to increased chain bonding. At lower CPS concentrations the material was very elastic and the profile is characterised by a plateau. The profiles generated at higher CPS concentrations lack this plateau and the deformation (max peak) occurs very quickly due to increased extension resistance. The profiles have a generally steep slope compared to that of the extensible membranes. Samples were tested in triplicate for each batch, and from the profiles it is evident that there is little variability amongst samples from the same batch (similar profiles), hence this confirms structural uniformity. Swelling studies revealed that the swelling degree was also dependent on the concentration of the CPS. Swelling was retarded by an increase in the concentration of the CPS (Figure3). Plain membranes and membranes that were crosslinked with 1% $K_2O_2S_8$ degraded rapidly in PBS. The degradation process was initially accelerated for the 3% $K_2O_2S_8$ and 5% $K_2O_2S_8$ crosslinked membranes and then proceeded in a gradual to a steady state fashion thought the entire experiment. For all other membranes formed, drug release was rapid (t=1hr). The 5% $K_2O_2S_8$ crosslinked membrane revealed slight control of drug release after an initial burst effect (Figure 4).

Conclusion

An array of physicomechanical and chemical properties can be obtained by varying the concentration CPS in a polymer blend. Prolonged degradation and minimal swelling of the biopolymeric membranes can be achieved at higher concentrations of CPS. Slow degrading devises are suitable for implantable drug delivery devises for diseases such as PCNSL that require long treatment periods. Drug release from the 5% $K_2O_2S_8$ was rapid and would not be ideally suited for this application, however other fabrication strategies can be employed to further retard drug release.

Appendix IV

A podium presentation entitled "An implantable hydrogel drug delivery system for chemotherapeutic applications". Bongani Sibeko, Viness Pillay, Yahya E. Choonara, Girish Modi, Sunny E. Iyuke and Michael P. Danckwerts. Research day and postgrad expo, University of the Witwatersrand, Faculty of Health Sciences, 2008.

An Implantable Hydrogel Drug Delivery Systems for Chemotherapeutic Applications

Introduction

- Systemically administered chemotherapy is not always effective in treating many solid malignant tumors of the brain, liver, colon, breast and prostate.
- Main reasons:

1. Complex biology of tumors-cell type, tumor size, location and vuscularization.
2. Difficulties in achieving therapeutic concentrations at the tumor site (BBB)
3. Drug toxicity to normal tissues.
4. Degradation of drug compounds in vivo.

- Several strategies for effective delivery and treatment of tumors have been investigated:

1. Administration of multiple drugs.
2. Chemical modification of drugs.
3. Identifying lipophilic drug analogs – ability to penetrate membranes.
4. Synthesizing analogs that require activation within host tissues.
5. **Improving the method of drug administration**

Local delivery of chemotherapeutic drugs with polymers as drug carrier materials

A. Suitability of polymers as drug carrier materials:

- Availability of a selected range of biocompatible and biodegradable polymers such as polyvinyl alcohol (PVA), poly (lactic acid) (PLA) and its co-polymers poly (lactide-*co*-glycolic acid), poly (ε-caprolactone) (PCL) ect.
- Polymers are a versatile class of materials with inherent diversity of chemical structures → modification → desired physicomechanical and physicochemical properties and drug release patterns.
- Extensive scientific knowledge and experience on the use of polymers for device and process design.
- Considerable advances in the development of mathematical models for controlled and targeted drug delivery with polymers → simulate therapeutic effects of various structural parameters of the device and operational parameters in the preparation process.

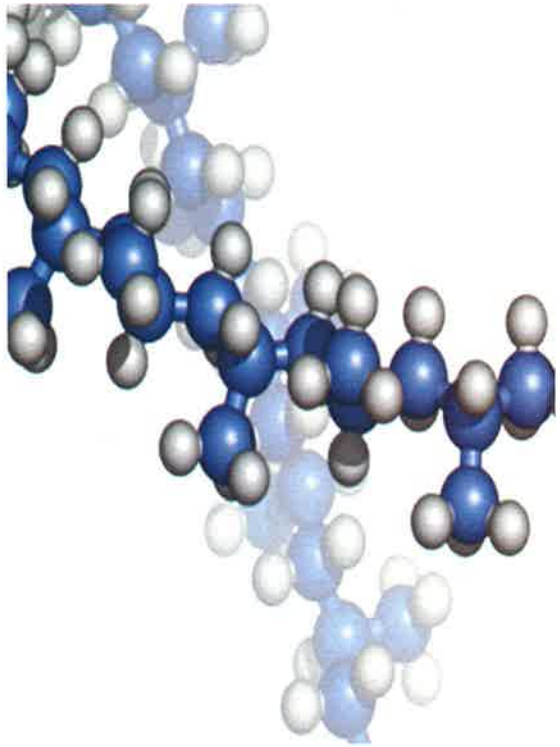

B. Pharmacokinetics of drug-polymeric implants

- Pharmacokinetic models based on compartmental drug descriptors are used to describe targeted chemotherapy.
- Complex mathematical models are used to evaluate the dynamics of drug transport into the tissue near the implant.

Once implanted:

1. The tissue adjacent to the polymer implant is treated as a material consisting of three phases, intracellular space (ICS), cellular membrane (CM) and extracellular space.
2. Drug is released at a local site and migrates away from the polymer/tissue interface by diffusion and fluid convection via the ECS.
3. Some of the drug molecules may be internalised by cells or enter the vascular system.
4. Therefore the fate of drug molecules delivered to the tumor depends on the rates of transport (diffusion and fluid convection), elimination (degradation, metabolism and transcapillary permeation) and internalization.

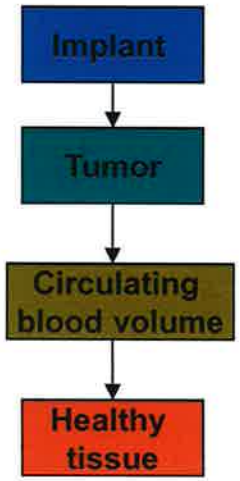

$$C = \alpha \cdot C^0_{ECS} + \beta \cdot C^0_{ICS} + (1 - \alpha - \beta) \cdot C^0_{CM} \qquad (1)$$

$$\frac{\partial C}{\partial t} = -\nabla \cdot (-\alpha \cdot D_{ECS} \nabla C^0_{ECS} + \alpha \cdot \bar{v}_r C^0_{ECS}) - (\alpha \cdot k_{ECS} \cdot C^0_{ECS} + \beta \cdot k_{ICS} \cdot C^0_{ICS} + (1 - \alpha - \beta) \cdot k_m \cdot C^0_{CM}) - \frac{\partial B}{\partial t} \qquad (2)$$

$$B = \alpha \cdot B^0_{ECS} + \beta \cdot B^0_{ICS} + (1 - \alpha - \beta) \cdot B^0_{CM} \qquad (3)$$

Eq. (2) can be combined with Eqs. (1) and (3) to yield:

$$\underbrace{\frac{\partial C^0_{ECS}}{\partial t}}_{\text{accumulation}} + \underbrace{\frac{\alpha}{\alpha^*} \nabla \cdot \bar{v}_r C^0_{ECS}}_{\text{convection}} = \underbrace{\frac{\alpha}{\alpha^*} D_{ECS} \nabla^2 C^0_{ECS}}_{\text{diffusion}} - \underbrace{\frac{\alpha \cdot k_{ECS} + \beta \cdot k_{ICS} \cdot P_{m:e}}{\alpha^*} C^0_{ECS}}_{\text{elimination}} \qquad (4)$$

with

$$\alpha^* = \alpha \cdot (1 + K_{ECS}) + \beta \cdot P_{l:e} \cdot (1 + K_{ICS}) + (1 - \alpha - \beta) \cdot P_{m:e} \qquad (5)$$

$$\frac{\partial C}{\partial t} + v \cdot \nabla C = D \nabla^2 C - k \cdot C$$

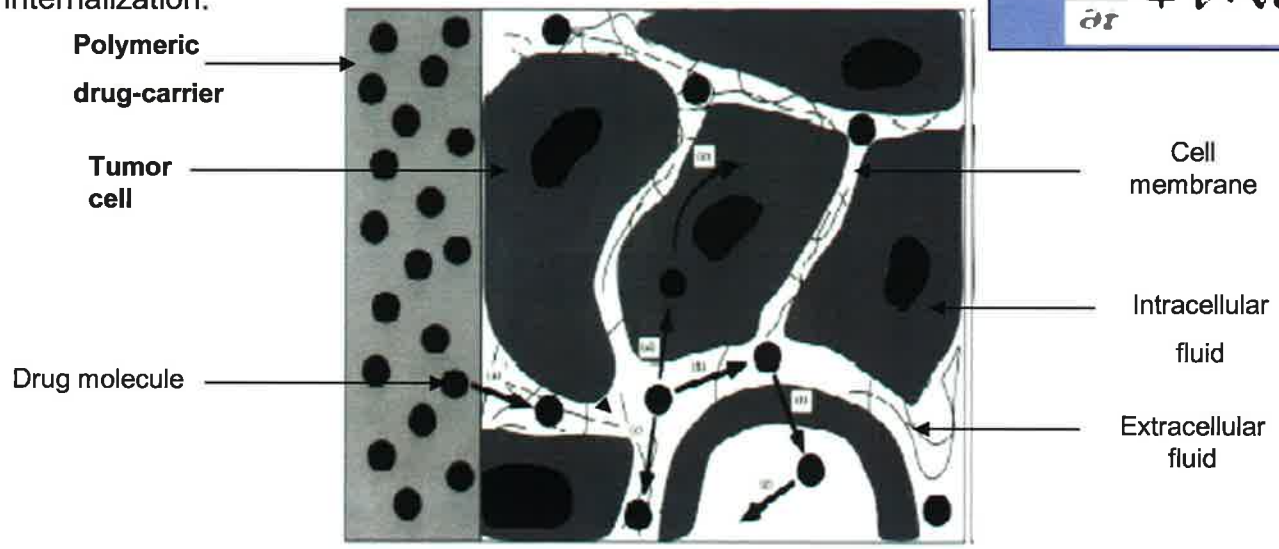

Advantages of local chemotherapy:

- Circumvents the barriers to efficient chemotherapeutic treatment – e.g. blood-brain barrier.
- Drug is in close proximity to the site of treatment.
- Cancer drugs can be delivered to the tumor in a sustained, continuous and predictable fashion.
- Localization of high doses of chemotherapeutic compound at the tumor site → increased antitumor activity.
- Reduction in systemic toxicities
- Improve drug stability → increase half- life (t1/2) of the drug → reduction in the dosing frequency.
- Implant dissolves in vivo after drug release – no need for second surgical procedure to remove the device.

Prostate cancer (polymer:PLGA; drug: GnRH)



Recurrent malignant gliomas (polymer: PCPP-SA; drug: carmustine)

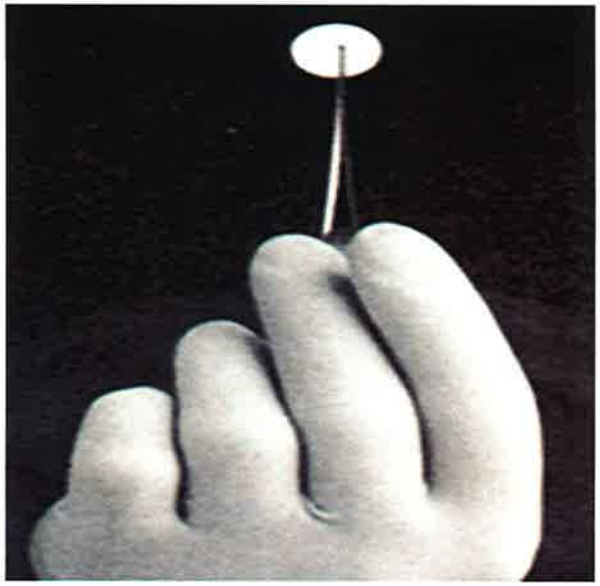

Aims and Objectives

A. Develop, characterise and assess the influence of varying formulation variables on the physicochemical properties, physicomechanical properties and release of folic acid from a composite biopolymeric membrane.

B. Perform computational and structural I modeling- rationalize the mechanisms of membrane formation.

C. Characterization of the implants:

1. Analysis of the mechanical properties by textural analysis
2. Analysis of drug entrapment efficiency (DEE) and swelling potential.
3. Perform in vitro drug release studies
4. Perform degradation studies

D. Determine the best combination of formulation variables that would result in the development of an optimum formulation.

Materials and Methods

Fabrication of the membranes

1. Membranes were fabricated by phase separation technique – immersion precipitation.
2. Homogenous solutions 10% $^{w}/_{v}$ of poly (vinyl alcohol) (PVA) and poly ($_{D,L}$-lactic acid) (PLLA) were co-blended after solubilisation in dimethylsulphoxide (DMSO).
3. Polymers were reacted in the presence of stannous octoate (catalyst) for 1 hour at a reaction temperature of 150°C.
4. The composite polymer was reacted for a further 1 hour with triethanolamine (TEA).
5. Folic acid (FA), a model drug was dissolved in DMSO and then reacted with 2.5mL of the composite polymer before casting onto a petri dish (15mm diameter).
6. The cast sample polymer solution was then immersed in a non-solvent coagulation bath comprising of acetone: methanol mixture in a ratio of 1:1.
7. The resultant biopolymeric membranes were recovered after 24 hours form the coagulation bath and allowed to dry at room temperature at 21±0.5°C.

Table 1: Box Behnken Design

Formulation	[PVA]	PVA vol	[TEA]
1	6	50	2.5
2	10	35	4.5
3	6	35	4.5
4	8	35	2.5
5	8	50	0.5
6	10	50	2.5
7	6	35	0.5
8	8	35	2.5
9	8	20	0.5
10	10	20	2.5
11	8	20	4.5
12	8	35	2.5
13	8	50	4.5
14	6	20	2.5
15	10	35	0.5

Characterization of the composite biopolymeric membranes

Physicomechanical investigations

Textural profiling was performed on a TA XT*plus* Texture Analyser (Stable Microsystems, Surrey, UK) equipped with a 2 mm flat cylindrical probe controlled via a 5kg load cell and Texture Exponent V3.2 software for data processing. Membranes were secured on a ring assembly with a 5mm diameter central hole using a raised secure platform. The probe was then lowered and embedded onto the membrane surface according to pre-set parameter settings. The bi-axial extensibility was determined from Force-Distance profiles generated.

Analysis of the swelling potential

Swelling studies were conducted by immersing a known weight of specimen in 10mL phosphate buffer saline (PBS, pH 7.4) and allowing the membranes to hydrate for 30 min. The swollen weight of the membranes was determined by weighing them immediately in an electronic balance after removing the membranes from the PBS and blotting them with filter paper to absorb water on the membrane surface. The swelling potential of the biopolymeric membranes in PBS were then calculated from the formula:

$$SD\ (\%) = \frac{(Ws - Wi)}{Wi} \times 100\%$$

where, SD is degree of swelling in PBS, and *Wi* and *Ws* are the weights of the membrane in a hydrated and unhydrated state, respectively.

Determination of the biopolymeric membrane drug entrapment efficiency

Drug entrapment efficiency (DEE) of the biopolymeric membranes was determined by completely dissolving the membranes in PBS, pH 7.4. The amount of folic acid (FA) entrapped within the membranes was determined by UV-spectroscopy by measuring the absorbance of the medium at 280nm. The DEE value was calculated by employing the equation:

$$\text{DEE (\%)} = \frac{(Mi - Md)}{Mi} \times 100\%$$

where, *Mi* is the initial mass of the drug dissolved in the casting polymer solution and *Md* is the mass of the drug quantified in the media after the membranes were completely dissolved.

Analysis of degradation kinetics

Degradation studies were carried out by placing the biopolymeric membranes in 10mL phosphate buffered saline (PBS, pH 7.4) in an orbital shaking incubator maintained at 37°C. At regular time intervals the membranes were removed from the buffer, dried to constant weight at 40°C in an oven and weighed. The degradation rate was determined as the percentage loss in weight over time. The experiment was continued by placing the membranes in fresh buffer solution until severe cracking or disintegration of the polymer was observed.

In vitro release of folic acid from the biopolymeric membranes

In vitro release studies were performed in PBS(pH7.4;37oC). The membranes were placed in jars containing 100mL of the release medium. The membranes were incubated at 37oC under shaking at 20rpm in the shaking orbital incubator. At predetermined time intervals samples of 5mL were collected from the release medium and were replaced with fresh buffer solution. The concentration of folic acid (FA) in the solution was assayed by UV spectroscopy (CECIL 3021 spectrophotometer, Cecil Instruments, Cambridge, England) at 280 nm using standard curve of known concentration in range of 0.25mg/mL – 1.0mg/mL with correlation coefficient R2=0.99.

Results and discussions

Computational and structural modeling

- The mechanistic formation of the composite biopolymeric membranes can be represented by a diverse contoured model in in various spatial conformations due to the inherent stereo-electronic factors at the matrix site **(a)**.
- The formation of the layer is induced by self assembly of conjugated FA,TEA, PLLA and PVA in different ordered orientations **(b)**.
- Chirality induces activation at one end of the of the optically active molecules through, linking, binding and association of the conjugated entities that ultimately lead to the formation of the multilayered membrane structure **(c)**.
- The process of membrane multi-layering is based primarily on sterochemical factors and weighted fusion of mono-layers to eventually form a multi-layered structure **(d)**.

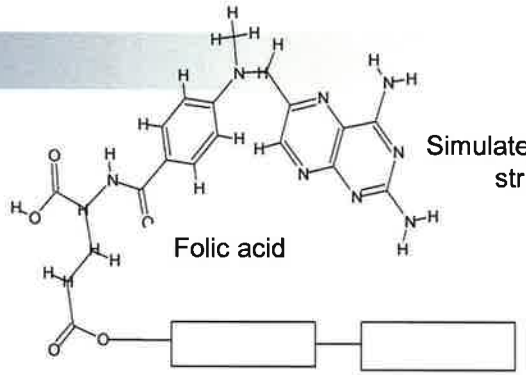

Simulated molecular structure

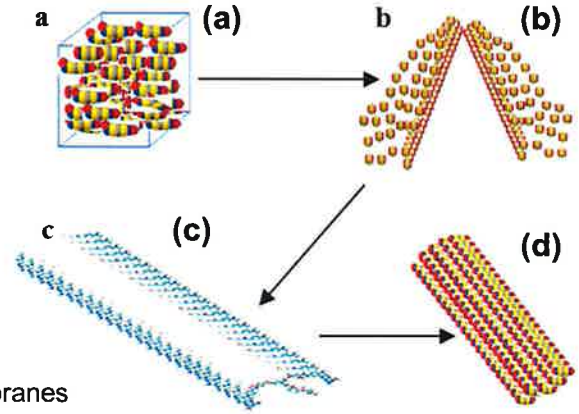

Schematic showing mechanistic formation of the biopolymeric membranes

Typical biopolymeric membranes



Mechanical properties of the membranes

- Microelectrodes → stiff and rigid materials → neural damage
- Mechanical testing is important in assessing the mechanical adaptability of medical brain implants for long term function.
- Ideal brain implants should mimic the viscoelastic mechanical properties of the brain tissue → minimal tissue damage
- Young's modulus **(E)** is a physical measurement of stiffness in a material, equaling to the ratio of applied load (stress) to the resultant deformation of the material such as elasticity).

$$E = \frac{\text{tensile stress}}{\text{tensile strain}} = \frac{F}{A0\Delta L}$$

E is the Young's modulus

F is the force applied to the membrane

A0 is the cross-sectional area through which the force is applied

ΔL is the amount (distance) by which the membrane is extended

Plain biopolymeric membrane

Drug loaded biopolymeric membrane

Swollen biopolymeric membrane

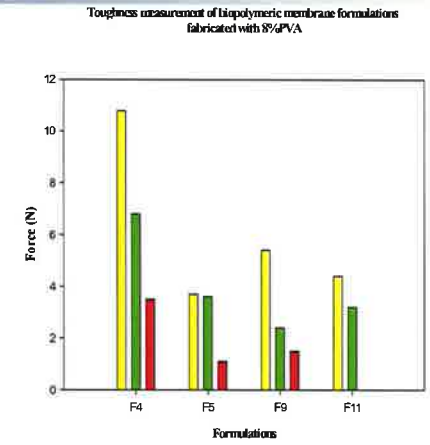

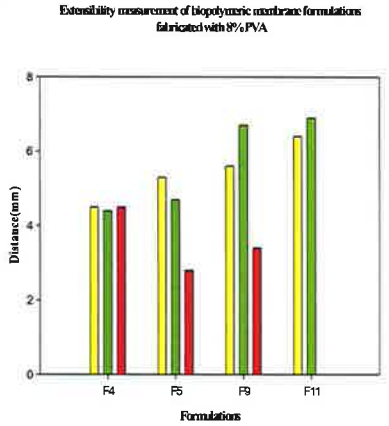

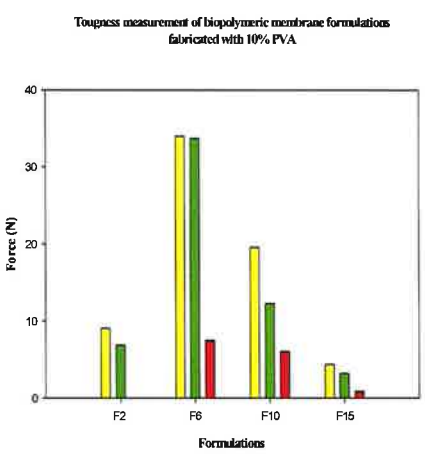

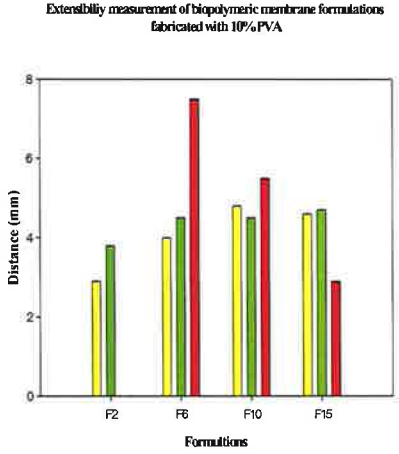

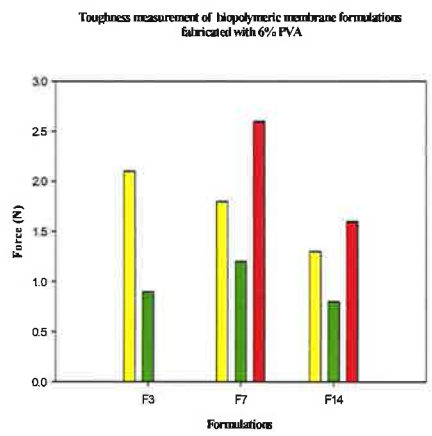

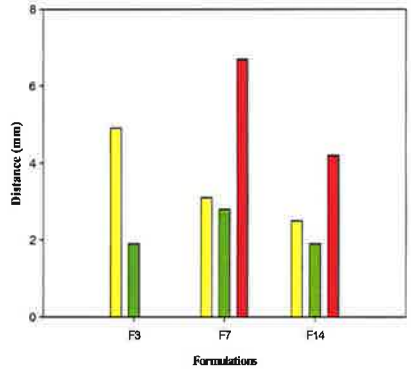

- Phase transitions associated with swelling and addition of the folic acid into the formulations led to changes in moduli.
- Mechanically adaptive biopolymeric membrane → initial high degree of stiffness to allow implantation into the brain parenchyma but then softens without excessive swelling upon implantation in response to the physiological environment (F4,F6,F7 and F10).
- Membranes showed good mechanical stability and integrity – showed by minimal factor change in moduli upon hydration and addition of the drug into the formulations.
- The membranes displayed viscoelastic mechanical behaviour, a property that enables hydrogels to integrate into neural tissue without causing mechanical pressure.

Table 2

Moduli (E) and factor change in moduli of biopolymeric membrane formulations

Form.No	E^a (MPa)	E^b (MPa)	E^c (MPa)	ΔE
F2	0.2	0.1	-	-
F3	0.06	0.3	-	-
F4	0.08	0.09	0.08	1
F5	0.06	0.06	0.2	3
F6	0.1	0.09	0.03	3
F7	0.1	0.2	0.03	7
F9	0.06	0.04	0.1	2.4
F10	0.07	0.09	0.05	2
F11	0.04	0.03	-	-
F14	0.2	0.3	0.8	3
F15	0.08	0.07	0.1	1.4

Swelling potential

- PVA, a hydrophilic component in the membranes was responsible for attracting water molecules into the membranes → hydration →swelling.
- The maximum water imbibing capacity of the formulations reached at equilibrium hydration was chiefly determined the concentration of PVA:
- 10% $^{w}/_{v}$ PVA formulations → greatest swelling degree
- 8% $^{w}/_{v}$ PVA formulations → intermediate swelling degree
- *6% $^{w}/_{v}$* PVA formulations → lowest swelling degree
- Inter-formulation variability in SD → amount of TEA and volume ratio of PVA.
- Minimal swelling favours greater stability and is a desirable property of brain implants.
- Therefore, desired swelling dynamics of the systems can be achieved by employing lowest concentrations of PVA .

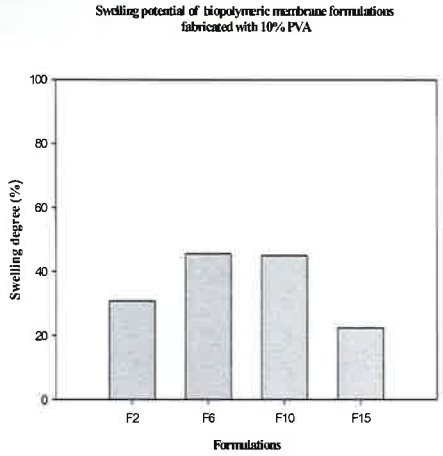

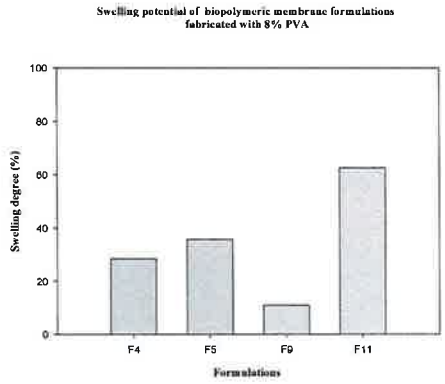

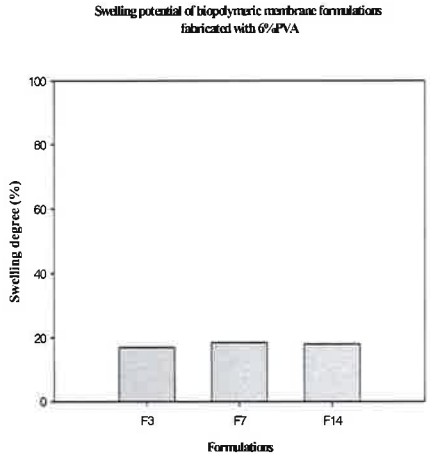

Degradation/ Erosion kinetics

- Degradation profiles of the membranes followed a similar biphasic kinetic pattern with initial rapid loss of weight followed by a constant loss of mass over time.
- Rapid loss of weight was indirectly proportional to the [PVA] and PVA vol ratio. Efficient grafting of PLLA onto PVA backbone seemed to have occurred at higher initial stoichiometric amounts and concentration of PVA (F6).
- The initial phase of the degradation profile may be attributed to the diffusion and solubilisation of partially reacted and/or unreacted polymer material trapped within the membrane matrices.
- The second phase of the degradation profiles may be attributed to hydrolytic cleavage of the PLLA branches grafted onto the the PVA backbone→ bulk degradation
- Stoichiometry of raw materials which favours long-term degradation pattern requires that the amount of TEA in the formulations be between 0.5-2.5mL.
- Higher TEA content ≥ 4.5mL → rapid degradation (within 12 hours)
- Long-term degradation behaviour was achieved with F4, F5, F6, F7, F9, F10 and F14.

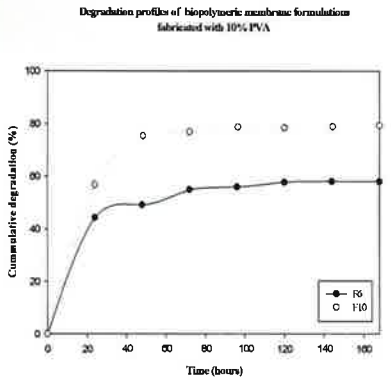

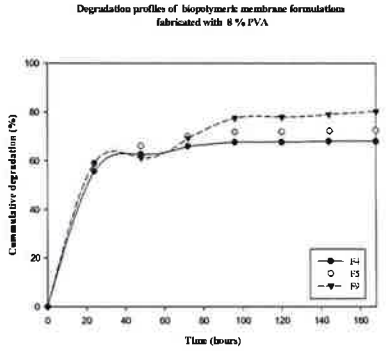

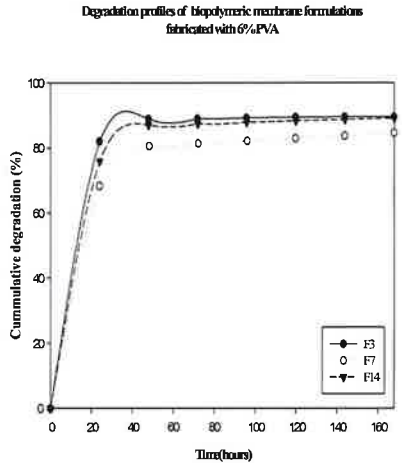

In vitro drug release

- The formulations displayed a wide array of folic acid release.
- Formulations fabricated with the same concentrations of PVA displayed similar release profiles.
- FA release from biopolymeric formulations fabricated with 10% w/vPVA followed zero-order kinetics with rapid release (8 hours) of the drug from the membranes.
- Drug release was lower for F2 and F6 with higher amount of TEA and PVA volume ratio.
- Reduction in the concentration of PVA, resulted FA acid release profiles with biphasic or triphasic kinetics. Initial burst release was observed in most formulations followed by steady state drug release.
- The greatest retardation in FA release was observed withF4 fabricated with intermediate concentration of PVA, intermediate volume ratio of PVA and intermediate amount of TEA.
- The FA release patterns of the biopolymeric membranes were not suitable for long-term drug delivery. The longest duration of drug release achieved was 12 hours.
- All three formulations variables showed a certain level of drug modulating effects.

Folic acid (FA) release profiles of biopolymeric membrane formulations fabricated with 10% PVA

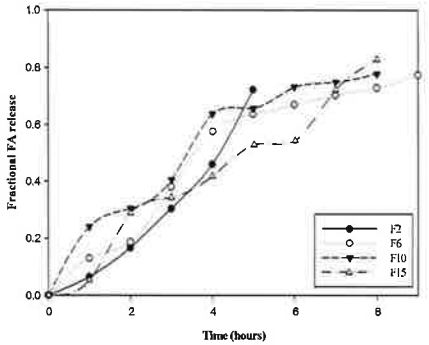

Folic acid (FA) release profiles of biopolymeric membrane formulations fabricated with 8% PVA

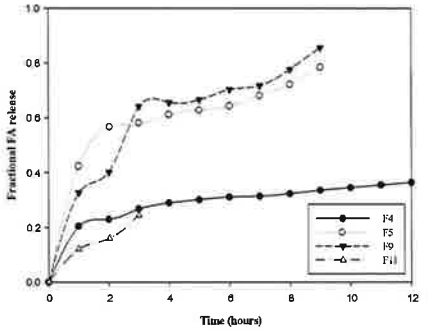

Folic acid (FA) release profiles of biopolymeric membrane formulations fabricated with 6% PVA

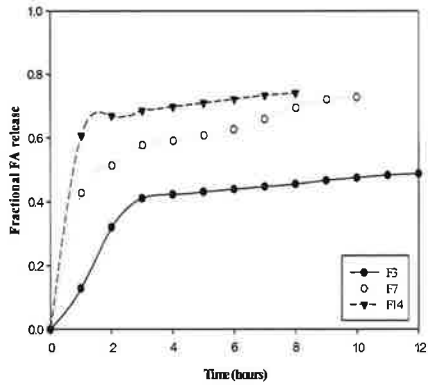

Conclusions

- Various composite biopolymeric membranes were successfully fabricated through Box-Behnken design.
- Characterization of the physicomechanical and physicochemical properties revealed important information on the effect of various formulation variables on the properties of the biopolymeric membranes.
- Membranes showing superior structural integrity, desirable swelling dynamics and degradation kinetics for long term-drug delivery were successfully fabricated.
- Drug release kinetics obtained with all composite biopolymeric membrane formulations were not ideal for long-term-drug targeted delivery.
- The results obtained from the experimental design will assist with the identification and subsequent combination of formulation variables that would translate into an optimum dosage formulation for long-term and targeted delivery of chemotherapeutic drugs.
- Shortfalls in drug release patterns will be addressed by investigating other formulation strategies such as embedding nanoparticulate systems within the optimised composite biopolymeric device.

Appendix V

A podium presentation entitled "Fabrication and Characterization of MTX-loaded PLA/PVA biopolymeric membranous drug delivery device". Bongani Sibeko, Viness Pillay, Yahya E. Choonara, Girish Modi, Sunny E. Iyuke and Michael P. Danckwerts. 29th Annual Conference of the Academy of the Pharmaceutical Sciences, Hunters Rest, Rustenburg on the, 2008.

Fabrication and Characterization of MTX-loaded PLA/PVA Biopolymeric Membranous Drug Delivery Device

Bongani Sibeko[1], Viness Pillay[1], Yahya E. Choonara[1], Girish M. Modi[2], Dinesh Naidoo[3], Riaz A. Khan[4], Leith Meyer[5], Michael P. Danckwerts[1] and Sunny E. Iyuke[6]

University of the Witwatersrand
[1]Department of Pharmacy and Pharmacology
[2]Department of Neurosciences, Division of Neurology
[3]Department of Neurosciences, Division of Neurosurgery
[4]Integral University, Department of Industrial Chemistry, Lucknow, India
[5]Central Animal Services
[6]School of Chemical and Metallurgical Engineering

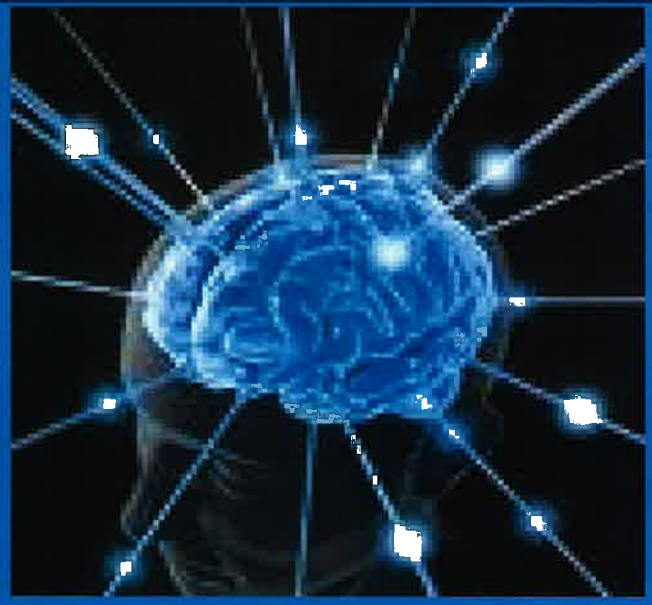

Wits Drug Delivery Platform
Department of Pharmacy & Pharmacology

University of the Witwatersrand, Johannesburg
School of Therapeutic Sciences

INTRODUCTION

- Systemically administered chemotherapy is not always effective in treating many solid malignant tumors.
- Example - Primary Central Nervous System Lymphoma (PCNSL)
- Non-Hodgkin's Lymphoma confined to the CNS
- Single tumors or multifocal tumors, size ranging between 2-4cm in diameter
- Immunocompetent and immunocompromised patients (Epstein Bar Virus)
- HD Methotrexate → Most efficient chemotherapy

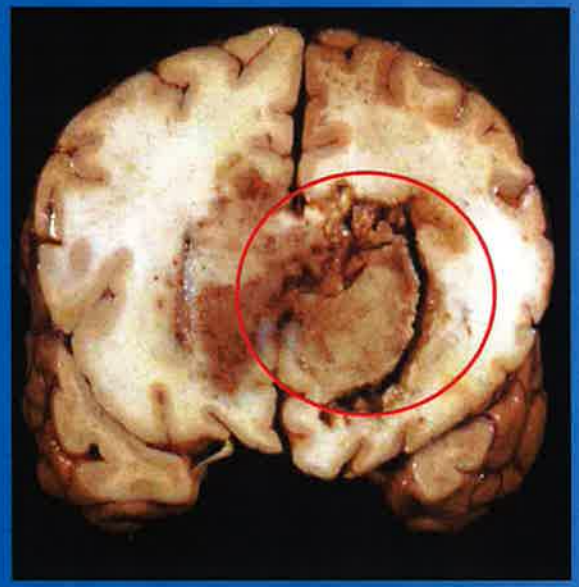

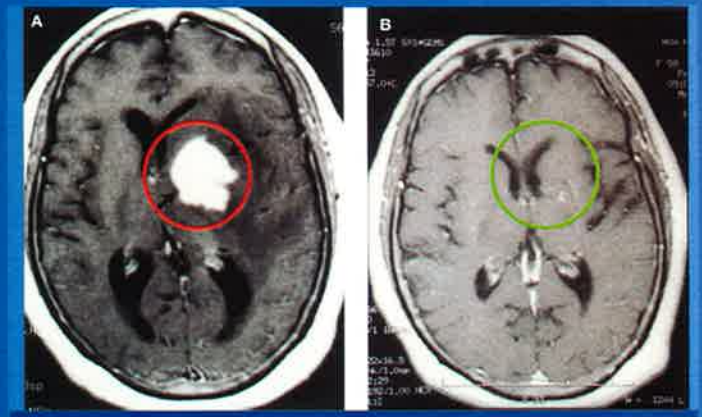

(A) Pre-MTX gadolinium-enhanced cranial magnetic resonance imaging (MRI) of a patient with PCNSL. (B) MRI of the same patient after four cycles (2months) of MTX.

Wits Drug Delivery Platform
Department of Pharmacy & Pharmacology
University of the Witwatersrand, Johannesburg
School of Therapeutic Sciences

TREATMENT STRATEGIES

Main reasons for therapeutic inefficiency:

1. Complex biology of tumors-cell type, tumor size, location and vascularisation
2. Blood-brain barrier restricts entry of drug molecules reaching the tumor site
3. Drug toxicity to normal tissues
4. Degradation of drug compounds *in vivo*

Strategies for effective drug delivery:

1. Administration of multiple drugs
2. Chemical modification of drugs
3. Identifying lipophilic drug analogs – ability to penetrate membranes
4. Synthesizing analogs that require activation within host tissues
5. Improving the method of drug administration



B. Osmotic disruption of the BBB



A. Convection enhanced drug delivery



C. Local delivery with polymer based implants

Wits Drug Delivery Platform
Department of Pharmacy & Pharmacology
University of the Witwatersrand, Johannesburg
School of Therapeutic Sciences

PHARMACOKINETICS OF DRUG-POLYMERIC IMPLANTS

- Pharmacokinetic models based on compartmental drug descriptors are used to describe targeted chemotherapy
- Complex mathematical models are used to evaluate the dynamics of drug transport into the tissue near the implant

Once implanted:

1. The tissue adjacent to the polymer implant is treated as a material consisting of three phases, intracellular space (ICS), cellular membrane (CM) and extracellular space.
2. Drug is released at a local site and migrates away from the polymer/tissue interface by diffusion and fluid convection via the ECS.
3. Some of the drug molecules may be internalised by cells or enter the vascular system.
4. Therefore the fate of drug molecules delivered to the tumor depends on the rates of transport (diffusion and fluid convection), elimination and internalization

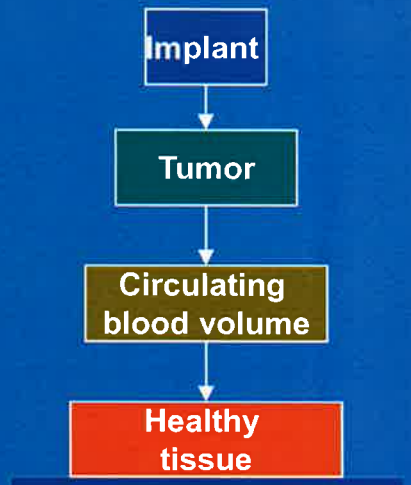

Compartmental Model

$$\frac{\partial C}{\partial t} + V.\nabla C = D\nabla^2 C - k.C$$

Mathematical model describing drug transport within the tissue

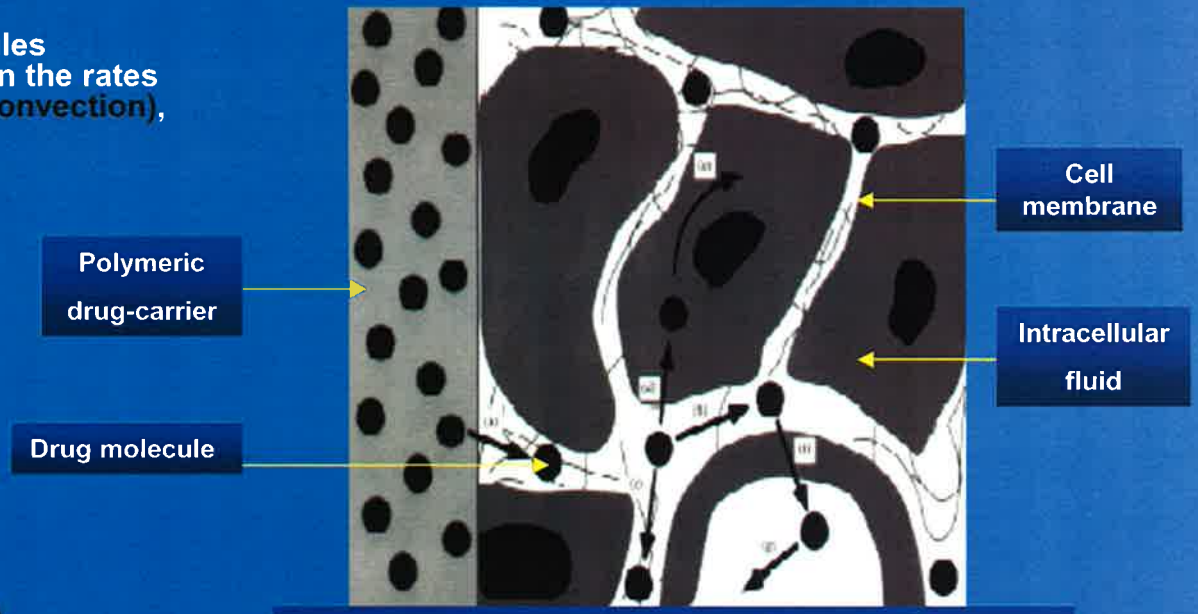

Schematic representation of local CNS drug delivery with polymeric implants

Wits Drug Delivery Platform
Department of Pharmacy & Pharmacology
University of the Witwatersrand, Johannesburg
School of Therapeutic Sciences

ADVANTAGES OF LOCAL CHEMOTHERAPY

- Bypasses the BBB
- Drug is in close proximity to the site of treatment
- Cancer drugs can be delivered to the tumor in a sustained, continuous and predictable fashion
- Localization of high doses of chemotherapeutic compound at the tumor site → increased antitumor activity
- Reduction in systemic toxicities
- Improve drug stability → increase half- life ($t_{1/2}$) of the drug → reduction in the dosing frequency
- Implant dissolves in vivo after drug release – no need for second surgical procedure to remove the device

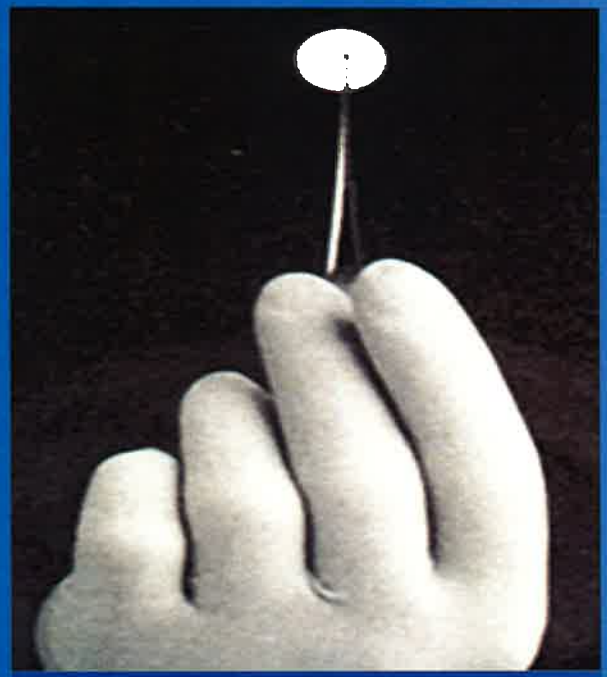

Gliadel®

Recurrent malignant gliomas

(Polymer: PCPP-SA; Drug: carmustine)

Wits Drug Delivery Platform
Department of Pharmacy & Pharmacology

University of the Witwatersrand, Johannesburg
School of Therapeutic Sciences

AIM AND OBJECTIVES

A. Development of a biopolymeric membrane device for targeted delivery of MTX

B. Computational and structural modeling of the mechanisms of membrane formation

C. Characterization of the implant:

1. Analysis of the mechanical properties by textural analysis
2. Analysis of drug entrapment efficiency (DEE) and swelling potential.
3. Perform in vitro drug release studies
4. Perform degradation studies

D. Fabrication of nanoparticulate structures for combined drug delivery

Wits Drug Delivery Platform
Department of Pharmacy & Pharmacology
University of the Witwatersrand, Johannesburg
School of Therapeutic Sciences

MEMBRANE DESIGN, FABRICATION AND OPTIMIZATION

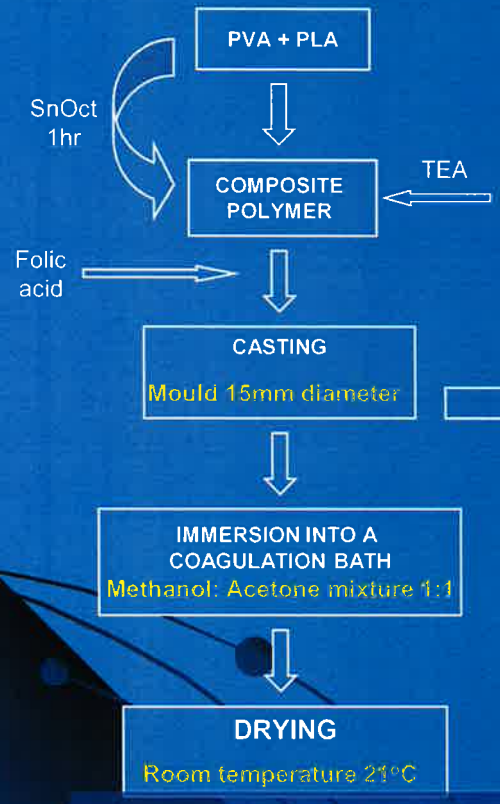

Immersion precipitation technique

Table 1: Box Behnken Design

F#	[PVA]	PVA Vol	[TEA]
1	6	50	2.5
2	10	35	4.5
3	6	35	4.5
4	8	35	2.5
5	8	50	0.5
6	10	50	2.5
7	6	35	0.5
8	8	35	2.5
9	8	20	0.5
10	10	20	2.5
11	8	20	4.5
12	8	35	2.5
13	8	50	4.5
14	6	20	2.5
15	10	35	0.5

Optimization

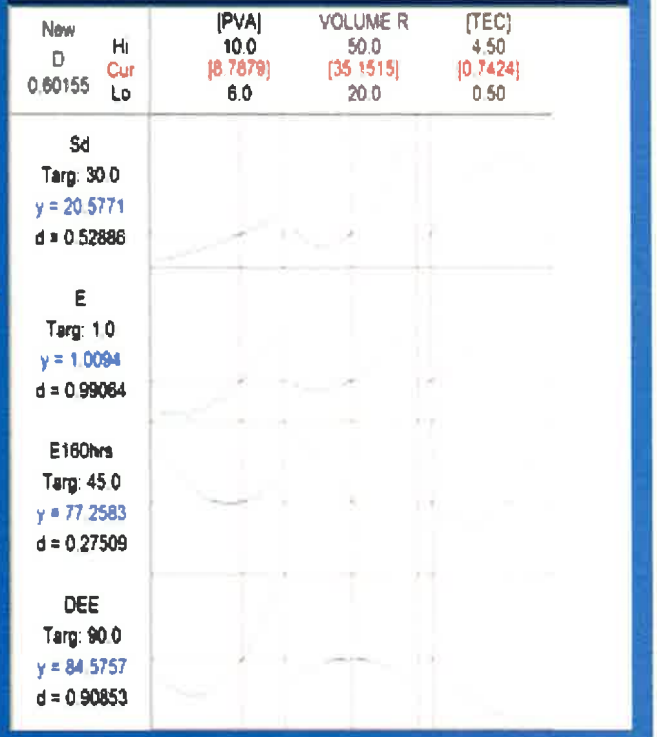

Wits Drug Delivery Platform
Department of Pharmacy & Pharmacology
University of the Witwatersrand, Johannesburg
School of Therapeutic Sciences

CHARACTERIZATION OF THE BIOPOLYMERIC MEMBRANES

Physicomechanical Investigation

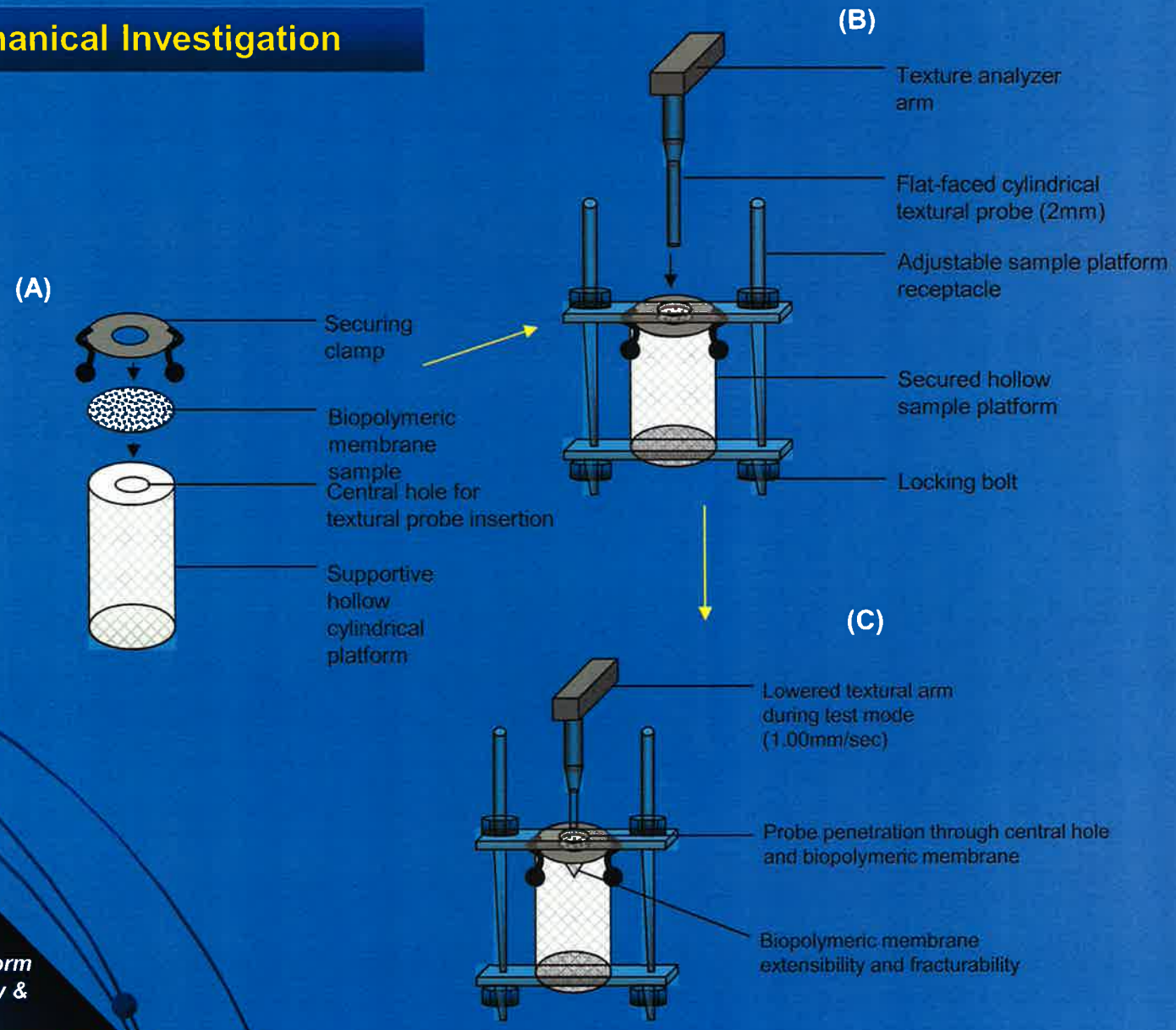

Wits Drug Delivery Platform
Department of Pharmacy & Pharmacology
University of the Witwatersrand, Johannesburg
School of Therapeutic Sciences

ANALYSIS OF THE SWELLING POTENTIAL

- Swelling studies were conducted in PBS, pH 7.4
- Membrane were allowed to reach equilibrium hydration
- Swelling potential was determined by gravimetric analysis

$$S_D(\%) = \frac{(Ws - Wi)}{Wi} \times 100\%$$

Where, S_D is degree of swelling in PBS, and *Wi* and *Ws* are the weights of the membrane in a hydrated and unhydrated state respectively

DETERMINATION OF THE DRUG ENTRAPMENT EFFICIENCY

Drug entrapment efficiency (DEE) was determined by re-dissolving the membranes PBS, pH 7.4. The amount FA entrapped within the membranes was determined by UV-spectroscopy DEE value was calculated by employing the equation:

$$DEE\ (\%) = \frac{(Mi - Md)}{Mi} \times 100\%$$

Where *Mi* is the initial mass of the drug dissolved in the casting polymer solution and *Md* is the mass of the drug quantified in the media

Wits Drug Delivery Platform
Department of Pharmacy & Pharmacology
University of the Witwatersrand, Johannesburg
School of Therapeutic Sciences

ANALYSIS OF DEGRADATION KINETICS

- Membranes were placed in buffer (PBS, pH 7.4) in an orbital shaking incubator set at 20rpm and maintained at 37°C
- At regular time intervals the membranes were removed from the buffer, and dried to constant mass
- Degradation rate was determined as the percentage loss in weight over time
- The experiment was continued until severe cracking or disintegration was observed

ASSESSMENT OF THE SURFACE MORPHOLOGY

- Scanning electron microscopy (SEM) on gold-platinum sputter coated samples

IN VITRO RELEASE OF FOLIC ACID

In vitro release studies were performed in buffer PBS (pH7.4;37°C). Membranes were placed in jars containing 100mL and incubated at 37 °C in shaking orbital incubator set at 20rpm. At predetermined time intervals samples of 5mL were collected from the release medium and were replaced with fresh buffer solution. The concentration of folic acid (FA) in the solution was assayed by UV spectroscopy

Wits Drug Delivery Platform
Department of Pharmacy & Pharmacology
University of the Witwatersrand, Johannesburg
School of Therapeutic Sciences

RESULTS AND DISCUSSIONS

Computational and structural modeling:

a) Formation of a composite amphiphilic polymer conjugated to FA.

b) Membrane is shaped through structural polymeric layering

c) Conformationally evolved biopolymeric membrane with inter-layering of PLLA and FA conjugated to the PVA backbone



Typical biopolymeric membranes
Thickness: 1mm
Diameter: 15mm

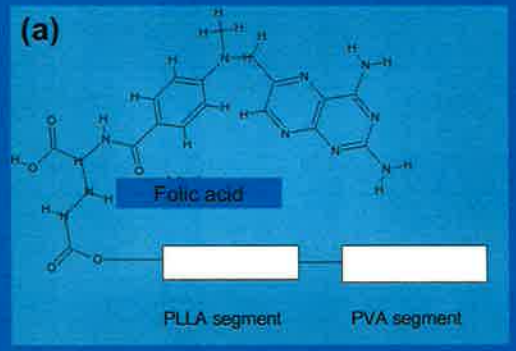

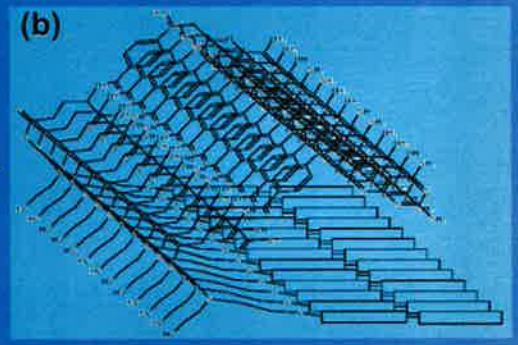

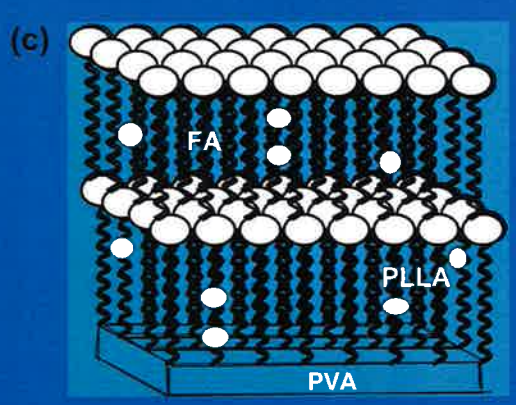

Wits Drug Delivery Platform
Department of Pharmacy & Pharmacology
University of the Witwatersrand, Johannesburg
School of Therapeutic Sciences

MECHANICAL PROPERTIES OF THE MEMBRANES

Equation 1: Elastic modulus (E)

$$E = \frac{tensile\ stress}{tensile\ strain} = \frac{F}{A\Delta D}$$

F = force (N)

A= area (Nmm)

D= distance (mm)

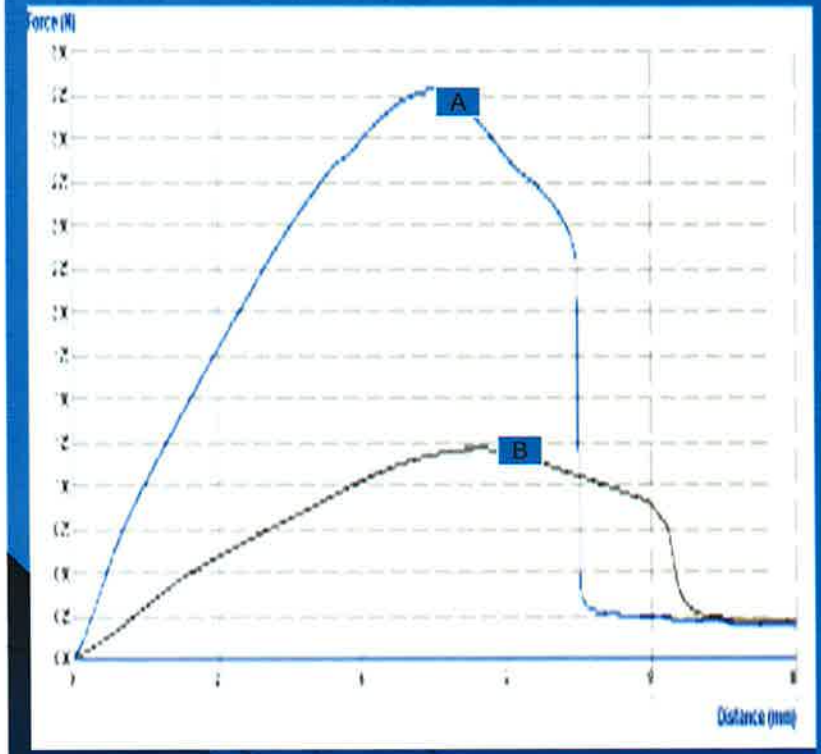

Textural profiles of an optimised formulation in an unhydrated (A) and hydrated (B) states

Elastic moduli and factor change in moduli upon equilibrium swelling of various PLA/PVA biopolymeric membrane formulations

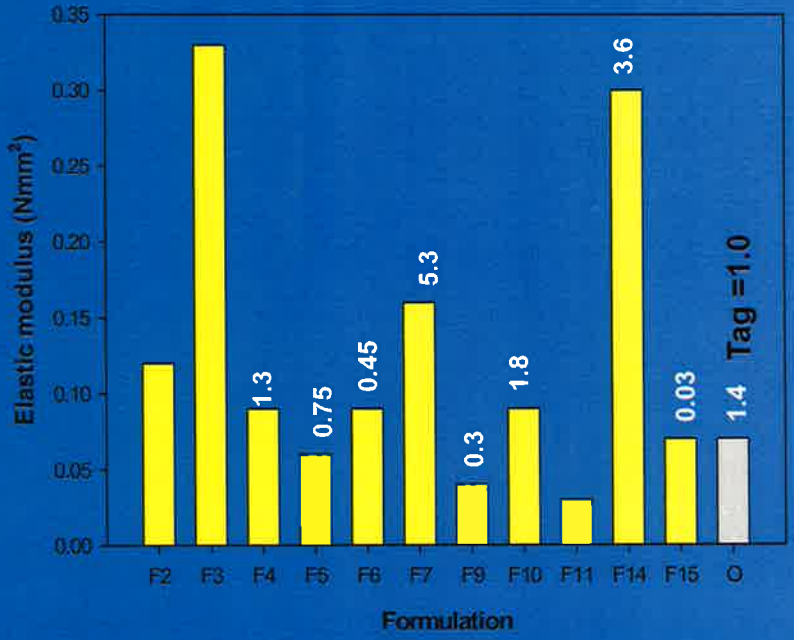

- Assess the potential for mechanical adaptability
- Stiff and hard materials→ neural tissue damage
- Elastic implants → possess the ability to integrate well into the neural tissue

Wits Drug Delivery Platform
Department of Pharmacy & Pharmacology
University of the Witwatersrand, Johannesburg
School of Therapeutic Sciences

SWELLABILITY

- PVA, a hydrophilic component in the membranes was responsible for attracting water molecules into the membranes → hydration →swelling.
- The maximum water imbibing capacity of the formulations reached at equilibrium hydration was chiefly determined the concentration of PVA:
- 10%$^{w}/_{v}$ PVA formulations → greatest swelling degree
- 8% $^{w}/_{v}$ PVA formulations → intermediate swelling degree
- 6%$^{w}/_{v}$ PVA formulations → lowest swelling degree
- Inter-formulation variability in S_D → amount of TEA and volume ratio of PVA
- Minimal swelling favours greater stability and is a desirable property of brain implants

Swellabiity of various PLA/PVA biopolymeric membrane formulations

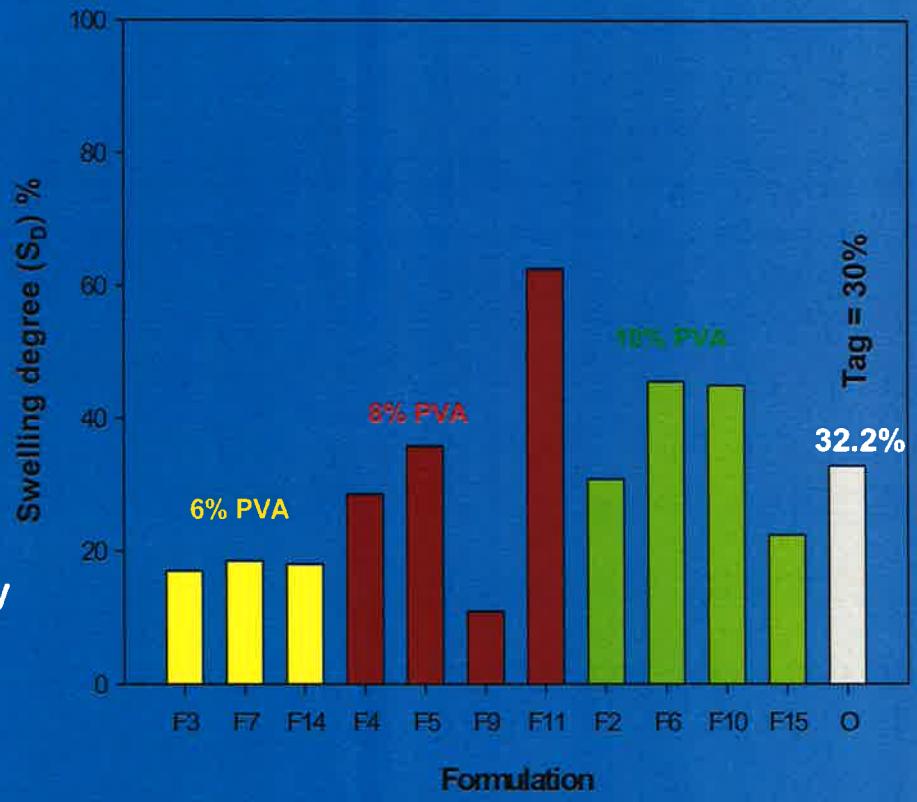

Wits Drug Delivery Platform
Department of Pharmacy & Pharmacology
University of the Witwatersrand, Johannesburg
School of Therapeutic Sciences

DEGRADATION/ EROSION KINETICS

- Membranes displayed biphasic degradation kinetics.
- Second degradation phase was due to constant surface erosion.
- Higher TEA content ≥ 4.5mL → rapid degradation (within 12 hours)
- Desired long-term degradation kinetics were achieved for the optimised formulation

Degradation profiles of various PLA/PVA biopolymeric membrane formulations

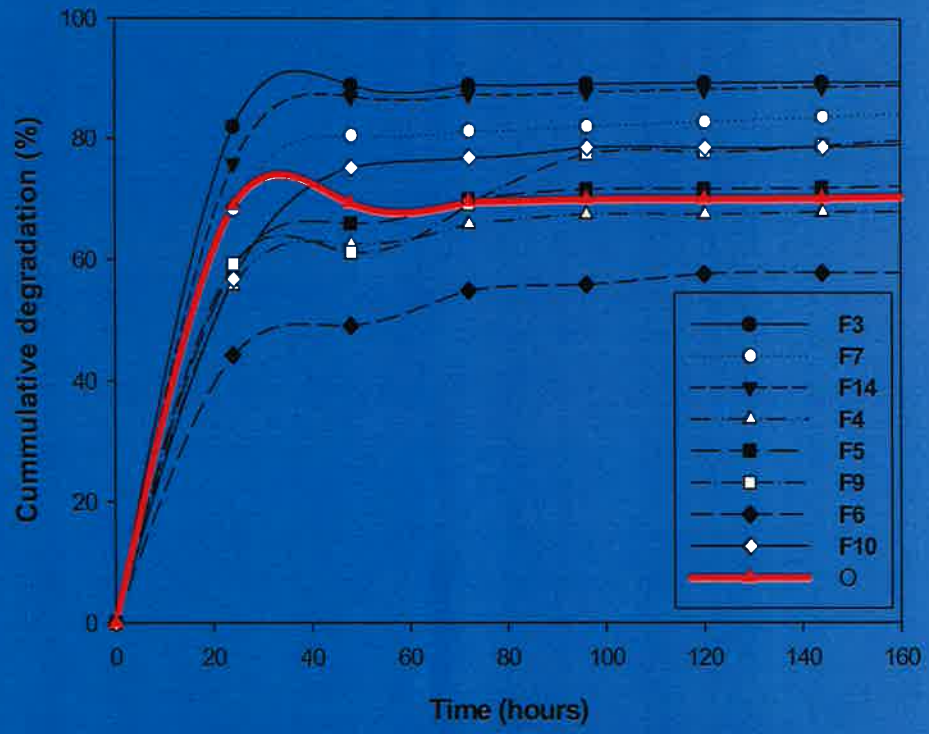

Wits Drug Delivery Platform
Department of Pharmacy & Pharmacology
University of the Witwatersrand, Johannesburg
School of Therapeutic Sciences

SURFACE MORPHOLOGY

- The resultant surface morphology of the membranes was determined by parameters such as [polymer] and arrangement of polymer chains during phase separation sequences
- Membranes displayed a layered and crystalline architecture (a) and (b)
- Differences in morphology of the aerial and bottom surfaces were observed (c) and (d)
- Surface morphology determines the extent of protein adhesion on implanted materials

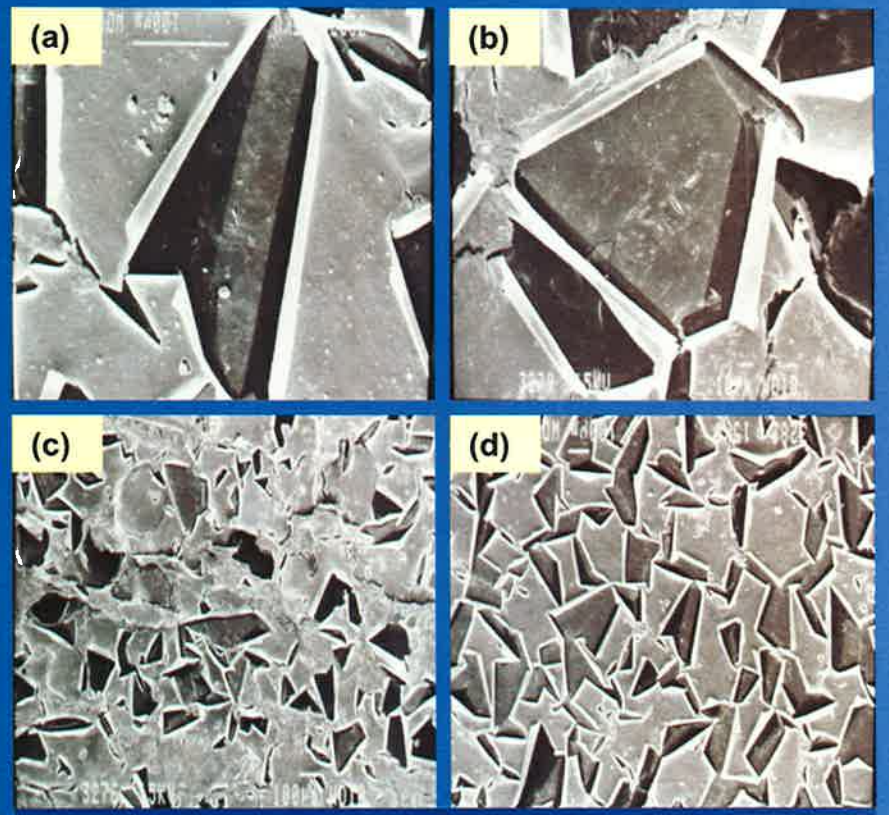

SEM photomicrographs of the biopolymeric membranes

Wits Drug Delivery Platform
Department of Pharmacy & Pharmacology
University of the Witwatersrand, Johannesburg
School of Therapeutic Sciences

DRUG ENTRAPMENT EFFICIENCY AND *IN VITRO* DRUG RELEASE

Drug entrapment efficiencies (DEE) of various PLA/PVA biopolymeric membrane formulations

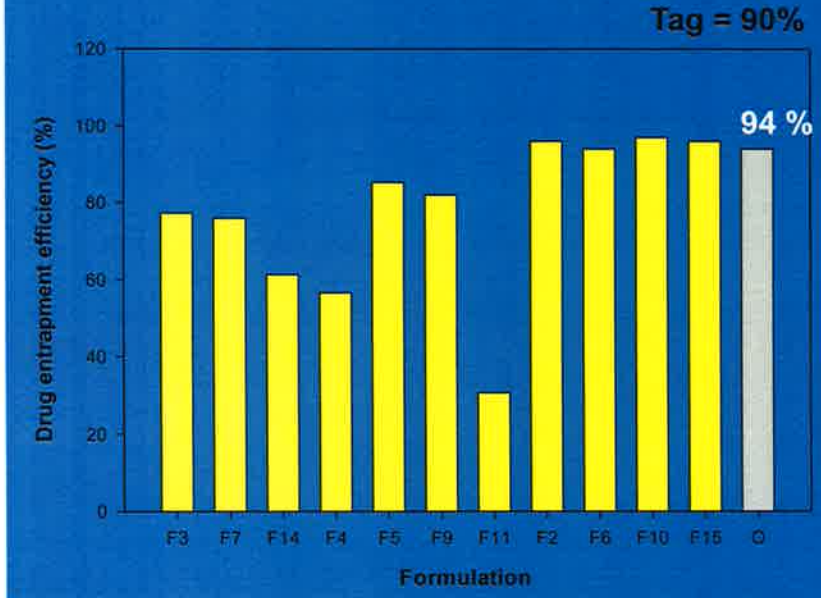

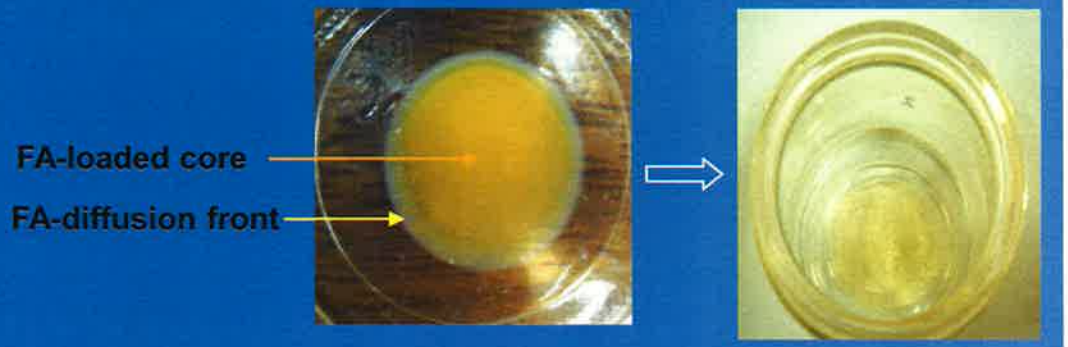

FA release profiles from various PLA/PVA biopolymeric membrane formulations

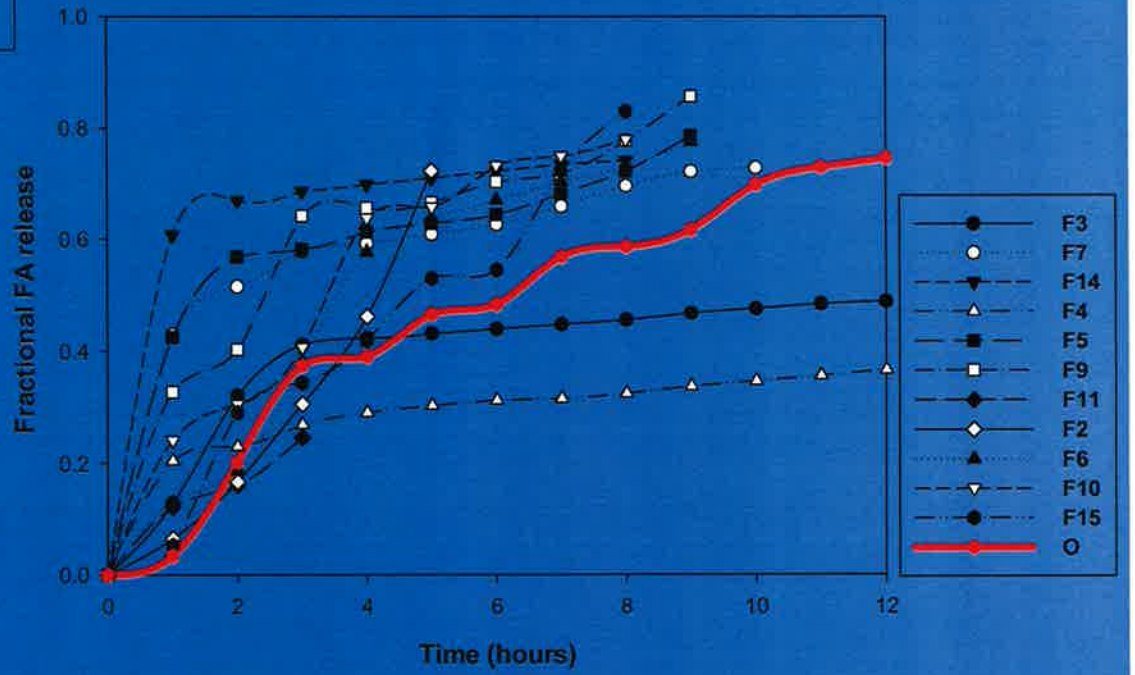

Wits Drug Delivery Platform
Department of Pharmacy & Pharmacology
University of the Witwatersrand, Johannesburg
School of Therapeutic Sciences

BIODISTRIBUTION AND BIOCOMPATIBILTY-TESTING SCHEDULE

Sprague Dawley Rat Model

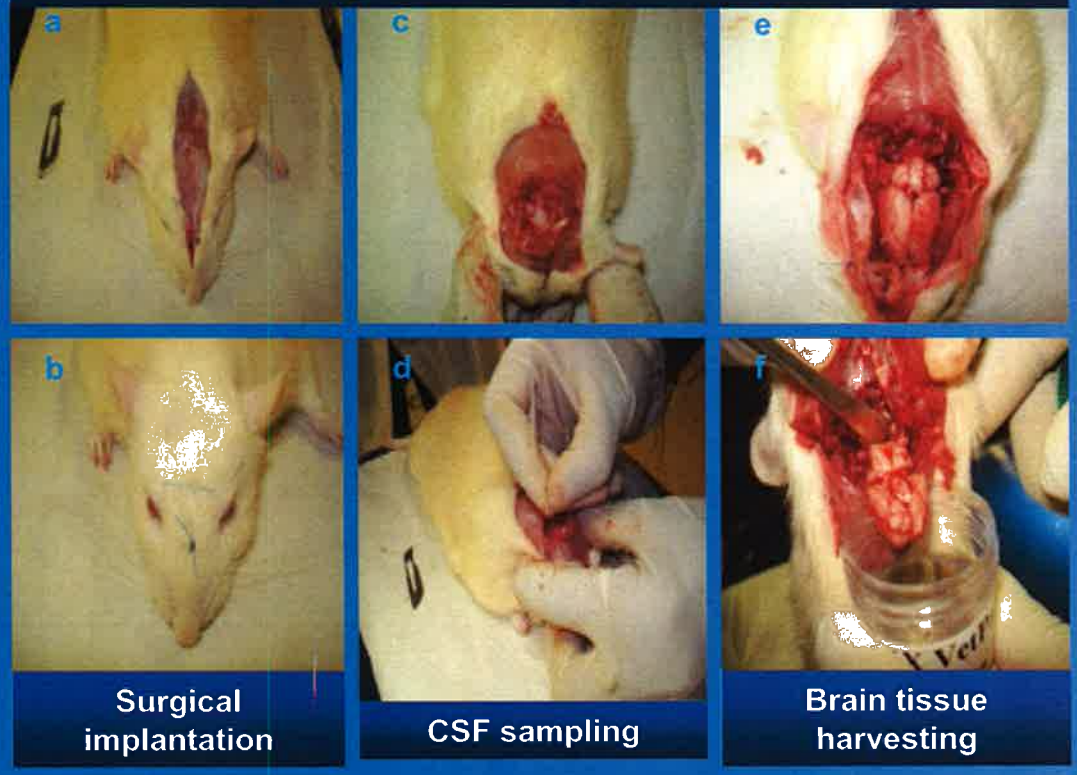

Surgical implantation

CSF sampling

Brain tissue harvesting

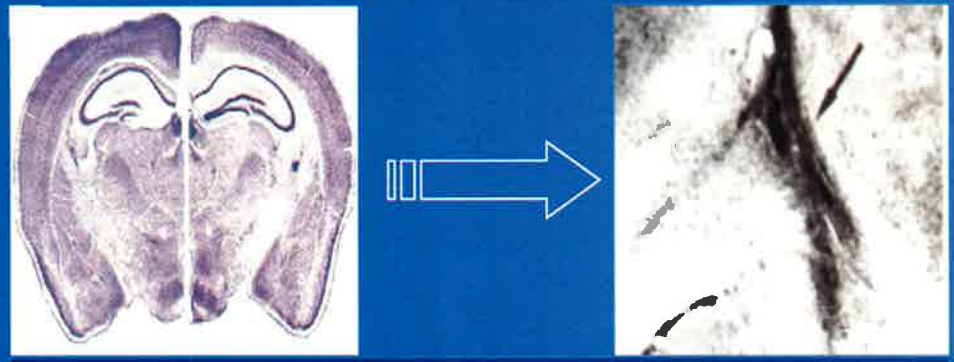

Cresyl Violet staining

Wits Drug Delivery Platform
Department of Pharmacy & Pharmacology
University of the Witwatersrand, Johannesburg
School of Therapeutic Sciences

CONCLUSION

Size distribution

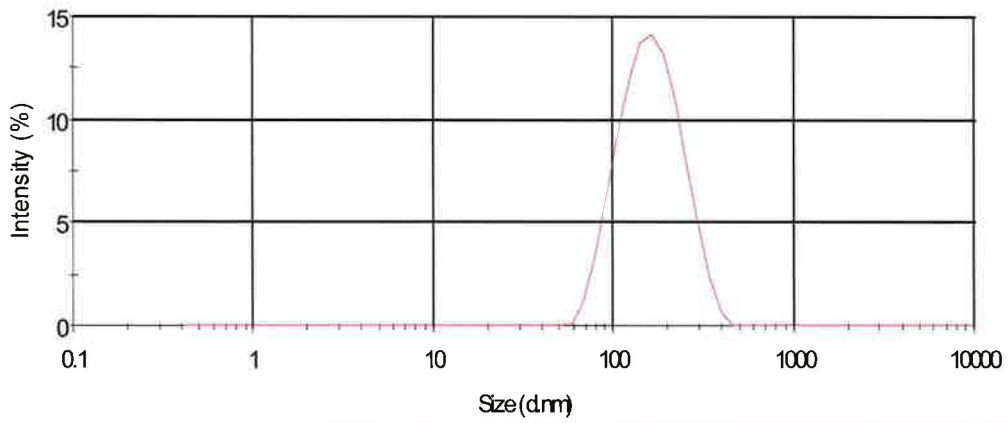



TEM photomicrographs:
PLA/Eudragit S 100 nanotube

- Optimized biopolymeric membrane.
- Fabrication PLA/Eudragit S 100 NT's
- Size = 140.6nm
- Optimization process
- Embedding NT's into the optimized biopolymeric membrane → desired drug release behaviour.

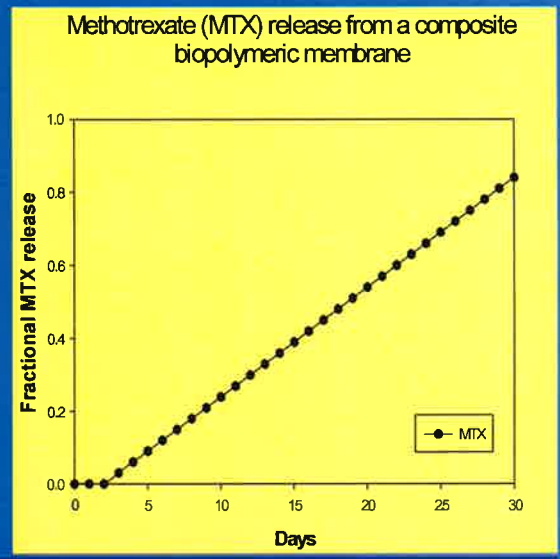

Desired drug release profile

Wits Drug Delivery Platform
Department of Pharmacy & Pharmacology
University of the Witwatersrand, Johannesburg
School of Therapeutic Sciences

THANK YOU

Wits Drug Delivery Platform
Department of Pharmacy & Pharmacology

University of the Witwatersrand, Johannesburg
School of Therapeutic Sciences